BEHAVIOURAL AND NEURONAL CORRELATES OF CENTRAL PAIN PROCESSING IN A RAT MODEL OF OSTEOARTHRITIS

by Carlota Montagut-Bordas

A thesis submitted to University College London for the degree of Doctor of Philosophy

Department of Neuroscience, Physiology and Pharmacology
Gower Street | London | WC1E 6BT

This work was funded by the European Union's Horizon 2020 research and innovation program under the Marie Skłodowska-Curie grant agreement No. 642720.

BonePain

I, ***Carlota Montagut-Bordas*** confirm that the work presented in this thesis is my own. Where information has been derived from other sources, I confirm that this has been indicated in the thesis.

ABSTRACT

Osteoarthritis (OA) of the knee join is a chronic condition characterized by the loss of articular cartilage around the joint leading to changes in joint capsule. Clinically, OA is manifested by joint stiffness, swelling, bone tenderness, discomfort upon movement and joint pain. The latter is the main reason why patients seek medical treatment. OA pain is often classified as nociceptive due to tissue damage leading to inflammation. However, a subgroup of OA patients exhibits pain with neuropathic pain-like features. Thus, it is important to understand the differences in pain processing between these two groups of patients, as it will have implications on treatment.

2mg of monosodium iodoacetate (MIA) was intra-articularly injected into the left knee of male Sprague-Dawley rats in order to study behavioural and electrophysiological changes that appear during the development of OA pain. The MIA model provides two distinct stages of OA pain. An early acute inflammatory stage (2-4 days after MIA injection) and a late stage that presents neuropathic pain-like features (14-21 days post MIA injection).

Cartilage damage scores differ between the early and late stage MIA animals with the latter exhibiting a more severe maximal OA score. Behaviourally, paw withdrawal thresholds decrease in the acute inflammatory stage and returned almost back to baseline in the late stage. Weight bearing deficits are present in both stages suggesting that both groups exhibit on going pain.

$Ca_V2.2$ is present in the pre-synaptic terminals of primary afferent fibers in the spinal dorsal horn and mediates neurotransmitter release. ω-conotoxin GVIA is a small peptide that acts as a state independent blocker of $Ca_V2.2$, while TROX-1 is a state dependent blocker of the channel. *In-vivo* electrophysiological recordings of WDR neurones revealed that ω–conotoxin was able to significantly inhibit neuronal evoked responses to electrical, dynamic brush, mechanical and thermal stimuli in the late stage MIA animals but had little or no effects in the early stage MIA animals. State dependent blocker TROX-1, had no effects in neuronal responses of WDR neurones, in any group. Additionally, *in-vivo* electrophysiological revealed an increased descending serotonergic drive in a subgroup of late stage MIA animals. Additionally, Descending noxious inhibitory controls (DNIC) disappeared in this stage of the model as observed after neuropathy. Suggesting that in the late stage descending modulation is altered.

PUBLICATIONS

Some of the work presented in this thesis has been previously presented or published:

Patel R, **Montagut-Bordas C**, Dickenson AH. Calcium channel modulation as a target in chronic pain control. Br J Pharmacol. 2017 Mar 20.

IMPACT STATEMENT

OA pain is often classified as nociceptive due to the tissue damage that the articular cartilage undergoes; yet a series of human studies have revealed the presence of a subgroup of patients that suffer from pain with neuropathic pain-like features. I have carried out a series of studies monitoring behavioural, locomotor effects, neuronal activity, effects of pharmacological agents and measured inflammatory mediators in order to help understand the peripheral and central changes that may occur in the MIA rat model of OA. I have tried to equate these to possible nociceptive and neuropathic changes.

The subgroup of patients that suffer from neuropathic pain-like features obtained high scores on the PainDETECT test (Soni et al., 2018), a test used to diagnose neuropathic pain patients. Additionally, this patients exhibit temporal summation (Clauw and Hassett, 2017), referred pain with mechanical and thermal hyperalgesia (Gwilym et al., 2009), ongoing pain even when at rest, and a reduced response to NSAIDs treatment (Thakur et al., 2014). Additionally, fMRI studies have demonstrated that upon mechanical stimulation of the injured area, these OA patients have increased midbrain activity compared to nociceptive OA and control patients. Suggesting, that this subgroup exhibits altered descending modulation. Identifying this subgroup of patients is crucial in order to provide them with proper treatment. Additionally, other studies have shown that three years after knee replacement surgery 19% of OA patients report severe to unbearable pain (Petersen et al., 2015). In line with these studies, brain imaging in human OA patients show that after knee replacement surgery a subgroup of patients that still suffers from chronic pain has altered brainstem activity. Therefore, knee replacement surgery is not a good treatment option for these patients as they might have nerve damage and will still suffer from pain years after the surgery

A possible way to diagnose these patients would be to address if they present Conditioned Pain Modulation (CPM) (Bannister et al., 2015). CPM works by the principle that of one pain inhibits another pain. In neuropathic patients, CPM is lost, thus the application of a conditioned stimulus in a part of the body away from injury site does not produce an inhibition of their already existing pain. In the work presented in this thesis, I have demonstrated that in the late stages of the MIA model a subgroup of animals exhibit an enhanced descending modulation. This is line with human data that shows increased PAG and RVM activity in neuropathic pain-like patients. In addition, during the late stages of MIA, DNIC was lost

suggesting that measuring CPM could be a good diagnosis tool for neuropathic pain-like OA patients. Additionally, new treatment for the subgroup of neuropathic pain-like patients is needed. In this thesis I have demonstrated that noradrenalin serotonin reuptake inhibitors (NSRIs), antidepressants commonly prescribed for the treatment of neuropathic pain, fail to reduce WDR neuronal evoked responses to dynamic brush mechanical and thermal stimulation in the late stages of MIA animals. Therefore, suggesting that NSRIs might not be the best line of treatment for OA patients. However, state dependent N-type voltage gated calcium channel blocker, ω-conotoxin, efficiently reduced neuronal evoked response to WDR neurones both in early and late stages of the MIA model, with more potency in the late stages. Thus, small molecules that target the channel in a state dependent way, could be good drug target for neuropathic pain-like OA patients.

ACKNOWLEDGEMENTS

First of all I want to thank my supervisor Professor Anthony Dickenson. Tony, thank you for giving me the opportunity to be part of 'The House of Pain'. I still remember the day you told me I got the PhD position. I was beyond happy and couldn't stop crying. Since then you have always given me your unconditional support, advice and encouragement.

I would also like to thank two people whom have been my mentors, teachers and friends during this past four years. These two women are not only amazing people but also amazing scientists. Dr. Leonor Gonçalves and Dr. Kirsty Bannister. Leo, thank you for always helping me when I needed, specially with my thesis, even if I didn't ask. Thank you for all the advice that you have given me (scientific/non-scientific) throughout the years, as well as all the fun moments spent together in or outside the lab. I would have been lost without you. Kirsty, you taught me everything I know about spinal electrophysiology, you have always been there for scientific advice and for moral support. I couldn't be more grateful for all the help you have given me even when at Kings. I want you both two know how much I look up to you and without your support I wouldn't have been able to complete my PhD and finish this thesis.

I also want to thank present HoP members. Thanks for such wonderful years and all the fun times we have spent together at NPP Christmas parties, summer days at the portico steps, conferences and most importantly at our favourite place, the LCC. Thank you Ryan for all the help you given me with stats, ephys and always opening the door for me when I forgot my key. I also want to thank Ana for arriving to the lab in a moment when I was feeling lonely. Ana, I had so much fun with you this past year, I want to thank you for always being there when I was down, had questions or needed a chat. I will never forget all the music we played in the ephys room. To past members of the House of Pain especially, to Mireia and to Liam. To my dearest PhD comrades, Candela, Rawan and Otto. I am very happy to have shared my PhD journey with the three of you, I couldn't have asked for better friends. To Heather, mi gran amiga! We started this journey together and we are ending it together, it could not be more special than that.

I would also like to thank all of the members of the BonePain Network. I am very proud to be part of such an amazing family of scientists. Special thanks to Ulla Kløve Jakobsen and Anne-Marie Heegaard for all their hard work they have done to make the BonePain Network possible. The BonePain Network allowed me two have the opportunity to carry out two amazing collaborations that I am super thankful for. I want

to say thank you to Professor Chantal Chenu. Chantal, thank you for giving me the opportunity to come to your lab and perform all the knee histology, it was a fun experience. I want to also thank Freija who showed me the ropes at the RVC and a special thanks to Elaine Shervill. Elaine, you always helped me with my knees when I needed it with a smile and no hesitation, for that I will always be grateful. The second collaboration was at Transpharmation where I was able to carry out some behavioural experiments. I want to thank both Dr. Neil Upton and Dr. Amy Fisher for taking me in at Transpharmatio. Amy, I had an amazing time with you at Transpharmation thanks for teaching me to perform the behaviour experiments and for all the support.

I want to thank all of my friends who have always encouraged and motivated me through my PhD even thought they had no idea or understanding of what I did in the lab. Special thanks goes to Berta, Carmen C, Carmen S and to my flatmates Maria Peiró and Maria Sanchez. Coming home after a long day of experiments was always better because you were there for me! To Mike, thank you for your unconditional love and support, even when I was grumpy. Also thanks for teaching me how to use Illustrator for my figures. I love you all so much!

Lastly, but most importantly this thesis is dedicated to my parents, Ana and Albert and to my sister Nina. You have done so much for me and I don't even know how to thank you. There are no words to describe how much I love you and how grateful I am for all the support you have given me through the years. I always try to make you all proud of me. You thought me from a very young age that if I work hard and stay motivated I can set my mind to achieve anything and so I did with this thesis. Superfamily, os quiero mucho!!

ABBREVIATIONS

-/-	Homozygous Knockout
5-HT	5-hydroxytryptamine
AC	Articular Cartilage
ACC	Anterior Cingulate Cortex
ACL	Anterior Cruciate Ligament
ACLT	Anterior Cingulate Ligament Transection Model
AMPA	α-Amino-3-Hydroxy 5-Methyl-4-Isoxazeloproprionic Acid
ANOVA	Analysis of Variance
APs	Action Potentials
ARA	American Rheumatism Association
ASIC	Acid Sensitive Ion Channels
ATP	Adenosine Triphosphate
ATF-3	Activating Transcription Factor 3
Ba^{2+}	Barium
BSU	Biological Services Unit
BMLs	Bone Marrow Lesions
Ca^{2+}	Calcium
CCI	Chronic Constriction Injury
CeA	Central Nucleus of the Amygdala
CFA	Complete Freud's Adjuvant
CGRP	Calcitonin gene related pepetide
COX	Cyclooxygenases
CNS	Central Nervous System
CPP	Conditioned Placed Preference
DLF	Dorsolateral Funiculus
DMM	Destabilisation of the medial meniscus
DNIC	Diffuse Noxious Inhibitory Controls
DOR	δ-opioid receptors
DRG	Dorsal Root Ganglia
EDTA	Ethylenediaminetetraacetic acid
ER	Endoplasmic reticulum
fMRI	Functional Magnetic Resonance Imaging
GAG	Glycosaminoglycan
GAL	Galanin
GAPDH	Glycolytic Enzyme Glyceraldehyde 3-Phosphate Dehydrogenase
GBP	Gabapentin
GPCR	G-Protein Coupled Recepots
HA	Hyaluronic acid
HTM	High-Threshold Mechanical Nociceptors
HVA	High voltage-activated channels
I	Input
IASP	International Association for the Study of Pain

IL	Interleukin
I.P	Intraperitoneal
IB4	Isolectin B4
LABORAS	Laboratory Animal Behaviour Observation Registration and Analysis System
LC	Locous coeruleus
LTP	Long Term Potentiation
LVA	Low Voltage-Activated Channels
MAPK	Mitogen-Activated Protein Kinase
Mg^{2+}	Magnesium
MIA	Monosodium Iodoacetate
MIDAS	Metal ion-dependent adhesion site motif
MMPs	Metalloproteinases
MMT	Medial Meniscal Tear Model
MRI	Magnetic Resonance Imaging
mRNA	Messenger ribonucleic acid
MOR	μ-opioid receptor
ms	Mili seconds
NE	Norepinephrine
NGF	Nerve Growth Factor
NK1	Neurokinin 1
NK1R	Neurokinin 1 Receptor
NMDA	N-Methyl-D-Aspartate
nNOS	Neuronal Nitric Oxide Synthase
NO	Nitric Oxide
NPY	Neuropeptide Y
NRI	Norepinephrine Reuptake Inhibitor
NS	Nociceptive Specific
NSAIDs	Non-Steroidal Anti-Inflammatory Drugs
NT	Neurotransmitter
OA	Osteoarthritis
PAG	Periaqueductal Grey
PB	Parabrachial
PBS	Phosphate buffer solution
PD	Post-discharge
PFA	Paraformaldehyde
PG	Prostaglandin
PGB	Pregabalin
PIC	Protease Inhibitory Cocktail
PKC	Protein Kinase C
PLC	Phospholipase C
PNS	Peripheral Nervous System
PSTH	Post-Stimulus Time Histogram
PV	Paravalumin

PW	Paw withdraw
PWF	Paw Withdraw Frequency
PWT	Paw Withdraw Threshold
QST	Quantitative Sensory Testing
R	Receptor
RM	Repeated Measures
ROS	Reactive Oxygen Species
RVM	Rostral Ventromedial Medulla
SB	Spinobulbar
SG	Substantia Gelatinosa
SNRI	Serotonin, Norepinephrine Reuptake Inhibitor
SNL	Spinal nerve ligation
SSRI	Selective Serotonin Reuptake Inhibitor
STT	Spinothalamic tract
T	Transmission
TAT	Trans-Activating Transcriptional Activator
TNF-a	Tumor necrosis factor alpha
Trk	Tyrosine Kinase Receptor
TREK	Two-Pore-Domain Potassium Channels
TROX-1	N-Triazole Oxindole
TRP	Transient Receptor Potential
TTX	Tetrodotoxin
UK	United Kingdom
USA	United States of America
USP	Ubiquitin specific proteases
VEGF	Vascular Endothelial Growth Factor
vF	von Frey
VGGC	Voltage gated calcium channels
VGLUT	Vesicular Glutamate Transporter
VP	Ventral Posterior
VEA	von Willebrand factor A
WDR	Wide dynamic range neurones
WOMBAC	Western Ontario and McMaster Universities Osteoarthritis Index
WU	Wind-up

TABLE OF CONTENT

Chapter 7. General Discussion

LIST OF FIGURES

SUPPLEMENTARY FIGURES

LIST OF TABLES

“I have declared war on pain.”

– John Bonica, The Management of Pain, 1954.

Chapter 1. Introduction

1.1. A brief history of Pain Theories

During the course of my PhD I have been studying the neuronal basis of pain in osteoarthritis (OA). This has made me think a lot about how we, as humans, experience, process and understand pain.

The International Association for the Study of Pain (IASAP) describes pain as "*an unpleasant sensory and emotional experience associated with actual or potential tissue damage, or described in terms of such damage*". However to get a proper understanding of how this description of pain came about, it is important to go back in history.

When reading about the history of pain, I came across philosopher, physiologist and mathematician René Descartes (1596-1650) and a drawing made by Louise La Forge (**Figure 1**) based on Descartes theory of the mechanisms behind pain transmission.

In his book *L'Homme* (1644), Descartes was the first western philosopher to describe a somatosensory pathway in humans (Moayedi and Davis, 2013). He did so by describing a model where a little kid is standing next to a fire with his foot near the flame **(Figure 1.1(A,B))**. The particles of the fire cause the activation of a fibril in the foot that then sends a signal from spinal cord to brain **(Figure 1.1 (C,F)).** Once the response has arrived to the brain the tubule that contains the fibril becomes active again, causing a motor response which includes moving the foot away from the fire and turning the body away from protection (Moayedi and Davis, 2013).

What was so ground breaking about Descartes theory, was the fact that he made a distinction between pain transmission, which we now call nociception, and pain perception. In his theory, the fibrils would be the primary afferent fibers, which encode sensor information and translate it into a neuronal signal. This signal travels to the brain where the messaged is process and perceived as "danger". In addition, Descartes also believed that intensity of the stimulus caused changes on the firing rate of the fibril, thus sending appropriate information to the brain about the intensity of the stimuli.

1.1

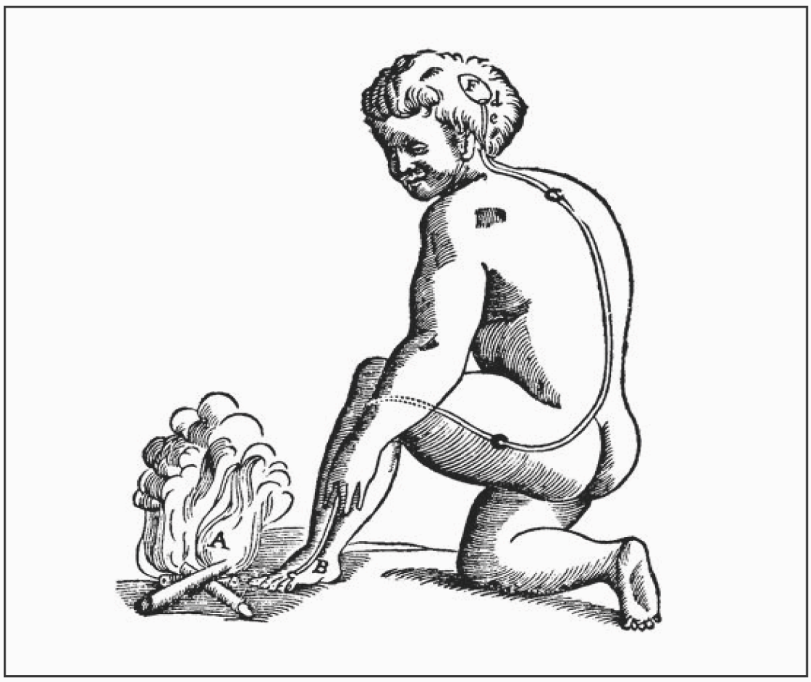

Figure 1.1. Drawing made by Louis La Forge base on Descartes pain pathway. The little boy is with his foot close to the fire (A). Particles of the fire activate the fibril on the foot (B), which activates and sends a message through the spinal cord (C) all the way to the brain (E). Once in the brain, the fibril opens a pore where the fibril terminated (D) which activates a specific brain region (F). This activates the motor responses and the little boy moves his foot away from the fire.

By 1965 the pain field was divided in two: Specificity Theory and Pattern Theory. The Specificity Theory postulated that touch and pain stimuli were encoded by different modality specific stimuli (e.g. touch, temperature, pain etc.) activating specific neuronal pathways in the periphery and sending messages to different centres in the brain. In contrast, the Pattern Theory argued that afferent fibers respond to a range of stimuli creating a particular firing pattern that encodes a type of stimuli, its intensity and location. The interpretation of a specific pattern occurs once the signal reaches the brain. Thus, it is the central nervous system (CNS) that is in charge of the perception of such stimuli and intense stimuli encode the perception of pain.

At this time, Ronald Melzack and Charles Patrick Wall postulated the Gate Control theory of pain, which revolutionized the pain field and became one of the most important concepts. The Gate Control theory proposed that both large diameter fibers (Aβ-fibers) and small diameter fibers (C-fibers) projected to the dorsal horn of the spinal cord (Melzack and Wall, 1965). The large fibers encoded touch and small fibers painful stimuli. In the dorsal horn, both fibers synapsed into two different sets of neurones, substantia gelatinosa (SG) neurones and another group of neurones that they called ‘transmission (T) neurones’. When active, the T neurones project to the brain, however the activity of the T neurones is modulated by the SG neurones. Thus, when large diameter fibers become active upon

touch, these activate the SG neurones causing the inhibition of T neurones. When small diameter fibers become active upon painful stimulation, the inhibition of SG neurones to T neurones is lost, thus the gate opens and T neurones are able to transmit painful stimuli to the brain. In addition, descending controls from the brain back to the spinal cord are also able to modulate the gate. All these theories proposed a series of discoveries that allowed the pain field to advance. However, they all had flaws and failed to propose a mechanism that explains the complexity of the pain system.

The question left to answer is, where are we now? While many questions remain unanswered, we now know that nociceptors are heterogeneous (e.g. they can respond to different modality stimuli, they have different sizes, myelination etc.) (Julius and Basbaum, 2001). Different subsets of nociceptors contain different receptors that respond to specific modalities of stimuli. However, nociceptors can also be polymodal as they can contain different receptors responding to thermal as well as mechanical stimulation. In addition, we also have noxious specific (NS) neurones (Duan et al., 2018) as seen in uninjured animals and wide dynamic (WDR) neurones that respond to both innocuous and noxious stimuli (Mendell, 1966). Behavioural pain responses are modality specific allowing us to distinguish between the different types of sensory information that is transmitted form the periphery to the brain (Braz et al., 2014). How the central nervous system translates the sensory information into a sensation and perceives pain remains unanswered.

Returning to the current description of pain by IASP we can understand that pain is, a sensory experience because we are able to distinguish the intensity of such pain, locate it and know its duration. We understand it is unpleasant because it triggers an emotion, which is encoded in the brain as a perception putting such pain into context (Moayedi and Davis, 2013).

1.2. Osteoarthritis

1.2.1. Definition and clinical features of osteoarthritis

In 1989 the American Rheumatism Association (ARA) published a report defining OA as: “a heterogeneous group of conditions that lead to joint symptoms and signs which are associated with defective integrity of the cartilage, in addition to the related changes in underlying bone and at the joint margins” (McAlindon and Dieppe, 1989). Thus, OA is a mechanically induced disorder and the changes produced in the joint give rise to a series of biological abnormalities mediated biochemically that lead to further destruction of the joint and surrounding area (Brandt et al., 2006).

Clinically, OA is characterized by joint stiffness, bone tenderness, discomfort upon

movement and joint pain. The latter being the key symptom that drives patients to seek medical care and makes OA one of the leading most common disabling joint diseases worldwide (Sandell, 2012). In addition, OA patients can experience pain at rest, bone enlargement, crepitus (the medical term that is used to describe the crackling or popping sound sensation experienced under skin or joints) and inflammation of the joint area.

OA can be classified into: primary or idiopathic when the cause of the disease is unknown or secondary when it is related to a known medical condition or event (e.g. caused by diabetes mellitus, obesity, etc.) (Altman et al., 1986). Because it is a mechanically induced disorder, OA can develop due to both or either (1) because the mechanical stress on the joints is excessive leading to changes in joint environment or (2) the biological environment of joint is abnormal (Brandt et al., 2006).

1.2.2. Anatomy and function of a healthy knee joint

A joint or articulation is defined as a junction that connects two bones in order to provide some movement. In the human body joints can be functionally classified based on the mobility that they provide:

- Synarthrosis or fibrous joints, which provide little or no mobility
- Amphiarthrosis or cartilaginous joints, which permit a slight mobility
- Diarthrosis or synovial joints, which allow joints to freely move. These are the most common type of joints.

The knee joint is a type of synovial joint comprised of two subjoints, the tibiofemural joint and the patellofemoral joint. Four bones make up the knee joint in order to provide support to the body. These are the tibia, femur, patella (or kneecap, triangular bone at the front of the knee) and the fibula. The meniscus, also part of the knee joint anatomy **(Figure 1.2.a)**, is an extra thick layer of cartilage that acts to prevent the deterioration and degeneration of the articular cartilage (Makris et al., 2011).

Additionally, the bones of the knee joint are connected to each other through ligaments. There are different types of ligaments in the knee joint: The anterior and posterior cruciate ligaments, which connect the femur and tibia providing stability and control movement. The lateral collateral ligament, found outside of the knee joint that attaches the femur and fibula. Lastly, the medial collateral ligament found on the medial inner side of the knee attaching femur and tibia. The tendons are also a crucial soft tissue that links muscle to bones and the bursa are small fluid field sacs that decrease friction between bones and tendons and other knee joint structures.

1.2

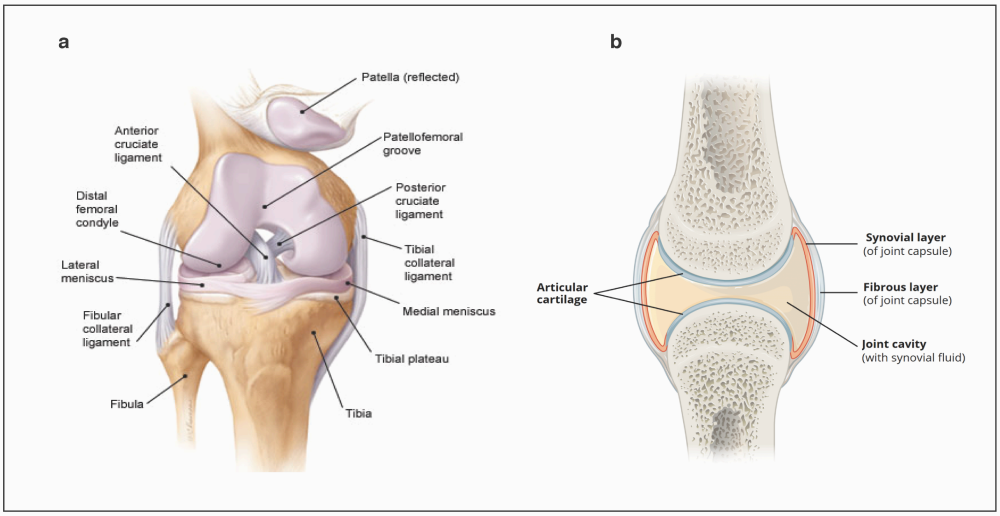

Figure 1.2. Anatomy of the knee joint. a) Coronal view of the knee indicating the different bones ligaments and menisci of the joint. **b)** Basic structure of the synovial joint and its components. (Image adapted from (Drake, 2009)).

Other essential components of synovial joints are the synovial cavity, synovium (or synovial membrane) and the articular cartilage **(Figure 1.2.b).** In the synovial joints, the synovial cavity emerges from the periosteum (a membrane of connective tissue that covers the bone) and marks the separation between the intra articular cavity and the extra articular cavity of the joint. The synovial cavity is sealed by synovium, which is composed of two layers of membranes. A fibrous membrane, which mainly contains type I collagen and a synovial membrane composed of macrophages and fibroblasts. The synovium is a crucial structure that maintains the production of synovial fluid by producing lubricant and hyaluronic acid (Mathiessen and Conaghan, 2017). In addition, the synovial fluid allows for the proper nutrition of the chondrocytes, which are the cells that form the articular cartilage. It also protects the cartilage from wear and tear through its production of lubricant.

The articular cartilage is an avascular and aneural tissue with no capacity of self-repair. Therefore, any changes in the structure of the cartilage are irreversible. The cartilage provides a smooth surface with a low coefficient of friction between the bones, that allow efficient gliding upon joint movement and transmits loading forces into the subchondrial bone (Loeser et al., 2012). Chondrocytes are the only cells that form the articular cartilage, they have different morphologies and depending on their location they exhibit different functions. For instance, chondrocytes in superficial layers are in charge of producing various lubricants such as hyaluronic acid (Goldring, 2012). Whereas, chondrocytes located in the middle areas are in charge of producing aggrecan, the most common type of proteoglycan present in this tissue, sitting along site the hyaluronic acid (Mathiessen and Conaghan, 2017). Proteoglycans are negatively charged which makes them able to bind to water molecules, which help

provide the cartilage with its mechanical properties.

Collagen II fibers are also part of the articular cartilage and are arranged differently along its structure. In the superficial layers the collagen II fibers are arranged parallel to the surface whereas in the middle their distribution is more random and then leading to a radial distribution in the deeper layers (Goldring, 2012). The collagen II fibers restrict over-swelling and give the tissue its ability to resist comprehensive forces (Cooke et al., 2018).

The osteochondral junction is another key structure in the knee joint. This structure is present between the deeper layers of the articular cartilage and the subchondral bone, which is present between the cartilage and the rigid skeleton. The structure of the osteochondral junction **(Figure 1.3a, b)** is as follows, deeper non-calcified cartilage, tidemark a basophilic line that separates the latter with the calcified cartilage and lastly the subchondral bone (Xiaoming Zhang, 2015). Beneath the subchondral plate lays the trabecular bone of the epiphysis, which contains blood vessels, sensory nerves, endothelium and bone marrow. The subchondral bone provide the deep layers of the cartilage with nutrients, thus it is very far to get nutrients from the synovium (Suri and Walsh, 2012).

Most of the described structures are compromised during the pathology of OA. Biochemical and structural changes in the knee joint together with both central and peripheral changes in sensory processing contribute to the maintenance and development of pain affecting the wellbeing of patients

1.3

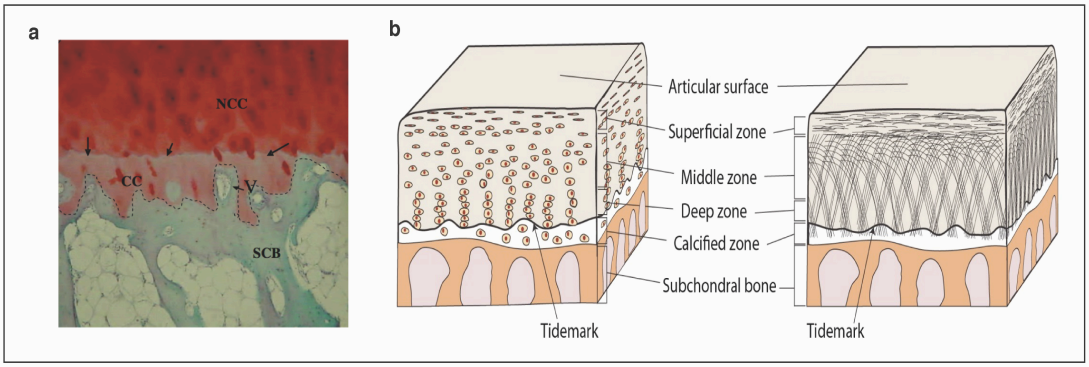

Figure 1.3. Osteochondral junction structure and layer in a normal joint. **a)** Photomicrograph showing osteochondral junction (indicated by dotted line) in medial tibia plateau of healthy patient. Image shows non-calcified cartilage (NCC), calcified cartilage (CC), vascular channel (V), tidemark shown in arrows and subchondral bone (SCB). (Image taken from (Suri and Walsh, 2012)) **b)** Diagram showing the different layers of separation between the subchondral bone of articular cartilage (Image taken from (Zhan et al., 2015)).

1.2.3. The pathology of osteoarthritis

A series of pathological changes occur during the development of OA that include, subchondral bone remodelling, osteophyte formation, synovial inflammation and cartilage loss (Walsh et al., 2007). In addition, degradation of joint structures such as the ligaments and meniscus can occur. In this section we are going to further investigate the mechanisms that drive these changes in OA.

1.2.3.1. Subchondral bone and osteochondral junction

Some of the first structures to be compromised in OA pathology are the subchondral bone and the osteochondral junction. The subchondral bone undergoes a remodelling process that includes thickening and bruising of the bone. The thickening of the subchondral bone plate might contribute to articular cartilage damage, since the subchondral bone provides nutrients to the deeper layer of the cartilage and once it thickens, it loses the ability to do so (Suri and Walsh, 2012). Increasing subchondral osteoclast activity causes the cutting of channels through the subchondral bone into the non-calcified cartilage. In addition, fissuring of the articular cartilage all the way to the tidemark cause the breaching of the barrier that separates the synovial cavity from the subchondral bone (Walsh et al., 2007).

The articular cartilage is avascular, blood vessels are never found beyond the tidemark; however in OA angiogenesis occurs. New blood vessels appear invading the osteochondral junction by breaching the tidemark together with sympathetic and unmyelinated sensory nerves, the latter might contribute to pain in OA (Walsh et al., 2010). Beneath the tidemark a new layer of ossification appears leading to the thickening of the subchondral bone and the formation of bony outgrowths, known as osteophytes, on the bone surface.

1.2.3.2. Articular cartilage

The main feature of OA is the loss of the articular cartilage, which is driven by a combination of factors. In healthy OA, chondrocytes resist proliferation and terminal differentiation and are in charge of regulating extracellular matrix (ECM) turnover and maintain tissue homeostasis (Akkiraju and Nohe, 2015). However, during OA, cartilage degeneration chondrocytes become hypertrophic leading to an enhanced metabolic activity, changes in expression of the ECM and activation of proteases that further destroy the cartilage (Dreier, 2010). Due to the remodelling of the subchondral bone the calcified cartilage undergoes vascularization in the later stages of the

disease progression (Goldring and Goldring, 2016). The articular cartilage is separated from the subchondral bone by a layer of calcified cartilage. However in OA, the calcified cartilage is penetrated with vascular elements that extend from the subchondral bone (Loeser et al., 2012). In human OA patients the vascularisation of the calcified cartilage is accompanied by both sympathetic and sensory fibers (Suri et al., 2007). The sensory fibers that innervate this structure are unmyelinated afferents and could be the potential source of symptomatic pain (Suri et al., 2007). Additionally, the region of vascularisation was associated with the expression of vascular endothelial growth factor (VEGF) and chondrocytes have also been shown to express VEGF. This provides further signals for recruitment of vascular elements (Walsh et al., 2010, Walsh et al., 2007). All these changes lead to the invasion of the deep layers of the articular cartilage by the calcified cartilage (Loeser et al., 2012).

Additionally, the cartilage undergoes changes in matrix composition causing the loss of proteoglycans and deterioration of the collagen II network. Driven by these changes, chondrocytes mediate the release of inflammatory factors, such as cytokines and chemokines, which contribute to the inflammation of the synovium as well as the release of proteolytic enzymes such as matrix metalloproteinase (MMPs) and aggrecanases, cause the further destruction of the cartilage matrix (Cooke et al., 2018). MMP, degrade aggrecan and increase activity of other enzymes such as collagenases that cause the degradation of collagen II. Once the collagen II network has been degraded, the changes cannot be reversed (Loeser et al., 2012). The degradation of the proteoglycans causes cartilage erosion and as this occurs, matrix proteins are degraded and this can stimulate further destruction of the cartilage. For instance, collagen fragments can induce the release of inflammatory cytokines and even MMPs. More so, the release of cytokines can induce the production of reactive oxygen species (ROS) contributing to cell death.

1.2.3.3. Synovium

During cartilage damage, inflammatory cytokines, chemokines and proteolytic enzymes released by the over active chondrocytes infiltrate into the synovial fluid. Such products are then phagocytosed by synovial cells and contribute to the inflammation of the synovial membrane, which is very common in early stages of OA disease. In response to inflammation, synoviocytes start producing more pro-inflammatory mediators, which attract immune cells, leading to the increase of angiogenesis and further activation of chondrocytes (Mathiessen and Conaghan, 2017). Another factor that contributes to synovitis is the infiltration of macrophages

and lymphocytes. These also contribute to the further production of cytokines. OA patients showed increased levels of IL-6 and IL-8 in synovial fluid (Siqueira et al., 2017) and other cytokines and chemokines involved in OA pathology such as, TNF-α and IL-8 (Kosek et al., 2018). Because the synovium is highly innervated by sensory fibers, these cytokines can cause the direct activation of receptors present on specific populations of fibers, contributing to pain and further destruction of the cartilage by activating chondrocytes and fibroblast (Loeser et al., 2012).

1.2.3.4. Meniscus and Ligaments

In addition to cartilage damage and synovitis many OA patients suffer from damage to both meniscus and ligaments. The prevalence of meniscal lesions in OA patients, shown both with clinical and with radiographic evidence, is 68-90% (Makris et al., 2011). When it comes to ligament damage, the most common ligament to be affected in OA patients is the anterior cruciate ligament (ACL). Functional magnetic resonance imaging (fMRI) studies in OA patients showed that 20-35% of patients suffer from damage to the ACL with no recollection of prior trauma (Amin et al., 2008).

The increase in inflammatory cytokines in early OA might contribute to the damage of the meniscus. fMRI studies in OA patients with meniscal damage show join effusion due to synovitis (Edd et al., 2015). In addition, it is thought that meniscal degradation could also be due to changes in joint loading after cartilage damage (Edd et al., 2015). Changes in meniscus during OA pathology are very similar to those that occur in the articular cartilage, thus the meniscus is a fibro cartilaginous structure. Such changes include damage to the matrix, calcification and cell death (Loeser et al., 2012), which lead to wearing and tearing of the meniscus (Katsuragawa et al., 2010).

ACL damage is often associated with damage to the meniscus. In OA, ACL damage is quite common, and several studies suggest that such damage can contribute to the development of OA (Simon et al., 2015). Histological changes that occur in ACL during OA are also very similar to those of the meniscus, including matrix disruption and collagen fiber disruption. After ACL damage there is also an increase in inflammatory cytokines which might also contribute to catabolic changes in the cartilage (Simon et al., 2015).

1.2.3.5. Vascularization and innervation changes

As previously described (1.2.2) the healthy cartilage is an avascular structure that is not innervated by nerve fibers. Sensory fibers innervate other areas of the knee joint such as the synovium, trabecular and subchondral bone, periosteum, meniscus and cruciate and collateral ligaments (Suri et al., 2007).

The increased angiogenesis observed in OA is driven by an increase in production of pro-angiogenic factors released by different joint structures, such as the synovium, subchondral bone and osteochondral junction as well as by chondrocytes themselves. The vascularization of the articular cartilage is accompanying unmyelinated sensory innervation (Grässel and Muschter, 2017).

Unmyelinated fibers reach the articular cartilage through vascular channels that appear upon damage to the subchondral bone (Suri et al., 2007). In human tibiofemoral OA patients these fibers have been identified as substance P (SP) and calcitonin gene related peptide (CGRP)-positive (Suri et al., 2007). Many OA patients describe their pain as a sustained burning sensation. The presence of these unmyelinated fibers in the articular cartilage may account for that and might be one of the main sources contributing to pain.

Additionally, the other joint structures that innervated can contribute to pain in OA. For instance, the subchondral bone contains both sympathetic and sensory nerves that might become active (Suri et al., 2007). Another source of OA pain could be the meniscus as it also undergoes increased vascularization together with increased density of sensory fibers (Ashraf et al., 2011).

1.2.3.6. Bone Marrow lesions

Radiography has been extensively used to visualize and describe OA severity; however radiographic evidence of cartilage damage alone is not enough to provide an extensive description on how joint are affected. In addition, the extent of cartilage damage does not correlate with pain reported by OA patients. Magnetic resonance imaging (MRI) allows us to visualize soft tissues as well as to quantitate inflammatory changes associated with OA. Bone marrow lesions (BMLs) are high signal intensity alterations detected on MRI fluid-sensitive and fat-suppressed sequences (Bonadio et al., 2017). These sequences can be present in several pathological conditions and have been recently linked to OA and joint pain (Alliston et al., 2018). BMLs appear

before bone degeneration and progress and increase size over time, therefore they can be used as a tool for early diagnosis. Presence of BML regions increases the risk of cartilage loss, likelihood of OA progression and development of knee pain (Alliston et al., 2018) and changes in mechanical loading could potentially lead to subchondral bone BMLs. Additionally, BMLs have also been shown to correlate with microdamage of the trabecular bone leading to subchondral bone attrition (Klement and Sharkey, 2019) . Some studies have addressed the relationship between BMLs and knee pain in OA patients. MRI studies revealed that knee pain and BMLs size had a positive association. Increase in BMLs was associated with greater knee pain addressed by WOMBAC test (Driban et al., 2013). In an other study, 77.5% of patients with BMLs had significant pain while 30% of patients reported no pain and presented no BMLs (Felson et al., 2001). The authors concluded that patients are more likely to report OA associated pain when BMLs are present. To conclude, the presence of BMLs and their sizes could provide with an early diagnosis tool and give information on OA severity and knee pain.

1.4

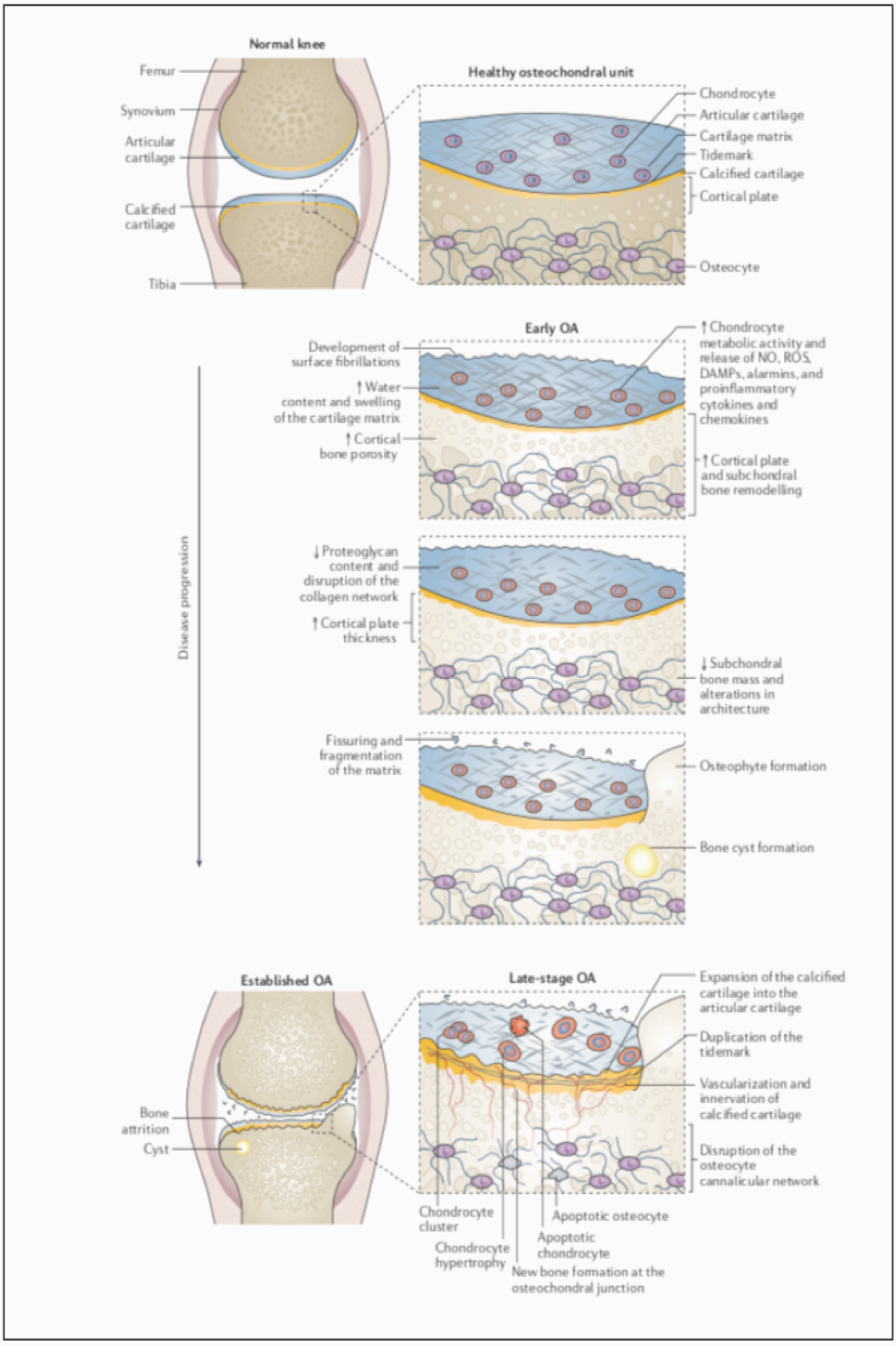

Figure 1.4. Changes in knee joint structures during the progression of osteoarthritis. The healthy osteochondral unit the articular cartilage comprised of healthy chondrocytes. The tidemark separates the articular cartilage from the calcified cartilage. The cortical plate also appears intact. In the early stages of OA progression, chondrocytes increase their metabolic activity leading to the production of pro-inflammatory factors such as cytokines and chemokines that contributes to swelling. The cortical plate thickens and the subchondral bone undergoes remodelling. Bone cysts and osteophytes are formed. In the late stages of OA, the calcified cartilage expands into the articular cartilage and the tidemark thickens. Vascularisation and innervation of the calcified cartilage occurs, chondrocytes become apoptotic and new bone is formed at the osteochondral junction. (Image taken from (Goldring and Goldring, 2016)).

1.2.4. Epidemiology: Incidence and prevalence

OA is currently one of the growing causes of disability worldwide, affecting >40million people across Europe (Organization, 2003) and 27 million people in the US (Neogi, 2017). It is predicted that by 2020 it will be the fourth-leading cause of disability (Kingsbury et al., 2014), as its incidence continues to rise with the increase in life expectancy and the increased prevalence of obesity (Neogi, 2017). In addition, the role the modern environment plays in the development of OA might also be a causal reason for the increase in prevalence. For instance, physical exercise playing a role in mechanical loading of the joint and diet affects the biological states of the body.

The incidence for the most common types of arthritis, (hip, hand and knee) increase with age and differ according to gender. Women have a higher incidence than men and according to a report by Versus Arthritis (UK), 49% of women and 42% of men of age 75 or over have sought treatment for OA. Of the reasons to seek medical treatment pain is the key symptom that drive therapeutic requests. Knee OA is the most common type of OA in the UK and it is estimated that by 2035, 8.3 million people in UK aged 45 and over could suffer from knee OA.

Epidemiological studies have mainly used radiographic evidence to assess damage to the joint in order to address OA prevalence. However only 50% of people with radiographic evidence of the disease suffer from pain or show any symptoms. Thus, symptomatic OA and radiographic OA are not comparable, because the amount of damage in the knee joint does not correlate the amount of pain the patient suffers and vice versa (Finan et al., 2013). Moving forward, epidemiological studies need to identify risk factors for diseases that cause suffering and discomfort. Functional magnetic resonance imaging (fMRI) is a good tool to directly visualize damage in OA, because it not only shows the important anatomical structures of the joint but also is able to show changes in soft tissue such as the cartilage (Yusuf et al., 2011) . Therefore, using fMRI scans to identify cartilage damage, bone erosion and synovitis is a good tool for the diagnosis of OA and could be use to study the epidemiology of OA (Felson and Nevitt, 2004).

1.2.5. Diagnosis of osteoarthritis

Diagnosis of OA can be usually made based on history and clinical features. MRI and radiography examinations allow clinicians to assess the degree of damage present in the knee joint. The American College of Rheumatology provides criteria to help

diagnose for OA shown in **Table 1**. (Altman et al., 1986). Additionally, the European League Against Rheumatism (EULAR) diagnostic criteria can also be used for OA diagnosis and are based on the presence of 3 symptoms and 3 signs (Heidari, 2011). The symptoms are as follows: persistent knee pain, limited morning stiffness and reduced function and the signs are crepitus, restricted movement and bony enlargement. When the 6 symptoms and signs are present this questionnaire can 99% predict the correct diagnosis of knee OA (Heidari, 2011).

Table 1. The American College of Rheumatology Clinical Classification Criteria and the Clinical plus Radiographic Classification Criteria for Osteoarthritis of the Knee**.**

Clinical One must have articular knee pain for most days of the prior month, in addition to at least 3 of the following:	**Clinical plus radiographical** One must have articular knee pain for most days of the prior month, PLUS radiographical evidence of osteophytes on joint margins in addition to 1 of the following:
1. Crepitus on active joint motion	1. Crepitus on active motion
2. Morning stiffness <30min duration	2. Morning stiffness <30min duration
3. Age > 38 years	3. Age > 38 years
4. Bony enlargement of the knee on examination	
5. Bony tenderness of the knee on examination	
6. No palpable warmth	

Pain associated with joint discomfort in OA is highly variable amongst patients and only shows little association with the extent of structural damage of the knee, therefore making the diagnosis of OA pain challenging for clinicians. There are different ways that clinicians can address joint pain and degree of sensitization in patients. The correct assessment of OA pain is crucial for the patient to get a proper treatment and management of their pain.

Human quantitative and mechanistic pain assessment tools such as quantitative sensory testing (QST) or the use of scores and/or questionnaires, are used by clinicians

to address the degree of sensitization in OA patients. Such tests, allow doctors to identify different subgroups of patients based on their degree of sensitization and pain experience (Arendt-Nielsen, 2017). When it comes to questionnaires there are different ones but the most commonly used are the Western Ontario and McMaster Universities Osteoarthritis Index (WOMAC), visual analogue scale, McGill Pain Questionnaire and its short form and Medical Outcomes Study 36-Item Short-Form Health Survey (Arendt-Nielsen, 2017). More recently, the PainDETECT Questionnaire has been developed in order to identify the subgroup of OA patients that has neuropathic-pain like features from those who form part of the nociceptive group.

QST has been developed to address specific pain mechanisms that contribute to sensitization in OA and are divided into two tests: stimulus-dependent and response-dependent methods. The stimulus-dependent tests consist of applying a stimulus and increasing its intensity until the patient detects pain or a tolerance threshold is reached. On the other hand the response-dependent method employs a range of fixed stimulus intensities with a specific score for each. There are four stimuli employed for such tests, pressure pain threshold, thermal threshold, cold pressor evoked pain and pin-prick (Arendt-Nielsen, 2017). These are applied around to three main areas: the knee, to muscles around the knee and at sites away from the knee. It is important to address if the patient reports referred pain meaning pain around areas away from the injury site as it will determine their degree of sensitization.

1.2.6. Risk factors

There are several risk factors that can influence the development of OA. The most common risk factor is obesity, which increases the risk factor for not only knee OA but also hip and hand arthritis. It is not clear how obesity contributes to OA, however it is not only through mechanical loading. It could be also through metabolic changes involving leptin which is thought to stimulate anabolic functions of chondrocytes (Wieland et al., 2005). Other risk factors include age, sex, ethnicity, smoking and previous joint disease

1.2.7. Economic burden of osteoarthritis

The economic burden of OA has been estimated to be at least £7.25 billion per year per population in the United States of America (USA) (Kotlarz et al., 2010), due to medical cost and the lost productivity of the patients that suffer from the disease. These were only indirect costs (loss of productivity, disability payment benefits, absenteeism and premature mortality). Direct costs would be considered surgery costs, hospital resources, caregiver times, cost of side effects from treatment research and

pharmacological and non-pharmacological treatment (Chen et al., 2012). Most studies that look at the economic burden of OA do not take into account both indirect and direct cost in addition to intangible costs such as pain suffering, decreased quality of life and the potential comorbidities that can arise from OA pain such as depression and anxiety (Chen et al., 2012).

The Oxford Economics report in March 2010 calculated that in 2008 the total economical cost of OA in the UK was £30.7 billion per annum and suggested that the cost would rise in the future.

1.3. Pain in osteoarthritis

1.3.1. Nature of pain in osteoarthritis

OA patients usually experience sensory gains and deficits and pain during evoked movement and loading of the knee (Hochman et al., 2010). Patients also experience increased sensitivity to noxious stimuli such as thermal heat, punctuated mechanical stimuli, pressure-induced pain and pinprick. Light touch thresholds are also increased in OA patients (Wylde et al., 2012). Even though radiographic evidence of joint damage predisposes to joint pain, the severity of pain experienced by patients does no correlate to the amount of radiographic damage (Moss et al., 2016). Therefore, making diagnosis of pain severity more difficult. In addition, OA patients also experience imbalance and deficits in vibratory sensation (Dua et al., 2018).

OA pain is often classified as nociceptive, resulting from tissue damage that the articular cartilage undergoes, leading to inflammation (Thakur et al., 2014). However, several studies have shown that some patients experience OA pain with neuropathic pain-like features. In a study 23% of OA patients described their pain as moderate to severe and 34% of patients defined their pain by using pain quality descriptors common amongst neuropathic pain patients such as a shooting and burning pain associated with numbness and tingling (Hochman et al., 2010). Burning sensation, suggests that unmyelinated fibers are possibly playing a role (Suri et al., 2007). As previously described unmyelinated fiber innervate the joint area and in some cases the cartilage itself. Thus damage to unmyelinated fiber could lead to the presence of neuropathic pain-like features in these patients.

Additionally, some OA patients report pain while at rest or at night, an indicator of spontaneous pain, as well as widespread mechanical and thermal hyperalgesia in areas, away from the joint such as the ankle and elbow (Moss et al., 2016). Other studies looking at cold stimuli showed that 13% of patients reported local hyperalgesia whereas 8% reported widespread cold hyperalgesia (Moss et al., 2016). The same study reported

that 3% of patients experienced both heat and cold widespread hyperalgesia, suggesting that there are subgroups of OA patients with different experiences of pain. The widespread hyperalgesia and ongoing pain experienced by this subgroup of patients suggest signs of central sensitization of second-order neurones, which will be further explained in section 1.3.3. However, central sensitization and referred pain is not specific of neuropathy (Thakur et al., 2014) but as it will be discussed in further sections these patients exhibit other changes in pain processing which resemble those present in neuropathy. Identifying the type of pain (nociceptive or neuropathic) that patients experience will allow for better, more efficient treatment and management of their pain.

1.3.2. Peripheral transmission of nociceptive signals

Without being able to detect harmful stimuli we wouldn't be able to properly protect ourselves from potentially life threatening events. Thus, the mechanisms by which painful harmful stimuli are detected are crucial for our survival. However, alterations in the pain pathways can lead to hypersensitivity, thus making pain chronic and debilitating for the individual as seen in osteoarthritis patients.

Nociception is described as the process by which intense thermal, mechanical and/or chemical stimuli are detected (Basbaum et al., 2009). Nociceptors or primary afferent fibers are a subgroup of peripheral nerve fibers in charge of detecting such noxious stimuli. The cell bodies of these neurones are located in the dorsal root ganglion (DRG) and have a peripheral axon, which innervate the target organ, and a central axon that terminates onto neurones in the spinal cord. Thus, primary afferent fibers are primarily responsible for transmitting signals from the periphery to the spinal cord. Under normal conditions, nociceptors only are only active when stimuli reach a noxious threshold. This threshold has to be sufficient to depolarize the resting membrane potential resulting in greater and rapid depolarization and full activation of the action potential. However, in the presence of an injury nociceptors undergo molecular changes as well as changes in their pain processing which causes non-painful stimuli to be detected.

1.3.2.1. Classification of primary afferent fibers

Primary afferent fibers can be classified in many different ways; the most common way of classifying them is by function and anatomy (shown in **Table 2)**, as they respond to different types of stimuli and their level of myelination varies, thus giving them different conductance velocities.

The first type of primary afferents are Aβ-fibers **(Figure 1.5).** These are large in diameter, thickly myelinated and therefore, have a fast conduction velocity **(Table 2**). They are the first fibers to become activated. Aβ-fibers mostly respond to innocuous mechanical stimuli like touch, while 20% of these fibers are nociceptive. These fibers innervate the basal epidermal layer of touch-sensitive areas in the skin and are in direct contract with Merkel cells, a set of sensory cells that transduce touch (Lumpkin and Caterina, 2007).

Aδ-fibers are medium in diameter, are thinly myelinated and are the first ones to produce a fast response acute pain **(Figure 1.5)**. They can also be subdivided into two groups based on the stimuli they respond to. Type I Aδ-fibers, also known as HTM: high-threshold mechanical nociceptors, respond to both mechanical and chemical stimuli **(Table 2).** However, they only respond to heat when the threshold is high (>50-53°C) (Julius and Basbaum, 2001). When the stimulus is maintained they will become sensitized which will cause them to respond to lower temperatures as well as to respond to lower threshold mechanical and chemical stimuli. Type II Aδ-fibers, have a low threshold for moderate heat (43°C) but a high threshold for mechanical stimuli **(Table 2**)(Julius and Basbaum, 2001). These are the first to get activated in response of noxious heat which is defined as temperatures of 45°C or higher (Caterina et al., 1997).

Lastly, the third type of afferents are C-fibers. These are small diameter unmyelinated fibres. They have a slow conductance velocity making them the last fibers to become activated upon noxious stimuli **(Figure 1.5)**. Unlike the others, most of C-fibers are polymodal, thus they respond to all types of noxious stimuli (mechanical, thermal and chemical) **(Table 2)**. A subset of C-fibers are known as the silent nociceptors which respond mainly to heat and chemical stimuli and are insensitive to mechanical stimuli (Michaelis et al., 1996). These are found in large number in the urinary bladder, the distal colon and the knee joint but are rare in rodent skin (Prato et al., 2017). However, in human skin silent nociceptors form a quarter of all C-fiber nociceptors (Schmidt et al., 1995). Under tissue damage or injury the silent nociceptors can develop mechanical sensitivity produced by a variety of compounds such as inflammatory mediators, thus contributing to mechanical hyperalgesia during inflammation (Prato et al., 2017).

Another way to classify C-fibers is by their neurochemical content. Peptidergic C-fibers are those that contain peptides such as substance P (SP) and calcitonin

gene-related peptide (CGRP), where as non-peptidergic C-fibers do not contain such neuropeptides and are isolectin B4 positive ($IB4^+$) **(Figure 1.7)** (Snider and McMahon, 1998).

During development, in the rat, 70-80% of DRG neurones express (TrkA), which becomes active by nerve growth factor (NGF), however in adult rats only 40-45% of DRG neurones still express TrkA and co-express substance P and CGPR (Snider and McMahon, 1998). Thus, suggesting that non-peptidergic C-fibers lose the expression of this receptor. Additionally, these neuronal subtypes differ in their central terminals. Non-peptidergic C-fibers project to interneurones in the inner lamina II of the dorsal spinal cord whereas peptidergic C-fibers synapses into projection neurones in more superficial areas lamina I and interneurones in the outer part of lamina II (Zylka et al., 2005, Zhang et al., 2013). Interestingly, C-fibers are not exclusively nociceptors, as certain subtypes, also involved in mediating itch, cooling and pleasant touch thus sometimes making them not nociceptors (Basbaum et al., 2009).

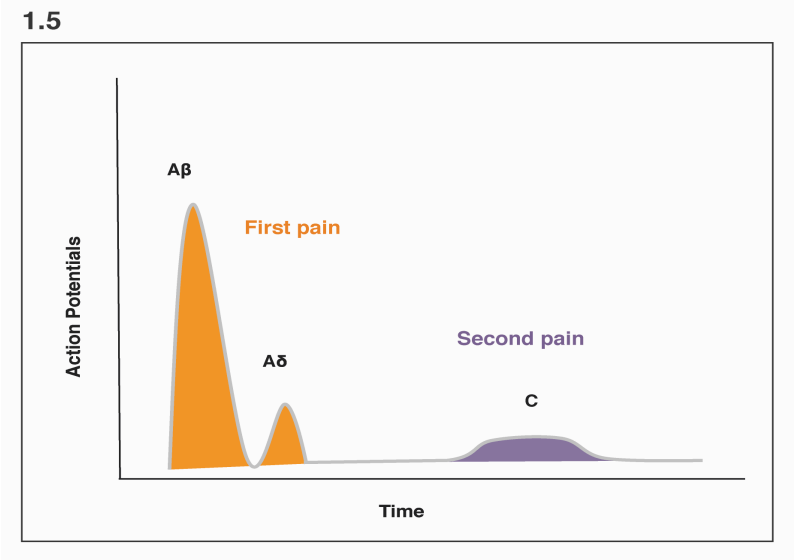

Figure 1.5. Timeline of activation of primary afferent fibers and activation response. Aβ-fibers are the first fibers to become active. They mostly respond to innocuous mechanical stimuli like touch, while 20% of these fibers are nociceptive. Aδ-fibers are the first ones to produce a fast response acute pain and together with Aβ-fibers they produce the first response to pain. C-fibers are the last to become activated upon noxious stimulation and they produce the second response to pain.

Table 2. The different types of primary afferent fibers and their characteristics.

Neuron Type	Conductance Velocity	Axonal diameter/ myelination	Stimuli Response to
Aβ	Rapid	Large/Highly	Innocuous
Aδ			
Aδ Type I	Medium	Medium/Thin	Mechanical and Chemical and high threshold response to heat (>50°C.)
Aδ Type II			Low threshold to Heat and high threshold response to mechanical stimuli.
C	Slow	Small/None	Polymodal: mechanical, heat and chemical.

1.3.2.2. Receptors and channels in primary afferent fibers

The role of nociceptors is to detect external noxious stimuli and translate this information into electrical current, in order to send the appropriate message through to higher brain centres. In order to do that, we need to understand what channels and receptors are involved in detecting noxious stimuli and distinguish between different modalities. It is also extremely important for us to be able to determinate what receptors are present in what subtype of fibers. Since it will provide information on which fibers become activated by modality and moving forward will allow us to specifically target populations of neurones to modify modality specific responses. In the following section I am going to discuss the different receptors and channels involved in detecting heat, cold, mechanical and chemical stimuli.

Noxious heat

The pain threshold for heat sensitivity lies around 43°C as explained in section 1.3.2.1. Type II Aδ- and C-fibers become active once temperature reaches such threshold. Around 45% of fibers (C and type II Aδ-fibers) become active in response to moderate heat (~45°C) and 5-10% of fibers (type I Aδ-fibers) respond to high threshold heat (~52°C). Most of the channels involved in detecting heat sensitivity are part of the transient receptor potential (TRP) channels family. TRPV1, also known as the capsaicin receptor was the first receptor to be identified with heat sensitivity almost 20 years ago (Caterina et al., 1997). This receptor becomes active in the presence of capsaicin, which is the main ingredient found in hot chili peppers and at temperatures >43°C. When temperatures exceed 42°C other members of the TRP

family become involved (Lumpkin and Caterina, 2007). At 52°C, TRPV2 is activated and this channel is present in type I Aδ-fibers. TRPV3 and TRPV4 also detect heat, the first one having a threshold of activation at temperatures 32-38°C and the latter at temperatures 27-35° (Bharate and Bharate, 2012). Interestingly, mice lacking TRPV1 only show a partial defect in their ability to sense responses to noxious heat, suggesting that this channel is not the only required for heat detection. An other TRP channel TRPA1, has been shown to mediate inflammatory pain and itch (Hill and Bautista, 2018). Recent studies have shown that a subset of sensory neurones, express these three channels (TRPV1, TRPM3 and TRPA1) **(Figure 1.6)**. Mice lacking these, do not display avoidance behavioural responses to noxious heat (Vandewauw et al., 2018). Therefore, the activity the three channels together might be required to mediate behavioural responses to noxious heat.

1.6

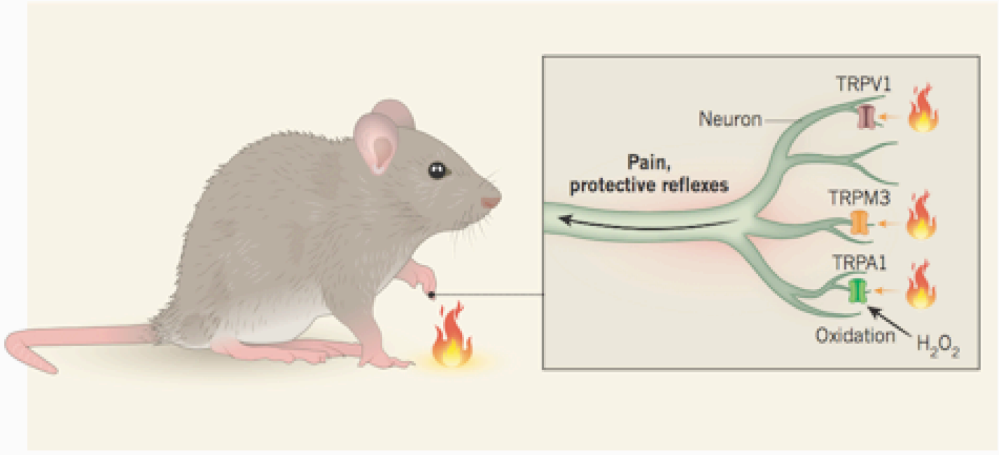

Figure 1.6. A subset of sensory neurones exhibit three types of TRP channels, TRPV1, TRPM3 and TRPA1. While TRPV1 becomes activated by capsaicin, TRPM3 becomes active by more noxious temperatures, while TRPA1 requires oxidation as well as thermal heat to become active. Mice lacking these, do not display avoidance behavioural responses to noxious heat (Vandewauw et al., 2018). (Image taken by (Hill and Bautista, 2018).

Noxious Cold

When it comes to the detection of noxious cold, which is defined as <17°C, only 10-15% of nerve fibers in the rodent hind-paw become activated (Julius and Basbaum, 2001). There are two TRP channels that become activated by cooling, these are TRPM8 and TRPA1 **(Figure 1.7)**. TRPM8 becomes activated by innocuous cooling temperatures ~25-28°C or by chemicals such as menthol that produce cooling sensation while TRPA1 is activated by noxious cold, icilin and pungent

compounds (Bharate and Bharate, 2012).

Mechanotransducers

How mechanical stimuli are detected in the skin and what cells or receptors are involved in translating touch stimuli into an electrical response remain a debate. Several channels present in primary afferent fibers have been proposed to play a role in mechanosensation. Additional, non-neuronal cells in the skin might also play a role in translating mechanosensation and communicating them by direct interaction with neuronal cells (Moehring et al., 2018).

Piezo2 is a stretch gated ion channel that mediates light touch, detects vibration and is involved in proprioception. Although Piezo2 is expressed in many cells, 20% of DRG neurones in adult mouse express Piezo2 mRNA and showed a 24% overlap with TRPV1 positive primary afferents, suggesting it might be involved in noxious mechanosensation (Coste et al., 2010). However more recent studies in humans and rodents, have suggested that Piezo2's role is not to detect noxious mechanical stimuli but rather light touch and suggest that blockage of this channel could prevent tactile allodynia in the presence of injury (Szczot et al., 2018).

Two-pore-domain potassium channels; TREK-1, TREK-2 and TRAAK and voltage gated potassium channels are thought to play a role in mechanotransduction **(Figure 1.7)**. The two-pore-domain potassium channels are force-sensitive channels that become activated by tension to the cell membrane (Moehring et al., 2018).

Chemical transduction

Environment irritants, endogenous irritants and pro-algesics released in presence of tissue damage can also cause the activation of primary afferent fibers. Yet again the TRP family is also involved in chemical transduction. TRPV1 and TRPA1 are activated by plant-derived irritants (Basbaum et al., 2009). Volatile irritants such as formalin and hydrogen peroxide can also cause the activation of primary afferent fibers (Hill et al., 2018, Caterina et al., 1997, Basbaum et al., 2009, Vandewauw et al., 2018)

When it comes to endogenous irritants and pro-algesics, these get produced and released upon tissue damage, promoting inflammation and sensitization of primary afferent fibers lowering their thresholds to noxious stimuli. These factors can be released both by neuronal cells and non-neuronal cells present in the damaged area or cells that infiltrate to the damage tissue. Such cells include immune cells, mast cells and macrophages. All together these cells release cytokines (IL-6, TNF-α, IL-1β), pro-inflammatory mediators, neurotransmitters, peptides, and chemokine

amongst others, that activate different receptors present in primary afferent fibers such as TRP channels, G-protein coupled receptors (GPCR), Acid sensitive ion channels (ASIC), two pore potassium channels and receptor tyrosine kinase (Basbaum et al., 2009).

During inflammation there is an increase of cyclooxygenases COX-2, which leads to an increase in prostaglandins levels. This can also be produced by other cyclooxygenases such as COX-1. The increase in prostaglandin E2 causes peripheral sensitization through the protein kinase A-mediated phosphorylation of sodium channels, increasing excitability and reducing pain thresholds (Wieland et al., 2005). NSAIDs act by inhibiting prostaglandin synthesis and COX-2 action.

The neurotrophin, nerve growth factor (NGF) is also released in the setting of an injury and plays a crucial role in activating TrkA receptors present in peptidergic C fibers and driving heat and mechanical hypersensitivity (Snider and McMahon, 1998). NGF can also activate the low-affinity neurotrophin receptor p75. There are two mechanisms by which NGF can produce heat and mechanical hypersensitivity. Firstly, NGF-TrkA interaction produces the activation of a series of downstream cellular mechanisms that include the activation of phospholipase-C (PLC), mitogen-activated protein kinase (MAPK) and phosphoinositide 3-kinase (Chuang et al., 2001). The activation of these leads to the potentiation of TRPV1 leading to heat sensitivity. Secondly, NGF can be retrogradlly transported into the nuclei where it promotes increased expression of substance P, TRPV1 and voltage gated sodium channel $Na_V1.8$ (Chao, 2003). Anti-NGF antibodies are currently under clinical trial as they could be used for the treatment of OA pain and this is further discussed in section 1.4.1 (Miller et al., 2017).

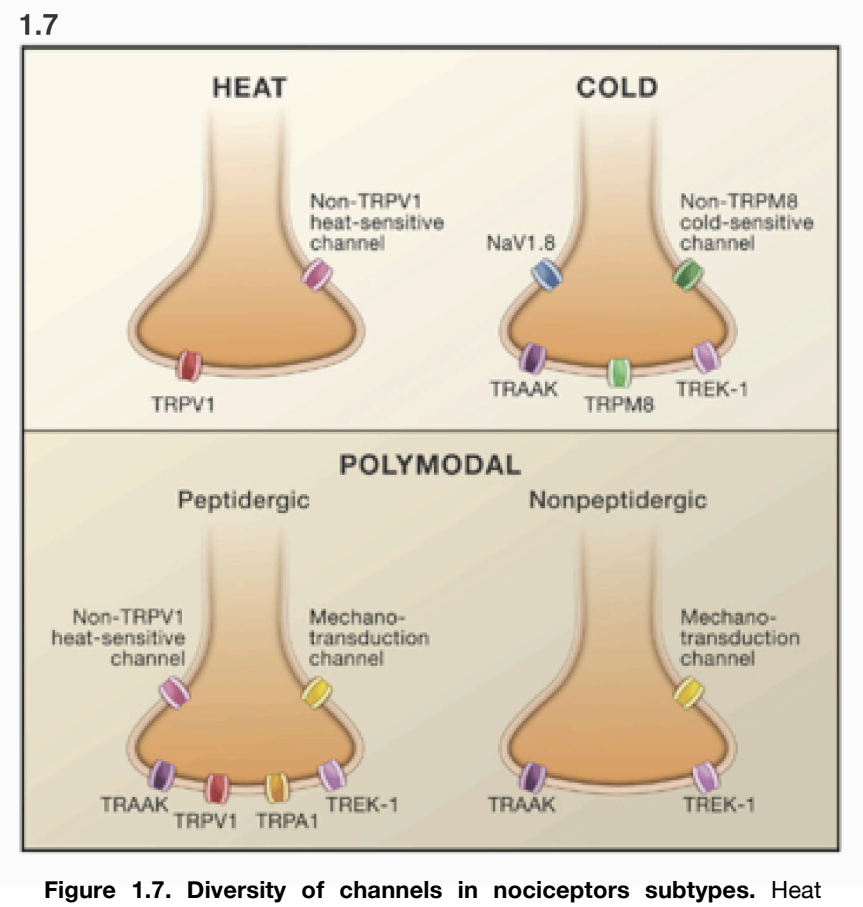

Figure 1.7. Diversity of channels in nociceptors subtypes. Heat nociceptors exhibit different types of TRP channels but mainly express TRPV1 channels. Cold nociceptors exhibit TRM8 as well as other receptors. Polymodal nociceptors respond to all modality stimuli. There are two types of polymodal nociceptors, peptidergic that express SP and CGRP and nonpeptidergic nociceptors that do not exhibit these neuropeptides. Both type of polymodal nociceptors express TRM channels that detect heat as well as mechanotransduction channels.

1.3.2.3. Transduction and conduction of action potentials in primary afferent fibers

The activation of primary afferent neurones in response to noxious mechanical, thermal or chemical stimuli triggers the activation of several ion channels with different functions, from initiation of action potentials, depolarization and repolarization and neurotransmitter release from central terminals in spinal dorsal horn. In this section we are going to discuss the different ion channels involved in such functions from periphery to the central terminals.

1.8

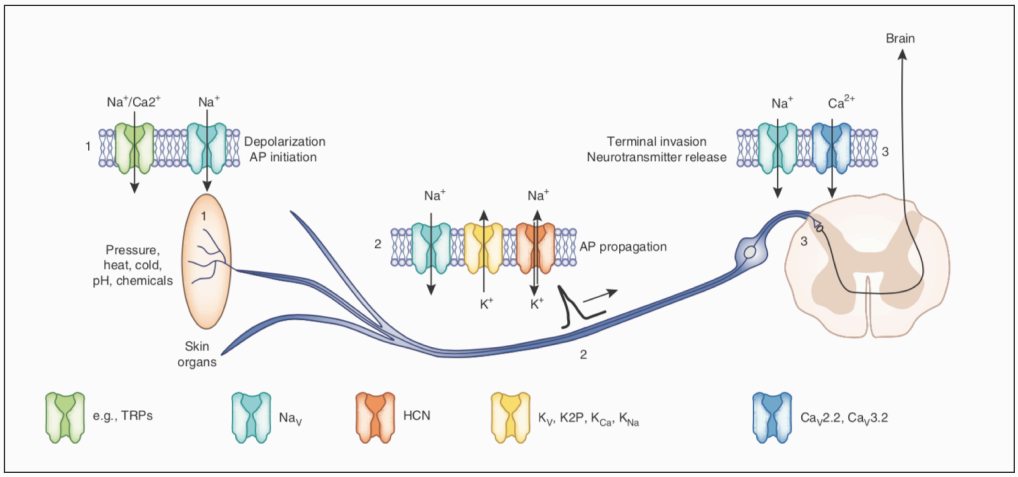

Figure 1.8. Transduction and conductance of action potentials by different ion channels in primary afferent fibers. In the periphery voltage gated sodium channels are in charge of initiation action potentials after pressure, heat, cold, chemical or electrical stimulation. Action potential propagation along the axon is mediated by potassium, sodium channels and by the sodium/potassium pump. Once the signal arrives to the spinal cord voltage gated calcium channels $Ca_V2.2$ and $Ca_V3.2$ are in charge of mediating neurotransmitter release from primary afferent fibers into spinal neurones. (Image taken from (Waxman and Zamponi, 2014)).

Voltage-Gated Sodium Channels

Sensory neurones express a range of voltage gated sodium channels, from $Na_V1.1$, 1.6, 1.7, 1.8 and 1.9 (Coste et al., 2007). From these, $Na_V1.7$ and $Na_V1.8$ play a crucial role in pain transmission by initiating action potentials **(Figure 1.8)**.

$Na_V1.7$ is expressed all along DRG neurones, from the periphery to the central terminations in the dorsal horn. Altered activity in this channel is related to a number of human pain disorders. Upregulation of this channel is seen upon inflammation and gain-of-function mutations of this channel in human causes excruciating burning pain for patients. In contrast, patients with $Na_V1.7$ loss-of-function mutations in the gene don't experience pain as they are unable to detect noxious stimuli, suggesting that this channel could be a good target for the treatment of pain (Waxman and Zamponi, 2014).

$Na_V1.8$, is expressed in small unmyelinated nociceptors (Akopian et al., 1996). Deleting $Na_V1.8$ in sensory neurones in mice, has been shown to reduce sensitivity to noxious mechanical and thermal stimuli as well as causing insensitivity to noxious cold (Renganathan et al., 2001, Abrahamsen et al., 2008)

Potassium Channels

Potassium channels are present along the axons of primary afferent neurones **(Figure 1.8)**. Their role is to regulate the membrane resting potential as well as to propagate the action potential generated in the periphery along the axons of primary afferents (Waxman and Zamponi, 2014). There are different types of potassium channels in primary afferent neurones such as voltage-gated potassium channels, two pore-potassium channels and calcium-sodium activated potassium channels. Recent studies have shown that voltage-dependent potassium channel KCNQ2/3 is involved in mediating excitability of Aδ fibers and are required for normal mechanonociceptive responses in dorsal horn neurones (Hill et al., 2018). Opening of this channel directly alleviates pain by decreasing excitability. However, inhibition of this channel promotes excitability and normal mechanical pain sensitivity.

Voltage-gated Calcium Channels

Different subfamilies of voltage-gated calcium channels (VGCCs) are expressed in primary afferent fibers. The different subfamilies are expressed along DRG neurones where they play different roles in pain transmission **(Figures 1.8, 1.9).**
$Ca_V3.2$ is a T-type VGCC, present in the nerve endings of D-mechanoreceptors where it plays a crucial role in action potential firing. It is present along the axon of nociceptors where it helps facilitate the opening of sodium channels helping the propagation of action potentials. It has been shown to be upregulated during neuropathy and inflammation (Waxman and Zamponi, 2014) and blocking this channel has been shown to attenuate responses to noxious stimuli in rodent models of neuropathic pain (M'Dahoma et al., 2016). $Ca_V2.2$ is an N-type VGCC present in the pre-synaptic central terminals of primary afferents **(Figures 1.8, .9)**. It plays a crucial role in mediating neurotransmitter release of glutamate, substance P and CGRP, from primary afferent fibers causing the activation of second-order neurones (Patel et al., 2018). This channel has been shown to be upregulated in neuropathy (Bauer et al., 2009) and its action is crucial for the proper transmission of pain messages making this channel a great target for the treatment of chronic pain. Lastly, Cav2.1 is a P/Q-type of VGCC also expressed in primary afferent terminals located in lamina II-IV of spinal dorsal horn and are also involved in mediating neurotransmitter release **(Figure 1.9)** (Patel et al., 2018, Basbaum et al., 2009).

1.9

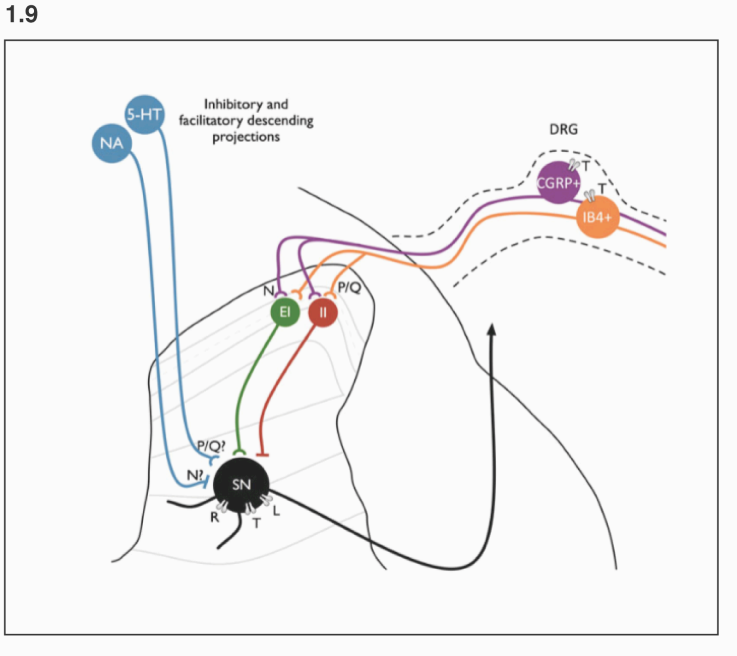

Figure 1.9. Expression of VGCC in dorsal horn. Peptidergic (CGRP+, purple) and non-peptidergic (IB4+, orange) primary afferent fibers exhibit T-type voltage gated channels in the DRG as well as in pre-synaptic site. N-type VGCCs are also present in the pre-synaptic terminal and are involved in neurotransmitter release. Inhibitory interneurones in the spinal cord (red) contain P/Q-type voltage gated calcium channels. Spinal neurones (black) express R, T and L-type VGCC channels. It is yet unclear if VGCC channels are expressed in descending projections. (Image taken from (Patel et al., 2018)).

1.3.2.4. Peripheral sensitization in osteoarthritis

As previously described (section 1.2.3) during OA pathology, the joint undergoes a series of changes, from bone remodelling to changes in vascularization and innervation. Altogether these contribute to pain in OA, however what joint structures are driving the pain are yet to be identified. In addition, biochemical changes in joint environment together with the activation of non-neuronal cells that either reside within or infiltrate the damaged tissue also contribute to pain by releasing an array of molecules leading to inflammation and activation of nociceptors. Nociceptors express one or more cell-surface receptors making them able to respond to these inflammatory mediators (Basbaum et al., 2009). The continuous activation of primary afferent fibers occurring in OA, can lead to heightened responsiveness, also known as sensitization, of both peripheral and central nociceptors. Peripheral sensitization leads to hypersensitivity to painful stimuli and responsiveness to non-noxious stimuli (Dua et al., 2018). Clinically, sensitization is explained as: allodynia, when non-painful stimuli become painful and hyperalgesia when there is an enhanced

response to a painful/noxious stimulus. In addition, peripheral sensitization can lead to central sensitization causing the spreading of pain into uninjured areas (Thakur et al., 2014). In this section, I am going to discuss the crucial players that mediate peripheral sensitization in osteoarthritis.

During inflammation and tissue damage occurring in OA, mast cells, T-cells, macrophages, osteoclasts, osteoblasts, neutrophils, basophils and fibroblasts amongst others, become activated and infiltrate the injury site (**Figure 1.10**). Each of these cells plays a different role in peripheral sensitization. They do so by releasing different molecules such as neurotransmitters including CGRP, substance P, bradykinin, prostaglandins, neurotrophins, cytokines and chemokines contributing to peripheral sensitization (Julius and Basbaum, 2001).

Mast cells are in charge of releasing histamine, bradykinin and NGF **(Figure 1.10)**. NGF is one of the most important mediators of OA pain, driving the activation of peptidergic C-fibers by acting on TrkA receptor and producing hypersensitivity to mechanical and thermal stimuli (Raoof et al., 2018, Cucchiarini et al., 2016, Kidd, 2012). Blocking NGF with monoclonal antibodies showed a reduction in OA knee pain, thus suggesting the important role of NGF as a target for the treatment of pain (Lane et al., 2010).

Macrophages have been shown to increase in number in animal models of arthritis causing the release of TNFα, which induces the release of CGRP, the release of inflammatory cytokines such as IL-6 and IL-1β as well as release of reactive oxygen species (Schaible et al., 2010), together promoting further inflammation and transmission of pain messages **(Figure 1.10)**. The role of cytokines in OA will be further discussed in section 3.1.2 as they play a crucial role in OA inflammation. In addition, macrophages have also been seen to infiltrate the DRG in a surgical model of OA (Segond von Banchet et al., 2009), contributing to sensitization in this model. Osteoclasts also increase in number in OA causing an increase in bone resorption that leads to the acidification and causing the activation of ASICs and TRPV1 (Raoof et al., 2018). Lastly, T-cells also infiltrate the damaged tissue contributing to the maintenance of pain **(Figure 1.10)**. T-cell infiltration is thought to coincide with the time when allodynia is developed (Kobayashi et al., 2015).

1.10

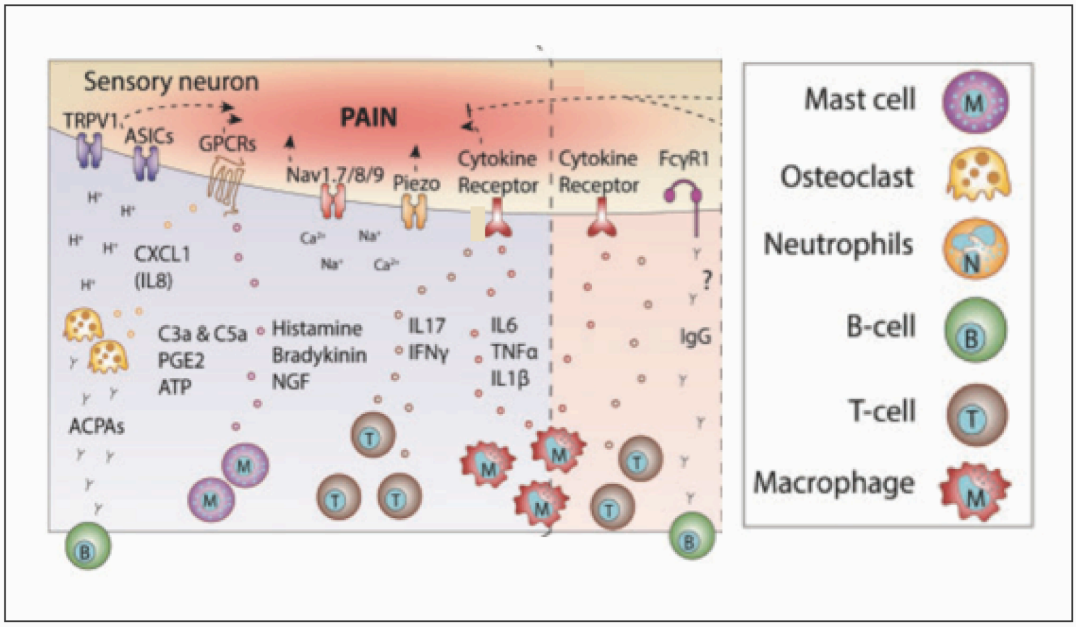

Figure 1.10. Inflammatory events that contribute to activation of sensory neurones during osteoarthritis. Upon cartilage damage in OA a series of immune cells infiltrate the damaged area contributing to inflammation by the release of inflammatory mediators. Mast cells are in charge of releasing histamine, bradykinin and NGF. Amongst these, NGF is one of the most important mediators as it drives the activation of peptidergic C-fibers by acting on TrkA receptor and producing hypersensitivity to mechanical and thermal stimuli. Macrophages release pro-inflammatory cytokines such as IL-6, IL-1β and TNFα together they cause the activation of cytokine receptors in primary afferent fibers. While other immune cells such as T cells help with the maintenance of pain. (Image taken from (Raoof et al., 2018)).

1.3.3. The spinal processing of nociceptive signals

The spinal dorsal horn is a site of complex processing and gating of nociceptive information. Primary afferent fibers innervating the skin and deeper tissue drive sensory information from periphery to dorsal horn. Once in dorsal horn the information is conveyed and processed by a complex circuitry composed of excitatory and inhibitory interneurones as well as projection neurones that are in charge of sending this nociceptive messages to the different brain areas involved in pain processing ((Todd, 2010) (Benarroch, 2016)).

The spinal information is also conveyed into the ventral horn to mediate nocifensive reflexes. In addition, descending excitatory or inhibitory projections from brain to spinal cord also modulate the spinal activity. Balance of excitatory and inhibitory inputs is required for normal sensory functions however these descending controls are altered during chronic pain and are also altered in OA (Rahman et al., 2009). The role of descending modulation will be discussed in section 1.3.4.3.

Primary nociceptors terminating in dorsal horn have a distribution pattern determined by sensory modality and by the part of the body that they innervate (Todd, 2010). In the following sections I will further describe how nociceptive signals are conveyed, processed and transmitted in the spinal cord.

1.3.3.1. Organization of spinal processing in the dorsal horn

The spinal cord is composed by a series of distinct laminae that were first described by Rexed in 1954 in the spinal cord of a cat and are now cytoarchitecturally classified. These laminae are divided in three based on their depth: superficial (lamina I-II), intermediate (lamina III-IV) and deep (lamina V-VI). Altogether, these laminas contain different types of neurones as well as non-neuronal cells. From different primary afferent fibers, to excitatory/inhibitory interneurones and projection neurones.

Primary afferent fibers

Primary afferent fibers terminate in different laminae in the spinal cord. Lamina I mainly receives input from Aδ fibers and peptidergic C-fibers. Additionally, lamina I also get inputs from a group of unmyelinated fibers activated by pruritic agents, suggesting that lamina I neurones respond both to pain and itch (Braz et al., 2014). TRMP8 positive C-fibers that respond to cooling also terminate in lamina I (Benarroch, 2016, Todd, 2010). Lamina II also receives projections from Aδ-fibers as well as from low threshold mechanoreceptors, which correspond to non-peptidergic C-fibers. The latter project to inner lamina II, thus making this lamina more responsive to mechanical stimuli and lamina I more sensitive to thermal stimuli. This difference in targeting suggests that peptidergic and non-peptidergic fibers have a district functional contribution to nociception (Braz et al., 2014). Lamina III and IV mainly receive projections from Aβ-fibers that respond to innocuous stimulation. Laminae V-VI respond to noxious and non-noxious stimuli as both Aβ-fibers and Aδ-fibers present monosynaptic projections to the deep lamina. C-fibers indirectly project to the deeper laminas either through polysynaptic projections through interneuron or via direct interaction through large dendritic trees that project to the more superficial laminas (Greenspon et al., 2019) (Braz et al., 2014).

Interneurones

The interneurones in spinal cord are the vast majority of neurones that have axons that remain in the spinal cord and arborise locally (Todd, 2010). They can be divided into excitatory and inhibitory. Excitatory interneurones use glutamate as their

neurotransmitter and they express vesicular glutamate transporter VGLUT2 (Santos et al., 2009). Inhibitory interneurones use GABA as their main neurotransmitter but some can also release glycine. In the rat, GABA is present in 25% of neurones in lamina I, 30% of neurones in lamina II and 40% of neurones in lamina III (Todd, 2010). Glycine is highly expressed in lamina III however it mainly co-expresses in GABA containing interneurones. Even though both neurotransmitters could be released from the same synaptic vesicle it is the expression of either GABA or glycine receptors that will determinate which neurotransmitter predominates (Braz et al., 2014).

Additionally, interneurones can also be divided by morphology (Braz et al., 2014). Lamina II interneurones can have the following morphologies: (1) Islet, mainly GABA interneurones that also express glycine, (2) Central, both inhibitory and excitatory interneurones exhibit this morphology; (3) Vertical, excitatory interneurones located in the outer body of lamina II in close proximity to lamina I; lastly (4) radial excitatory interneurones. Lamina I interneurones can also be divided into the following morphologies: pyramidal, fusiform or multipolar (Todd, 2010). However, the different function amongst these is hard to dissect due to the presence of projection neurones. There are different subpopulations of inhibitory interneurones classified based on their neurochemical expression. GABAergic interneurones can co-express with neuropeptide Y (NPY), galanin (GAL), parvalbumin (PV), and neuronal nitric oxide synthase (nNOS) (Benarroch, 2016). These subpopulations have different properties and different afferent input which reflect modality specificity.

Projection neurones

Most of projection neurones are concentrated in lamina I, with lamina II containing very few projection neurones in the lumbar region and some projection neurones scattered between lamina III-VI (Todd, 2010). Most of lamina I projection neurones are nociceptive specific (NS) as they receive direct input from Aδ- and C-fibers (D'Mello and Dickenson, 2008). Therefore, they respond to heat or mechanical induced pain, noxious heat, noxious mechanical stimuli (pinch) or cold stimuli, with some also responding to innocuous cold (Todd, 2010, Benarroch, 2016). 80% of lamina I projection neurones express neurokinin 1 receptor (NK1R) for substance P and terminate in the parabrachial nucleus (PB) (Todd, 2002). These neurones are excitatory, however the NK1R can also be present in some excitatory interneurones (Braz et al., 2014). NK1 projection neurones can also send signals to areas in the midbrain such as the rostral ventromedial medulla (RVM), which sends back projections to the spinal cord modulating spinal responses (Mantyh et al., 1997). Other lamina I projection neurones send signals to thalamus and periaqueductal grey (PAG) but interestingly only 5% of the total of lamina I neurones are projection neurones, thus they represent a

small population of neurones in the spinal cord (Spike et al., 2003).

In deep dorsal horn (lamina V-VI), most of the projection neurones are wide-dynamic range (WDR) neurones. They respond to both noxious and innocuous stimuli. These neurones target the amygdala and hypothalamus as well as projecting to the ventraobasal thalamus (Benarroch, 2016). WDR neurones fire action potentials in a graded fashion depending on the intensity of the stimuli. They also exhibit 'wind-up', an NMDA dependent event, where constant repetitive stimulation of these neurones causes an increase in evoked responses as well as in increase in post-discharge after each stimulus (D'Mello and Dickenson, 2008). Glutamate released from primary afferent fibers acts on NMDA receptors causes depolarization and calcium (Ca^{2+}) influx. This causes an increase in wind-up and amplification and propagation of response (Dickenson, 1995). Wind-up contributes to central sensitization and will be further explain in section 1.3.3.3.

Projection neurones can also be classified by their morphology. Multipolar and fusiform neurones are mainly NK1(+) which makes the nociceptive specific. Pyramidal neurones do not express NK1 in uninjured animals, however under injury conditions these neurones respond to noxious stimuli (Saeed and Ribeiro-da-Silva, 2013). Perhaps under an injury setting the observed *de novo* gene up-regulation of NK1 plays a role in these pyramidal cells allowing them to respond to noxious stimuli (Saeed and Ribeiro-da-Silva, 2013).

1.3.3.2. Information flow: from primary afferents to projection neurones

The information flow that arrives to the dorsal horn through the activation of primary afferent fibers can either directly or indirectly activate projection neurones. This mechanisms are strictly regulated and involve the activation of interneurones that act as meditors of signals between primary nocicpetors and spinothalamic neurones through a circuit known as feed-forward excitation. Additionally interneurones can also inhibit projection neurones through feed-forward inhibitiory circuits.

Feed-forward excitation

NK1 projecting neurones are located in lamina I (Todd et al., 2000). These fibers can become active upon direct interaction with peptidergic C-fibers in response to heat stimuli. However, feed-forward excitatory circuits driven by interneurones can also activate them. Non-peptidergic C-fibers can activate excitatory interneurones in lamina II, which the will activate vertical cells located in the outer lamina II. Vertical

neurones then project to NK1 expressing neurones in lamina I causing their activation (Benarroch, 2016). Additionally Aδ-fibers can directly activate vertical neurones in lamina II that project to NK1 neurones in lamina I. When it comes to tactile stimuli, Aβ-fibers can activate excitatory interneurones in lamina II, causing the activation of PKC positive interneurones in lamina II. These then project to vertical neurones. Low threshold C-mechanoreceptors which also transmit tactile information also activate excitatory interneurones in lamina II, which then project to NK1 (+) neurones (Braz et al., 2014). Thus, lamina II is crucial in integrating signals and sending them to lamina I where projection neurones are mainly located. Also, vertical neurones are in charge of conveying a range of stimuli as they receive indirect input of almost all primary afferent fibers (Benarroch, 2016, Braz et al., 2014).

Feed-forward inhibition

Feed-forward inhibition is required in order to provide some gate control mechanisms in order to reduce the input from primary afferent fibers to projection neurones. Inhibitory interneurones are crucial in reducing nociceptive inputs as well as itch and tactile information (Benarroch, 2016). The first theory provided on feed-forward inhibition was by Melzack and Wall (Melzack and Wall, 1965) as explained in section 1.1. Also, low threshold Aβ-fibers and low threshold C-mechanoreceptors activate GABA/glycinergic interneurones located in laminas II-IV and inhibit primary afferent fibers in response to innocuous stimuli. Other inhibitory interneurones inhibit descending controls that terminate in spinal cord. This allows the dorsal horn circuitry to distinguish between noxious and innocuous stimuli. The gate control theory also proposed that upon noxious stimulation, inhibitory interneurones were inhibited.

1.3.3.3. Central sensitization in the spinal cord

Primary afferent fibers release glutamate in response to acute and persistent noxious stimuli. Glutamate acts on a series of receptors present post-synaptically in the spinal dorsal horn. The initial baseline responses to glutamate release by nociceptors are set by the a-amino-3-hydroxy 5-methyl-4-isoxazeloproprionic acid (AMPA) receptor. This receptor becomes active very fast upon glutamate release.

Glutamate can also act on N-methyl-D-aspartate (NMDA) receptor. Under normal conditions the NMDA receptor is blocked by magnesium (Mg^{2+}). This Mg^{2+} block is not affected by normal acute or low frequency noxious stimulation. It is only under prolonged depolarization of the plasma membrane caused by repetitive C-fiber firing and release of substance P and CGRP that removes the Mg^{2+} block leading to the activation of the NMDA receptor. NMDA receptor activation causes the influx of

calcium allowing wind-up to occur. Wind-up appears after acute high intensity C-fiber stimulation (Dickenson and Sullivan, 1987), peripheral nerve damage or inflammation and leads to central sensitization. Central sensitization causes increased responsiveness to noxious stimuli also known as hyperalgesia and pain resulting from non-noxious stimuli known as allodynia as well as a spread in the receptive field of the neurones (D'Mello and Dickenson, 2008, Dickenson, 1995, Dickenson and Sullivan, 1987).

1.3.3.4. Clinical evidence of central sensitization in osteoarthritis

As joint degeneration progresses during OA, some patients report a transition from localized joint to wide spread allodynia and hyperalgesia, suggesting the development of central sensitization (Arendt-Nielsen et al., 2015). This will result in higher levels of pain, disability, poorer quality of life, higher concentration of pro-inflammatory cytokines and poorer outcome after knee replacement surgery (Arendt-Nielsen et al., 2015). Studies have shown that three years after knee replacement surgery 19% of OA patients report severe to unbearable pain, suggesting that central sensitization is driving the pain in this patients rather than peripheral nociceptive input (Petersen et al., 2015) and that facilitatory CNS alterations might be contributing to the experience of pain in this patients.

Another indicator of central sensitization in OA is when patients report diffuse radiating pain also known as referred pain. Sensory abnormalities are found in the area with referred pain including cutaneous mechanical hyperalgesia and allodynia as well as pressure-induced pain (Gwilym et al., 2009) Mechanical hyperalgesia requires central sensitization in spinal cord initiated by ongoing peripheral input driven by primary afferent fibers and is thought to cause chronic pain state in OA (Clauw and Hassett, 2017). Knee OA patients usually report referred pain in areas around the knee joint and the tibia (Lesher et al., 2008).

As explained in the previous section, wind-up drives central sensitization, thus causing an increase in neuronal excitability in spinal cord neurones upon repetitive stimulation. When translating this into the clinic, OA patients who exhibit central sensitization and are presented with a defined painful stimulus applied repeatedly will perceive such stimulus as increasingly painful (Thakur et al., 2014). This phenomenon is called temporal summation. Temporal summation can be evoked by a series of stimulus such as tactile pin-prick, pressure, heat and electrical pulses. When looking at temporal summation in a subgroup of OA patients that report high pain a facilitation of the temporal summation was observed compared to other groups (Finan et al., 2013).

Descending inhibitory and excitatory controls might also contribute to the maintenance of central sensitization in spinal cord by exciting or inhibiting neuronal activity in dorsal horn. OA patients present altered descending modulation and altered brain activity, which will be further discussed in section 1.3.4.4.

1.3.4. Central processing of nociceptive signals

Second-order neurones in spinal cord cross the midline to enter ascending tracts which will then project to different areas in the CNS such as the thalamus, periaqueductal grey (PAG) and parabrachial area (PB) sending the nociceptive information. In the CNS these signals will be processed and perceived as pain. Ascending projections can also send signals to rostral ventromedial medulla (RVM) in the brainstem. RVM descending projections will feed-back information to the spinal cord modulating the spinal circuitry.

Recent neuroimaging data have shown the different brain regions that are activated during a painful experience. These areas are the following: primary somatosensory cortex (S1), secondary somatosensory cortex (S2), the anterior cingulate cortex (ACC), prefrontal cortex (PFC), insula, amygdala, thalamus, cerebellum and the ventral tegmental area VTA and the nucleus accumbens (NAc) which are part of the reward system (Gwilym et al., 2009). Together they are referred as the "pain matrix". The S1, S2 and thalamus are the fundamental network for human nociceptive processing without them we wouldn't feel pain. Whereas the prefrontal region and the limbic system (ACC, PGC, amygdala, VTA and NAc) encode emotional and motivational responses and are implicated in the affective aspects of pain (Ossipov et al., 2014). Additionally, interaction amongst these brain regions can alter the experience and perception of pain by engaging descending pathways (Denk et al., 2014). In the following section I am going to further explain both ascending and descending pathways, which modulate nociceptive processing.

1.3.4.1. The spinothalamic tract

The spinothalamic tract (STT) sends sensory discriminative messages from the spinal cord to the contralateral thalamus making it the main relay site for nociceptive inputs to cortical and subcortical structures. Lamina I and lamina V neurones, project to different nuclei of the thalamus.

In primates, lamina I STT neurones send projections to posterior part of the ventral medial nucleus, the ventral posterior inferior nucleus, the ventral posterolateral nucleus and to the ventral caudal portion of the medial dorsal nucleus (Craig, 2003). Lamina I, STT also send projection to the ventral posterior thalamus (VP) however a much larger

number of STT projections to VP arise from lamina V. The deep laminas also send projections to VPI, ventral lateral nucleus and intralaminar nuclei (Craig, 2003).

The ventral posterolateral nucleous signals to the somatosensory cortex and vice versa and the posterior triangular nucleus projections to second somatosensory area and the insular cortex (Todd, 2010). Altogether the thalamus contributes to both the sensory-discriminative and the affective-motivational aspects of pain that generate the overall perception of pain (Tracey and Mantyh, 2007).

Spinothalamic tract neurones have been identified using anterograde and retrograde tracing methods. In primates 50% of spinothalamic tract neurones originate in lamina I, 25% in lamina IV-V and the rest in lamina VII-VIII (Craig, 2003). However, this is not the case in rats, where only 5% of lamina I STT neurones projecting to thalamus and a much larger number of STT neurones project from lamina V (Todd, 2010).

1.3.4.2. The spino-bulbo-spinal pathway

Spinobulbar (SB) projection neurones originate mainly from lamina I (63-69%), and project to areas in the medulla and brainstem like the parabrachial nucleus and the periaqueductal grey (PAG) (Andrew et al., 2003). Once SB projections have reached the parabrachial nucleus and the PAG they project to limbic regions such as the amygdala and the hypothalamus, which play a role in processing the emotional and affective components of pain. Microinjection of opioids or electrical stimulation applied into this region produce antinociceptive effects in both animals and humans (Ossipov et al., 2014). The PAG plays a crucial role in converging ascending and descending pathways. Ascending projections by way of the parabrachial nuclei and descending projections through projections to the rostorventromedial medulla (RVM) and the locus coeruleus (LC) (Ossipov et al., 2014). The latter modulates nociceptive transmission by either inhibiting or exciting neuronal signals in spinal cord (Patel and Dickenson, 2018).

1.3.4.3. Descending monoaminergic controls

The RVM is considered to be the final relay in descending modulation of pain projecting back into the spinal cord and sending both, facilitatory or inhibitory messages (Zhuo and Gebhart, 1992). In the RVM there are two distinct groups of neurones that exhibit different firing patterns in response to noxious stimulation. These are the ON-cells considered to modulate descending facilitation and the tonic firing OFF-cells which cease firing upon noxious stimulation and are considered to play a role in descending inhibition (Patel and Dickenson, 2018). ON-cells exhibit increased activity after injury or inflammation. On the other hand, inhibiting on-cell causes the

excitation of off-cell, which produces analgesia (Ossipov et al., 2014). Thus, activity of these cells provides a regulatory mechanism by which signals into the spinal cord modulate nociceptive inputs.

Descending facilitation from RVM is mediated by the release of serotonin into the spinal cord. Serotonin binds 5-HT receptors expressed in nerve terminals of primary afferent fibers or spinal interneurones. There are different types of 5-HT receptors and they can be pronociceptive or antinociceptive depending on what subtype becomes active. 5-HT_3 receptors are pronociceptive, while 5-HT7 and 5-HT2 are proposed to be antinociceptive (Rahman et al., 2011, Bannister and Dickenson, 2016). Descending inhibition arises from the locus coeruleus (LC) and it is mediated by the release of norepinephrine (NE) in spinal cord, which predominantly acts at the α2-adrenoceptor inhibiting the release of NTs from primary afferent fibers suppressing the firing of projection neurones (D'Mello and Dickenson, 2008). Evidence suggests that descending faciliatory pathways predominate (Patel and Dickenson, 2018). For instance, block of neuronal activity within the RVM using lidocaine or depletion of 5-HT causes a decrease in neuronal excitability of spinal cord neurones in normal states (Bee and Dickenson, 2007, Rahman et al., 2006). Additionally, depletion of NK1+ projection neurones using a substance P-saporin (SP-SAP) conjugate reduced neuronal excitability of WDR neurones revealing that descending influences are mainly faciliatory and act via 5-HT3 as blocking this receptor with an antagonist mimicked effects observed with the (SP-SAP) conjugate (Suzuki et al., 2002).

During chronic pain states, both excitatory and inhibitory pathways undergo plastic changes. Descending faciliatory pathways from RVM appear to be increased in neuropathy and are though to contribute to the maintenance of chronic pain states by increasing excitation and masking descending inhibitory inputs and acting alongside central sensitization (Patel and Dickenson, 2018).

1.3.4.4. Diffuse noxious inhibitory controls

One pain inhibits another pain is the principle by which Diffuse Noxious Inhibitory Controls (DNIC) exerts its action. Thus, DNIC is an endogenous descending inhibitory pathway that originates in the subnucleus reticularis dorsalis and it is triggered by a noxious stimulus distant to the control response and acts by modulating the activity of WDR neurones in spinal cord (Bannister and Dickenson, 2016). It is important to note that this pathway is different than the descending controls originating in the RVM. Interestingly, DNIC disappears in spinal nerve ligated (SNL) rats but can reappear after blockage of 5-HT3 receptor or by enhancing descending inhibitory controls (Bannister

et al., 2015). Therefore, it suggests that enhanced RVM activity post-injury masks the actions of this pathway. In the clinic, Condition Pain Modulation (CPM) is the equivalent to DNIC in humans. It also requires descending controls and it is also absent in certain pain patients (Bannister and Dickenson, 2016). CPM is a useful measure to assess if OA patients have altered descending modulation, thus those patients that exhibit neuropathic signs will not exhibit CPM and if they undergo knee replacement surgery have higher chances of exhibiting post-injury pain.

1.3.4.5. Central processing in osteoarthritis

Processing of pain signals in the CNS can be altered during different pain states. *In-vivo* electrophysiological studies in the monoiodoacetate (MIA) model of OA pain in rats where neuropathic pain-like features are present have shown that spinal administration of ondansetron a 5-HT3 antagonist, reduced neuronal responses to mechanical and thermal stimulation in the late stage of the disease (Rahman et al., 2009). On the other hand, in the rat carrageenan model, ondansetron failed to inhibit neuronal evoked responses to evoked stimuli (Rahman et al., 2004). Therefore, these studies suggest that there is a differential role of descending facilitation in inflammatory pain and neuropathic pain. Further studies in the late stage of this model showed that in condition placed preference (CPP), inactivation of the RVM by injection of lidocane causes CPP, reversing ongoing pain (Havelin et al., 2016).

Differences in DNIC have also been shown in the MIA animal model. Recent work by our laboratory has shown that in the early stages of MIA were inflammation predominates DNIC is present but it is lost in the later stage of the model (Lockwood et al., 2019a).

Clearly descending faciliatory controls play a role in modulating responses in animal models, but in humans, the role of descending modulation has also been researched. Neuroimaging studies in patients with OA show increased activity in the PAG than control patients (Soni et al., 2018). Furthermore, when OA patents were divided into two groups: nociceptive patients versus patients with neuropathic pain like features that presented greater responses to punctuated hyperalgesia (Soni et al.,) showed that the latter group presented increased PAG activity perhaps due to an increased faciliatory drive that would explain the increase in pain hyperalgesia and presence of referred pain.

1.4. Current treatment for osteoarthritis pathology and associated pain

The treatment of OA remains challenging as there has not been a single agent identified that can treat both, symptomatic and structural effects of OA pathology. This is most likely because there is little correlation between cartilage preservation and OA pain the extent of damage and pain varies between patients. There are different ways to treat OA pain, either by using a pharmacological approach to relieve pain, using disease-modifying treatments that target the changes that occur in the joint or by surgical management. Additionally, the combination of non-pharmacological and pharmacological treatments is also available, but drug therapy becomes necessary when OA becomes painful. In the following section I am going to discuss the pharmacological approaches for the treatment of OA pain, as pain is the main symptom, as well as the surgical management.

1.4.1. Treatments for OA-associated pain

Non-Steroidal Anti-Inflammatory Drugs (NSAIDs)

NSAIDs exert both an anti-inflammatory and analgesic action. They act mainly on the periphery by inhibiting cyclooxygenase (COX) enzymes 1 and 2 which causes the decrease of prostaglandins and centrally possibly by increasing serotonin levels (Majeed et al., 2018). They can be given topically or orally, but due to the number of gastrointestinal side effects the oral NSAIDs can cause, topical NSAIDs are the first to be prescribed specially amongst the elderly patients (≥75years). The topically available NSAIDs need to be applied in pain causing structures around the knee joint and the most commonly prescribed is diclofenac. Recent studies have shown that topically applied diclofenac produces a 50% reduction of pain of 60% of patients over a period of 8-12 weeks (Derry et al., 2016).

Orally prescribed NSAIDs such as ibuprofen and naproxen are usually prescribed once the topically available is insufficient for the patients. However, depending on the dose and duration of treatment with orally available NSAIDs they can cause several side effects and individual risk factors need to be taken into account before preserving them to the patients.

Acetaminophen (Paracetamol)

Paracetamol used to be the first in line analgesic for OA pain management and freely available over the counter medication. Even though the mechanisms of action of paracetamol are complex and still not fully understood, it is thought to have both a

peripheral and a central action. In the periphery it is thought to inhibit COX-1 and COX-2 and centrally it acts on the descending serotonergic pathway as well as in the endocannabinoid system (Majeed et al., 2018). Recent studies have shown that paracetamol even at high doses exerts a small and not clinically relevant analgesic effect and that NSAIDs are more efficient for the treatment of OA pain (Majeed et al., 2018, Steinmeyer et al., 2018).

Capsaicin

Capsaicin as previously described is a TRPV1 activator. It is prescribed as a cream, which can be topically applied to alleviate pain. It initially causes a burning sensation because TRPV1 channel becomes active leading to enhanced sensitivity followed by a period with reduced sensitivity and persistent application of the cream leads to persistent desensitisation (Derry et al., 2017). It has limited efficacy and does not improve function, however it can be used as combination with other treatments.

Opioids

Prescription of opioids for the management of OA pain is strongly discouraged due to the fact that they are highly addictive, can cause tolerance and in some patients can cause opioid-induced hyperalgesia when taken for a prolonged time (Bannister and Dickenson, 2010). They also produce a range of side effects from vomiting, nausea, dizziness and somnolence. Therefore, opioids are only prescribed when necessary and at the lowest does for the shortest amount of time possible (Steinmeyer et al., 2018, Majeed et al., 2018)

Anti-NGF treatment

As discussed in previous section NGF is upregulated during inflammation and by binding to its receptor TrkA causes the activation of downstream cellular mechanisms leading to peripheral sensitization. Injection of NGF into the knee joint of naïve rat induces pain behaviour and synovitis and when injected into the knee of an animal model of OA exacerbates pain behaviour. NGF blockage can be achieved by using antibodies that prevent its binding to TrkA. Human monoclonal antibodies against NGF have been developed and are currently under clinical trials. There are different antibodies that have been developed by different pharmaceutical companies; the most studied is tanezumab (Pfizer and Eli Lilly). In a randomized double-blinded control trial with tanezumab OA patients reported dramatic pain relief (Lane et al., 2010). Even though this result was promising a number of subjects

developed progressive OA and osteonecrosis in non-target joints. The risk of developing progressive OA was higher when the treatment was given in conjunction with NSAIDs. The clinical trials for anti-NGF treatment are still ongoing, however it is important to take into consideration the potential risk and recognize patients that would be in risk of toxicity (Miller et al., 2017).

1.4.2. Treatments for OA pathology

Intra-articular therapies

Intra articular injections of glucocorticoids or hyaluronic acid (HA) are also common treatments for management of OA and associated pain. Glucocorticoids reduce pain and restore mobility; however they can only be applied at a low dose and over a short period of time. High doses of glucocorticoids can inhibit cartilage metabolism, reduce cartilage mass, produce soft tissue calcification, atrophy and can induce acute crystal synovitis (Steinmeyer et al., 2018, Majeed et al., 2018).

Hyaluronic acid is found in the synovial fluid of a healthy joint, thus injections of HA aim to change the pathological HA with new healthy one. HA injections help with lubrication and show a delayed analgesic effect observed at a maximum of 2 months after injection and can last up to 6month (Steinmeyer et al., 2018). They have shown to have little side effects although the literature is divided on the use of HA.

Surgical Management

When it comes to surgical management there are two types of surgical approaches that can be used for the treatment and management of knee OA. These are arthroscopic surgery or total knee replacement surgery (total knee arthroplasty).

Arthroscopic surgery consists of inserting an arthroscope into the knee joint which allows the removal of cartilage fragments, calcium crystals, and debridement of the knee joint where the articular surface and osteophytes can be smoothen. This reduces synovitis and eliminates mechanical interference with joint motion (Kirkley et al., 2008). This surgery is performed in many joints but most commonly in the knee joint and there are very little risks for the patients. Less than 1% of patients die and fewer than 5% develop serious complications (Marx, 2008). However, studies have shown that arthroscopic surgery is not more effective than non-operative treatment (Kirkley et al., 2008).

Total knee arthroplasty consists in the removal of articular surfaces form the knee joint and replacement of these with synthetic materials, usually metal, ceramic and plastic. This surgery is thought to improve function 3-6 months post surgery, with men

benefiting more than women from the procedure, and relieving pain in people with OA that have failed to respond to pharmacological treatment (Ethgen et al., 2004). The surgery recovery takes 6-10 weeks and prosthetic knee remains functional up to 10 years.

As explained in previous sections (1.2.5, 1.3.3.4, 1.3.4.4) it is crucial to properly assess the type of pain and level of sensitization the patient suffers before the surgery. Thus, increasing evidence suggest that the subgroup of patients that have neuropathic pain-like feature would not be good candidates for this surgery as it is likely they would continue suffering from chronic pain post surgery (Thakur et al., 2014, Soni et al., 2018).

1.5. Induced animal models of osteoarthritis-associated pain

There are a number of rodent animal models available to study osteoarthritis-associated pain. Even though none of these models mimics the pathophysiological changes the joint undergoes during OA, they prove to be useful for the study of OA-associated pain. As pain is the main symptom of OA pathology, it is important to get a better understanding of the molecular and cellular mechanisms involved in generating and maintain chronic pain in pre-clinical models (Malfait et al., 2013). The different rodent models to study OA associated pain are:

Chemically induced models

In this method an inflammatory or toxic compound is injected into the knee joint in which OA is to be induced causing the destabilization of the knee joint and surrounding structures.

• *Rat/Mouse monosodium iodoacetate model (MIA):* Intra-articular injection of MIA causes cartilage destruction leading to intra-articular inflammation. The animal model used for the work described in this thesis has been the MIA model of OA pain and it will be further described in detail in future sections.

• *Rat/Mouse collagenase induced arthritis:* This method consists on delivering an intra-articular injection of collagenase into the knee joint causing patellar dislocation on the medial side and destruction of collagen fibers within the cartilage. Additionally, collagen fibers in tendons and ligament also become damaged leading to joint instability. Two injections tend to be made in this model, the second one 3-5days

after the first one and subchondral sclerosis appears 6 weeks after injection (Bapat et al., 2018) (Lampropoulou-Adamidou et al., 2014).

Surgical induced models

They represent post-traumatic OA and work through a combination of joint destabilization, altered articular surface contact forces and intra-articular inflammation (Teeple et al., 2013). The most common of these are:

• *Rat/Mouse anterior cingulate ligament transection model (ACLT):* This surgical method consists of performing a transection of the ACL causing joint destabilization and inducing post-traumatic OA in the knee joint following a similar pattern of pathogenesis seen in humans. The advantages of this method are that its quick, the OA develops rapidly and it is reproducible (Lampropoulou-Adamidou et al., 2014).

• *Rat/Mouse medial meniscal tear model (MMT):* This method consists of cutting the medial collateral ligaments to expose the meniscus. Once the meniscus is exposed, the surgeon splits the meniscus; either the medial or lateral meniscus can be split. The medial meniscus tends to be the chosen one as it bears more weight. This method is also quick and the OA progression is also rapid. 50% of humans that have a menisectiomy develop OA within 20 years, which makes this model a very interesting model to study as it mimics human pathology. In 4 weeks the rat has developed mild to moderate OA (Fang et al., 2018, Bapat et al., 2018). This model is more severe than the ACL transection model (Kuyinu et al., 2016).

Spontaneous OA Models

Several animals such as horses, dogs, sheeps, and rabbits exhibit naturally occurring OA. However, the most commonly used animal models of naturally occurring OA are the *Dunkin Harley* guinea pig, which develops lesions similar to those present in OA in humans and the *STR/ort* mice which are normally used to study disease pathogenesis (Kuyinu et al., 2016).

Mechanical Joint Loading Model of OA

Recent studies have been focused on finding new non invasive models of OA.
The mechanical joint loading model of OA uses the repetitive mechanical loading of the joint in mice for a period of 2 weeks, 3 times a week at 9N (Ter Heegde et al., 2019). This model has been shown to induce changes to the articular cartilage as well

as changes in the subchondral bone, similar to OA in humans. Additionally mice in this model develop pain phenotype (Ter Heegde et al., 2019). Thus, this model could be used for both the study of OA pathology as well as the study of OA associated pain.

1.5.1. The monosodium iodoacetate model of osteoarthritis

The rat monosodium iodoacetate model (MIA) is different from human OA however it is considered useful to study pain mechanisms as it generates long-lasting mechanical hyperalgesia (Eitner et al., 2017). Intra-articular injection of MIA into the knee joint inhibits glycolysis leading to chondrocyte death. The pathology of OA develops rapidly and the amount of damage and inflammation will vary depending on the concentration of MIA injected into the knee joint (Havelin et al., 2016). With the higher doses of MIA (2mg/animal) the model provides two distinct stages. An early acute inflammatory phase (2-6 days post injection) where chondrocytes shrunken and become lost, the synovial membrane expands and the joint becomes infiltrated by macrophages, neutrophils, plasma cells and lymphocytes causing inflammation and cartilage collapses (Combe et al., 2004). By day 7 inflammation in the synovium has resolved and it does not play a role in mediating pain. At later stages (14 days post injection and forward) inflammation has decreased the cartilage damage continues, new trabecular bone appears and the subchondral bone collapses (Eitner et al., 2017). Even though in both stages animals show differences in weight bearing asymmetry and mechanical hypersensitivity to punctuated stimuli compared to naïve or sham animals, in the late stage, animals also exhibit ongoing pain driven by central mechanisms (Rahman et al., 2015, Havelin et al., 2016, Lockwood et al., 2019a). In this thesis further research of the mechanisms driving pain in the two distinct stages of the MIA model will be described.

1.6. Aims of the thesis

Recent magnetic resonance brain imaging studies have revealed the presence of a subgroup of OA patients that present increased rostral ventromedial medulla (RVM) and periaqueductal grey (PAG) activity (Gwilym et al., 2009). These patients score high on the PainDETECT test and use indicators of neuropathic pain to describe their OA associated pain (Soni et al., 2018). Additionally these patients are insensitive to non-steroidal anti-inflammatory drugs (Gwilym et al., 2009). Thus, suggesting that there is a subgroup of OA patients that present neuropathic-pain like features and there is a need to develop or prescribe alternative drugs to these patients in order for them to obtain proper pain-relief.

The monoiodoacetate (MIA) model of OA has been widely used for the research of OA-associated pain. While articular cartilage damage and pain severity in this model can vary depending on dose and volume injected into the intra-articular space of the knee joint, several studies using the MIA model in rats report that a 2mg dose of MIA provides joint degradation with two distinct stages of the model (Thakur et al., 2012). There is first an early acute inflammatory stage that appears at day 2 post MIA-injection with inflammation subsiding around day 7 post MIA-injection and then there is a later stage that presents neuropathic-pain like features (Thakur et al., 2012). The latter remains controversial but several studies report behavioural changes in the late stage of the model that are not present in the early acute inflammatory stages. Such as, severe damage to the articular cartilage, the presence of cyclic AMP-dependent transcription factor-3 (ATF-3) immunoreactivity in DRG neurons during the later stages (Orita et al., 2011) (Thakur et al., 2012) which is suggestive of nerve damage, and increased descending serotonergic controls (Rahman et al., 2009), which are present in neuropathic pain models. These studies report the appearance of neuropathic-pain like features as soon as days 14-21; however several other studies do not see the presence of ATF-3 expression (Lockwood, 2018) (Ogbonna et al., 2013) and others do not report the appearance of neuropathic-pain like features until later stages of the model (around day 28 post-MIA injection) or with higher doses of MIA injected into the knee joint (Liu et al., 2011).

In this thesis a dose of 2mg of MIA dissolved in a volume of 25μL 0.9% saline was intra-articularlly injected into the knee joint of male Sprague-Dawley rats. The first aim of this thesis was to address behavioural and articular cartilage histological differences between early stage MIA (2-4 days post MIA-injection) and late stage MIA (14-21) rats Additionally, extracellular *in-vivo* electrophysiological recordings of WDR deep dorsal horn neurons were carried out to compare any differences in baseline responses between early and late stages MIA animals in response to evoked innocuous and noxious stimuli.

The second aim of this thesis was to address the role of voltage-gated calcium channels $Ca_V2.2$ and $Ca_V3.2$ in MIA-induced OA associated pain. $Ca_V2.2$ are present in pre-synaptic terminals of primary afferent fibers and plays a role in neurotransmitter release. $Ca_V3.2$ are present in various locations along the axon of primary afferent fibers where they mediate transmembrane calcium influx and are also present in pre-synaptic terminals of these fibers where they contribute to spontaneous neurotransmitter release (Cassidy et al., 2014). While pharmacologically agents targeting these channels are not used for OA pain treatment, Cav2.2 blockers such as ziconotide have been used the treatment of neuropathic pain in humans, as well as Gabapentinoids drug which act by inhibiting channel trafficking into the plasma membrane and thus, reducing neurotransmitter release (Patel et al., 2018). Additionally, $Ca_V3.2$ channels have been used in rodent models where they were shown to attenuate pain in both neuropathic and inflammatory models. Therefore, the use of voltage gated calcium channel modulators could be a potential alternative to OA

treatment. For the subgroup of patients with neuropathic-pain like features, targeting these channels could be an alternative to NSAIDs. In this thesis, we wanted to address if targeting $Ca_V2.2$ with the use state-dependent blocker TROX-1 and state independent blocker ω-conotoxin could inhibit neuronal evoked responses of WDR neurons in both early and late stages of the MIA model. Additionally, $Ca_V3.2$ was also targeted in the late stages of the MIA model with a recently developed peptide TAT-cUBPI-USP5 (Garcia-Caballero et al., 2016).

The third and last aim of this thesis was to address changes in descending modulation both in early and late stages of the MIA model in rats. Descending serotonergic controls do not appear altered in inflammatory pain (Rahman et al., 2004), thus we would expect this mechanism not to be enhanced in the early acute inflammatory stage of the MIA model. However, increased descending serotonergic drive has been previously reported in the late stages of the model but remains controversial (Rahman et al., 2009). Diffuse noxious inhibitory controls were also measured in order to further address changes to descending modulation. Duloxetine, a serotonin/noradrenaline reuptake inhibitor (SNRI), recently approved for the treatment of OA pain, was also used to in order to address its inhibitory effects on WDR neurons in the late stages of the MIA model (Abou-Raya et al., 2012).

Chapter 2. Materials and Methods

2.1. Animals

Male Sprague-Dawley Rats (Central Biological Services, University College London, UK) were used for all behavioural and electrophysiological experiments. Animals were grouped at a maximum of 4 animals per cage and housed at a conventional 12 hour: 12 hour light/dark cycle with access to food and water *ad libitum*. Temperature (20-22°C) and humidity (65-75%) of the holding and procedure rooms, were closely regulated by the Biological Services staff. The specific number of animals used per study is stated in the methods section of each chapter.

All experiment procedures were licensed by local laws (UK Animals (Scientific Procedures) Act 1986 and the European Communities Council Directive of 22 September 2010 (2010/63/EC)) and followed the guidelines under the International Association for the Study of Pain (Zimmermann, 1983).

2.2. Induction of the MIA model of osteoarthritis pain

The MIA model of OA pain involves an intra-articular injection of monosodium iodoacetate (MIA) into the intra-articular space of the left knee in rats. MIA reduces glycolysis by inhibiting glycolytic enzyme glyceraldehyde 3-phosphate dehydrogenase (GAPDH). Disrupting glycolysis causes a reduction in ATP production at the mitochondria thus interrupting cellular respiration. Injection of MIA into the knee joint causes chondrocyte death, which leads to structural changes in the articular cartilage, bone and other joint structures. For more information on the MIA model please refer to Chapter 3.

2.2.1. Protocol for MIA induction

Male Sprague-Dawley rats (Early Stage 190-200g; Late Stage 90-100g) were placed into a transparent sealed chamber that received a constant flow of isoflurane (4%) in a mix of N_2O:O_2 for inhalation. Once animals had gone under the anaesthesia and showed no signs of reflexes, the ventral surface of their left knee was shaved off in order to expose the skin. Skin was then cleaned with an anti-bacteria 4% chlorexidine gluconate solution (Hibiscrub antibacterial wash, Mölnycke Health Care).

Rats were then placed in a supine position on the surgery table on top of a thermo-regulated head matt and placed into a nose-cone. Through the nose-cone the animals received a constant supply of isoflurane for anaesthetic maintenance 2.5% v/v. Left knee was flexed and animals received an intra-articular injection into the infrapatellar ligament of 2mg of MIA (MIA; Sigma,UK) in 25uL of 0.9% saline solution.

Injection was done by using a 50µL sterilized Hamilton syringe and a 27G sterile needle. Needle was then removed slowly to avoid leakage from the knee joint space. Control sham animals were injected with 0.9% saline only. The knee was flexed and extended in order to distribute the MIA in the joint cavity. Following injection, animals were placed into a recovery incubator and supervised. Once awake and mobile, animals were placed into a clean cage and monitored over the following hours and days by the experimenter and BSU staff. **Figure 2.1**. shows a diagram of the different stages of MIA-induced OA. The early acute inflammatory stage, appearing from days 2-4 and a later stage, with neuropathic-pain like features, appearing at days 14-21. Behavioural measurements were taken before injection at Baseline and at days 2, 4, 7 and 14 post MIA-injection. In-vivo electrophysiological recordings were taken in both early and late stage and rats were sacrificed after each experiment. For Catwalk Gatway System and LABORAS, rats were sacrificed at day 14 post MIA-injection.

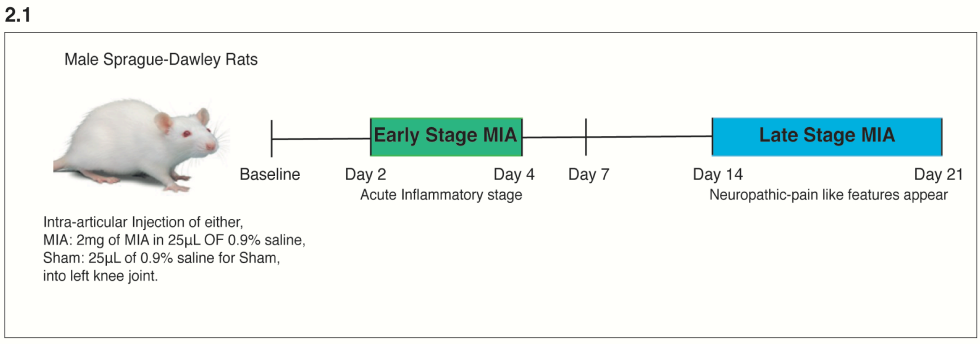

Figure 2.1. MIA induced OA timeline. Male Sprague-Dawley rats are injected into the intra-articular space of their left knee with 2mg of MIA dissolved in 25µL of 0.9% saline. The early acute inflammatory stage is comprised from day 2 post MIA injection to day 4. By day 7 inflammation resolves and the late stage with neuropathic pain-like features are seen at day 14. Behavioural measurements are taken in both MIA and sham groups before injection at baseline and post injection at days 2, 4, 7 and 14. *In-vivo* electrophysiological recordings are performed for the early stage group between days 2-4 post injection and for the late stage group between days 14-21 post injection.

2.3. Behavioural Assessments in Rats

2.3.1. Mechanical Hypersensitivity

In order to assess mechanical hypersensitivity animals were first placed in separated transparent Plexiglas chambers mounted on a wire mesh floor. Animals were left to habituate for 30min prior to the test. Mechanical hypersensitivity was assessed using von Frey (vF) filaments (Touch-Test, North Coast Medical, USA) of different weights (1g, 4g, 10g, 15g).

Filaments were applied from lower to higher weight. First round of testing began by applying the lowest vF into the plantar surface of contralateral hind paw 5 times for 5 second in each animal with 30s wait between each stimuli. Once each animal had been tested, same vF was then applied to the ipsilateral hind-paw. Second round of testing consisted on applying the second lowest vF on the contralateral site and so on. Full paw lift was considered a positive withdrawal and partial lifts were ignored.

Baseline behaviour was tested twice, 4 and 3 days prior to MIA/Sham injection, and an average baseline was calculated. Paw withdrawal behaviour was then tested at days 2, 4, 7 and 14 post MIA/Sham injection. Percentage response was calculated for each von Frey filament based on how many times the animal had withdrawn (1 PW – 20%; 2 PW- 40%; 3 PW – 60%; 4 PW – 80% and 5 PW – 100%) at each time point.

Paw withdrawal thresholds (PWT) (g) were also calculated per animal at each time. PWT was assessed by applying a series of vF filaments (1g-15g) in ascending order into the plantar surface of the animal's hind-paw. Paw withdrawal thresholds was assigned to each animal when the lowest weight of vF filament that elicited a 100% withdrawal reflex. For analysis, a PWT of greater than 15g was recorded as 26g. 26g was assigned as that is the most noxious vF that can be applied into the hind-paw of an awake rats.

2.3.2. Weight bearing

Weight bearing behaviour was assessed using an incapacitance tester (Linton Instruments, Norfolk, UK). Rats were placed in a plexiglass enclosure while each hind paw rested on separate electronic weight plates. Front paws rested on the plexiglass **(Figure 2.2).**

Animals were habituated for 5min to the equipment prior to test. Once they were settled, three consecutive measurements were recorded for each rat and average of these was calculated for both ipsilateral and contralateral hind paws. Baseline readings were recorded on days 4 and 3 prior to MIA/Sham injection. Following injection readings were taken at days 2, 4, 7 and 14 for all animals. The percentage for the ipsilateral hind paw is presented as a percentage of the total weight bearing of both contralateral and ipsilateral limbs.

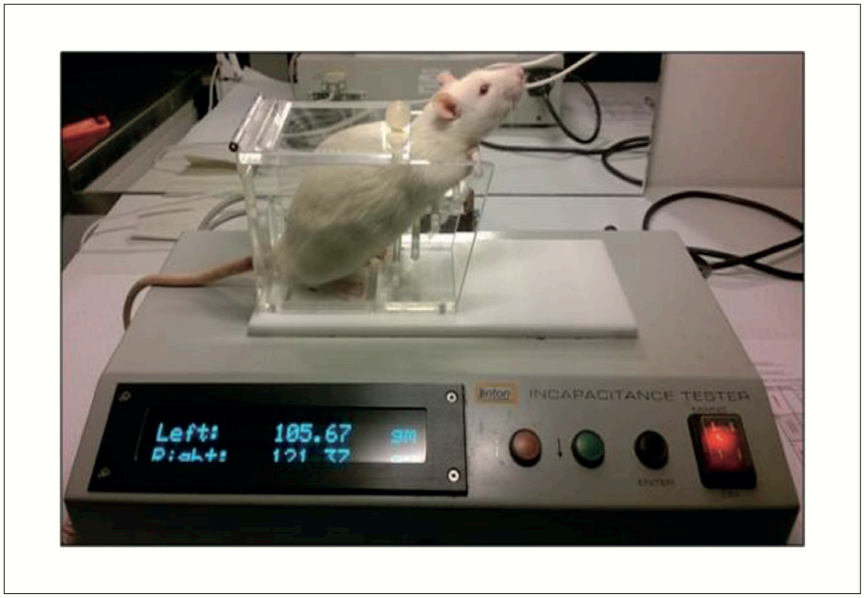

Figure 2.2. Weight bearing measurements with incapacitance tester. The rat stands inside the plexiglass enclosure with its tail out of the box. Each hind-paw rests on a separate electronic plate. The electronic screen gives the reading of the weight (grams) that the animal is putting into each hind-paw. Three consecutive readings per rat are taken at every time point (Baseline, day 2, 4, 7 and 14 post injection) and a average is obtained for each time-point.

2.3.3. CatWalk XT System

2.3.3.1. Overview of the CatWalk XT system

Gait abnormalities in the MIA were measured using the CatWalk XT system. CatWalk XT system consists of an enclosed walkway on a glass plate. Rats are placed on the platform and they are able to walk freely from one side to the other of the walkway. The room where the CatWalk is located has to be in the dark due to the fact that the catwalk is illuminated in a dim red light. In addition a green light enters at the long edge of the plate and is reflected internally so that when the animal walks through the catwalk the paws in contact with the plate become illuminated in green fluorescence **(Figure 2.3a)**.

The CatWalk XT system incorporates an Illuminated Footprints^{TM} technology that captures the paws through a high-speed video camera that is positioned vertically right under the glass plate at a 70cm distance from the platform. Videos are then transformed into images and because the system is also connected to a computer this images are then transferred into the CatWalk XT 10.5 computer program **(Figure 2.3b)**. The Illuminated Footprints^{TM} technology is able to detect differences in paw intensity between animals **(Figure 2.3b)**. Once animal runs have been acquired, the computer program allows you to either manually or automatically label each

illuminated paw in each video image **(Figure 2.3c)**. It is recommended to ensure that the automatic labelling has been done correctly as the system sometimes labels paws wrongly. Once the classification has been done the program automatically calculates a range of parameters in order to address any possible gait abnormalities.

2.3.3.2. Protocol for data acquisition on CatWalk XT system

Rats were habituated to the Catwalk by allowing them to freely move from one side to the other of the platform for 5min. For each animal 3 compliant runs were acquired at each time point after habituation. These runs were then averaged to obtain the value for that animal at that specific time point. Run criteria were set at a minimum run duration of 1 second and maximum run duration of 5 seconds.

A run was considered compliant when it fell under these parameters. The run criteria parameters were taken from the CatWalk XT 10.6 reference manual recommendations. If the animal was slower or faster than the parameters set on the computer, the system classified the run as non-compliant and had to be repeated. This parameter is crucial to ensure that all animals are walking at the same pace as sometimes rats could walk either too fast or too slow along the platform. In addition, the camera gain (dB) was set at 20.00, the green intensity threshold was set at 0.10, red ceiling light (V) was set at 17.7 and the green walkway light (v) was set at 16.0 for all time runs and time point.

MIA/Sham injections were carried out as explained above 2.2.1. Three runs were recorded at each time point and averaged to obtain one run average value. Additionally, two baselines were recorded MIA/Sham pre-injection per animal and then averaged, in order to obtain one baseline value per animal. Following injection CatWalk measurements were taken at days 2, 4, 7 and 14, post injection. In order to measure gait abnormalities a series of parameters were obtained. Ratios were calculated between left/right hind-paw and left/right front paw for each parameter measured.

2.3

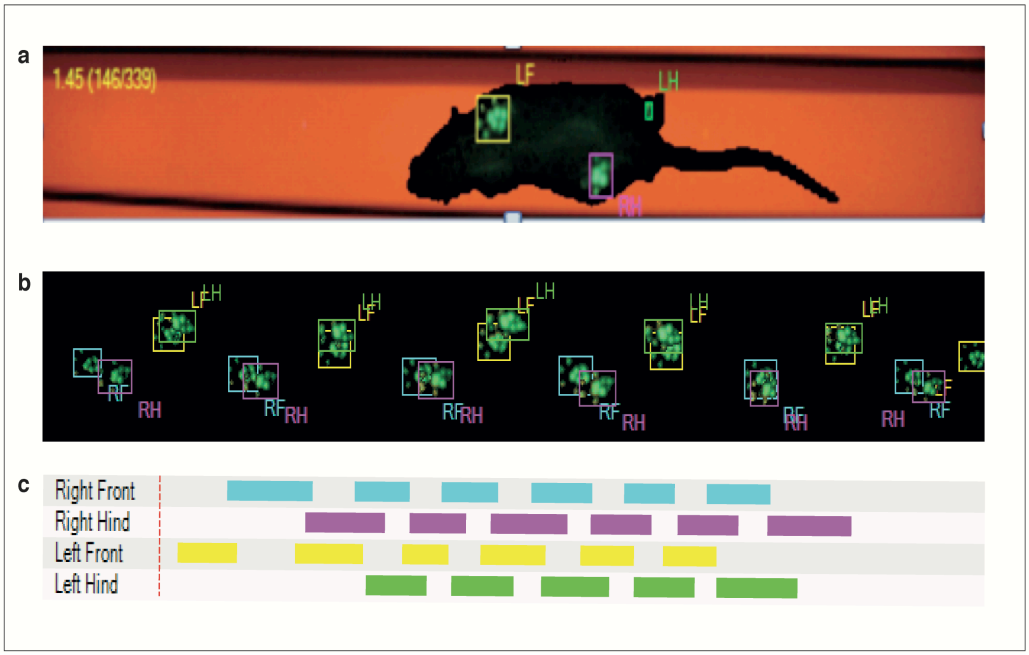

Figure 2.3. Catwalk Gateway System overview a) The rat walks through the illuminated platform (green and dim red light) while a high-speed video camera connected to the computer system is recording the run from below the platform. As the animal places its paws on the platform, these become illuminated with green fluoresce and the computer detects each paw. **b)** The Catwalk software recognizes each paw, and labels it accordingly left hind-paw, right hind-paw, left front-paw and right front-paw and produces a running pattern which each paw. The green luminescences of the paws are further analysed in order to produce different gait parameters. c) The catwalk software also process a stance pattern in order to measure the number of seconds a specific paw spent on the platform. Every paw is assigned with a colour. (All images obtain from Catwalk experiment reported in Chapter 3).

2.3.4. LABORAS

2.3.4.1. Overview of LABORAS

LABORAS (Laboratory animal behaviour observation registration and analysis system) is a system that allows the automatic recognition of a range of normal and special behaviours of rats. Animals are placed on a cage (that resembles their home cage), which is hold at a fixed position on top of a platform. This platform is able to measure the vibrations and forces evoked by the movement of the animal and determinates both behaviour and position in the cage. In addition, the LABORAS software provides information how much time the animal spends carrying different types of behaviour as well as information on movement and speed **(Figure 2.4)**.

2.4

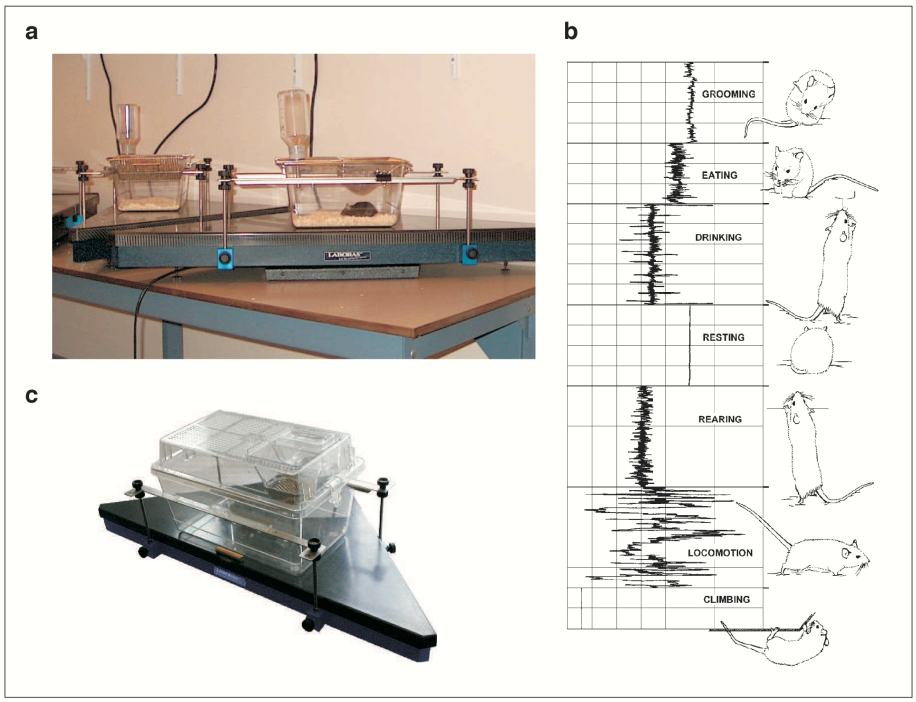

Figure 2.4. LABORAS system. **a)** Animals are housed individually in cages that resemble their home cage and contain a wood chip bedding as well as access to food and water for 20h. The cages are housed at a 12h:12h light/dark cycle. **b)** The LABORAS platform is connected to the computer, which reads the vibration of the platform and assigns them to specific behaviours giving 1h bin measurement of either the time or frequency, spend for each behaviour. **c)** View of the cage, which the animal is housed in, fixed on top of the LABORAS platform. (Images taken from LABORAS, Metris B.V. brochure).

2.3.4.2. Protocol for LABORAS

For this study 12 MIA animals and 6 Sham animals were used. These were the same animals as used for the CatWalk Gateway measures. Animals were habituated 2 days prior to baseline recordings. For habituations, animals were placed into LABORAS clean cages containing wood chip bedding, food pellets and water for 20h, as they would on the day of the experiment. The LABORAS cages were on a 12 hour: 12 hour light/dark cycle at a constant temperature (20-22°C) and humidity (65-75%). After habituation animals were placed back into their home cages.

On the day of the experiment cages were cleaned, placed into the platforms and calibrated. Once calibrated weights of each animal were typed into the LABORAS software in the computer and animals were placed into each corresponding cage. The experiment started at 14:00h and lasted 20h until the following day at 9:00am. Only BSU staff and experimenter were allowed to enter the room to check on the

animals to minimize vibrations that could affect the experiment. After the experiment finished animals were placed back into their home cages in groups of 4. The LABORAS software analysed the different parameters in 1h bins over the course of 20h and when data was exported from the computer it was separated between light and dark cycle. Dark cycle measurements were taken over the course of 13h (From 18:00-6:00), while light cycle measurements were taken over the course of 7h (14:00-16:00 and from 07:00-09:00). Measurements were taken at baseline (before MIA/Sham-injection) and at days 2, 4, 7 and 14 post-MIA or Sham-injection.

The total of specific behaviours per animal were plotted per cycle. For example for Grooming Frequency, total grooming frequency for each animal in dark cycle (18:00-6:00) was calculated by summating total grooming frequency activity per hour (18:00-6:00). This was calculated for each time point (baseline, post injection day 2, day 4, day 7 and day 14). An average of total grooming frequency/animal was then calculated and plotted. For further information on how data was analysed for each parameter please refer to the methods section of Chapter 3.

2.3.5. Pharmacology and Behavioural Assessments

Paw withdrawal thresholds and weight bearing measurements were used in order to address the effects of a specific drug (TROX-1, refer to Chapter 4 for further details) or vehicle in the MIA rat model of OA. All behavioural measurements were performed while experimenter was blind to treatment but not to the injury state. Rats were first habituated to the equipment as described in sections 2.3.1. and 2.3.1. Once habituated controls responses (baseline) were recorded and then animals were dosed intraperitoneally with either vehicle (10% DMSO, 5% cremophor and 85% saline) or 20mg/kg of TROX-1 in a volume of 1.2mL (please refer to Chapter 4 for further information on the specific experiment and drug). Each animal received the same volume of drug, thus concentrations were calculated for each animal based on their weight on the day of the experiments

Mechanical sensitivity was tested by using the up-down method previously described by (Chaplan et al., 1994a) with von Frey forces of 1.4g, 2g, 4g, 6g, 8g, 10g and 15g. Test began with 6g vF and the next filament was chosen depending on the response of the animals. If the response was positive (animal withdraw to the filament) test continue by using 4g vF. However if the response was negative (animal did not withdraw) the 8g vF was used. Four further filaments were applied increasing or decreasing the weight, following the direction of the responses. Four animals were

tested at a time. Test began by applying the vF filaments to the ipsilateral paw of the first animal, then the ipsilateral side of the second animal, third and fourth. Then the contralateral paw of the fist animal was tested following the contralateral paw of the second animal and so on. 50% paw withdrawal thresholds (50 % PWT) were calculated using the following formula: PWT = (10^(x + kδ)/10,000). In the formula, x represents the log of the last von Frey tested, δ represents the mean difference between the von Frey filaments in log units (0.17) and k, a value dependent on the series of responses.

2.4. In-vivo electrophysiological recordings from dorsal horn neurones

2.4.1. Set-up

In-vivo electrophysiology experiments were preformed following the same protocol previously described (Urch and Dickenson, 2003). Animals were briefly anaesthetised in a Perspex induction box with 4% isoflurane in a gaseous mix of 3:2 ratio of nitrous oxide and oxygen. Once animal showed loss of reflexes, they were transferred to a nose cone, laid in a supine position on top of a heat blanket and isoflurane was lowered to 3%.

Trachea was then exposed through a blunt dissection of the surrounding muscles in order to perform the tracheotomy. Once exposed, a transverse incision was made into the trachea and a polyethylene cannula was inserted. Cannula was then secured with 3-0 silk threads and connected to the anaesthesia circuit. This allowed the constant delivery of isoflurane for the reminder of the experiment. Rats were then placed into a stereotaxic frame with their head secured by ear bars. A homeothermic heath blanket was placed under the animal's ventral side. The blankets temperature was linked to a rectal probe that allowed to maintain the animals body temperature constant at 37°C.

Laminectomy was performed under 2.5% isoflurane. A longitudinal incision was made into the skin along the vertebrae to get a better exposure of the spine. Two smaller incisions were then made on either side of the vertebra above of L1-L3 lumbar segments in order to clamp the vertebra tightly and secure it to the stereotaxic frame. Connective and muscular tissue surrounding the lumbar region was removed and a laminectomy was performed in order to expose L4-L6 segments of the spinal cord. The dura was removed with fine forceps. Once segments were exposed, two smaller incisions were made caudal to the exposed spinal cord allowing a second spinal clamp

to tighten the cord. Having the clamps into place allowed the spinal cord to be levelled on all axes. In addition the muscular, connective tissue and bone left around the exposed segments created a natural well that allowed the topical application of drugs for pharmacological studies. Anaesthesia was then lowered to 1.5% and maintained for the reminder of the experiment.

2.4.2. A guide to the recording system

Recordings of neuronal evoked activity of lamina V/VI wide dynamic range (WDR) neurones with an AC recording system (NeuroLog System, Digitimer, UK). A parylene coated tungsten microelectrode (125μm diameter, 2MΩ impedance, A-M system Inc., USA), inserted into a head stage fixed to a micromanipulator that allows for the electrode to be moved up and down as well as sideways. One the electrode is in the head stage; the micromanipulator is lowered from the surface of the dorsal spinal cord allowing the electrode to penetrate the cord to the deeper laminas (500-1500μm). In order to perform an extracellular recording a single WDR neuron has to be isolated and electrode needs to be inserted close to the central blood vessel on the ipsilateral (injured) side. Hind-paw is then gently tapped in order to stimulate the neuron and electrode can be moved up or down accordingly until the neuron is isolated.

In order to be able to read the neuronal signal and exclude both the interference of the recording system and the animal's body, two leads are used. The first lead is attached to the stereotaxic frame and lead ("B") is attached to the animal's body and subtracted from ('A'). Lead ('A') corresponds to the electrode. The neuronal signal needs to be amplified, filtered and displayed in the oscilloscope, for that a series of modules are required in the recording system **(Figure 2.5)**.

The head stage is connected to the AC Pre-Amplifier (Amp), which amplifies the neuronal signal and its gain is set at 5k. The AC Pre-Amp is then connected to the AC-DC Amp, which amplifies the neuronal signal to 62000 (Gain 100; 1.4 gain; 5K gain of the A.C. PREAMP = 62000k). Two different band pass filters allow us to set our frequency (Hz) in order to pick up action potentials with a good signal-to-noise-ration. The low frequency filter is set at 1.5 kHz, while the high frequency filter is set 2 kHz. The filter is then connected to the oscilloscope in order to visualize the neuronal firing pattern. Additionally, the Audio Amp is connected to the speaker and allows for the neuronal signal to be heard. The filters also connect to the spike trigger and this sends outputs to both the oscilloscope and the CED 1401 Interface, which is coupled to Spike2 software (Cambridge Electronic Design, UK). Spike trigger allows for

manipulation of the aperture, which decides the capture of the correct width of the action potential. In addition, adjusting the window height is used to determine if a single neuron is being counted. When dots appear on the oscilloscope screen and the consecutive spikes have the same amplitude and shame, it is presumed a single neuron is being recorded **(Figure 2.5)**.

2.5

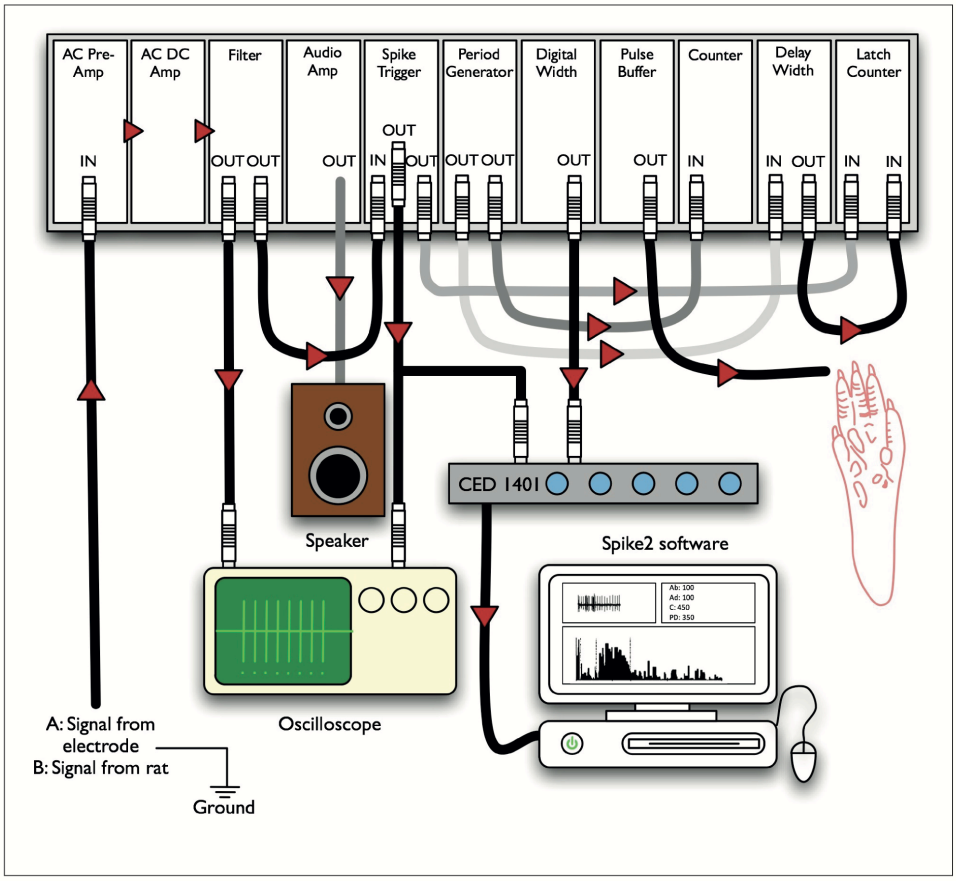

Figure 2.5. Overview of the NeuroLog System and its modules. In order to read the neuronal signal and exclude both the interference of the recording system and the animal's body, two leads are used. Lead ("A") is the signal from the electrode and lead ("B") is attached to the animal's body. These are fed into the head stage and the head stage connects to the NeuroLog system. Once the signal is send to the NeuroLog it becomes amplified and filtered and outputted both into the audio amplifier and to the oscilloscope. This allows hearing and visualizing action potentials. For electrical stimulation, the pulse buffer is in charge of delivering the 16 train pulses to the receptive field, in this case the animals hind-paw. The period generation controls the frequency of the signal while the delay width and delay/width modules control the duration of the pulse. The spike trigger outputs into the latch counter, which display the cumulative number of action potentials, evoked during electrical stimulation. The evoked action potentials are captured by the CED 1401 and separated according to latency by the Spike2 software. Results are displayed in the computer screen. (Diagram produced by Dr. Ryan Patel).

For electrical stimulation a series of modules are required to generate the signal: The frequency of stimulation, duration, amplitude of the current and number of pulses delivered are set by the period generator, the digital width, the pulse buffer and the counter. The period generator outputs into the delay/width module and this allows us to set a 2s delay between each pulse (i.e 0.5 Hz) that we want to consecutively deliver. In addition, it also outputs into the counter, which is set at 16 pulses, allowing the signal to stop after the pulses have been delivered. The action potential input generated by the spike trigger outputs into the latch counter. The number of action potentials evoked will be displayed on the latch counter as well as on the computer. The pulse buffer determines the amplitude of the stimulation and this is always set at 3 times the C-fiber threshold in order to ensure we obtain C-fiber stimulation. The pulse buffer outputs into the isolator box, which allows the signal to be, send through the stimulating electrodes to the receptive field of the hind-paw causing the electrical stimulation of the neuron. Once a single neuron has been isolated and identified we can proceed and record the neuronal evoked responses to electrical, dynamic brush, mechanical and thermal stimulation of the receptive field **(Figure 2.6)**.

2.6

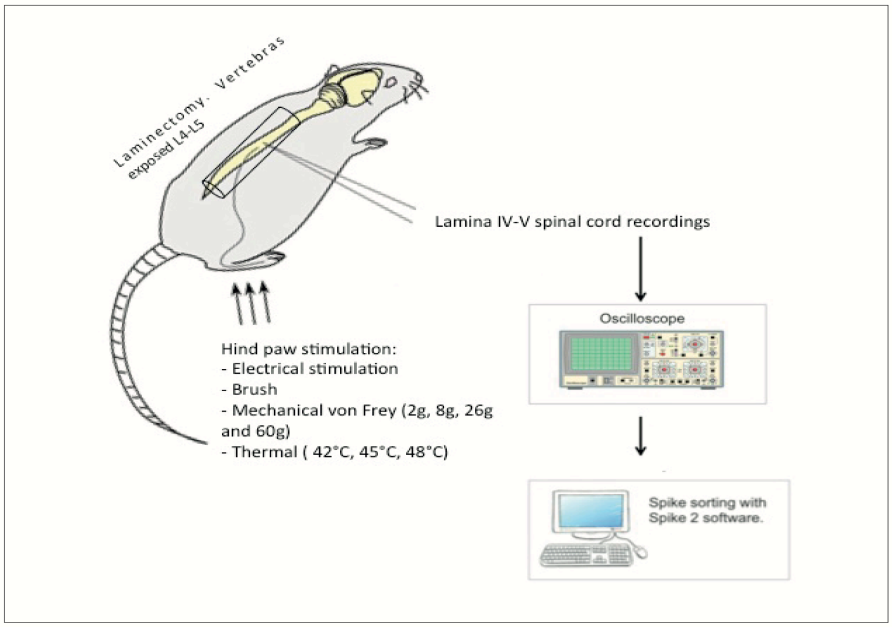

Figure 2.6. *In-vivo* electrophysiology set-up. Extracellular single cell WDR neuronal recordings in lamina IV-V of spinal dorsal horn are performed in anaesthetized animals that underwent laminectomy surgery. Once neuron is found and isolated neuronal evoked activity is recorded. Different modality stimuli are applied into the receptive field (electrical, dynamic brush, mechanical and thermal) in this case the hind-paw of the animal. Neuronal evoked responses are processed by the NeruoLog (**Figure 2.5),** shown on the oscilloscope and presented in the computer through the Spike2 software. Three consecutive baselines are recorded for each modality stimuli in order to obtain a baseline average response before pharmacology experiments are carried out.

2.4.3. Electrical evoked responses

On isolating a single WDR neuron electrical stimulation of these was delivered via needles into the receptive field allowing a constant current to transcutaneously activate sensory afferents that innervate that region without causing tissue damage. Threshold for Aβ and C-fibers were determined by delivering a single stimulus and observing at what point action potentials were generated. Once the threshold had been set a train of 16 consecutive stimuli was applied at three times the C-fiber threshold and the C-fiber evoked response was counted. Each stimulus was delivered at 0.5Hz at 2ms pulses.

During the 16 pulses a post-stimulus time histogram (PSTH) was generated on spike 2 allowing the response to be analysed and separated based on **latency (Figure 2.7a)** . Thus responses recorded at 0-20ms were classified as Aβ responses, 20-90ms to Aδ, 90-35ms to C-fibers. All neuronal response occurring after C-fiber latency (350-800ms) were classified as Post-discharge (PD) **(Figure 2.7a)**. Electrical stimulation allowed us to then calculate the input and wind-up for the isolated WDR neuron. The input is the theoretical non-potentiated response, meaning the firing response of the neuron we would expect if the response would not change during the course of the experiment **(Figure 2.7b)**. It can be calculated by the following formula. Input = (number of action potentials evoked on the first pulse) x total number of pulses (in this case 16). The wind-up can be calculated by subtracting the Input from the total number of action potentials obtained after the 16 train stimuli **(Figure 2.7b)**.

2.7

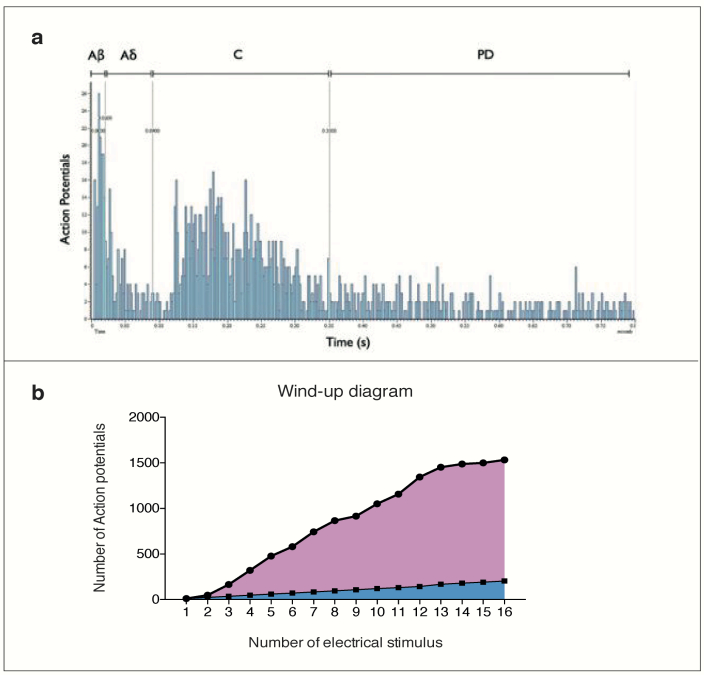

Figure 2.7. Electrical stimulation of WDR neurones. a) Histogram of electrical evoked responses showing the number of action potentials fired by each of the primary afferents separated by time. The computer is able to detect which action potentials corresponds to what type of fiber based on their conductance velocity. Aβ fibers are the first to become activated and have the quickest conductance, thus will be the first to arrive. Neuronal activity that continues after stimulation has cessed corresponds to the post-dischatge (PD) **b)** Area in blue shows the Input, which is the non wind-up predicted response to the electrical stimulation. The area in purple is the wind-up, which is the potentiated neuronal response after repetitive stimulation.

2.4.4. Natural evoked responses

Natural stimuli were also applied into the receptive field of the animal and responses to these were recorded during 10s by the computer **(Figure 2.8)**. Dynamic brush was used to measure innocuous evoked responses. Mechanical punctuated stimuli were measured by applying calibrated von Frey filaments (Touch-Test, North Coast Medical, USA) of different weights (2g, 8g, 26 and 60g). Higher weight filaments (26 and 60 g) allowed to record supra-threshold responses that cannot be measured during behaviour. Thermal responses where measured by applying jets of water through a syringe fitted with a (21g needle) of temperatures 42°C, 45°C and 48°C into the receptive field. Natural stimuli were applied in the following order dynamic brush, mechanical and thermal. Within each modality, stimuli were applied from lowest to highest intensity with gaps between stimuli that allowed neuron to stop firing before

next stimulus was applied and neuronal traces were obtained with Spike2 software **(Figure 2.8**).

2.8

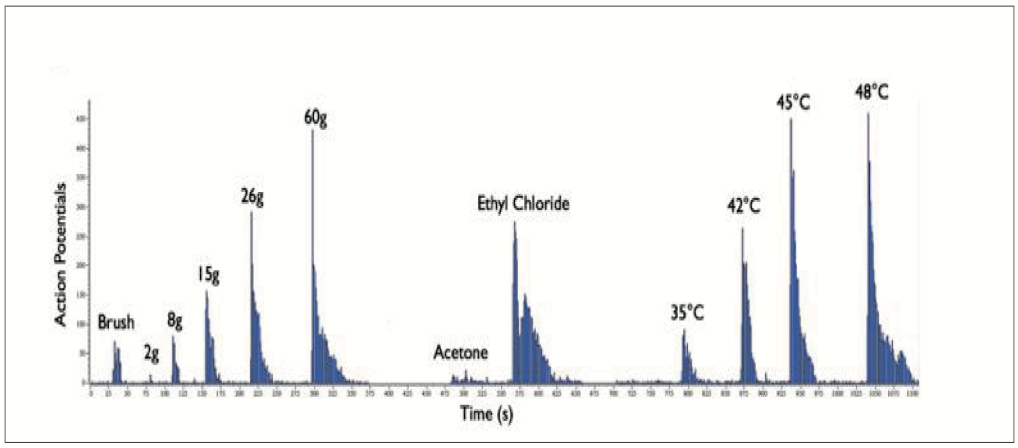

Figure 2.8. Neuronal traces of natural evoked stimuli. Histogram traces of single unit responses of WDR neurons to dynamic brush, mechanical, cold and thermal heat stimulation of receptive fields. Stimulations are carried for 10s and neuronal activity is recorded. Recorded by Spike2 Software and displayed in computer screen. (Image produced by Dr. Ryan Patel)

2.4.5. Drugs

Detailed description of drugs used, the dosage chosen, pharmacology and administration route are described in the methods section of each individual chapter.

2.5. Knee Histology

After in-vivo electrophysiological experiments, knees were dissected post mortem from early and late stage MIA and sham animals in order to assess cartilage damage severity. While dissecting, tissue around the joint area was carefully removed. Tibia and femur were left almost intact. After dissection, knees were placed in a 50mL falcon tube and left in 4% paraformaldehyde (PFA, pH=7) for 28-48h. Each knee was given a code in order for experiment to be blinded and tubes were labelled with the code. Following fixation, tissue was washed with dH_20 and dehydrated following a series of ethanol washes (30% ethanol for 30min, 50% ethanol for 30min and 70% ethanol.) Knee samples could be stored in the fridge at 2°C for a long period of time while collecting more knees or process could be continued straight away.

2.5.1. Decalcification

Decalcification process started by rehydrating the knees with a sequence of washes in ethanol (50% ethanol for 1h, 30% ethanol for 1h) following a wash in dH_20 water. Knees were then placed in EDTA (100g EDTA, 5g NaOH in 1L of dH_20) at pH= 7.4 and left for 12-15 days. EDTA was replaced with fresh one every 5 days and knee bone consistency was checked in order to see if they were decalcified. Once decalcified, the knees acquired a soft, gummy texture. In addition knees were scanned on microCT (SkyScan 1172) to check if decalcification had been completed.

2.5.2. Embedding in wax

Once decalcified knees were first rinsed in ddH_20, dehydrated again as described in section 2.5. They were then placed in individual cassettes and processed overnight in a Tissue-Tek® VIPTM (Vaccum Infiltration Processor, Sakura, USA) machine in a protocol that involved a series of ethanol and wax washes. Knees are first washed in 70% Industrial Methylated Spirits (IMS) for one hour, followed by a 90% IMS wash for an other hour, then four consecutive washes with 100% IMS for 90min each, two consecutive Xylene washes for 90min each, two more Xylene washes of 105min each and finally a one hour wax wash followed by two wax and vacuum steps for one hour each.

Following overnight processing, knees were taken out of the cassette and placed in individual plastic moulds labelled with the knee code. The orientation of the knee in the mould is crucial, as the wrong orientation will affect the cutting during sectioning of the knee. The patella has to be placed facing down, the tibia needs to be perpendicular to the front of the mould and the femur has to be sticking upwards. Once knee were in the mould in the correct orientation, the mould is then filed with paraffin, left to cool and placed in the fridge until used for sectioning.

2.5.3. Slicing

Moulds contained the knees embedded in paraffin were taken out of the fridge and opened releasing the block of paraffin. The block was then placed in a microtome (Microtome HM 360) with the tibia parallel to the blade in order to start sectioning. A sterile blade was used to cut the section starting at a 15μm thickness in order to trim the

excess wax until the knee joined started to be visible. Thickness was then changed to 6µm and sections started to be collected in ribbons and placed orderly in black paper mat. The slicing room was kept at 17°C in order to keep the wax blocks cool. Around 400 sections were collected per knee sometimes more in order to assure the whole knee had been sliced. Ribbons were then cut in groups of 3-4 sections and placed in a 45°C water bath allowing them to flatten and straighten. 3-4 sections were then picked up on a superfrost plus slide (ThermoFisher) and they were then left to dry in 37°C oven in order to stick to the slide

2.5.4. Staining

In order to visualise the cartilage, slides were stained with Toluidine Blue (0.1%ToluidineBlue: 0.1g in 100ml of acetate buffer), which consists of submerging the slides in a series of solutions for specific period of time.

Toluidine blue is a cationic dye that stains proteoglycans and glycosaminoglycans. It has a high affinity to the sulphur present in cartilage allowing the staining of the cartilage matrix and nuclei in a deep violet colour while staining the cytoplasm and rest of the tissue in various shades of dark blue.

Every 3rd slide from each knee was selected and placed in a plastic rack. Solutions used for Toluidine blue staining were poured into crystal containers and placed next to one another in the order of staining. An important step to notice was that the solution fully covered the rack of slides to ensure they were going to be stained properly. Racks were then placed on each crystal container for specific time and moved onto the next container until staining was finished. **Table 3**. shows the steps followed in the staining. Xylene containers were located in a fume hood to prevent inhalation of toxic fumes. After staining procedure, slides were mounted with coverslips (22mm x 70mm, 0.17mm thickness. Thermo Scientific) using DPX in order for coverslip to attach to the slide and left to dry overnight at room temperature.

Table 3. Order and staining time of solutions for Toluidine blue staining of knees.

SOLUTION	TIME
NeoClear	10min
NeoClear	10min
100% IMS	1min
100% IMS	1min
90% IMS	1min
70% IMS	1min
50% IMS	1min
dH20	1min
Acetate buffer (pH 5.6 combine: 20ml acetic acid + 180ml sodium acetate).	1min
Toluidine blue	2min
dH_20	2min
Acetone	2min
Acetone	2min
Xylene	5min
Xylene	2min
Xylene	Mount with DPX

2.5.5. Grading

In order to address the cartilage damage present every third slide per knee was stained and one section from each slide was scored. OA severity score was measured using the Osteoarthritis Research Society International grading system (Gerwin et al., 2010). Figure 2.9 shows the different examples of damage present to the articular cartilage and assigns a OA severity score. Slides were analysed under a Zeiss light microscope at a 10x magnification. Each condyle (lateral femur, medial femur, lateral tibia and medial tibia) was given a score. Cartilage degeneration score in each condyle is scored from none to sever with numerical values (0-6, with 6 being the maximum score) details for each grade are explained below (Figure 2.9):

Grade 0: Normal articular cartilage (AC) surface
Grade 0.5: loss of toluidine Blue staining but no lesions
Grade 1: lesions in the superficial zone of the AC
Grade 2: lesions down to the intermediate zone
Grade 3: lesions down to the tidemark with or with or out possible loss of AC up to 20% of the surface of the condyle
Grade 4: loss of AC tissue from 20% to 50% of the condyle surface
Grade 5: loss of AC tissue from 50% to 80% of the condyle surface
Grade 6: more than 80% loss of surface and/or exposed subchondral bone

All scoring was done blinded and carried out by two different experimenters. For each knee, the lesion with the highest score determined the OA maximum score. Additionally, maximum score per slide was also recorded for every knee and average was plotted per group (early stage MIA, early stage sham, late stage MIA and late stage sham). Image acquisition was done with an Axios Scan (Zeiss) set at bright field at 2.5x magnification.

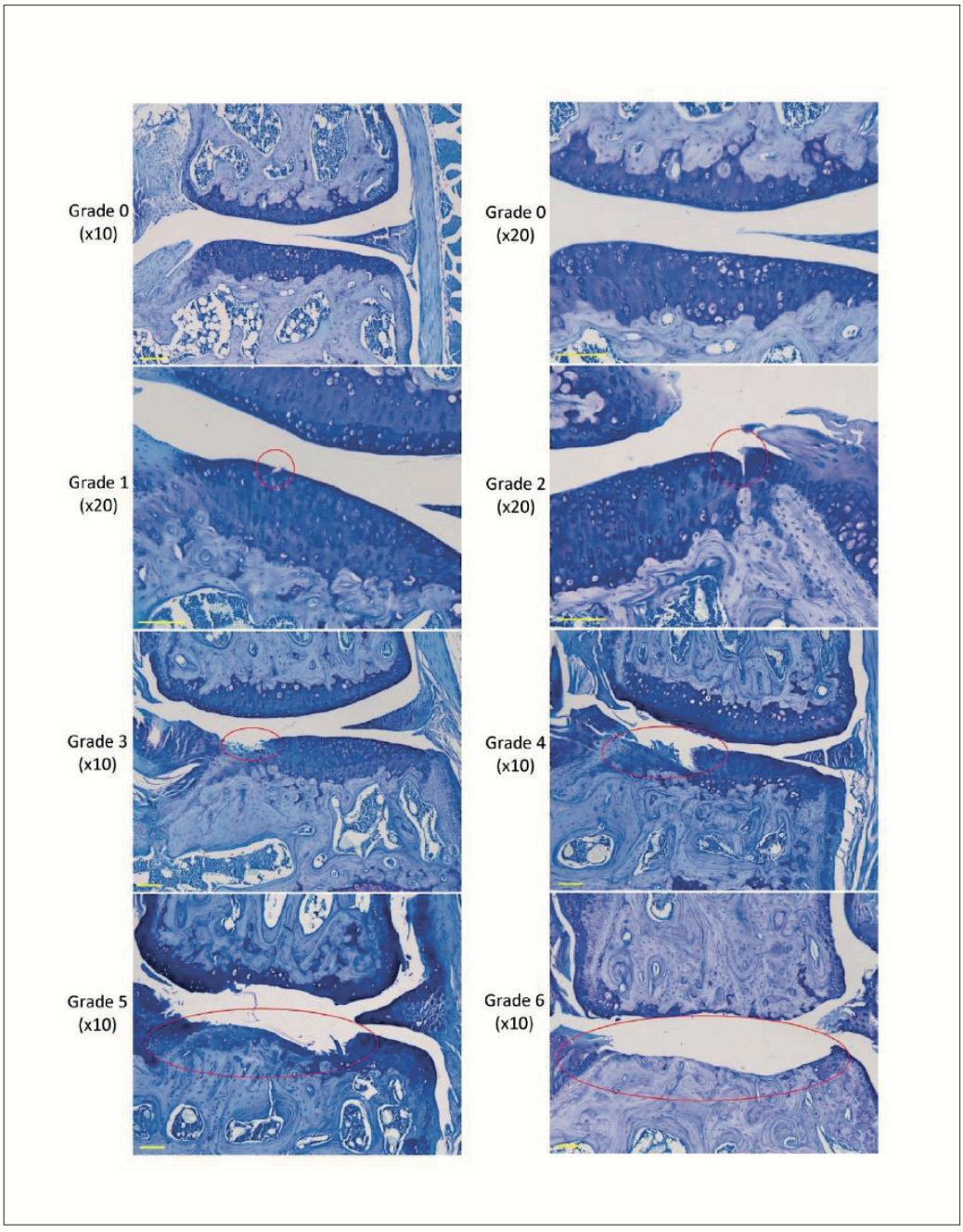

Figure 2.9. Grades of articular cartilage degeneration in knee joint. The following image shows microscopic pictures (x10 magnification) of toluidine blue stain sections of knee joint with different cartilage damage scores. The cartilage is intact in grade 0 while damage starts to appear in the other grades. The red circles represent the damage observed in the other grades. (Image taken from (Lockwood, 2018)).

2.6. Cytokine Profile in serum in the rat MIA model of osteoarthritis

2.6.1. Blood extraction

Blood extraction of MIA animals took place at baseline (before MIA injection) and days 4, 7 and 14 post MIA-injection. In order to extract blood animals were first placed in a – chamber in order to get their blood flowing. Blood was extracted from their tails by the examiner while another member of the team restricted the rats. Blood was collected into 1.5mL microcentrifuge tubes and labelled with date and animal number. Each blood samples was mixed by slow inversion of the tubes and these were immediately placed in ice.

The next step was to separate the plasma from platelets in each animal sample. First, the whole blood samples were centrifuged for 15min at 200g at room temperature (21°C). The supernatant was then collected and transferred into a new labelled 1.5mL tube. For each supernatant a volume of 1mL was expected for a 250-300g rat. Once the supernatant was in the newly labelled tube it was centrifuged for 10min at 2100g at 4°C. The new supernatant represents the platelet free plasma and it was carefully removed and placed in a separate 1.5mL tube and labelled Plasma and animal number. The original 1.5mL tubes containing the pellets are inverted on a tissue to let all the liquid out and then it was re-suspended in a 50µL PBS + 0.01%EDTA solution.

For the plasma tubes, volume of each plasma collected was measured and the protease inhibitory cocktail (PIC) (Sigma P834) was added to a final concentration of 2%. For the platelets tubes a volume of 1 µL of PIC was added. Samples were stored in a -80°C freezer until samples of all animals at all time points were collected and then send for reading.

For PBS + 0.01%EDTA solution

- For a 100mL
  - 10mg of EDTA (Sigma EDS)
  - 100mL PBS Buffer (PBS tablets, Sigma P4417)

2.6.2. Cytokine profile reading

The principle of the MSD multi-spot assay system is a rapid method that allows measuring protein levels with a single, small sample volume. Essentially the assay is a sandwich immunoassay. The multi-spot assay is carried out in a 96-Well 10-spot MULTI-

SPOT plate **(Figure 2.10)**. Each well is pre-coated with capture antibodies, the user adds their sample and a solution containing detection antibodies conjugated with an electrochemiluminescent label (MSD SULFO-TAG™) over the course of several incubation periods **(Figure 2.10)**. The analytes in the sample will then bind to the capture antibodies that are immobilized on in the pre-coated wells on top of a working electrode **(Figure 2.10)**. The detection antibody will also bind to the analyte completing the sandwich **(Figure 2.10)**. Lastly a buffer is loaded into the wells in order to create the perfect environments for electrochemiluminescence and the plate is then loaded into the MSD instrument. A voltage is applied to the plate causing the conjugated antibodies that have been captured to emit light through their electrochemiluminescent label. The MSD instrument measures the intensity of the emitted light and provides a measure of each analyte present in the sample.

Serum samples loaded into the well were the samples of 9 MIA animals at baseline and days 4, 7 and 14 after MIA-injection. The MSD instrument was able to measure the amount of cytokine levels in serum per animal at each time point. Cytokines measured were the following, IFN-γ, IL-β, IL-4, IL-5, IL-6, KC/GRO, IL-10, IL-13 and TNF-α.

2.10

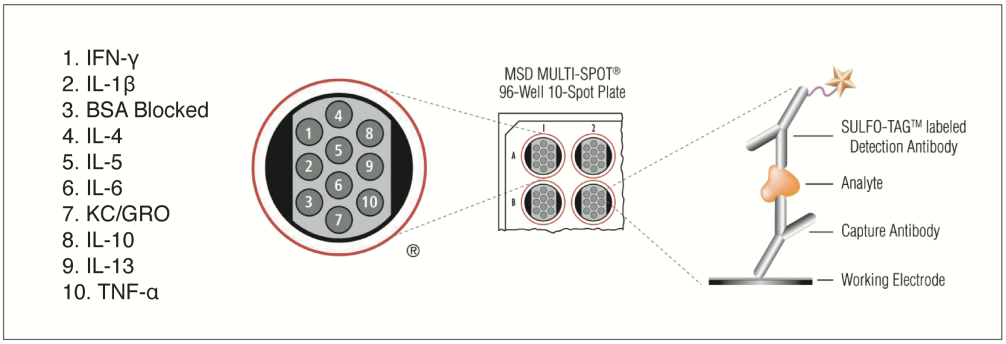

Figure 2.10. MSD multi-spot assay system. The assay consists on a MSD multi-spot plate containing 96wells with 10 spots per well. Every spot is pre-coated with a captured antibody, the serum sample is loaded into each well following by adding a solution containing the detection antibodies conjugated with an electrochemiluminescent label that will emit light once the plate is loaded into the MSD instrument and voltage is applied. The intensity of the emitted light will be measured providing the protein levels present of each cytokine per serum sample. (Figure obtained from Meso Scale website www.mesoscale.com).

2.7. Statistical Analysis

All statistical analysis for all experiments were performed using SPSS v25 (IBM, NY, USA). Detailed information of tests used for statistical analysis of each specific experiment is described in the methods section of each individual chapter.

Chapter 3. Characterization of the rat MIA model of Osteoarthritis

3.1. Introduction

3.1.1. Knee joint pathology in the rat MIA model of Osteoarthritis

The monosodium iodoacetate (MIA) rat model of osteoarthritis (OA) is a chemically induced OA model commonly used to study arthritis-associated pain (Malfait et al., 2013). The model consists of an intra-articular injection of MIA into the rat femorotibial joint space leading to the inhibition of the glycolytic system and resulting in chondrocyte destruction. MIA-induced OA progression is dose and time dependent. Lower doses of MIA (0.1mg-1mg in 25μL or 50μL) have been reported to induce a degeneration of the cartilage matrix, synovial fibrosis, osteophytosis and synovial inflammation (Mapp et al., 2013, Udo et al., 2016, Guzman et al., 2003). Other studies report that a high dose (2mg) MIA-induced OA is characterized by an early acute inflammatory stage while the later stage has neuropathic-pain like features, initiated by nerve damage around the knee joint area (Thakur et al., 2012, Orita et al., 2011).

Several studies have followed the progression of MIA-induced arthritis. Guzman et al. followed the changes that occur in the joint cavity following injection of a lower dose (1mg/50μL) of MIA into the femorotibial joint space of male Wistar rats (Guzman et al., 2003). At day 1 the authors reported chondrocyte degradation, synovial membrane expansion and thickening of the articular cartilage. At day 5 the inflammatory response in the synovium started to subside, the cartilage matrix had collapsed and there was an extensive loss of chondrocytes. By day 7 the inflammatory response had fully subsided and subchondral bone remodelling started to occur. They also reported an increased in the number of osteoclasts present along the junction between the damaged cartilage and the subchondral bone. Fibrosis of the subchondral bone barrow occurred at day 14, followed by its fragmentation at day 28 (Guzman et al., 2003).

Previous work from our laboratory compared the effects of a low dose (1mg/25μL) and high dose (2mg/25μL) MIA on the histological knee features of male Sprague-Dawley rats at different time points (Thakur et al., 2012). Thakur and colleagues observed that at day 7, at both doses, there were no signs of inflammation in the knee joint in line with the Guzman et al data. At day 14 no differences in articular cartilage loss were observed between the two doses. However, in the high-dose group, immunohistochemical studies revealed a significant increased expression of ATF-3 positive neurones in DRG of lumbar regions 4 and 5 at days 7 and day 14, which were

not present with the lower doses (Thakur et al., 2012). Other histological studies using the same high-dose of MIA (2mg/25μL), showed that at day 14 there was a loss of articular cartilage integrity and a moderate to severe reduction in chondrocyte density with the tidemark not visible (Orita et al., 2011). The same study revealed reduction of glycosaminoglycan (GAG) protein levels in both tibia and femur (Orita et al., 2011). Higher doses of MIA-induced arthritis (3mg/25μl) resulted in a subchondral bone 3 and 6 weeks post-MIA injection as well as increased knee diameters and an increase in the number of calcitonin gene related peptide (CGRP)-positive neurones innervating the knee joint is seen (Yu et al., 2013).

Therefore the effects of lower doses of MIA appear to be predominantly characterized by cartilage loss, inflammation of the synovial cavity and thickening of the cortical plate. These changes are also observed in early stages of human OA where there are no changes in the subchondral bone (Ene et al., 2015). However these studies also suggest that in the late stages (day 14 onwards) following injection of high dose of MIA (2mg-3mg) injected animals there may be a neuropathic pain-like component due to the presence of nerve damage in these animals (Thakur et al., 2012). Both the articular and calcified cartilage are aneural structures. However, in the late stages of OA in humans, the calcified cartilage undergoes vascularisation, which is accompanied by small unmyelinated sensory nerve fibres as well as sympathetic nerves. Eventually the calcified cartilage takes over the articular cartilage, lead to the vascularisation and innervation of the latter (Goldring and Goldring, 2016). I would hypothesise that innervation of the cartilage is present in a subgroup of OA patients who describe their pain as containing neuropathic-like features (as seen in animal models). Additionally, it is possible that certain areas of the cartilage have a greater nerve innervation and so are more susceptible to the development of neuropathy.

3.1.2. The role of inflammatory cytokines in OA and in the MIA rat model of OA

During the progression of OA and under the context of inflammation and tissue damage, chondrocytes, synovial cells, and other types of cells can produce and respond to a series of cytokines (Wojdasiewicz et al., 2014). Cytokine levels can change during OA progression, and they can either promote or reduce inflammation or help reduce it (Miller et al., 2014). Pro-inflammatory cytokines contribute to inflammation and cartilage damage and may also activate and excite nociceptive neurones both in the DRG and in the dorsal horn (Miller et al., 2014), thus contributing to pain signalling in OA pathology.

Pro-inflammatory cytokines play an important role in promoting the pathogenesis of OA. Amongst these, tumour necrosis factor alpha (TNF-α) is a key cytokine that

promotes and coordinates inflammation in OA (Wojdasiewicz et al., 2014). TNF-α is synthesized and secreted by chondrocytes, osteoblasts, synovial membrane cells and mononuclear cells that are present in the joint or infiltrate the joint after tissue injury (Wojdasiewicz et al., 2014). The main role of this cytokine is to block chondrocytes from synthesizing proteoglycans and type II collagen. It also increases the production of metalloproteinases (MMPs) and decreases the production of ATP in mitochondria. TNF-a also increases the production of other cytokines such as IL-6 and IL-8 as well as other inflammatory mediators such as COX-2, PGE2 and iNOS.

In human OA patients TNF-α is not increased in serum (Finn et al., 2014, Sohn et al., 2012) but is highly expressed in chondrocytes (Melchiorri et al., 1998) and synovial fluid (Sohn et al., 2012). Thus, most likely in knee OA, TNF-α is only increased locally around the injured area.

High dose (2mg) of MIA coincides with an increase of TNF-α in the knee joint tissue of the ipsilateral injured side is present (Orita et al., 2011). Here the authors reported that the significant increase for TNF-α is present as early as day 1. There is a maximum peak at day 4 followed by a decrease at day 7 that continues until day 28, whereas levels of TNF-α are lower than at day 1 (Orita et al., 2011). However, other studies investigating TNF-α levels in synovial fluid in the same model did not report any significant changes in levels of this cytokine (Finn et al., 2014).

Interleukin-1β (IL-1β) plays a crucial role in promoting inflammation and cartilage destruction by enhancing the expression of other cytokines, chemokines, inflammatory mediators, enzymes and reactive oxygen species (ROS) (Wojdasiewicz et al., 2014). Like TNF-α, IL-1β is produced by chondrocytes, synovial cells and monocytes and is increased in synovial fluid of OA patients. However with regard to serum levels, some studies report an increase of IL-1β in OA patients compared to controls while others do not report this increase (Finn et al., 2014, Sohn et al., 2012). In the MIA rat model of OA, IL-1β levels in synovial fluid do not appear to be increased during MIA progression (Finn et al., 2014). In the same model, in the late stages of MIA, increased mRNA expression levels of IL-1β were observed in the ipsilateral injured side of the spinal dorsal horn (Lockwood et al., 2019b).

Interleukin-6 (IL-6) strongly activates the immune system in order to enhance the inflammatory response and is also involved in OA pathology (Raoof et al., 2018). This cytokine is produced in response to TNF-α by chondrocytes, osteoblasts, macrophages and adipocytes. Its main action is to decrease type II collagen and it produces MMP which induces cartilage destruction and changes to subchondral bone. In human OA patients, IL-6 is increased in both synovial fluid and in serum (Finn et al., 2014). In the MIA rat model of OA, IL-6 is also increased both in serum and synovial fluid. In synovial fluid this increase was observed at day 1, day 10, day 21 and day 28 post-injection (Finn

et al., 2014). Authors observed that IL-6 peaked at day 1 in the synovial fluid, decreased at day 10 and peaked again at day 21 and 28 (Finn et al., 2014). The levels of IL-6 in serum also showed a similar biphasic pattern (Finn et al., 2014). Interestingly this coincided with increased swelling of the knee, which was present at day 1 post-injection followed by a decrease of swelling at day 7 and a second peak increase at day 28 (Finn et al., 2014). Other studies have also reported increased IL-6 levels in knee joint tissue samples of MIA-injected animals but timelines have differed (Orita et al., 2011). In this study authors report an increased IL-6 expression at day 1 and day 4 followed by a decreased, but still significant, expression at day 7,14,21 and 28 (Orita et al., 2011).

Interleukins 4 (Il-4), 10 (IL-10) and 13 (IL-13) have an anti-inflammatory and chondroprotective role in the cells of the articular cartilage and synovium in OA pathology (Wojdasiewicz et al., 2014). IL-4 is secreted by T-cells that infiltrate the synovium through blood vessels under the context of tissue injury, inhibits the secretion of metalloproteinase, pro-inflammatory cytokines and other inflammatory mediators. IL-4 is increased in synovial cell and synovial fluid of OA patients (Schlaak et al., 1996). IL-10 is expressed by chondrocytes and its main role it to stimulate the synthesis of extracellular matrix components such as type II collage and aggrecans. In addition, it also inhibits apoptosis of chondrocytes (John et al., 2007) (Wojdasiewicz et al., 2014). IL-13 has shown to have inhibitory effects on the synthesis of IL-1β, TNF-α and MMPs. IL-10 also decreases the levels of PGE2 and blocks the synthesis of COX-2 (Wojdasiewicz et al., 2014).

3.1.3. A role for microglia in the rat MIA model of OA

Microglia regulate neuronal activity in the spinal cord during the development and maintenance of different chronic pain states (Clark et al., 2007). Increased peripheral nociceptive drive heightens spinal cord activity and excitability, which can lead to activation of microglial cells (Tran et al., 2017). In OA, microglia become active after injury, increasing the release of pro-inflammatory cytokines such as IL-1β and TNF-α (Tran et al., 2017, Eitner et al., 2017).

Several studies have looked at microglial activation in the MIA-rat model of OA. Previous work by our laboratory has reported an increased expression of the microglial marker ionized calcium binding adaptor molecule 1 (Iba1) within the dorsal and ventral horn 7 days post-MIA injection (2mg) (Thakur et al., 2012). Interestingly, in the same model of OA, Orita and colleagues showed that Iba1 expression was only increased in the late stages (14, 21 and 28 days post-MIA injection) but not 7 days post-MIA injection (Orita et al., 2011). Similarly, in MIA-injected mice, increased Iba1 expression and

microglial activation in dorsal horn of spinal cord was only observed 28 days post-MIA injection (Clark et al., 2007). High dose of MIA (3mg) in rats revealed a significant increase in microglial activation on the ipsilateral injured side to the injury in the spinal cord 3 and 6 weeks post-MIA injection (Yu et al., 2013).

One hypothesis is that activation of microglia in the MIA model could appear in the late stages of the disease, contributing to cytokine release in the spinal cord and promoting central mechanisms of hyperalgesia.

3.1.4. Pain behaviour in the rat MIA model of OA

Pain behaviour in the MIA model has been extensively studied. Intra-articular injection of MIA into the knee joint causes a significant decrease in hind-paw withdrawal thresholds in response to von Frey (vF) filaments as soon as 2 days post-MIA injection (Lockwood et al., 2019b, Orita et al., 2011, Rahman et al., 2015, Thakur et al., 2012, Finn et al., 2014, Ivanavicius et al., 2007). Paw withdrawal thresholds have been shown to slightly increase at day 7 and day 8 compared to days 2 and 4, and decreasing again at days 14 and 21 for low (0.5mg) and high (2mg and 3mg) dose MIA-injected rats (Thakur et al., 2012, Ferland et al., 2011, Devonshire et al., 2017, Abaei et al., 2016). Mechanical hyperalgesia and tactile allodynia are present in this model on the ipsilateral injured hindpaw (Liu et al., 2011). Additionally, thermal hyperalgesia is present in MIA-induced OA as well as sensitivity to acetone cooling (Liu et al., 2011, Thakur et al., 2012).

Weight bearing asymmetry has been reported in the MIA model in rats. Weight bearing deficits are present as soon as day 2 post-MIA injection and this is maintained both in early and late stages of the disease (Thakur et al., 2012). The ipsilateral injured side shows a decrease in weight bearing while the contralateral uninjured side shows increased weight bearing (Rahman et al., 2015, Thakur et al., 2012, Yu et al., 2013, Lockwood et al., 2019b, Havelin et al., 2016, Orita et al., 2011, Abaei et al., 2016).

Gait analysis using the CatWalk Gateway system has shown that MIA-induced OA rats exhibit changes in gating parameters. In MIA-induced OA in mice, a decrease in duty cycle, swing speed and print area of the ipsilateral injured side was present 5 days post injection (Miyagi et al., 2017). Similarly, following high doses (3mg/25μL) of MIA, swing speed was also decreased in the ipsilateral hind-paw compared to the contralateral side (Ferland et al., 2011). The same authors reported a decrease in duty cycle of the ipsilateral injected side that returned back to baseline at days 8 and 12 while swing phase was longer for the ipsilateral side but also returned to baseline at day 8 (Ferland et al., 2011). Print paw area measurement in 1mg and 2mg injected MIA-animals was decreased in the ipsilateral side as soon as 3 days after injection, with a slight increase in print paw area at days 6 and 13 that decreases again at day 17-27 (Ferreira-Gomes et al., 2012). Interestingly, this increase in both paw print and duty cycle

at days 7-13 correlates with the increase in paw withdraw thresholds at days 7 and 8. This correlation might be related to the decrease in pro-inflammation observed at the same time point in the same model (Orita et al., 2011). It is shown that, in the early acute inflammatory stage behavioural measurements show hyperalgesia and allodynia which decrease as inflammation ceases and returns in the later stages when neuropathic-pain like features may be present.

Ongoing pain has also been reported in the MIA-induced OA in rats. Conditioned place preference studies where clonidine was spinally administrated in one of the chambers showed that late stage MIA animals (28 days post-MIA injection, 4.8mg of MIA in 60μL saline) spend more time in the clonidine-paired paired-chamber (Kang et al., 2013, Liu et al., 2011). The spinally administrated clonidine reversed ongoing pain in these animals.

3.1.5. Electrophysiological changes in the MIA rat model of OA

During OA pathology, primary afferent fibers innervating the knee joint capsule may become activated and sensitized by release of a series of inflammatory mediators and neurotransmitters, leading to changes in neuronal firing of spinal dorsal horn neurones. In the MIA model of OA electrophysiological changes in spinal neuronal firing can be investigated using electrophysiological recording techniques.

In-vivo electrophysiological recordings of wide dynamic range (WDR) neurones located in the deep (lamina V-VI) layers of the spinal dorsal horn revealed an increase in responses to mechanical punctuate stimuli in the late stages of MIA compared to sham-injected animals (Rahman et al., 2009). Meanwhile, thermal- and dynamic brush-evoked responses of WDR neurones are unchanged between the MIA and sham group (Rahman et al., 2009). The same results were found in MIA-injected mice, where mechanical-evoked neuronal responses appeared to be facilitated compared to sham injected animalsm yet thermal-evoked neuronal responses remained unchanged (Harvey and Dickenson, 2009).

Unpublished thesis work revealed that both early and late stage MIA-injected rats had enhanced WDR neuronal evoked responses to thermal stimuli (45 and 48°C) compared to naïve animals, as well as enhanced responses to 60g vF stimulation (Burnham, 2012). In addition, late stage MIA animals showed increased neuronal evoked responses to 8g and 26g vF compared to naïve animals. Repetitive electrical stimulation of the receptive field (hind-paw) also revealed differences in WDR neuronal evoked responses between early and late groups and naïve animals. Aβ, Aδ and C-fiber

responses were enhanced in both experimental groups compared to naïve animals, while indicators of neuronal excitability post-discharge (PD) and wind-up (WU) were only enhanced in late stage animals compared to naïve. Non-potentiated input (I) was enhanced in both early and late stages compared to naïve group ((Burnham, 2012)).

In contrary to these results, recent work by our laboratory using the same approach has shown that there is no differences in baseline WDR neuron firing in response to mechanical, thermal and dynamic brush evoked stimuli between the early acute inflammatory stage of the MIA model, a later stage with neuropathic pain-like features and sham-injected animals (Lockwood et al., 2019b). Additionally, other unpublished work by our laboratory reported no changes in lamina I nociceptive specific (NS) neurones and lamina V WDR neuronal evoked activity to electrical, mechanical and thermal evoked stimulation between the late stages of MIA model and naïve animals (Thakur, 2012). Overall, these data suggest that changes in evoked neuronal activities for the hindpaw are subtle and not seen in all studies.

Interestingly, while most patients with knee OA develop mechanical hypersensitivity, not all patients develop thermal hyperalgesia (Bevilaqua-Grossi et al., 2019). Some studies have reported lower heat thresholds in such patients while other human studies do not (Bevilaqua-Grossi et al., 2019). This suggests that a cohort of patients develop heat sensitivity while others do not develop it. This could also occur in MIA-induced OA in rat since some *in-vivo* electrophysiological report differences between neuronal evoked responses to thermal heat between MIA and sham animals.

3.2. Chapter aims

The aims of this chapter are as follows (1) to identify any possible differences in cartilage damage scores between early and late stage MIA groups and compare data to shams. (2) To measure changes in levels of various cytokines present in the serum of MIA-injected animals during the course of MIA progression. (3) To assess differences in noxious-evoked behaviours between early and late stage MIA animals as well as to sham groups. (4) To address differences in gaiting parameters in MIA animals as well as differences in naturalistic behaviour of MIA and sham-injected groups. (5) To detect possible differences in neuronal firing patters of lamina V WDR evoked neuronal firing patterns in early stage MIA, late stage MIA and sham groups.

3.3. Methods

3.3.1. Animals

In this study, a total of 43 Male Sprague-Dawley rats, bred by the Biological Service Unit (UCL, London, UK), were used for paw withdrawal, paw frequency, weight bearing and electrophysiological experiments. For cytokine profile, Catwalk Gateway system and LABORAS a total of 19 animals were used. These were bred by the Biological Unit service at the Royal Veterinary College (Potters Barn, UK). Additionally all weights of animals can be found on Appendix I: Chapter 3.

3.3.2. MIA induction

MIA and Sham induction protocol can be found in Chapter 2: Materials and methods, section 2.2

3.3.3. Knee histology

For details on knee histology experiments please refer to Chapter 2: Materials and Methods, section 2.5.

3.3.4. Cytokine Profile

For details on how cytokine profile in serum was quantified please refer to Chapter 2: Materials and Methods, section 2.6.

3.3.5. Behavioural Assessment

Description of each behavioural assessment protocol can be found in Chapter 2: Materials and Methods, section 2.3.

3.3.6. In-vivo electrophysiology

Three consecutive baseline neuronal responses were taken per neuron recorded in early and late MIA-injected and sham groups for all modality stimuli in the following order: electrical, dynamic brush, mechanical and thermal stimulation. One neuron was recorded per animal; therefore the n relative to animal numbers is the same as the n for neuron numbers. The average of the three consecutive baselines was obtained and baseline averages are plotted per group.

3.3.7. Statistics

All statistical tests were performed on raw data using SPSS, version 25 (IBM, Armonk, NY). Additionally all statistical values for these studies can be found in Appendix I: Chapter 3.

For knee histology, two blinded experimenters scored all knees and an average of those scores was obtained. For knee histology statistics, a non-parametric 2-independent samples Kruskal-Wallis test was used to address differences between MIA and sham groups for the average histological maximum knee score and for the average maximum knee score/slide. Differences in condyle average knee histological scores between MIA animals and sham animals were addressed by using a non-parametric 2-indpendent samples Mann Whitney-U test.

Differences in cytokine profile during the course of MIA-induced OA were quantified for each individual cytokine. A paired sampled t-test was used to see differences between baseline and each different time point (day 4, 7 and 14 post-MIA injection).

For behavioural tests, paw withdraw threshold (g), paw withdraw frequency (%), weight bearing, Catwalk gateway and LABORAS measurements a non-parametric related samples Friedman test with Bonferroni correction was used to measure behavioural changes before and after MIA-injection at different time points. For the same behavioural tests, to measure differences between either MIA-sham groups or ipsilateral vs. contralateral paws a non-parametric 2-related samples Wilcoxon test was used.

To address differences in electrophysiological firing rates of WDR neurones between early MIA vs. early sham, late MIA vs. late sham, early MIA vs. late MIA and early Sham vs. Late sham groups, 2 different statistic methods depending on stimulus modality were used. Mechanical and heat coding of neurones were compared using a Multivariate repeated measures test. Dynamic brush and electrical neuronal responses between groups were compared using an independent sample t-test. $*p < 0.05$, $**p < 0.01$, $***p < 0.001$. All data is expressed as mean ± SEM.

3.4. Results

3.4.1. Knee Histology

Knee histological studies were carried out to address the possible damage in the articular cartilage in both early and late stage MIA animals as well in sham animals.

The maximum knee score average represents the greatest score obtained per knee in every group, while the average maximum score per slide represent the greatest knee damage score observed in each group. Additionally, the average score for each condyle (Medial Tibia, Medial Femur, Lateral Tibia and Lateral Femur) was also analysed.

Analysis of early MIA and early sham animals showed no significant difference when comparing the average histology score per condyle (**Figure 3.1e)**. However, Mann Whitney-U test revealed a significant difference when comparing the medial femur (*p=0.017(*)*) and lateral femur (*p=0.008(**)*) of late stage MIA animals with late stage sham animals, while the other condyles were not significantly different (**Figure 3.1f**).

When analysing the maximum knee score obtained per group, Kruskal-Wallis test revealed a significant difference (*p=0.050(*)*). This was followed by paired-comparisons that revealed a significant difference in knee scores between early MIA and late MIA (*p=0.040(*)*) (**Figure 3.1g**). Lastly, no significant difference was observed when analysing the average maximum score per slide for each group (early MIA, early sham, late MIA and late Sham) (**Figure 3.1h**).

3.1

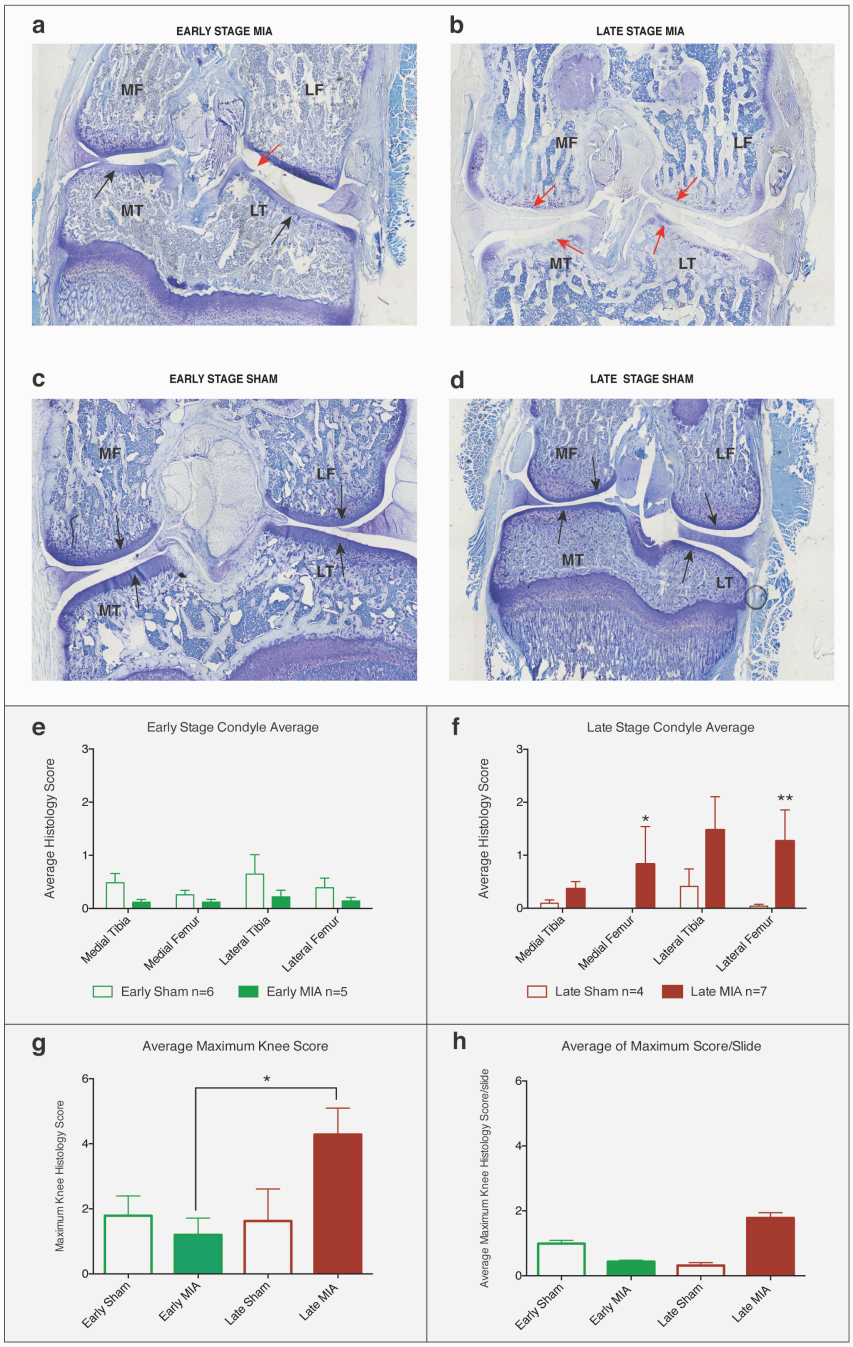

Figure 3.1. Severity of MIA induced OA in rats. **a-d)** Examples of knee histological cross-sections of ipsilateral (left, injured) side of sham and MIA rats. Dark arrows point out the articular cartilage and by assessing changes to this structure, severity scores are assigned to each condyle as explained in method section 2.5. (Medial femur (MF), medial tibia (MT), lateral femur (LF) and lateral tibia (LT)). Red arrows point out the damaged area in the articular cartilage of each condyle.
a) Early stage MIA ipsilateral (injured) knee cross-section. The red arrow shows a damaged area in the articular cartilage of the LT condyle with a damage score of 2. **b)** Late stage MIA ipsilateral (injured) knee cross-section. The red arrow shows a damaged area in the articular cartilage of the LT condyle with a damage score of 4, and additional damage to MF, MT and ML. **c,d)** Both early stage and late stage ipsilateral knee cross-sections of sham rats present little to no damage to the articular cartilage structure, black arrows show intact articular cartilage. **e)** No significant differences were observed in the condyle knee damage score averages between early stage MIA and sham animals. **f)** Both MF (*p=0.017(*)* and LF (*p=0.008(**)*) damage scores of late stage MIA animals were significantly increased compared to damage scores of late stage sham group. **g)** Average maximum damage knee scores were higher in late stage MIA animals (Kruskal-Wallis *p=0.05(*)*; Paired comparison *p=0.04(*)*) compared to early stage MIA animals. **h)** No significant differences were observed for the average maximum damage knee scores per slide.

3.4.2. Anti-inflammatory cytokine IL-10 levels are increased in serum of MIA-injected rats while pro-inflammatory cytokines remain unchanged

Significant differences in the cytokine profile in serum of the anti-inflammatory panel were observed before (baseline) and after MIA-induction in rats (Figure3.2b and c). Anti-inflammatory cytokine IL-4 levels remained unchanged (**Figure 3.2a**). One Way ANOVA test revealed that IL-10 was also significantly increased at day 14 post-MIA injection ($F_{(8,24)}=6.116$, $p=0.0093(**)$, Multiple comparisons with Bonferroni correction $t_{(8)}=5.980$, $p=0.0003(***)$), while at other time points post-MIA injection, levels remained unchanged (**Figure 3.2b**). Lastly anti-inflammatory cytokine IL-13 remained unchanged (**Figure 3.2c**).

In contrast to the anti-inflammatory panel, the pro-inflammatory panel of cytokines IFNγ, TNFα in serum showed no changes before and after MIA-injection (**Figure 3.2d-g**). IL-5 and IL-6 levels in serum were too low to be detected in some rat serum samples therefore no statistical analysis was carried out in this group as the sample number was too low. (**Figure 3.2f and g**). In addition, One Way ANOVA test revealed that pro-inflammatory chemokine KC/GRO also showed increased levels at day 4 ($F_{(8,24)}=4.184$, $p=0.035(*)$, Multiple comparisons with Bonferroni correction $t_{(8)}=3.036$, $p=0.016(*)$) while other timepoints were unaffected **Figure 3.2h**).

3.2

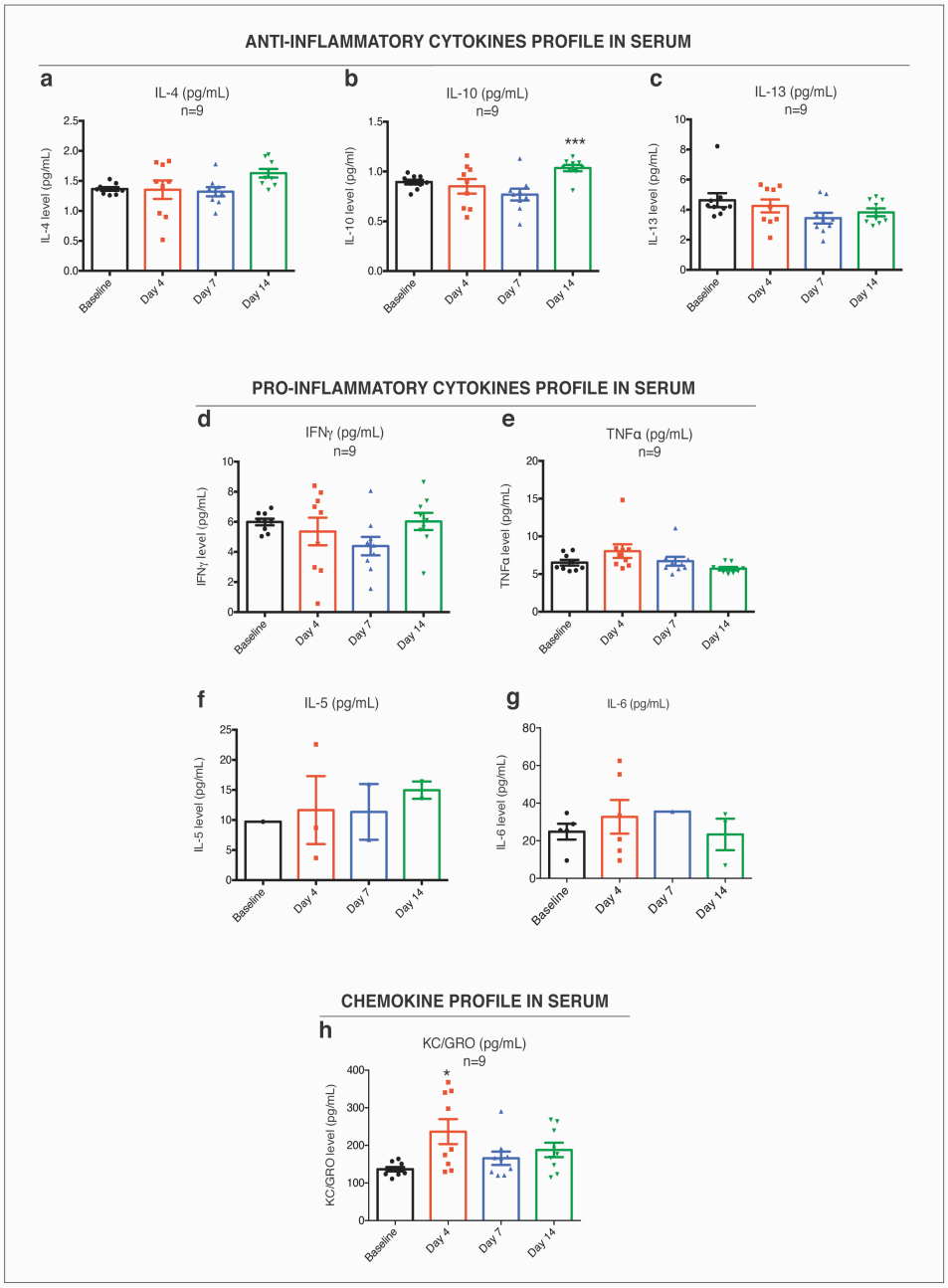

Figure 3.2. Panel of cytokine profile levels (pg/mL) in serum in the MIA rat model of OA. **a)** Cytokine profile panel of anti-inflammatory cytokine IL-4. IL-4 levels in serum remained unchanged at days 4, 7 and 14 post MIA-injection. **b)** Cytokine profile panel of anti-inflammatory cytokine IL-10. IL-10 levels in serum were significantly increased at day 14 post-MIA injection (One Way ANOVA, $F_{(8,24)}=6.116$ $p=0.0093(**)$, post-hoc test with Bonferroni correction $t_{(8)}=5.980$, $p=0.0003(***)$). IL-10 serum levels remained unchanged at other time points. **c)** Cytokine profile panel of anti-inflammatory cytokine IL-13. IL-13 serum levels remained unchanged at days 4, 7 and 14 post MIA-injection.
d) Cytokine profile panel of pro-inflammatory cytokine IFNγ. IFNγ serum levels remained unchaged at days 4, 7 and 14 post MIA-injection. **e)** Cytokine profile panel of pro-inflammatory cytokine TNFα. TNFα serum levels remained unchanged at days 4, 7 and 14 post MIA-injection. **f,g)** Cytokine profile panel of pro-inflammatory cytokines IL-5 and IL-6. Both IL-5 and IL-6 levels in serum were only detected in some MIA rat samples, while in other MIA rat samples the levels of these cytokines were to low to be detected.
h) Chemokine profile panel of pro-inflammatory chemokine KC/GRO. KC/GRO chemokine levels in serum were significantly increased at day 4 post MIA-injection (One Way ANOVA ($F_{(8,24)}=4.184$ $p=0.035**$), post-hoc test with Bonferroni correction shows ($t_{(8)}=3.036$, $p=0.016(*)$)).

3.4.3. Behavioural characterization of the rat MIA model of OA

3.4.3.1. Paw withdrawal thresholds (g) were decreased in the early acute inflammatory stage of the MIA rat model of OA

Paw withdrawal thresholds (g) were measured using von Frey (vF) filaments, before injection (baseline) and at days 2, 4, 7 and 14 after MIA or sham injection. These withdrawal thresholds measured for both ipsilateral (injured) and contralateral (uninjured) hind paws in MIA and sham groups. Analysis of the ipsilateral hind-paw withdrawal thresholds (g) of MIA-injected animals with Friedman two-way ANOVA test and Bonferroni correction showed a significant decrease at day 2 (*p=0.046(*)*) and day 4 (*p=0.049(*)*) post-injection compared to the baseline withdrawal threshold **(Figure 3.3a)**. Interestingly at day 4 post-injection, withdraw thresholds (g) appeared to be the lowest, while at day 7 and day 14 post-injection withdrawal thresholds increased and were not significantly different to baseline **(Figure 3.3a)**.

When comparing ipsilateral (injured) to contralateral (uninjured) hind-paw withdrawal thresholds, Wilcoxon tests showed that ipsilateral hind-paw thresholds were significantly lower than the contralateral ones at day 2 (*p=0.042(#)*), 4 (*p=0.046(#)*) and 7 (*p=0.04(#)*) post-injection **(Figure 3.3a).** Withdrawal thresholds between ipsilateral and contralateral hind-paws of MIA animals were not significantly different at day 14 post-injection.

Paw withdrawal thresholds (g) for the sham-injected group remained unchanged when comparing baseline ipsilateral hind-paw withdraw thresholds to day 2, 4, 7 and 14 post sham-injection (**Figure 3.3b**). In addition, when comparing ipsilateral to contralateral hind-paw sham withdrawal thresholds, no significant difference was found. Lastly, there was no significant difference when comparing ipsilateral withdrawal thresholds (g) of MIA and Sham animals at baseline and post-injection at days 2, 4, 7 and 14 (**Figure 3.3c**).

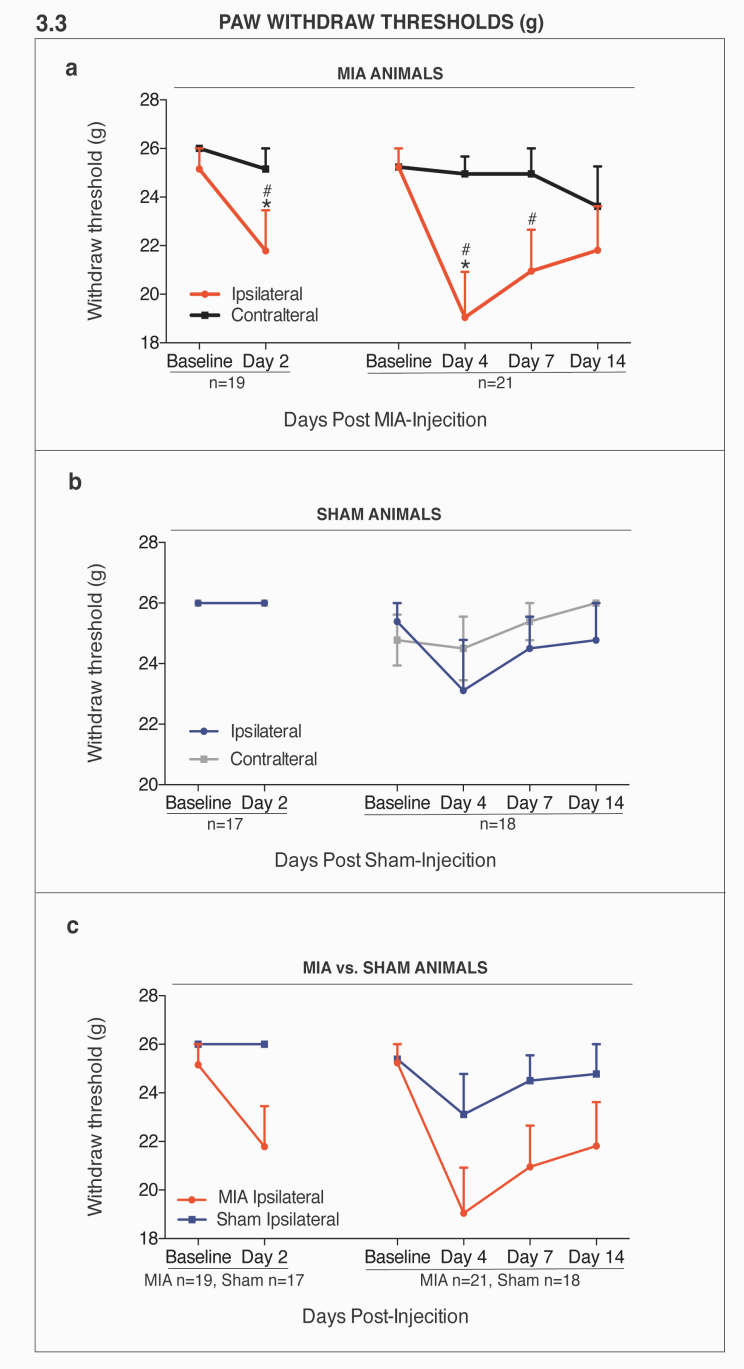

Figure 3.3. Paw withdrawal thresholds (g) of ipsilateral and contralateral hind-paws in MIA and sham-injected groups. a) Paw withdrawal thresholds in MIA animals. Ipsilateral (injured) hind-paw withdrawal thresholds were significantly decreased at day 2 post-MIA injection compared to baseline (Friedman test, p=0.0046(*)). Additionally, a significant decrease was also observed at day 4 compared to baseline (p=0.049(*)). Paw withdrawal thresholds increased at day 7 and day 14 and are not significantly different to baseline. Wilcoxon test revealed significant differences in paw withdrawal thresholds (g) between ipsilateral and contralateral hind-paws at days 2 (*p=0.042(#)*), 4 (*p=0.046(#)*) and 7 (*p=0.04(#)*) post-MIA injection. **b)** Paw withdrawal thresholds in Sham animals. No significant differences in paw withdrawal thresholds (g) were recorded between baseline ipsilateral and any of the time points post-sham injection and no differences were observed between ipsilateral and contralateral paws. **c)** When comparing paw withdrawal thresholds (g) of ipsilateral hind-paws of MIA vs. Sham animals, no significant differences were observed over time.

3.4.3.2. Paw withdrawal frequencies (%) of ipsilateral injured hind-paw were increased compared to contralateral hind-paw in the MIA rat model of OA

No significant differences were observed over time when comparing ipsilateral paw withdrawal frequency (PWF) (%) to contralateral in the MIA group in response to 1g and 4g vF stimulation **(Figure 3.4a,b)**. However PWF (%) of contralateral (uninjured) hind-paw in the MIA group was decreased compared to baseline in response to 10g and 15g vF.

10g vF stimulation significantly reduced contralateral PWF (%) at day 4 (*p=0.03(**)*), day 7 (*p=0.000(***)*) and day 14 (*p=0.006(**)*) post-MIA injection compared to baseline (**Figure 3.4c**). Similarly, 15g vF simulation significantly decreased contralateral PWF (%) at day 7 (*p=0.025(*)*) and day 14 (*p=0.002(**)*) post-MIA injection compared to baseline (**Figure 3.4d**).

When comparing MIA ipsilateral to MIA contralateral PWF (%), a significant increase of ipsilateral PWF (%) to 4g vF was observed at day 4 (*p= 0.01(##)*) and day 14 (*p=0.045(#)*) post-MIA injection compared to contralateral responses (**Figure 3.4b**). After 10g vF stimulation, PWF (%) of ipsilateral hind-paw of MIA animals was increased at days 4 (*p=0.009(##)*), 7 (*p=0.03(#)*) and 14 (*p=0.004(##)*) compared to contralateral responses (**Figure 3.4c**). Lastly, after 15g vF, PWF (%) of ipsilateral hind-paws was significantly increased at days 4 (*p=0.024(##)*), 7 (*p=0.001(###)*) and 14 (*p=0.001(###)*) compared to contralateral hind-paw in the MIA group (**Figure 3.4d**). Supplementary Figure 1 found on Appendix 1: Chapter 3, shows the comparison of ipsilateral paw withdraw frequency (%) between sham and MIA groups.

3.4 PAW WITHDRAW FREQUENCY (%): MIA IPSILATERAL vs. MIA CONTRALATERAL

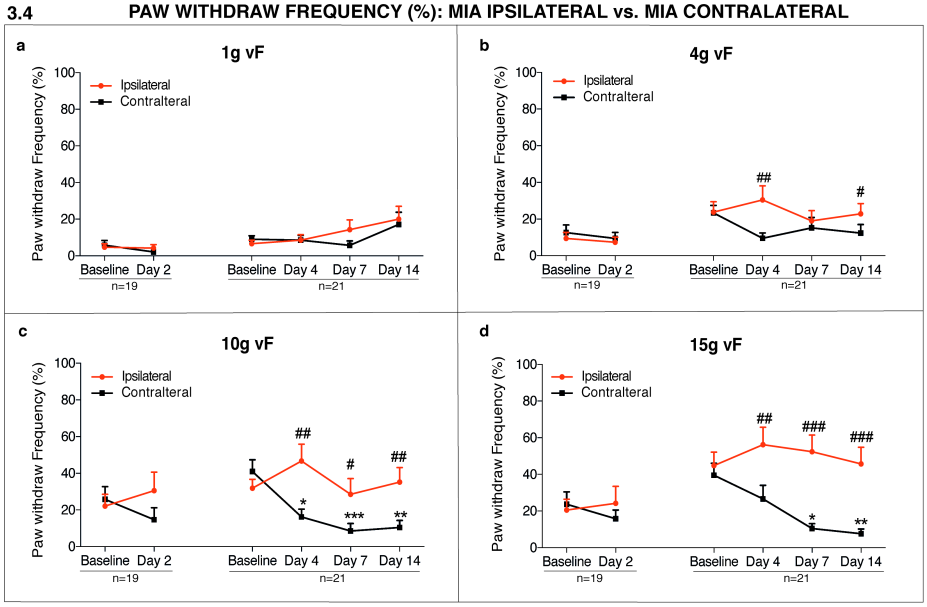

Figure 3.4. Paw withdrawal frequencies (%) of MIA ipsilateral vs. MIA contralateral hind-paws. a) Stimulation of ipsilateral and contralateral hind-paws with 1g vF filament had no effects on paw withdrawal frequency (%). **b)** Stimulation of ipsilateral hind-paw with 4g vF caused a significant increased in paw withdrawal frequency (%) at days 4 (*p=0.01(##)*) and 14 (*p=0.045(#)*) compared to contralateral hind-paw frequency. **c)** Paw withdrawal frequency (%) of contralateral hind-paw was significantly decreased at day 4 (*p=0.03(**)*), day 7 (*p=0.000(***)*) and day 14 (*p=0.006(**)*) compared to baseline after stimulation with 10g vF. Additionally, ipsilateral withdrawal frequency (%) was significantly increased compared to contralateral one at days 4 (*p=0.009(##)*), 7 (*p=0.03(#)*) and 14 (*p=0.004(##)*). **d)** Paw withdrawal frequency (%) after 15g vF in contralateral hind-paws was significantly decreased at day 7 (*p=0.025(*)*) and day 14 (*p=0.002(**)*) post-MIA injection when compared to baseline. Paw withdrawal thresholds of ipsilateral hind-paw were significantly increased compared to contralateral frequency at days 4 (*p=0.024(##)*), 7 (*p=0.001(###)*) and 14 (*p=0.001(###)*) post MIA-injection.

3.4.3.3. Weight Bearing (%) is altered in the MIA rat model of OA but not sham animals

Weight bearing percentages were measured for both ipsilateral and contralateral hind-paws for MIA and sham-injected animals. At baseline both MIA and sham-injected groups exhibited 50% of weight bearing over both ipsilateral (injured) and contralateral (uninjured) hind-paws, indicating that the same weight was used for both hind-paws. After injury, MIA animals exhibited altered weight bearing post-MIA injection (**Figure 3.5**).

Analysis of weight bearing post-MIA injection revealed that animals exhibited a significant decrease of weight bearing (%) in their ipsilateral hind-paws at days 2 (*p=0.02(*)*) and 4 (*p=0.000(***)*) compared to baseline. Post-MIA injection days 7 and 14 were not significantly different to baseline. Additionally, the contralateral uninjured hind-paw exhibited increased wright bearing (%) compared to baseline at day 2 (*p=0.033(*)*), 4 (*p=0.001(**)*) and 7 post (*p=0.023(**)*) post-MIA injection.

Significant differences between contralateral and ipsilateral hind-paw weight bearing (%) at day 2 (*p=0.005(##)*), 4 (*p=0.0002(###)*), 7 (*p=0.001(###)*) and 14 (*p=0.001(###)*) post-MIA injection were observed (**Figure 3.5**).

Sham animals exhibited no differences in weight bearing (%) before and after sham-injection. Both ipsilateral and contralateral hind-paws exhibited 50% to 50% weight bearing (%), indicating that equal weight was used in both hind-paws (**Figure 3.5**).

When comparing both ipsilateral and contralateral weight bearing (%) between MIA and sham groups, significant differences were found on all time points. A significant decrease in ipsilateral MIA hind-paws weight bearing (%) at days 2 (*p=0.003(^^)*), 4 (*p=0.006(^^))*, 7 *p=0.001(^^^))* and 14 *p=0.007(^^))* compared to ipsilateral sham hind-paws was present. Contralateral MIA hind-paws weight bearing (%) was increased also at days 2 (*p=0.003(^^)*), 4 (*p=0.001(^^^))*, 7 *p=0.000(^^^^))* and 14 *p=0.002(^^))* compared to contralateral hind-paw of sham animals at those time points (**Figure 3.5**).

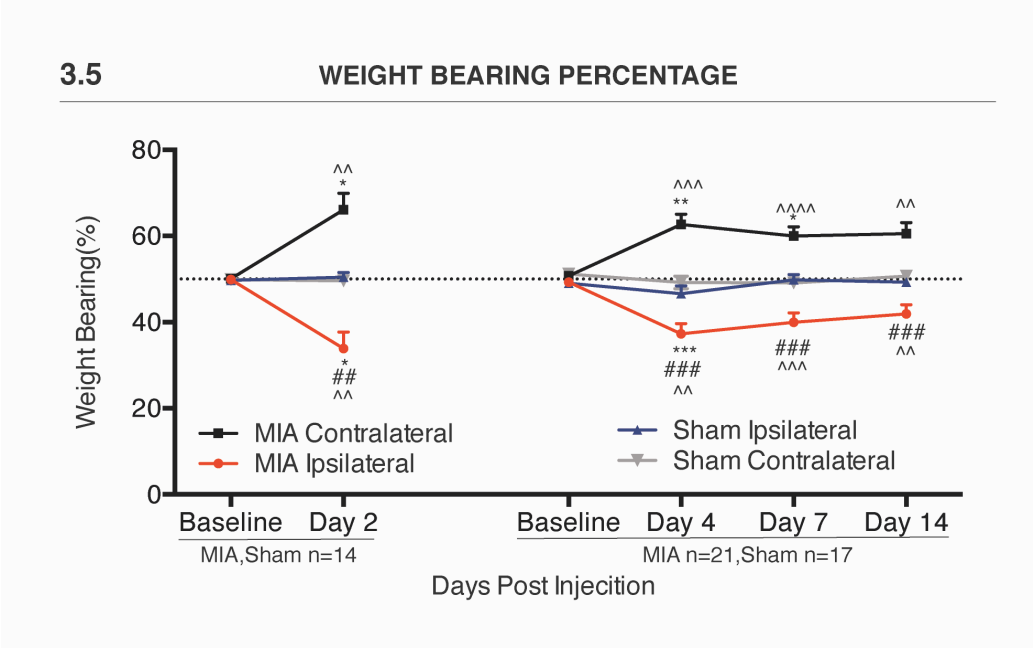

Figure 3.5. Weight bearing (%) of ipsilateral and contralateral hind-paws in MIA and sham groups. While at baselines there is no significant difference in weight bearing percentage in both MIA and sham-injected groups, post-MIA injection ipsilateral and contralateral weight bearing (%) was altered. Compared to baseline, ipsilateral (injured) weight bearing (%) was decreased at day 2 and day 4 (Friedman test; *p=(0.02(*))*, *p=(0.000(***)).* Contralateral (uninjured) weight bearing (%), was increased post-MIA injection compared to baseline at day 2, 4 and 7 (Friedman test; (*p=0.033(*)*), (*p=0.001(**)*), (*p=0.023(**)*)), post-MIA injection. Additionally, weight bearing (%) differs between ipsilateral and contralateral hind-paws in MIA group at all time points (Wilcoxon test; day 2 *(p=0.005(##)),* day 4 (*p=0.0002(###)*), day 7 (*p=0.001(###)*) and day 14 (*p=0.001(###)*)) post-MIA injection. Wilcoxon test revealed a decrease of Ipsilateral MIA hind-paws weight bearing (%) at days 2 (*p=0.003(^^)*), 4 (*p=0.006(^^))*, 7 *p=0.001(^^^))* and 14 *p=0.007(^^))* compared to ipsilateral sham hind-paws. Contralateral MIA hind-paws weight bearing (%) was increased also at days 2 (*p=0.003(^^)*), 4 (*p=0.001(^^^))*, 7 *p=0.000(^^^^))* and 14 *p=0.002(^^))* compared to contralateral hind-paw of sham animals at those time points.

3.4.3.4. CatWalk Gateway System shows significant differences in gait parameters during the early acute inflammatory stage in MIA-induced OA

The CatWalk Gateway System can be used to measure gait abnormalities in rats by providing a series of parameters and paw statistics.

In the study presented in this thesis significant differences were observed when measuring 4 different parameters in MIA animals. Data is expressed as ratios between left and right paws for both hind and front paws in sham and MIA-injected groups. MIA and sham injections were performed in the left hindpaw of the rats.

Print area (cm^2), is the surface area of the complete paw print when it touches the glass catwalk platform. When comparing hind-paw ratios of MIA-injected animals before (baseline) and after MIA-injection a significant decrease in hind-paw ratios (LH/RH) at day 2 post-MIA injection (*p=0.003(**)*) (**Figure 3.6a**) was revealed. A significant decrease of hind-paw ratios in MIA-injected animals compared to sham animals was also present. These differences appeared at day 2 (*p=0.028(#)*), day 4 (*p=0.0028(#)*) and day 14 (*p=0.046(#)*) post injection (**Figure 3.6a**). No differences in front-paw ratios were observed over time or between MIA and sham groups (**Figure 3.6b**).

Swing (s) measures the duration in seconds that a paw has no contact with the glass catwalk platform. A significant increase in swing (s) at day 2 (*p=0.001(***)*) post-MIA injection was present when compared to baseline while other time points were not significantly changed (**Figure 3.6c**). A significant increase at day 2 post-MIA injection compared to day 2 post sham-injection (*p=0.028(#)*) with regards to front-paw ratios was present.

Swing Speed (cm/s) measures the speed of the paw during swing. Formula is as follows: Swing Speed=(Stride Length/Swing); stride length refers to the distance between successive placements of the same paw. A significant decrease in swing speed hind-paw ratios at day 2 post-MIA injection *(p=0.003(**)*) compared to baseline was present (**Figure 3.6e**). Additionally the decrease in hind-paw ratios, was significantly different compared to sham-injected animals at day 2 (*p=0.028(##)*) (**Figure 3.6e**). No other significant changes were observed. A significant decrease in baseline front-paw MIA ratios was present when compared to baseline sham but it disappeared overtime (*p=0.028(*)*) (**Figure 3.6f**).

Single Stance (s) measures the duration in seconds of ground contract of a single paw, while the other paw is not touching the ground. This is one of the most used parameters to measure gait analysis in pain models. A significant decrease in hind-paw Single Stance (s) ratios at day 2 post-MIA injection (*p=0.000(***)*) compared to baseline was recorded (**Figure 3.6g**). Additionally a significant decrease in the hind-paw ratios of MIA group at day 2 (*p=0.028(##)*) and day 7 (*p=0.0046(#)*) was present when compared to sham groups (**Figure 3.6g**). MIA front-paw ratios were significantly decreased at baseline when compared to day 2 (*p=0.012(**)*), day 4 (*p=0.001(***)*), day 7 (*p=0.005(**)*) and day 14 (*p=0.003(*)*) post-injection. Baseline front-paw sham ratios were also significantly decreased at baseline compared to day 14 post-sham injection (*p=0.0001(^^^)*) (**Figure 3.6h**).

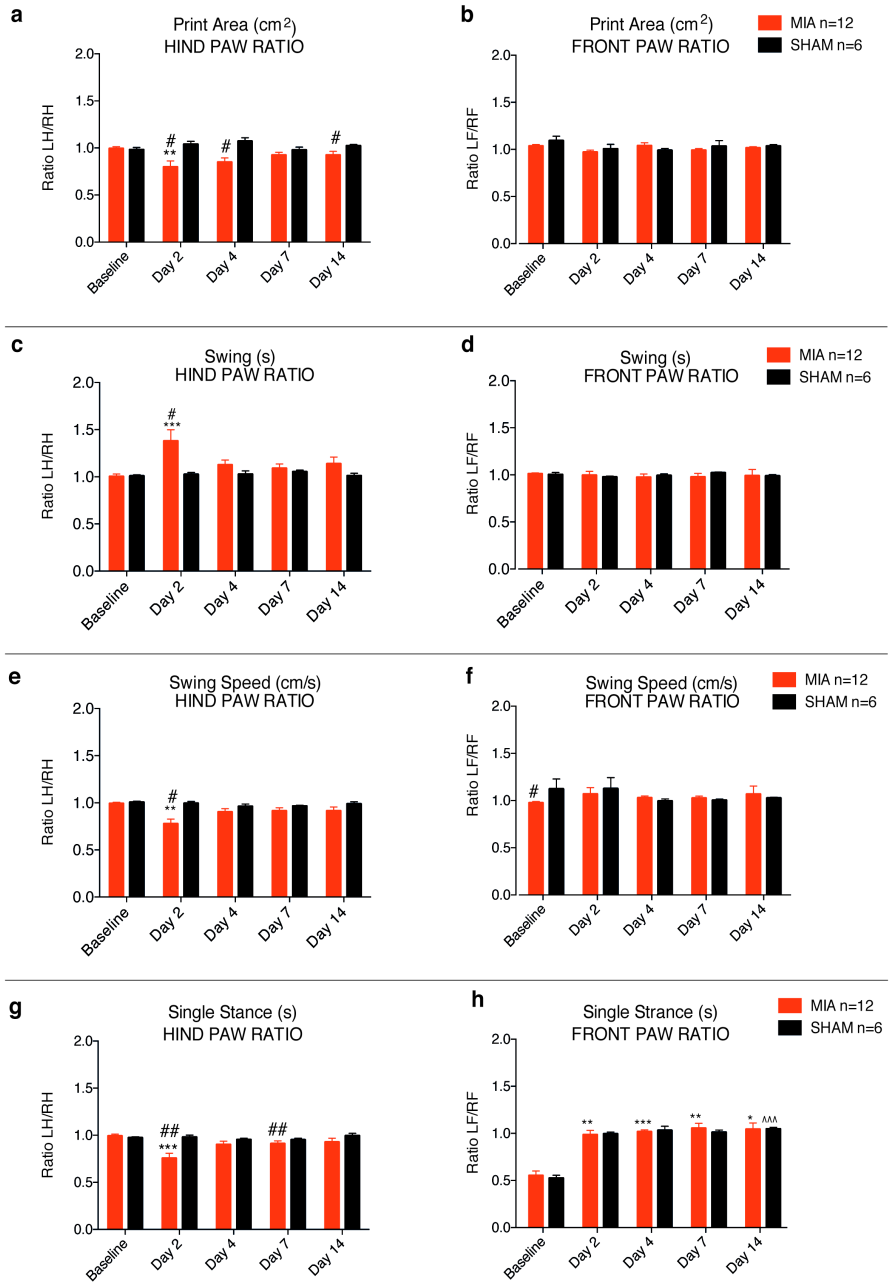

Figure 3.6. Catwalk gateway system measured parameters in both MIA (n=12) and sham groups (n=6). a) Print Area (cm^2) of left (injured)/right (uninjured) hind-paw (LH/RH) ratios. Decreased print area (cm^2) LH/RH ratios were significantly decreased at day 2 post-MIA injection compared to baseline (Friedman test; (*p=0.003(**)*). Print area (cm^2) ratios also were significantly decreased at day 2, day 4 and day 14 (Wilcoxon test; *p=0.028(#)*, *p=0.0028(#)* and *p=0.046(#)*) when comparing MIA to sham group. **c)** Swing (s) hindpaw ratios were significantly increased at day 2 post-MIA injection compared to baseline (Friedman test; *p=0.001(**)*) and compared to day 2 sham-injected group (Wilcoxon test; *p=0.028(#)*). **e)** Swing speed (cm/s) appeared decrease at day 2 post-MIA injection compared to baseline (Friedman test; *p=0.003(**)*). When comparing day 2 post MIA to sham-injected group swing speed also were decreased in the MIA group (Wilcoxon test; *p=0.0028(#)*). **f)** Swing speed (cm/s) LF/RF ratios were significantly decreased when comparing baseline MIA animals to baseline sham rats (Wilcoxon test; *p=0.028(*)*). **g)** Single stance (s) LH/RH ratios were significantly decreased at day 2 post-MIA injection compared to baseline (Friedman test; *p=0.000(***)*). When comparing MIA to sham group, decreased single stance was present at day 2 and day 7 (Wilcoxon test; *p=0.0028(**), p=0.046(**)*). **h)** Single stance (s) front paw ratios were significantly increased in MIA animals at all days (2,4,7 and 14) post injection compared to baseline (Friedman test; *p=0.012(**), p=0.001(***), p=0.005(**), p=0.03(*)*). Sham front paw ratios also appeared increased at day 14 post-sham injection compared to baseline sham (Wilcoxon test; *p=0.001(^^^)*).

3.4.3.5. LABORAS

A decrease in total locomotor duration (s) in the MIA group during the light cycle at days 4 (*p=0.019(*)*) and 7 (*p=0.001(**)*) post-MIA injection compared to baseline locomotor duration was present. Locomotor duration (s) was also decreased in the sham group, at days 7 (*p=0.035(*)*) and 14 (*p=0.035(*)*) post-sham injection compared to baseline. No changes in locomotor duration were observed during the dark cycle in both MIA and Sham-injected groups when comparing baseline to different post injection time points. Additionally, no differences were observed when comparing MIA to Sham in both dark and light cycle at all time points (**Figure 3.7a**).

Significant differences in the total maximum speed (mm/s) of MIA animals compared to Sham group were recorded at day 2 post-MIA injection compared to day 2 sham in the light cycle (*p=0.028(#)*). Interestingly, at day 14 post-MIA injection, maximum speed was increased when compared to sham injected animals during the light cycle (*p=0.028(#)*). Lastly, during the dark cycle a decrease in total maximum speed was present at day 14 of MIA-injected group compared to sham at the same time point (*p=0.046(#)*) (**Figure 3.7b**).

Total distance travelled (m) was unaffected in the MIA group after MIA induction in both dark and light cycle and no differences where observed when compared to sham. However, a significant decrease in total distance travelled (m) was observed at day 2 post sham-injection (*p=0.003(**)*) compared to baseline distance travelled. No changes were observed for other time points in the sham group (**Figure 3.7c**).

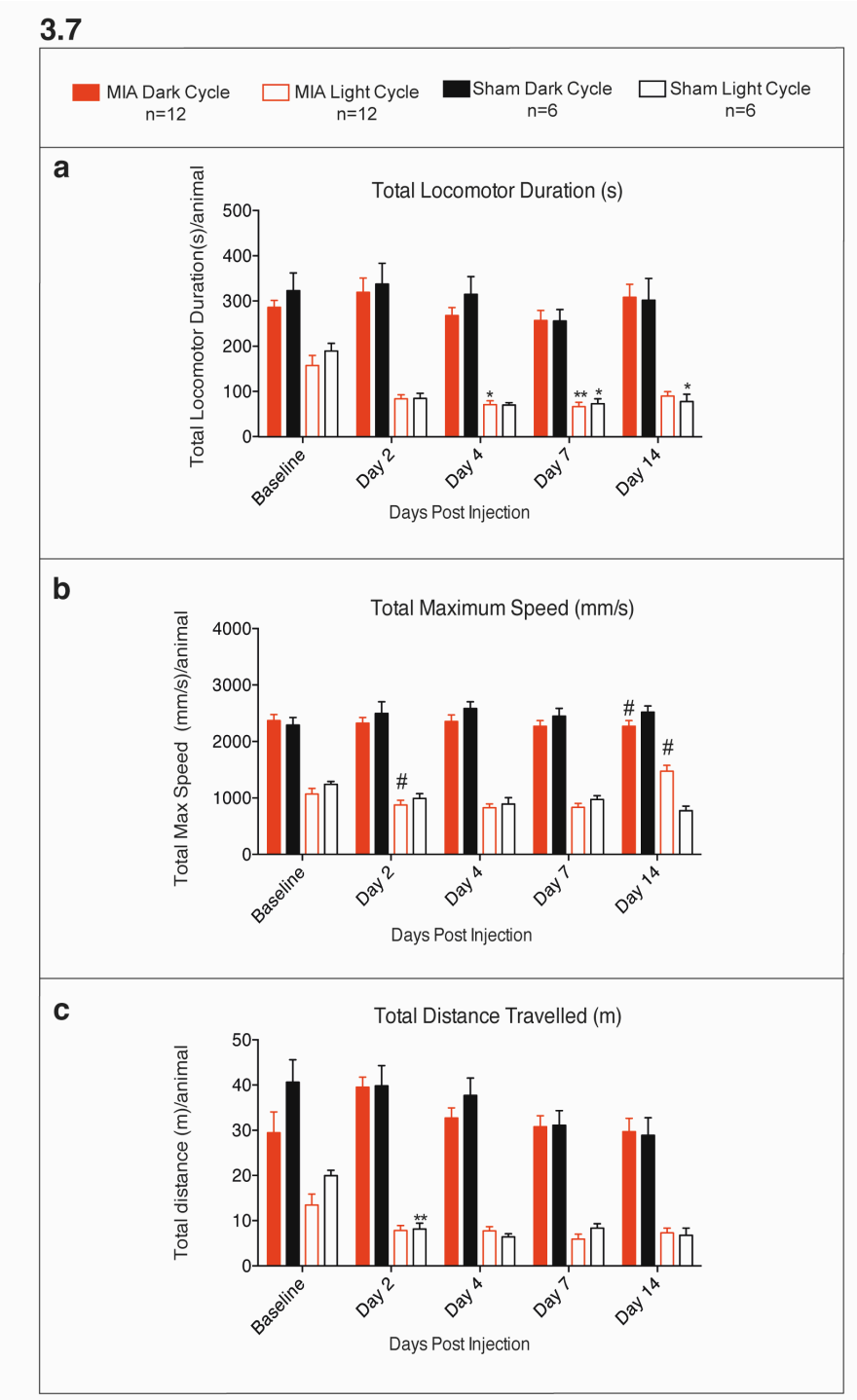

Figure 3.7. LABORAS locomotor related results during Dark and Light cycle in MIA and sham-injected animals. a) Total locomotor duration (s) was significantly decreased (Friedman test) in the MIA group during the light cycle at days 4 (*p=0.019(*)*) and 7 (*p=0.001(**)*) post-MIA injection compared to baseline locomotor duration. Locomotor duration (s) also was decreased in the sham group, at days 7 (*p=0.035(*)*) and 14 (*p=0.035(*)*) post-sham injection compared to baseline. **b)** Wilcoxon test revealed a decrease in the total maximum speed (mm/s) at day 2 post-MIA injection compared to day 2 sham in the light cycle (*p=0.028(#)*). At day 14 post-MIA injection, maximum speed was increased when compared to sham injected animals during the light cycle (*p=0.028(#)*). During the dark cycle a decrease in total maximum speed was present at day 14 of MIA-injected group compared to sham at the same time point (*p=0.046(#)*). **c)** Friedman test revealed a significant decrease in total distance travelled (m) was observed at day 2 post sham-injection (p=0.003(**)) compared to baseline distance travelled.

Total drinking frequency (counts) of MIA animals remained unaffected after MIA-induction for both light and dark cycle. In the sham group, total drinking frequency during the dark cycle also remained unchanged. However in the light cycle, a significant decrease in drinking frequency at day 14 post sham-injection (p=0.003(**)) compared to baseline was present. No significant differences in drinking frequency were observed when comparing MIA to sham groups for both dark and light cycle (**Figure 3.8a**).

Total feeding frequency (counts) was significantly decreased in the MIA light cycle at days 7 (*p=0.01(*)*) and 14 (*p=0.01(*)*) post-MIA injection compared to baseline (Friedman test). Additionally, a significant difference in total feeding frequency of MIA animals at day 7 (*p=0.028(#)*) compared to sham group at the same time point during the light cycle appeared. No changes were observed overtime during the dark cycle for both MIA and sham-injected groups (**Figure 3.8b**).

During the dark cycle, total grooming frequency (counts) appeared significantly increased at day 2 (p=*0.000(****)*) and day 4 (*p=0.005(**)*) post-MIA injection compared to baseline. During the light cycle, a decrease in total grooming frequency (counts) at day 7 (*p=0.001(**)*) and day 14 (*p=0.019(*)*) post MIA injection compared to baseline was present. Total grooming frequency during the light cycle in sham group appeared decreased at day 4 (*p=0.035(*)*) and day 14 (*p=0.019(*)*) compared to baseline. No differences between MIA and sham groups were observed at any time point for both dark and light cycle (**Figure 3.8c**).

Lastly, total rearing frequency (counts) appeared increased at day 2 post-MIA injection (*p=0.024(*)*) during the dark cycle compared to baseline. During the light cycle, rearing frequency was decreased at days 7 (*p=0.008(**)*) and 14 (*p=0.019(**)*) in MIA group and decreased at day 4 in the sham group (*p=0.010(**)*). No differences were observed when comparing MIA to sham groups for both dark and light cycle (**Figure 3.8d**).

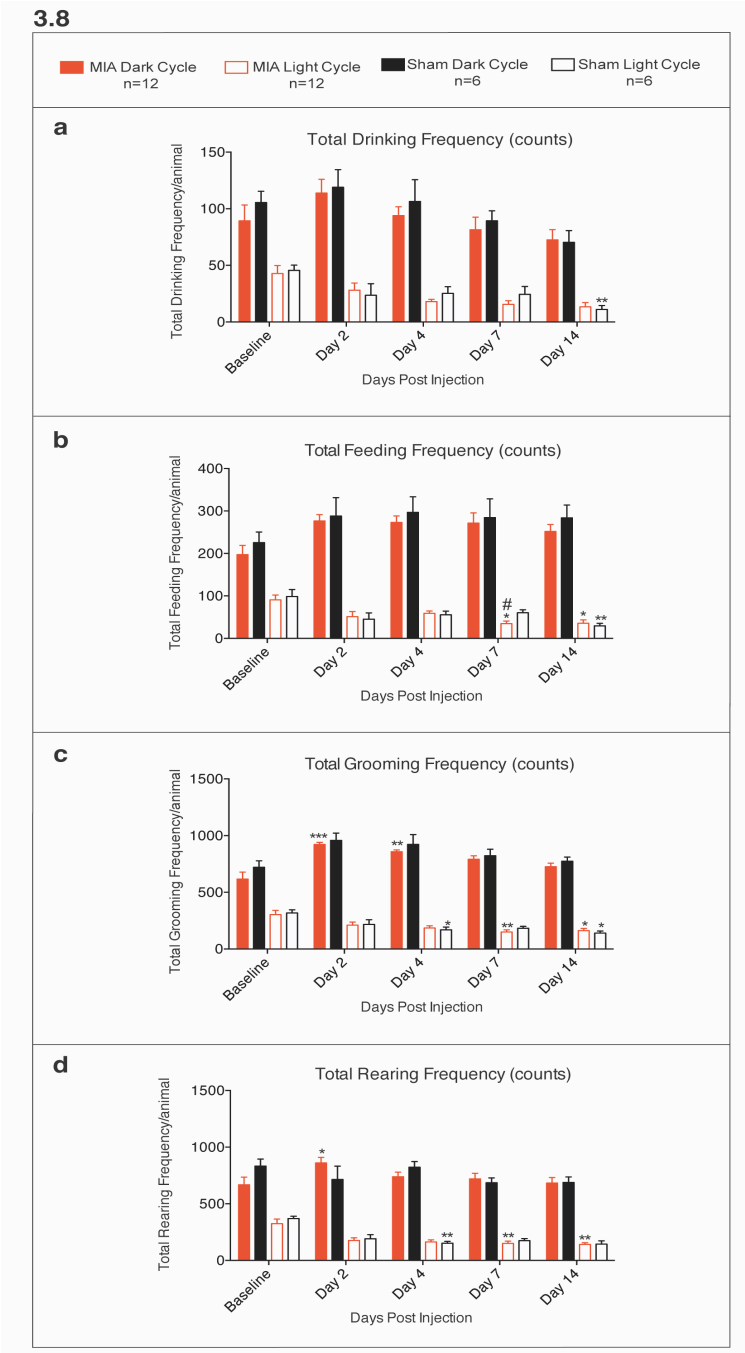

Figure 3.8. LABORAS naturalistic behavioural frequencies during dark and light cycle in MIA and sham-injected rats . a) In the light cycle, Friedman test revealed a significant decrease in drinking frequency at day 14 post sham-injection (p=0.003(**)) compared to baseline drinking frequency. **b)** Total feeding frequency (counts) was significantly decreased in the MIA light cycle at days 7 (*p=0.01(*)*) and 14 (*p=0.01(*)*) post-MIA injection compared to baseline (Friedman test). Wilcoxon test revealed a significant difference in total feeding frequency of MIA animals at day 7 (*p=0.028(#)*) compared to sham group at the same time point during the light cycle. **c)** During the dark cycle, total grooming frequency was significantly increased at days 2 (p=*0.000(***)*) and day 4 (*p=0.005(**)*) post-MIA injection compared to baseline. During the light cycle, Friedman test revealed a decrease in total grooming frequency (counts) at day 7 (*p=0.001(**)*) and day 14 (*p=0.019(*)*) post MIA-injection. Total grooming frequency during the light cycle in sham group appeared decreased at day 4 (*p=0.035(*)*) and day 14 (*p=0.019(*)*) compared to baseline. **d)** Total rearing frequency (counts) was increased at day 2 post MIA-injection (*p=0.024(*)*) during the dark cycle compared to baseline. During the light cycle, rearing frequency was decreased at days 7 (*p=0.008(**)*) and 14 (*p=0.019(**)*) in MIA group and decreased at day 4 in the sham group (*p=0.010(**)*).

3.4.4. Electrophysiological characterization of the rat MIA model of OA

3.4.4.1. Comparison of baseline evoked responses of WDR lamina V neurones in early stage MIA and early sham-injected groups

Baseline WDR neuronal responses to evoked stimulation of the peripheral receptive field in the early stage MIA rats were compared to baseline early sham-injected responses. Electrically parameters were not significantly different between early MIA and sham animals (**Figure 3.9a**). Neuronal evoked firing rates in response to dynamic brush, mechanical punctuated stimuli and thermal heat also showed no significant differences between MIA-induced and sham-injected early stage groups (**Figure 3.9b, c and d**).

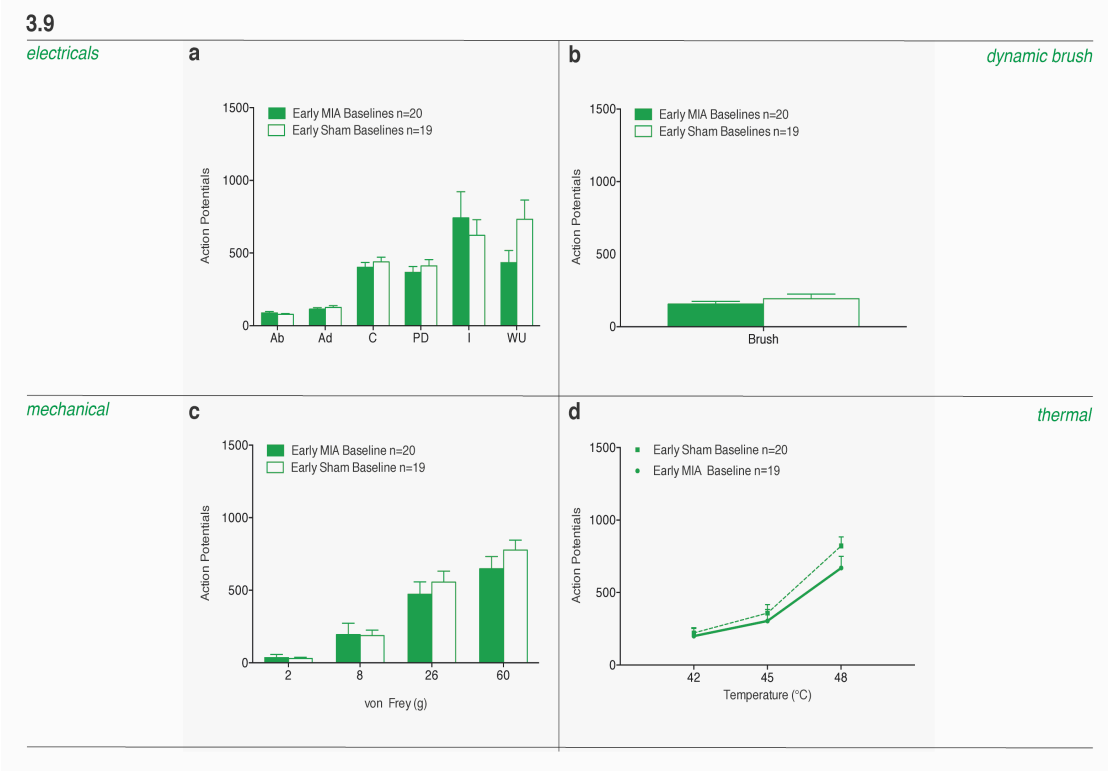

Figure 3.9. Baseline neuronal evoked responses of WDR neurones in the early stages of the MIA rat model of OA and in sham-induced animals. **a)** Electrical evokes responses of WDR neurons were not significantly different between early MIA and sham groups. **b)** WDR neuronal evoked responses to dynamic brush responses were not significantly different between both eary MIA and sham groups. **c)** No significant differences in neuronal evoked responses of WDR neurons were observed after mechanical stimulation of receptive field with 2g, 8g, 26g and 60g vF in both early MIA and sham groups. **d)** WDR neuronal evoked responses to thermal stimulation were not significantly different between both early MIA and sham groups.

3.4.4.2. Comparison of baseline evoked responses of WDR lamina V neurones in late stage MIA and late stage sham-injected groups

Comparison of baseline WDR neuronal evoked responses to electrical, dynamic brush, mechanical and thermal stimulation showed no significant differences between late stage MIA and late stage sham animals firing rates (**Figure 3.10a,b,c and d**).

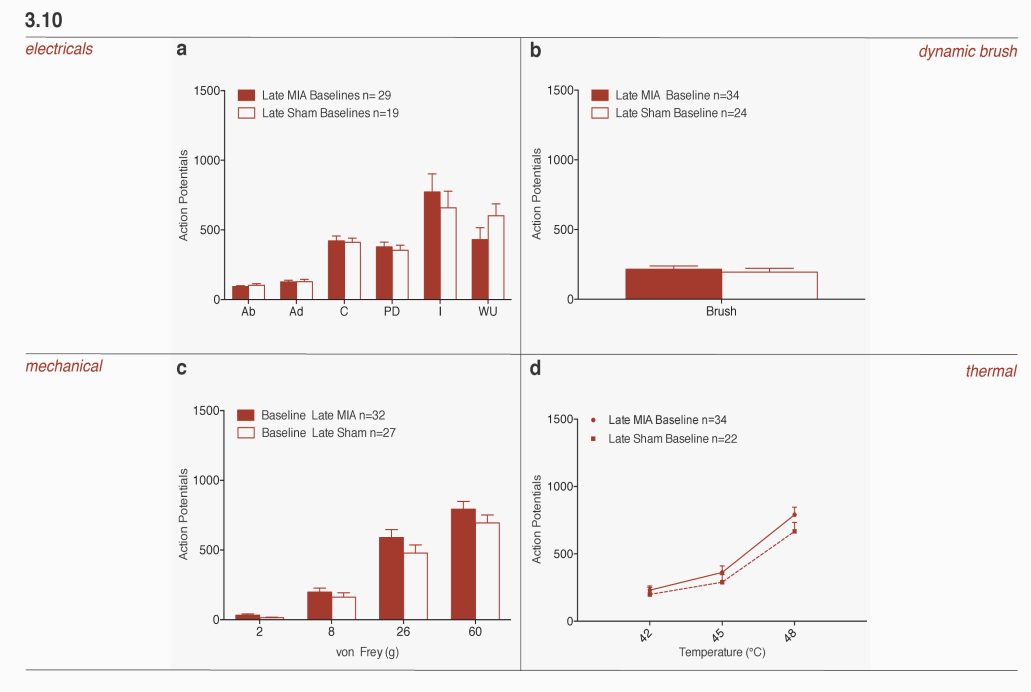

Figure 3.10. Baseline neuronal evoked responses of WDR neurones in the late stages of the MIA rat model of OA and in sham-induced animals. **a)** Electrical evoked responses of WDR neurones were not significantly different between late sham and MIA groups. **b)** WDR neuronal evoked responses to dynamic brush were not significantly different between both MIA and sham groups. **c)** WDR neuronal evoked responses to mechanical stimulation with 2g, 8g, 26g and 60g vF were not significantly different between late MIA and sham groups. **d)** WDR neuronal evoked responses to thermal stimulation were not significantly different between late MIA and sham groups.

3.4.4.3. Comparison of early and late stage MIA neuronal evoked responses of lamina V WDR neurones

Neuronal evoked responses of WDR neurones to electrical stimulation, dynamic brush, mechanical punctuated stimulation and thermal heat were not significantly different between early stage MIA and late stage MIA groups (**Figure 3.11a,c and d**). Additionally, early sham neuronal evoked responses were not significantly different to late stage sham group neuronal response (data can be found in Supplementary Figure 2 on Appendix I: Chapter 3).

To conclude, administration of saline had no significant effects on neuronal evoked responses to all modality stimuli for both MIA and sham animals. Statistical data for saline experiments can also be found on Appendix I: Chapter 3 and neuronal responses of Sham and MIA animals to saline are plotted on Supplementary Figure 3.

.

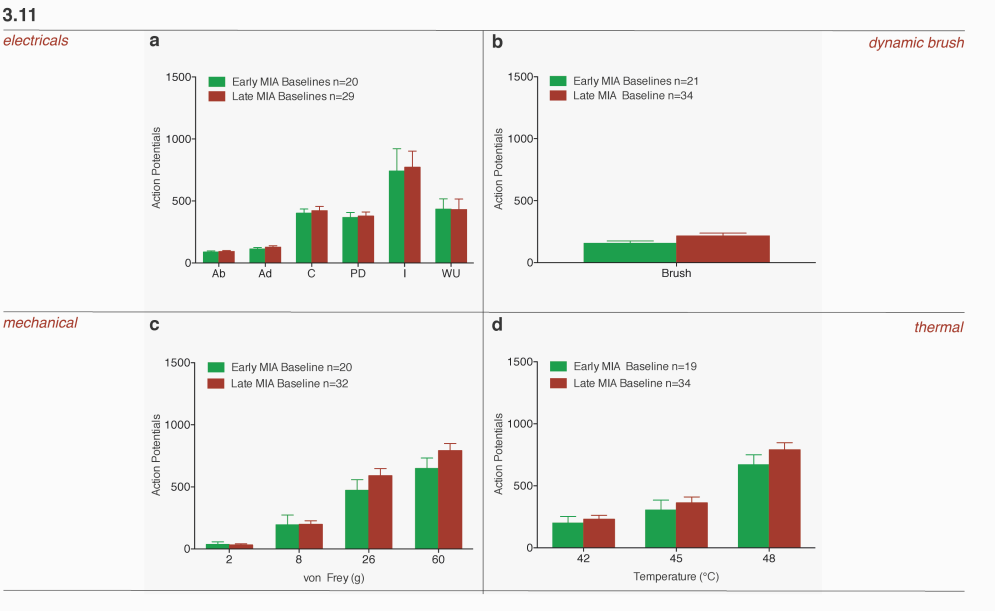

Figure 3.11. Baseline neuronal evoked responses of WDR neurones in early stages and in late stages of MIA induced rat model of OA. **a)** Electrical evoked responses of WDR neurones were not significantly different between early and late stage MIA groups. **b)** WDR neuronal evoked responses to dynamic brush were not significantly different between both early and late stage MIA groups. **c)** WDR neuronal evoked responses to mechanical stimulation with 2g, 8g, 26g and 60g vF were not significantly different between early and late stage MIA groups. **d)** WDR neuronal evoked responses to thermal stimulation were not significantly different between early and late stage MIA groups.

3.5. Discussion

3.5.1. Cartilage damage of the knee joint in the MIA rat model of OA over time

Knee histology of both early stage and late stage MIA and sham animals has revealed several differences in the OA damage score present per group. The average maximum knee score of late stage MIA animals, was above 4 and significantly higher than the damage present in early stage MIA animals, which was lower than 2. Interestingly, for early and late stage sham animals the average maximum knee score was also lower than 2, but not significantly different to neither early stage or late stage MIA animals. The injection itself can cause some tissue damage to the knee joint and that might explain why they exhibit a score higher than 0.

Surprisingly, the average of maximum scores per slide was not significantly different between groups. This might suggest that damage to the knee might be localized to a specific region of the knee rather than along the whole knee, since in the late stages of the MIA model both the medial femur and the lateral femur exhibited a significant increased in average condyle scores compared to late sham animals. This might be indicative of predominant damage in the femur of these animals. Additionally, the lateral tibia also had increased scores suggesting that damage was mainly restricted to the lateral side. Therefore explaining why perhaps the average of maximum score per slide was not significantly different between groups. Additionally, early stage MIA and sham animals showed no differences in condyle average.

While, in the early stages of MIA animals show little or no damage to the articular cartilage, behavioural studies presented in this thesis show that early stage MIA animals exhibit pain-like behaviours (decreased paw withdrawal thresholds, altered weight bearing and gait abnormalities). Conversely, both early sham and late stage sham animals do not. Thus it is unclear what is driving the pain in the early stages of the model. However other studies also report little damage in the early stages of the disease (Bove et al., 2003). Perhaps the increase of inflammation is one of the main drivers and although pro-inflammatory cytokines IL-6, TNF-α and IL-5 levels were not increased in serum during the early stages of the model, pro-inflammatory chemokine KC/GRO was.

Even thought the cartilage is aneural during the early stages of OA (Goldring and Goldring, 2016), the synovium, trabecular and subchondral bone, periosteum, meniscus and cruciate and collateral ligaments have unmyelinated nerve endings (Suri et al., 2007). MIA toxicity and the presence of inflammation could lead to the activation of sensory nerves in these regions of the joint cavity. Perhaps addressing damage to any of these areas would give us additional information on how the MIA affects the joint structures and how comparable it is to human OA. Additionally, we need to remember

that in human OA the amount of radiographic knee damage shows a modest association with OA pain that the patients report (Finan et al., 2013). Therefore, cartilage damage does not correlate with levels of pain experienced.

In the late stages of the MIA model a more severe OA damage score is present compared to the early stages. However the damage was mild, as it did not reach a score of 5-6. This is in line with other studies that used the same amount of MIA in Male Sprague-Dawley rats (Thakur et al., 2012) (Pomonis et al., 2005). Other studies using lower doses and higher volume of MIA injected (1mg/50μL) in Wistar rats report a more severe OA score in the late stages of the MIA model (Udo et al., 2016). Other studies in Wistar rats injected with a 3mg/50μL dose of MIA show a mild to sever OA damage score of the cartilage 15 days post-MIA injection, with more severe damage to the femoral condyles (Guingamp et al., 1997), as observed in the study presented in this thesis. There is quite a lot of variability in regards of OA damage scores amongst studies using the MIA model. There are several factors that could affect cartilage damage, such as the strain of animals used, the weight of the animals at time of MIA induction, and the volume and dose of MIA injected. Therefore all these factors should be taken into consideration when planning an experiment.

3.5.2. Pain behavioural changes in the early vs. late stages MIA rat model of OA and the role of cytokines in OA-associated pain

The MIA rat model of OA is the most used model for the research of OA-associated pain. The progression of the disease and pathological changes that occur in the MIA model vary over time and the severity of the model can also vary depending of the dose of MIA used to induce OA in the rats.

Previous studies have shown that a high dose of 2mg of MIA injected into the knee joint of rats leads to the development of two different stages of the pathology overtime (Thakur, 2012). An early acute inflammatory stage (day 2-4 post MIA-induction) followed by a later stage with neuropathic pain-like features (day 14-onwards). These two distinct stages have also been shown to have different behavioural and electrophysiological characteristics (Thakur, 2012) (Burnham, 2012).

In the work presented in this thesis, animals were intra-articularly injected with a 2mg dose of MIA dissolved in a volume of 25μL of 0.9% saline into their left knee joint. Sham animals were injected with 0.9% saline only. Behavioural and electrophysiological changes in these animals were monitored over time to observe differences between the early stage and the late stage. In this chapter it is shown that paw withdrawal thresholds appeared decreased during the early acute inflammatory stage (day 2 and day 4 post-

MIA injection) when comparing to baseline and to the contralateral uninjured hind-paw thresholds. Paw withdrawal thresholds increased at day 7 post-MIA injection as has been observed in other studies (Abaei et al., 2016, Sagar et al., 2015). As mentioned by the authors this increase in paw withdrawal thresholds at day 7 could be accounted for the decrease in inflammation that has been observed in other studies at this time point. Additionally, paw withdraw thresholds were also increased at day 14 compared to baseline and to contralateral uninjured hind-paw. While some studies report a decrease in withdraw thresholds at day 14 (Thakur, 2012), others report this decrease at later days post-injection at 21 and 28 days (Ferreira-Gomes et al., 2012). We can speculate that if we kept testing and analysing paw withdrawal thresholds until later time points we would also have been able to observe the same decrease, but we cannot confirm it due to UK Home Office regulations.

Withdrawal frequency (PWF) (%) of ipsilateral (injured) hind-paw was unchanged when comparing baseline PWF (%) to post-MIA injection frequency (%) upon stimulation with different von Frey (vF) filaments (1g, 4g, 8g and 15g) (**Figure 3.3**). Whilst paw withdrawal (g) in the MIA animals is significantly changed overtime, withdraw to a specific von Frey is not necessarily increased. This could explain why there is no change in PWF (%).

Contralateral (uninjured) hind-paw exhibited a significant decrease in PWF (%) at different time points compared to baseline after 10g and 15g vF stimulation. This decrease in PWF (%) on the contralateral side might be to that animal becoming habituated to the filament stimulation and, as days go by, the frequency of withdrawal decreases. Interestingly, while no significant changes in PWF (%) between baseline ipsilateral to post injection time points were observed, comparing ipsilateral to contralateral hind-paws of MIA animals shows differences in PWF (%). Ipsilateral PWF (%) appeared increased at various post injection (mainly days 4, 7 and 14) time points compared to contralateral PWF (%) when stimulating the receptive field with higher von Frey hairs 10g and 15g (**Figure 3.3c,d**). This indicates differences in mechanical evoked allodynia between ipsilateral and contralateral hind-paws.

Similarly, weight bearing (%) analysis also revealed differences between the early stage and the late stage in the MIA rats, that were similar to changes observed in paw withdrawal thresholds. Weight bearing (%) of ipsilateral (injured) hind-paw was significantly decreased compared to baseline at day 2 and day 4 post-MIA injection while the contralateral (uninjured) side was significantly increased at those time points. No differences in weight bearing (%) were observed at day 7 and 14 post-MIA injection compared to baseline. Sham animals did not exhibit any differences in weight bearing (%) when comparing to baseline and between each hind-paw. Differences between

sham ipsilateral and MIA ipsilateral hind-paws were present in all post injection time points compared to baseline (**Figure 3.4**).

Additionally, analysis of cytokine profiles in serum of MIA animals showed that anti-inflammatory cytokines IL-10 was significantly increased at day 14 post-MIA injection. Thus, this increase of IL-10 in the serum of MIA-injected animals could be contributing to a decrease in inflammation, an increase in paw withdrawal thresholds at days 7 and 14 post-MIA injection as well as increased weight bearing (%) of the ipsilateral (injured) hind-paw of MIA animals.

Pro-inflammatory chemokine KC/GRO levels are significantly increased at day 4 post MIA injection.. It is interesting that this chemokine is highly elevated in the acute inflammatory stage at (day 4) while it is decreased as inflammation ceases (at day 7). Perhaps the increase of this cytokine could be present at later days post-injection not measured in this study such as day 28 and could contribute to the decrease in paw withdrawal thresholds observed in other studies, at later time points of the late stage MIA group (21 and 28 days) (Ferreira-Gomes et al., 2012). Levels of pro-inflammatory cytokines IL-5 and IL-6 were too low to be detected in serum. While in human OA patients IL-6 levels have been detected both in serum as well as in synovial fluid, it is possible that in these animals, levels of IL-6 were not increased in serum. However, previous studies report increased IL-6 levels both in serum and synovial fluid in the same rat model of OA (Finn et al., 2014, Orita et al., 2011). This difference in results could be to the fact that those authors observed increased of IL-6 levels at day 1, day 10, day 21 and day 28 post-injection that were not measured in the study presented in this thesis (Finn et al., 2014). TNF-α was also not increased in serum levels of MIA animals in this study. Some studies, report increased levels of TNF-α in serum while others do not (Finn et al., 2014, Orita et al., 2011). Sample size could also play a role, as a higher number of animals could provide a better representation of the proportion of animals that exhibit increased levels of pro-inflammatory cytokines in serum. Additionally measuring the level of cytokines in synovial fluid rather than serum could have been a better approach. Inflammatory events are restricted to the local area of the knee joint, thus perhaps an increase of pro-inflammatory cytokines in synovial fluid could have been detected. Additionally measuring pro-inflammatory cytokines as soon as days 1-2 post-injection could also have provided further information as the acute inflammatory response starts promptly after MIA-injection.

The Catwalk gateway system revealed some differences in gait parameters between the early and late stages of the MIA animals. While no gait parameters appeared changed at days 7 and 14 post-MIA injection, gait abnormalities were observed in the early acute inflammatory stage (day 2 post-MIA injection). Print area

(cm^2), swing speed (cm/s) and single stance (s) ratios of left/right hind-paws of MIA animals, were decreased at day 2 post-MIA injection compared to baseline as well as compared to sham. Swing (s) was increased at day 2 post-MIA injection, also compared to baseline and to sham group. This suggests that at day 2, MIA animals spend less time with their injured paw on the ground and more time with the injured paw in the air, as observed by the decrease in print area and increase in swing. Additionally, the speed at which they put down the injured hind-paw in the platform become slower and the time the injured hind-paw spends in the ground is less as shown by the decrease in both swing speed and single stance. Single stance front-paw ratios were increased post MIA and post sham injection compared to baseline. However, ratios were not significantly different between MIA and sham animals, suggesting that perhaps these changes have to do with the rats adapting to the catwalk platform overtime.

Interestingly, LABORAS system did not provide with much information on MIA and sham-injected animals during disease progression regarding differences on locomotor duration, total maximum speed, distance travelled and naturalistic behaviours such as grooming, feeding and rearing. Even though changes were present in the MIA group at different time point compared to baseline, these were not significant when compared to the sham group. Only feeding frequency (counts) appeared decreased at day 7 post-MIA injection, in the light cycle, both compared to baseline and sham group. In the OA model of destabilization of the medial meniscus (DMM), animals exhibited a decrease in distance travelled (m), average number of climbs per hour and average number of rears per hour compared to naïve and sham animals (Miller et al., 2012). However, in the present study in the MIA model of OA, no changes were observed in rearing frequency and distance travelled. Although the DMM model is much more invasive than the MIA model. However, one would expect a decrease in rearing frequency post-MIA injection, since the injured hind-paw bears less weight and animals avoid using it (as reflected in weight bearing (%) and catwalk data). It might be possible that LABORAS is not a good method to use in the assessment of the MIA rat model of OA. It is also possible that animals might suffer ongoing pain as observed in the late stages of the MIA model but continue their normal behaviours (Liu et al., 2011).

To conclude, most of the behavioural changes observed in this study appeared at the early acute inflammatory phase. Namely, a decrease in paw withdrawal thresholds, altered weight bearing (%) on the ipsilateral (injured) paw and altered gait parameters. These changes in the early acute inflammatory stage were accompanied by an increase in levels of pro-inflammatory chemokine in serum at day 4 post-MIA injection, which might be contributing to the mechanical allodynia and hyperalgesia observed. In the late stages of the MIA model, where neuropathic pain-like features appear, ipsilateral paw

withdrawal thresholds appeared increased at day 14 compared to withdraw thresholds of contralateral hind-paw. However, paw withdrawal frequency (%) in response to stimulation with vF filaments 10g and 15g revealed a significant increase at day 14 compared to contralateral uninjured site. Weight bearing (%) of ipsilateral hind-paw in the late stage MIA group (day 14) also appeared decreased compared to sham ipsilateral and MIA contralateral. Thus suggesting that ongoing pain and allodynia is also present in these stage, perhaps at a lower degree that might develop into a more sever state at later time-points. Additionally, anti-inflammatory cytokines were increased at day 14 and day 7 which may contribute to the shift from the acute inflammatory state into a different state. Perhaps day 14 is an intermediate time point between the two states and behavioural features would reappear at later time points as seen in other studies. Unfortunately, home office regulations prevented the examination of this later time point in the present study.

3.5.3. Deep dorsal horn neurones in the MIA rat model of OA

In this study I have demonstrated that deep dorsal horn WDR neuronal evoked responses in early acute inflammatory and late stage MIA groups are not potentiated compared to each other as well as compared to baseline responses in the sham groups (**Figure 3.9-3.11**). Three different studies by colleagues in the same rat model of OA have investigated differences between MIA and sham baseline response of WDR neurones. From these studies, one reports an increased in electrical evoked activity of WDR neurones in early and late stage MIA animals compared to sham, as well as increases in mechanical and thermal-evoked activity (Burnham, 2012).

In contrary to these results, the two other studies report that neuronal responses of deep layer WDR neurones from experimental MIA groups do not appear potentiated compared to sham responses (Thakur, 2012) (Lockwood, 2018) In line with the data present in this study, Lockwood demonstrated that both early and late stage MIA baseline responses are not significantly different to each other as well as to sham animals. Thakur, only addressed changes in the late stage MIA group and saw no differences in baseline responses of WDR lamina V neurones compared to naïve animals. However, Thakur demonstrated that lamina I neuronal responses of WDR appeared potentiated compared to sham/naïve neuronal responses in the same lamina I. In the same study, Thakur did report an increase in action potential responses to specific stimuli when comparing WDR neuron responses in lamina I to lamina V.

Previous studies in other pain models, such as in the SNL model of neuropathic pain, have also reported that neuronal evoked responses of WDR neurones in SNL

animals are not significantly potentiated compared to sham/naïve neuronal evoked responses although in some cases a non significant trend for potentiation is present (Chapman et al., 1998, Patel and Dickenson, 2016, Patel et al., 2014). Interestingly, in the cancer-induced bone pain (CIBP) model an increased in WDR neuronal evoked activity in lamina V was present compared to the sham group (Urch et al., 2003). This increased WDR activity in the CIBP model was specific to electrical and thermal stimulation, while dynamic brush and mechanical evoked responses did not appear potentiated compared to sham group (Urch et al., 2003).

There are several possible reasons on why evoked responses of WDR neurones in the MIA model are not potentiated compared to WDR responses in the sham group. For instance, a single WDR neuron can integrate inputs for a wide variety of neurones. This includes, nociceptive and non-nociceptive neurones, neurones from different laminae as well as interneurones. Additionally, tonic inhibitory controls in the spinal cord might also affect WDR activity. Thus, the increase in lamina I WDR neurones does not necessarily mean that lamina V WDR neuron activity will be potentiated (Thakur, 2012). Perhaps a higher portion of WDR neurones in the deeper laminas becomes activated due to an increase in the receptive field, but this increase is not observed in the in-vivo electrophysiological recordings, as this are single unit recordings.

In the SNL model, as previously mentioned, spinal WDR neuronal responses are not potentiated compared to sham. However recent studies have demonstrated that, in the ventral posterior thalamus, WDR neuronal activity is potentiated in response to mechanical and cold stimuli compared to sham (Patel and Dickenson, 2016). Thus, perhaps in the MIA model, deep dorsal horn WDR neuronal responses do not appear potentiated as compared to shams animals, but an increased number of WDR neurones becomes activated. This would alter and enhance the sending of information to higher centres of the brain, such as the thalamus causing the potentiated response of WDR thalamic neurones compared to WDR sham neurones seen in the SNL model. A plausible mechanism would be the enlarged receptive fields of these neurones after neuropathy, so that a given defined stimulus would activate more spinal neurones (Suzuki et al., 2005). Future studies should aim to address this issue in the MIA model.

In addition, in this study MIA baseline neuronal responses were recorded at days 2-4 post-injection for early stage MIA group and days 14-21 post-injection for late stage MIA group. It is possible that increased neuronal activity of WDR neurones in the MIA group would appear at later time points. This has been observed in a previous study where WDR neuronal responses to mechanical punctuated stimuli (10g and 15g vF) appeared potentiated 28-31days post-MIA injection, as compared to sham animals (Sagar et al., 2010).

Spontaneous activity could also contribute to increases in WDR neuronal firing in the MIA group, as neuropathic pain-like features develop over time. Although spontaneous activity has not been reported in the MIA model, it could appear at later time points if ectopic activity at either the injured site or DRG appear due to nerve damage (Chapman et al., 1998). Ectopic activity could then lead to WDR spontaneous activity, as it has been observed in the SNL model (Chapman et al., 1998).

3.6. Summary

The behavioural data presented in this chapter shows that in the early acute inflammatory stage, MIA animals exhibit decreased paw withdrawal thresholds, weight bearing asymmetry as well as altered gaiting properties. This is accompanied by mild damage in the cartilage and increase in pro-inflammatory chemokine such as KC/GRO at day 4 post MIA injection. This suggests that there is an inflammation leading to mechanical hyperalgesia and allodynia. Inflammation resolves at day 7, with paw withdrawal thresholds increasing and no altered weight bearing asymmetry. In the late stages, animals display increased paw withdrawal frequency (%) to more noxious stimuli and altered weight bearing asymmetry compared to shams. The presence of anti-inflammatory cytokines, (IL-4, IL-10 and IL-14) in serum at day 7 and day 14 might contribute to the increase in paw withdrawal frequency observed in these data points. Additionally, baseline early stage and late stage neuronal responses of deep dorsal horn WDR neurones do not appear potentiated compared to sham or to each other.

Chapter 4. The impact of N-type Voltage Gated Calcium Channel blockers on behavioural and spinal neuronal hypersensitivity in the rat MIA model of OA

4.1. Introduction

4.1.1. Structure and properties of voltage gated calcium channels

Voltage gated calcium (Ca^{2+}) channels (VGCC) are expressed in excitable cells and mediate Ca^{2+} influx to the pre-synaptic terminals as they open in response to action potential-evoked membrane depolarization (Dolphin, 2013). The influx of Ca^{2+} leads to the activation of second order messaging system that lead to cellular and molecular changes. Physiological events are then initiated. VGCC comprise a main α1 transmembrane pore-forming subunit composed of 2000 amino acids residues organized in four repeated domains (I-IV), each composed by six membrane-spanning helices (S1-S6), a S4 segment that controls voltage-dependent activation and a membrane associated re-entrant P loop motif between S5 and S6 **(Figure 4.1)** (Catterall, 2011, Simms and Zamponi, 2014). The P loop region contains highly conserved negatively charged amino acid residues that form the pore forming subunit which is permeable to barium (Ba^{2+}) and calcium (Ca^{2+}) (Simms and Zamponi, 2014). Cytoplasmic linker regions with N and C termini connect the major membrane domains. There are great variations in the sequence of these cytoplasmic regions in different types of VGGC subtypes that determine the function and protein-protein interactions (Catterall et al., 2007) (Simms and Zamponi, 2014). Additionally, all calcium channels, except Ca_V3 (T-type), are associated with auxiliary subunits β and $\alpha_2\delta$ with an additional γ subunit present in skeletal muscle **(Figure 4.1)**. The β subunit has a α-helix structure with no transmembrane segments whereas the γ subunit is a glycoprotein with four transmembrane segments (Catterall, 2011). It is proposed that the β subunit interacts with the main subunit of the VGCC α_1 at the endoplasmic reticulum (ER) protecting it from polyubiquitylation, proteasome degradation and promotes folding. The β subunit also promotes forward trafficking of VGCCs out of the ER and into the plasma membrane which consequentially evokes the release of neurotransmitters (Dolphin, 2016).

The $\alpha_2\delta$ subunit is an extracellular membrane-tethered protein, encoded by a single gene that is post-translationally cleaved into 2 moieties, α_2 and δ, which are bound together via disulphide bonds (Davies et al., 2010). The subunit is attached to the plasma membrane by a GPI anchor in the δ region **(Figure 4.1)**.

VGCC can be divided into three different classes that are defined by different α1 subunits (Ca_V1-3) **(Table 4)**. These different families are expressed in different molecular VGCC subtypes; they become activated by different voltages and mediate currents with different physiological, pharmacological and regulatory properties (Dolphin, 2013). The various subfamilies of VGGC also exhibit different functions and can be divided into two categories based on their activation: high voltage-activated (HVA) channels, which open in response to large membrane depolarization and low voltage-activated (LVA) channels, which become activated by smaller voltages near neuronal resting potential (Simms and Zamponi, 2014).

The Ca_V1 (L-type) subfamily is HVA channel with a slow voltage-gated dependent inactivation making Ca^{2+} currents long lasting **(Table 4)**. Ca_V1 channels are present in neurones both in the CNS and PNS where they are in charge of regulating gene expression and initiating synaptic input, as well as in endocrine cells where they mediate hormone release (Catterall, 2000).

The Ca_V2 subfamily is divided into HVA and intermediate voltage activated **(Table 4)**. Alternative splicing and auxiliary subunit assembly gives rise to two types of HVA channels, P/Q-type channels ($Ca_V2.1$) and R-type channels ($Ca_V2.3$). N-type channels ($Ca_V2.2$) have intermediate activation voltage dependence and their rate of inactivation is more negative and faster than the L-type but more positive and slower than T-type. They are exclusively expressed in neurones where they are responsible for initiating synaptic transmission in fast synapses by mediating neurotransmitter release (Simms and Zamponi, 2014, Catterall, 2000).

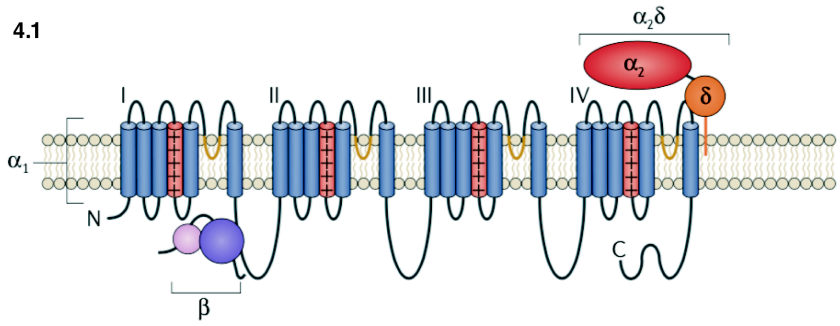

Figure 4.1 Voltage-gated calcium channel structure. The α1 subunit of the channel is composed of 24 transmembrane α-1 helices with 4 homologous repeats (I-IV). The voltage-sensing domain of the channel is comprised by the 4th transmembrane domaine segment of each homologous repeat and contains positively charged amino acids. The pore of the α1 domain is composed of yellow segments as depicted in the figure. The β auxiliary subunit binds to the intracellular linker domain (I-II) of the α1 subunit. The α2δ subunit is an extracellular membrane-tethered protein composed by two moieties, α2 and δ. These are bound together through disulphide bonds and the δ region is attached to the plasma membrane by a GPI anchor. (Image taken from (Dolphin, 2012)).

The Ca_V3 subfamily (T-type), is activated at more negative membrane potentials compared to L-type, they are a LVA subtype, inactivate rapidly and deactivate slowly and have a slow calcium conductance (**Table 4**). This subfamily is present in different cell subtypes were it plays a role in initiating and maintain repetitive firing of action potentials in DRG neurones as well as in projection neurones from lamina I (Catterall, 2000). These channels will be further discussed in chapter 5.

Table 4 Different types of VGCC, their location and function (adapted from (Catterall, 2000)

Ca^{2+} current type	***α1 subunits***	***Voltage***	***Primary location***	***Function***
L-type	$Ca_V1.1$	High voltage activated (HVA)	Skeletal muscle	Excitation-contraction coupling Calcium homeostasis Gene regulation
	$Ca_V1.2$		Cardiac muscles Endocrine cells Neurones	Excitation-contraction coupling Hormone secretion Gene regulation
	$Ca_V1.3$		Endocrine cells Neurones	Hormone secretion Gene regulation
	$Ca_V1.4$		Retina	Tonic neurotransmitter release
P/Q-type	$Ca_V2.1$		Nerve terminals Dendrites	Neurotransmitter release
N-type	$Ca_V2.2$			
R-type	$Ca_V2.3$		Cell bodies Dendrites Nerve terminals	
T-type	$Ca_V3.1$	Low voltage-activated (LVA)	Cardiac and skeletal muscle Neurones	Repetitive action potential firing
	$Ca_V3.2$		Cardiac Muscle Neurones	
	$Ca_V3.3$		Neurones	

4.1.2. The role of $Ca_V2.2$ in nociceptive signalling

The N-type VGCC, also known as $Ca_V2.2$, is distributed in the central and peripheral nervous system (**Figure 1.7**). In the periphery, $Ca_V2.2$ is present in pre-synaptic terminals of primary afferents that terminate at the superficial lamina (lamina I and II) of the dorsal spinal cord **(Figure 1.9)** (Simms and Zamponi, 2014). Calcium influx through the α1 pore-forming subunit of this channel in these neurones mediates neurotransmitter (NT) release of NTs such as calcitonin gene-related peptide (CGRP) glutamate and substance P amongst others, causing activation of projection neurones into different brain regions such as the parabrachial nucleus (PB) and periaqueductal grey (PAG) (Basbaum et al., 2009). Therefore, this channel plays a key role mediating pain transmission.

$Ca_V2.2$ contains a synaptic protein interaction site in the intracellular domain II-III linker region that allows its interaction with proteins from the synaptic vesicle release complex such as syntaxin 1 and SNAP-25 (Simms and Zamponi, 2014). This allows the channel to be in close proximity with the synaptic vesicles and, upon calcium influx, the calcium-channel-SNARE protein complex rearranges leading to vesicle release.

A number of studies have investigated the role of $Ca_V2.2$ in nociception. In an animal model of neuropathic pain, immunohistochemical studies demonstrate an up regulation of the α1 pore-forming subunit of this channel, this accompanied by mechanical and thermal allodynia (Winquist et al., 2005). Genetically modified mice have also been used to examine the role of $Ca_V2.2$ in behavioural hypersensitivity. Mice that lack $Ca_V2.2$ show no signs of motor dysfunction but exhibit abnormal pain-related behaviour. Even though acute nociceptive stimuli is normal in $Ca_V2.2$ -/- compared to $Ca_V2.2$ +/- and $Ca_V2.2$ +/+, when knock out mice undergo spinal nerve ligation they show reduced signs of neuropathic pain compared to the two other groups suggesting that this channel plays a crucial role in pain processing (Saegusa et al., 2001). Electrophysiological recordings in DRG neurones of $Ca_V2.2$ -/- mice reveal a reduction in current densities with no effects in L- and P/Q-type currents. Regarding inflammatory pain, $Ca_V2.2$ -/- mice exhibit reduced licking nociceptive behaviour in the second phase of the formalin test compared to wild-type mice, a phase normally known to induce inflammatory processes that produce persistent pain (Hatakeyama et al., 2001). No changes in liking behavioural responses were observed on the first phase of the formalin test. The same authors observed an increase in hot plate (50°C) latency in the knock-out group but no changes were observed in tail pinch test, suggesting that perhaps the role of this channel varies depending on stimuli modality (Hatakeyama et al., 2001).

Altogether, these data shows that $Ca_V2.2$ mediates neurotransmitter release from primary afferent fibers into spinal neurones and knockout studies reveal a specific role of this channel in nociception as knock-out mice show decreased pain behaviours in various chronic pain models.

4.1.3. The role of the $\alpha_2\delta$ auxiliary subunit of VGCC

The $\alpha_2\delta$ auxiliary subunit plays a major role in VGCC trafficking and function. There are four $\alpha_2\delta$ auxiliary subunits, $\alpha_2\delta$-1, $\alpha_2\delta$-2, $\alpha_2\delta$-3 and $\alpha_2\delta$-4. With $\alpha_2\delta$-1,2 and 3 are widely expressed in both the CNS and PNS while $\alpha_2\delta$-4 is mainly expressed in endocrine tissue with less in the brain (Dolphin, 2012). $\alpha_2\delta$-1 is located in pre-synaptic terminals of DRG neurones and in cell bodies to a much lower extent. $\alpha_2\delta$-2 expression is restricted to GABAergic neurones and Purkinje neurones and $\alpha_2\delta$-3 is located in some brain regions including hippocampus and cortex (Dolphin, 2013).

The α_2 and δ protein are expressed by the same gene, which encodes for a $\alpha_2\delta$ pre-protein and is post-translationally proteolysed into α_2 and δ proteins. The disulphide bone formation between α_2 and δ occurs in the ER and the N-glycosylation in the Golgi apparatus (Dolphin, 2013).

The N-terminus of the $\alpha_2\delta$ pre-protein contains a signal that allows the protein to be trafficked to the ER where the protein is cleaved. Additionally, $\alpha_2\delta$ has a von Willebrand factor A domain (VWA domain) which contains a metal ion-dependent adhesion site motif (MIDAS motif). The MIDAS motif is intact in $\alpha_2\delta$-1 and $\alpha_2\delta$-2 whereas $\alpha_2\delta$-3 and $\alpha_2\delta$-4 have missing polar residues (Dolphin, 2018).

The VWA domain interacts with the first loop in both Ca_V1 and Ca_V2 domain I, through the MIDAS motif. The interaction between VWA and Ca_V1 and Ca_V2 is essential for the proper trafficking of the channels into the plasma membrane as well as their function (Cassidy et al., 2014). Mutations in the MIDAS motif cause a reduction in trafficking of $\alpha_2\delta$-1 alone but also trafficking of the VGCC complex into the plasma membrane (Cassidy et al., 2014). Cell surface co-expression of $\alpha_2\delta$-1 and $Ca_V2.2$ is reduced in the absence of β subunit, suggesting that $\alpha_2\delta$-1 probably binds with the channel in the ER before the β subunit traffics the Ca_V1 and Ca_V2 out of the ER (Cassidy et al., 2014). As previously mentioned, the $\alpha_2\delta$ subunit also affects VGCC function by increasing current density; it does this by promoting the trafficking of VGCC and augmented expression in the plasma membrane (Dolphin, 2018). Mutations in the MIDAS motif in both, $\alpha_2\delta$-1 and $\alpha_2\delta$-2, reduces the ability of this subunit to enhance calcium because less channels are trafficked into the plasma membrane (Bernstein and Jones, 2007, Dolphin, 2012).

4.1.4. The role of the $\alpha_2\delta$-1 subunit in rodent models of chronic pain

The $\alpha_2\delta$ subunit is the target of the gabapentinoid drugs (gabapentin (GBP) and pregabalin (PGB)) (Patel et al., 2018). These drugs are the most frequently prescribed calcium channel modulators for the treatment of neuropathic pain.

Gabapentinoids bind to both $\alpha_2\delta$-1 and $\alpha_2\delta$-2 with similar affinity (Dolphin, 2018). However studies in mice with mutations in the gabapentin (GBP) binding site of either $\alpha_2\delta$-1 or $\alpha_2\delta$-2 have revealed that alleviation of neuropathic pain only occurred upon interaction with $\alpha_2\delta$-1 (Field et al., 2006). The mechanism of action of GBP has been extensively studied both in-vitro and in-vivo. Incubation of transfected cells and DRG cultures with GBP decreases cell surface expression of both $\alpha_2\delta$-1 or $\alpha_2\delta$-2 as well as causing a reduction in calcium currents (Dolphin, 2012). This suggests that GBP reduces VGCC trafficking in the plasma membrane and thus a reduction of calcium currents are observed, as fewer channels are present in the plasma membrane.

Additional studies supported this hypothesis, as they showed that Gabapentinoids inhibit $\alpha_2\delta$-1 trafficking into pre-synaptic terminals as well as inhibit the recycling of calcium channel complexes between intracellular compartments and the synaptic membrane (Bauer et al., 2009, Tran-Van-Minh and Dolphin, 2010).

Chronic treatment in SNL rats with PGB, significantly reduced paw withdrawal frequencies to mechanical and cold stimulation as well as reducing $\alpha_2\delta$-1 expression in the ipsilateral injured superficial layer of spinal dorsal horn (Bauer et al., 2009).

In the same study, Bauer et al., found increased mRNA levels of $\alpha_2\delta$-1 in DRG neurones of SNL animals indicating that upon neuropathy, $Ca_V2.2$ is upregulated to mediate increased levels of NTs release that could contribute to the continuous activation of projection neurones. *In-vivo* electrophysiological recordings of neuronal evoked responses of WDR neurones in the deep dorsal spinal cord of $\alpha_2\delta$-1 knock out mice, revealed a decreased in baseline neuronal responses to both mechanical and cold evoked stimulation. This suggested the presence of Cav2.2 in primary afferent (Patel et al., 2013).

In neuropathic pain states there is an enhanced descending serotonergic drive that causes the activation of 5-HT3 receptors in spinal cord (Suzuki et al., 2005). This enhanced facilitatory drive is thought to be crucial for the inhibitory action of gabapentinoid drugs. In-vivo electrophysiological recordings in SNL animals revealed that pharmacological spinal blockade of excitatory 5-HT3 receptors with antagonist ondansetron, diminished the inhibitory potency of GBP (Suzuki et al., 2005). In naïve animals, pre-treatment with 2-methul 5-HT agonist producing a modest facilitation in the

naïve animals and subsequent administration of GBP caused an inhibition of neuronal evoked responses of WDR neurones to both mechanical and thermal stimulation. In the absence of 5-HT agonist treatment, GBP failed to inhibit neuronal evoked responses in naïve animals (Suzuki et al., 2005). This study conducted by Suzuki et al., revealed that 5-HT3 receptor activation, is required for GBP inhibitory action.

But is it the increase in $Ca_V2.2$ trafficking via $\alpha_2\delta$-1 subunit interactions alone, or the combination of this and an enhanced serotonergic drive by actions of 5-HT at 5-HT3 receptor that maintains chronic pain states in neuropathic animals? More importantly, is targeting calcium channel action alone enough to alleviate such states?

The roles of $\alpha_2\delta$-1 and $Ca_V2.2$ have also been extensively studied in the late stage MIA model of osteoarthritis. A small but significant increase in $\alpha_2\delta$-1 mRNA expression has been reported in DRG neurones of late stage MIA animals (Rahman et al., 2009). However a more recent study reported no increase in $\alpha_2\delta$-1 mRNA DRG expression in the same animal model of OA (Lockwood et al., 2019). However both authors report an altered descending pain modulation as well as a decrease in neuronal evoked responses of WDR neurones to mechanical and thermal stimulation after spinally administrated PGB in late stage MIA animals.

Rahman et al., reported an increase in descending serotonergic drive that was activating excitatory spinal 5-HT3 R in these animals, which was blocked by using a 5-HT3 antagonist ondansetron. Lockwood et al., revealed a loss of Diffused Noxious Inhibitory Controls (DNIC) in the late stage of this animals.

Interestingly, *in-vivo* electrophysiological recording in the early acute inflammatory stage of MIA animals revealed that treatment with pregabalin has no effects on neuronal evoked responses of WDR neurones in response to mechanical stimulation (Lockwood, 2018). Furthermore, another study *in-vivo* electrophysiological study revealed that, in the late stage MIA animals (2mg/25µL), injected with a low dose of MIA (1mg/25µL) were animals do not develop neuropathic pain-like features and inflammation is predominant, pregabalin failed to reduce neuronal evoked responses of WDR neurones to electrical, mechanical and thermal stimulation (Thakur et al., 2012). Therefore, these studies suggest that $Ca_V2.2$ could play a different role between the early acute inflammatory stages and late stages with possible neuropathic-pain like features in the MIA model.

4.1.5. $Ca_V2.2$ blockers for the treatment of chronic pain

Gabapentinoids are one of the most prescribed drugs for the treatment of neuropathic pain and have proved to be effective in patients with peripheral and central neuropathy (Moore et al., 2014, Wiffen et al., 2005). However, treatment of gabapentin can produce adverse effects on patients such as suffer from dizziness, somnolence,

peripheral oedema and gait disturbance (Moore et al., 2014). Therefore, we are in need of finding new $Ca_V2.2$ blockers that cause less adverse effects. In this section I am going to discuss the different types of blockers that target $Ca_V2.2$ that and are being currently developed for novel analgesics in the treatment of neuropathic and inflammatory pain.

Zinconotide (Prialt™) was developed and approved as the first-in-class synthetic drug targeting $Ca_V2.2$. The structure of this drug is a synthetic version of ω-conotoxins. ω-conotoxins are small peptides (24-29 amino acid residues) derived from the venom of marine cone snail (Bourinet and Zamponi, 2017). They are thought to physically occlude the main pore forming subunit of $Ca_V2.2$ regardless of their state (**Figure 4.2**). They block the pore regardless of whether the channel is in an open or closed conformation. This blockage causes an inhibition of calcium influx into the cell, consequentially inhibiting peptide release and post-synaptic hyperexcitability. Some of the ω-conotoxins, such as GVIA, selectively block $Ca_V2.2$. This block virtually irreversible due to its slow onset and recovery kinetics, complicating their usage (Schroeder and Lewis, 2006).

25 years ago, ω-conotoxin was shown to be antinociceptive in neuropathic animals; intrathecal administration of the toxin in SNL animals produced a dose-dependent reduction in tactile allodynia (Chaplan et al., 1994b). Many more studies have examined the role of these toxins in neuropathic and inflammatory disorders. *In-vivo* electrophysiological studies have also looked at the role of $Ca_V2.2$ in nociceptive signalling. In the SNL model of neuropathic pain, spinal application of ω-conotoxin GVIA inhibited spinal WDR neuronal responses to mechanical and heat stimulation as well as neuronal wind-up (Matthews and Dickenson, 2001). Ziconotide, a MVIIA ω-conotoxin, was approved by the FDA for the management of chronic pain in 2004 (Patel et al., 2018). It since been shown that even though ziconotide does not produce tolerance or addiction, its usage can cause neurological side effects such as confusion, memory impairment and hallucinations (Nair et al., 2018). Additionally, Ziconotide is a large peptide; this presents challenges in terms of manufacturer and delivery as it is expensive and does not cross the blood brain-barrier (intrathecal administration is required) (Patel et al., 2018). Altogether, these challenges restrict the use of ziconotide.

N-triazole oxindole (TROX-1) is a state dependent blocker of the Ca_V2 subfamily. It is orally bioavailable and penetrates the blood-brain barrier. In cultured DRG cells TROX-1 blocks channels only when the membrane is depolarized (Patel et al., 2018, Swensen et al., 2012) (Abbadie et al., 2010). Therefore, only blocking Ca_V2 channels when they are in an active open state **(Figure 4.2).** This is preferable as TROX-1 will not have any action on channels in inactivated states and will not affect normal physiological function. In $Ca_V2.2$ knockout mice, TROX-1 failed to reverse CFA-induced hyperalgesia while it had an inhibitory effect in normal CFA-treated mice (Abbadie et al., 2010). Therefore,

suggesting that TROX-1 primarily mediates its effects through blockage of $Ca_V2.2$ channels

In the CFA model of inflammation a 3-day chronic oral treatment with TROX-1 produced a reduction in mechanical withdrawal thresholds in treated CFA rats (Abbadie et al., 2010). Additionally, oral administration of TROX-1 caused a ~70% reversal of allodynia in the SNL model of neuropathic pain in rats (Abbadie et al., 2010). In the iodoacetate (IOA) induced model of knee OA, Abbadie et al reported a 43% reversal to weight bearing post TROX-1 administration. These studies suggest that TROX-1 produces pain relief in both inflammatory and neuropathic animals models.

Previous *in-vivo* electrophysiological studies from our laboratory revealed that spinal administration of TROX-1 in SNL animals reduced neuronal evoked responses WDR neuronal to mechanical stimulation (Patel et al., 2015). However dynamic brush-, heat- cold-evoked and wind-up responses were unaffected by TROX-1 (Patel et al., 2015). Therefore TROX-1 could possibly have a modality specific role in reducing mechanical responses. In the same study Patel and colleagues showed that subcutaneous administration of TROX-1 revealed an increase in mechanical paw withdrawal thresholds in both ipsilateral (injured) and contralateral hind-paws of SNL animals 30min and 1h post-dosage. While, intrathecal injection of TROX-1 had no effect in mechanical paw withdrawal thresholds, suggesting that intrathecal injection is not the best rout of administration for this drug (Patel et al., 2015).

In the late stages of the MIA model, spinal administration of TROX-1 inhibited evoked neuronal responses to dynamic brush, heat and mechanical stimulation in a dose-dependent manner, while systemic administration of the drug only reduced evoked neuronal responses to mechanical stimulation (Rahman et al., 2015). Electrical stimulation of the receptive field showed that wind-up was not reduced in neither SNL nor late stage MIA animals in response to TROX-1(Rahman et al., 2015, Patel et al., 2015). Suggestive that NMDA receptor driven neuronal excitability of recorded spinal WDR neurones are unaffected by the drug.

In summary, these studies suggest that targeting the main $\alpha 1$ pore-forming subunit of $Ca_V2.2$ channels could be a good approach for the treatment of chronic pain as seen in rat models where behavioural and neuronal responses to evoked stimuli were decreased after administrating pharmacological agents that target the a1 subunit. What remains unclear is whether state-dependent blockers, such as TROX-1, that target the channel under open state are better than state-independent blockers, such as ω-conotoxin, that bind to the channel regardless of conformational state.

4.2

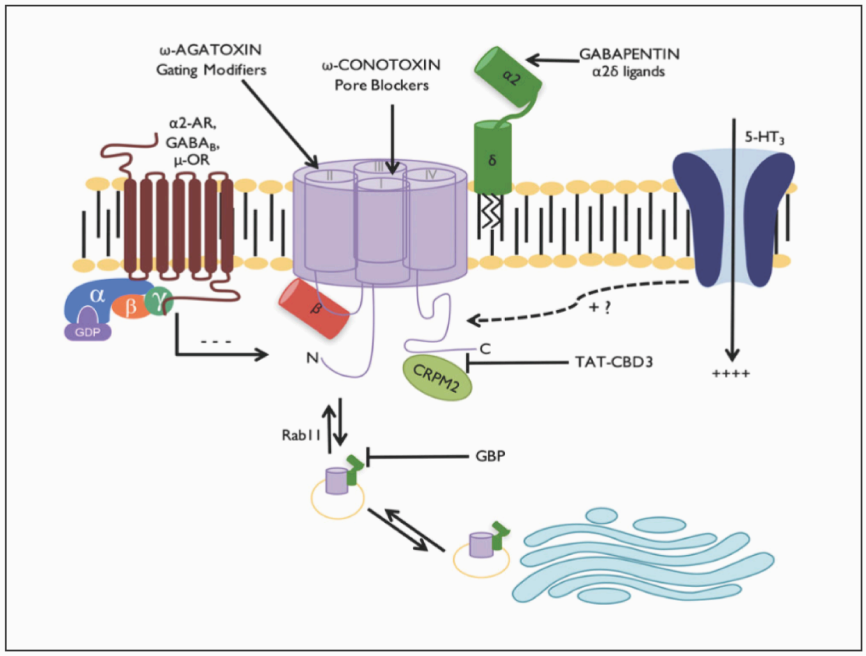

Figure 4.2 Approaches to the modulation of calcium channels in chronic pain. Gabapentinoids target the α$_2$δ-1 and α$_2$δ-2 auxiliary subunit of VGCCs inhibiting axonal trafficking as well as the endosomal recycling of the channel via Rab11, which leads to a reduction of the number of channels present in the plasma membrane. ω-conotoxins act by occluding the main α1 pore of the channel and blocking calcium entry consequently reducing neurotransmitter release. Additionally 5-HT3 receptors may contribute to VGCC activity. (Image taken from (Patel et al., 2018)).

4.2. Chapter Aims

The aims of this chapter were (1) to address if pharmacologically targeting voltage-gated calcium channel Ca$_V$2.2 decreased neuronal evoked responses to different modality stimuli in WDR neurons (2) if Ca$_V$2.2 played a differential role during the early acute inflammatory stage and the late stage with neuropathic-pain like features in the MIA model in rats and lastly, (3) whether state dependent vs. state independent blocker of the channel provided a better modulation of channel activity without affecting normal physiological function.

4.3. Methods

4.3.1. Animals

In this study, a total of 50 (TROX-1, 24; ω-conotoxin, 26) Male Sprague-Dawley rats (230g-300g), bred by the Biological Service Unit (UCL, London, UK), were used for electrophysiological experiments.

4.3.2. Behavioural assessment of mechanical hypersensitivity

In order to get more information on how the behavioural assessment of mechanical hypersensitivity **(Figure 4.3)** was addressed refer to the Methods section 2.3.5.

4.3.3. In-vivo electrophysiology

In-vivo electrophysiology was performed between day 2 and day 4 post-injection in early stage MIA and sham groups and between day 15 and day 21 post-injection in late stage MIA and sham groups. Single unit spinal WDR neuronal recordings in responses to repeated electrical stimulation followed by dynamic brush, mechanical and thermal stimulation were characterised. Three consecutive baseline were recorded per animal in both the TROX-1 and ω-conotoxin study.

For the TROX-1 study, TROX-1 was dissolved in 0.9% saline and 1μg in a volume of 25μL was topically administrated in the spinal cord. Responses to TROX-1 to all modality stimuli were recorded in both early and late stage MIA and sham animals, 10, 30 and 50min post dosing. Maximal change in response to TROX-1 compared to baseline mean was plotted for each neuron and shown in graphs (**Fig. 4.4, 4.5**). TROX-1 was gifted by Grünenthal.

For the ω-conotoxin study, drug was dissolved in 0.9% saline to a concentration of 0.5μg in a 50μL volume. Thus was topically applied into the spinal cord. Neuronal responses following ω-conotoxin administration to all modality stimuli were recorded in both early and late stage MIA and sham animals, 10, 30, 50, 70 and 90min post dosing. The maximal effect post dosing compared to mean baseline was always observed at 90min for each neuron as shown in graphs (**Fig. 4.6, 4.7**).

4.3.4. Statistics

All statistical tests were performed on raw data using SPSS, version 25 (IBM, Armonk, NY). Mechanical and Heat coding of neurones were compared using a two-way repeated-measures (RM) ANOVA, followed by a Bonferroni post-hoc test for pair

comparisons. Electricals and brush neuronal responses were compared using a paired sample Student's *t*-test. $*p < 0.05$, $**p < 0.01$, $***p < 0$ .001. All data is expressed as mean ± SEM. Additionally all statistical values for both studies can be found in APPENDIX II: Chapter 4.

4.4. Results

4.4.1. Intra-Peritoneal (I.P) injection of TROX-1 fails to increase paw withdraw threshold in MIA animals

Paw withdrawal responses in MIA rats were measured before TROX-1 and pre-vehicle I.P injection in both ipsilateral and contralateral hind-paws (**Figure 4.3**).

Post administration paw withdrawal responses were measured at time points 10, 30 and 50min post treatment. TROX-1 failed to increase paw withdrawal thresholds in both early stage and late stage MIA animals on ipsilateral and contralateral hind-paws **(Figure 4.3)**. Vehicle treated animals showed no change in paw withdraw thresholds post I.P injection.

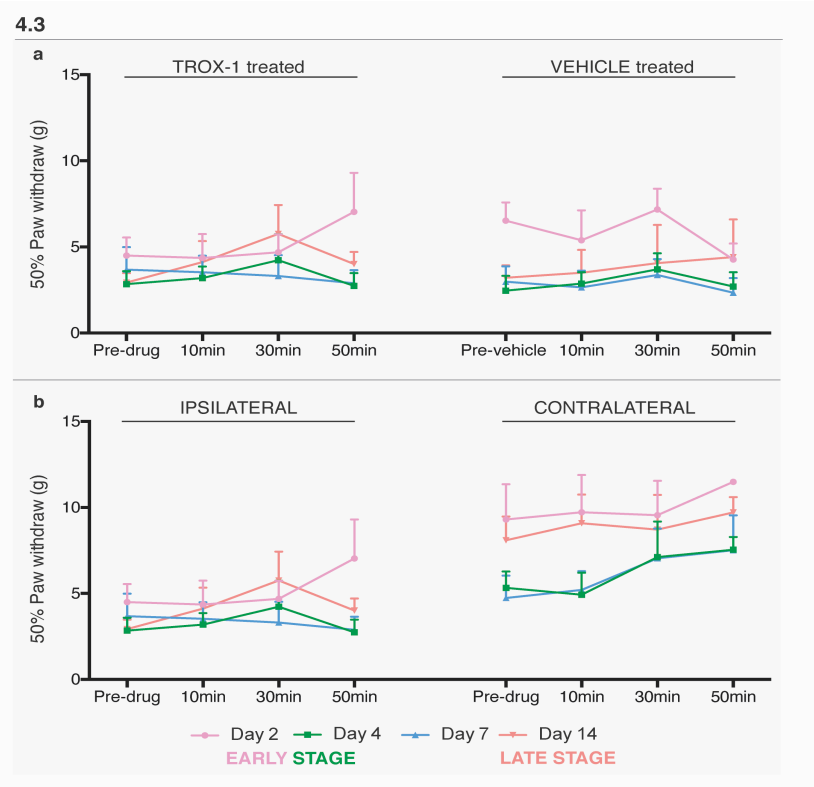

Figure 4.3. 50% Paw withdrawal thresholds (g) after TROX-1 and vehicle I.P. delivery in the early and late stages of the MIA rat model of OA. **a)** Ipsilateral (uninjured) withdrawal thresholds (g) remained unaffected 10, 30 and 50min after both, TROX-1 and vehicle I.P. administration, at day 2, 4, 7 and 14 post MIA-injection. **b)** TROX-1 I.P. treated animals showed no significant difference when comparing ipsilateral and contralateral withdrawal thresholds at day 2, 4, 7 and 14 post MIA-injection. Additionally, TROX-1 had no effects on contralateral withdrawal thresholds 10, 30 and 50min after I.P delivery of TROX-1 at days 2, 4, 7 and 14 post MIA-injection.

4.4.2. TROX-1 inhibits mechanical WDR neuronal evoked responses in the early stage of the MIA-induced rat model of OA

In early stage MIA animals 1µg of TROX-1 had no impact on neuronal evoked responses to electrical stimulation. Neither action potentials attributed to Aβ, Aδ and C-fibers, or indicators of neuronal activity post-discharge (PD), input (I) or wind-up (WU), appeared significantly changed compared to baseline **(Figure 4.4a)**. Action potential activity in responses to dynamic brush also remained unchanged post dosage **(Figure 4.4c)**. No changes were observed in electrical or dynamic brush evoked stimulation in the sham group **(Figure 4.4b and d)**.

A significant inhibitory effect of TROX-1 on mechanical evoked WDR neuronal responses was observed in the early MIA group ($F_{(3,5)}$=7.478, p=0.041(*)), however post-hoc test showed no effect when comparing post-dosage vF (2g, 8g, 26g, 60g) to baseline **(Figure 4.4e)**. Early stage sham-operated mechanical evoked action potentials also remained unchanged **(Figure 4.4f)**. Responses to thermal stimulation were not inhibited after TROX-1 administration in both MIA and sham-operated early stage animals **(Figure 4.4g and h)**.

4.4.3. TROX-1 administration does not inhibit neuronal evoked responses in the late stage MIA rat model of OA

In the late stage MIA group, TROX-1 caused a significant inhibition to evoked action potentials attributed to Ab-fibers ($t_{(4)}$=*3.259, p=(0.031(*))*. However, Aδ, C-fibers activity and indicators of neuronal excitability, post-discharge (PD), input (I) and wind-up (WU) remained unaffected. **(Figure 4.5a)** Dynamic brush, mechanical and thermal evoked responses in WDR neurones compared to baseline remained unchanged in both late stage MIA and sham-operated groups **(Figure 4.5c,e and g)**. Electrical responses in the late sham-operated control group were also unaffected after spinal TROX-1 application **(Figure 4.5b).**

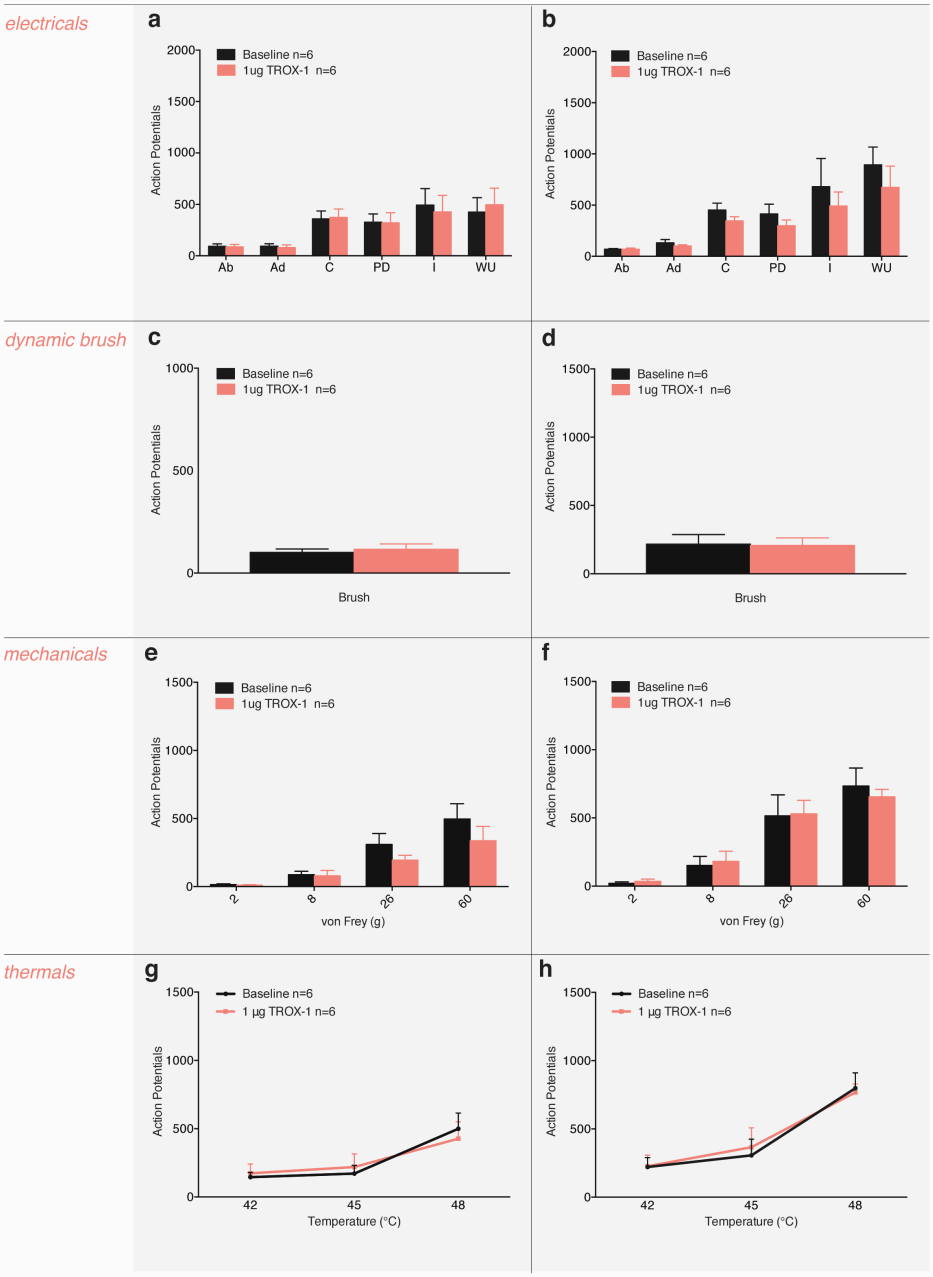

Figure 4.4. Effects of spinally applied TROX-1 on spinal neuronal evoked responses in both early stage MIA and sham-operated animals. **a,b)** Extracellular *in-vivo* electrophysiological recording of deep dorsal horn WDR neurons. Electrical stimulation of the receptive field in MIA and sham-operated groups had no effects on WDR neuron responses in both early MIA and sham-operated groups after spinally applied TROX-1. Inputs from Aδ, Aβ and C-fibers remain unchanged compared to baseline and indicators of neuronal excitability non-potentiated input (I), wind-up (WU) and post discharge (PD) also remained unchanged. **c,d)** Neuronal evoked responses to dynamic brush in both early MIA and sham-operated control group were not affected after spinally applied TROX-1. **e)** Neuronal evoked responses to mechanical punctuated stimulation were overall significantly inhibited after TROX-1 spinal administration in the early MIA group (Two-way RM ANOVA, ($F_{(3,5}$=7.478, p=0.041(*)). Pairwise comparisons with post-hoc test showed no significance differences when comparing 2, 8, 26 and 60g vF to baseline. **f)** Neuronal evoked responses to punctuated mechanical stimulation of the receptive field with vF filaments, in the sham-operated group remained unchanged after spinal administration of TROX-1 **g,h)** WDR neuronal responses to thermal stimulation were unchanged after spinally applied TROX-1 in both early stage MIA and sham-operated control group.

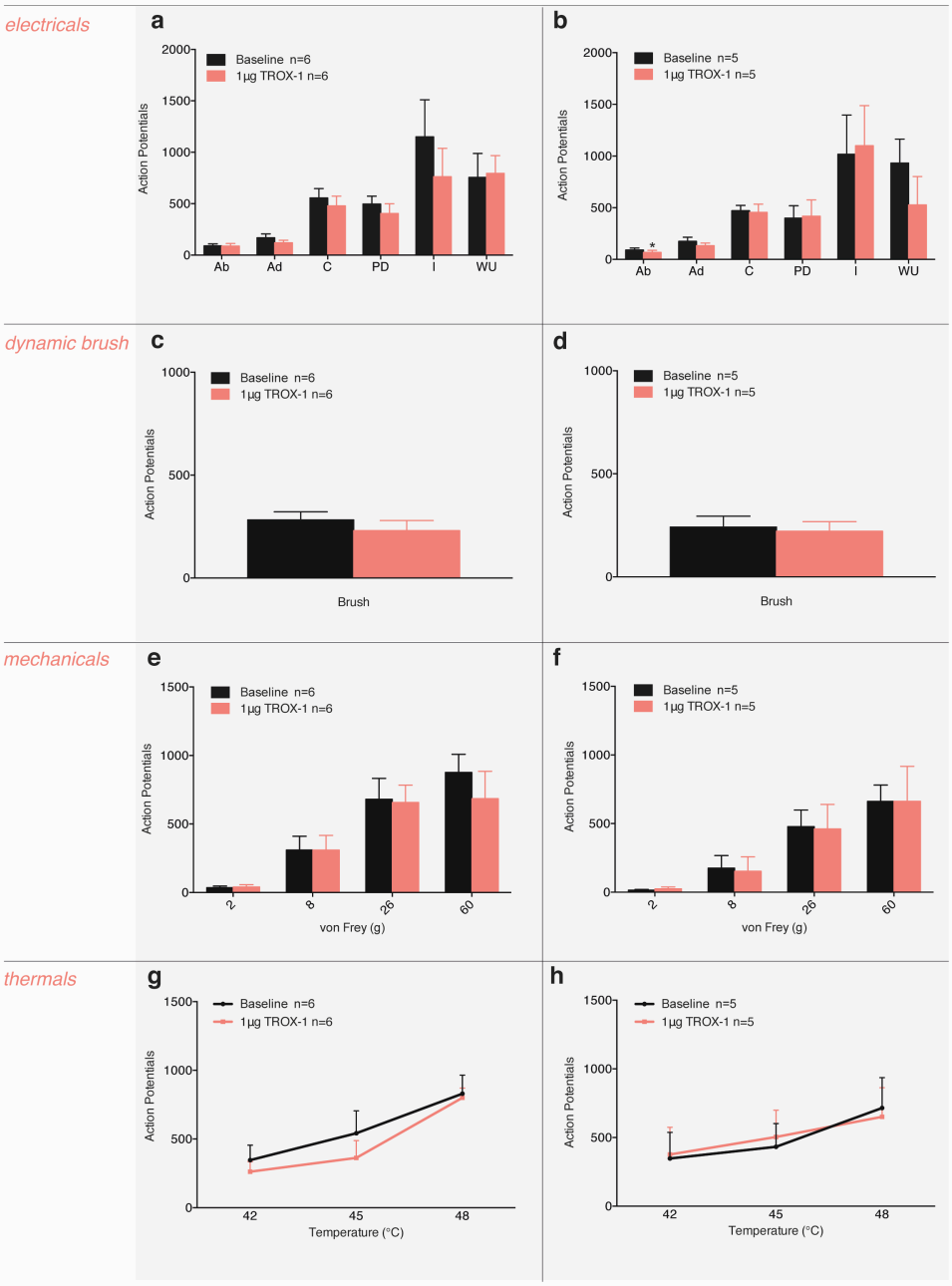

Figure 4.5. Effects of spinally applied TROX-1 on spinal neuronal evoked responses in both late stage MIA and sham-operated animals. **a)** WDR neuronal evoked responses to electrical stimulation showed that TROX-1 had no effect on inputs from primary afferent fibers and did not change indicators of neuronal excitability (I, PD and WU). **b)** WDR neuronal evoked responses to electrical stimulation in late stage sham-operated rats showed that TROX-1 significantly inhibited responses attributed to Aβ-fibers ($t_{(4)}$=*3.259, p=(0.031(*))* but did not have any effects on Aδ, C-fibers activity, post-discharge (PD), input (I) and wind-up (WU) **c,d)** WDR neuronal evoked responses to dynamic brush in both late stage MIA and late stage sham-operated rats were unaffected after spinal administration of TROX-1. **e,f)** TROX-1 had no significant effects on WDR neuronal evoked responses to mechanical punctuated stimulation in late stage MIA and sham-operated groups. **g,h)** WDR neuronal evoked responses to thermal simulation remained unaffected after spinal administration of TROX-1 in late stage MIA and sham-operated rats.

4.4.4. Spinally applied ω-conotoxin inhibits electrical and mechanical neuronal evoked responses in the early stage MIA rat model of OA

To further investigate whether or not occlusion of $Ca_V2.2$ has a differential role in WDR neuronal evoked activity in early vs. late MIA/Sham animals, ω-conotoxin was spinally administrated in both groups.

A dose of 0.5μg of ω-conotoxin GVIA was topically applied to the spinal cord in early MIA and sham-operated animals. The maximum effect of the drug was consistently observed 90min post drug administration. ω-conotoxin failed to attenuate electrical evoked action potentials attributed to Aβ, Aδ and C-fiber responses. However indicators of neuronal excitability post-discharge (PD) and input (I) were significantly inhibited while wind-up remained unaffected (PD: $t_{(6)}$=2.478, p=0.047(*); I: $t_{(6)}$=3.345, p=0.015(**); **Figure 4.6a**). Interestingly, in the sham-operated group post-discharge and input were also significantly inhibited (PD: $t_{(6)}$=2.596, p=0.041(*); I: $t_{(6)}$=3.974, p=0.007(**); **Figure 4.6b**).

WDR neuronal evoked responses to dynamic brushing were unaffected in both the MIA and sham-operated group before and after drug administration (**Figure 4.6c and d**). Spinal administration of ω-conotoxin had an overall inhibitory effect to in mechanical evoked-responses ($F_{(3,6)}$=8.220, p=0.035(*)) in the MIA group. Post-hoc test showed that ω-conotoxin only caused a small but significant inhibition in mechanical punctuated stimulation of the receptive field with 26g vF (p=0.022(*)) only in the MIA group while 2g, 8g and a 60g vF were not inhibited by the drug (**Figure 4.6e**). No effects were observed in the sham-operated group in response to mechanical punctuate stimuli (**Figure 4.6f)**. Thermal evoked responses were unaffected after spinally delivered ω-conotoxin in both early MIA and sham animals (**Figure 4.6g and h**).

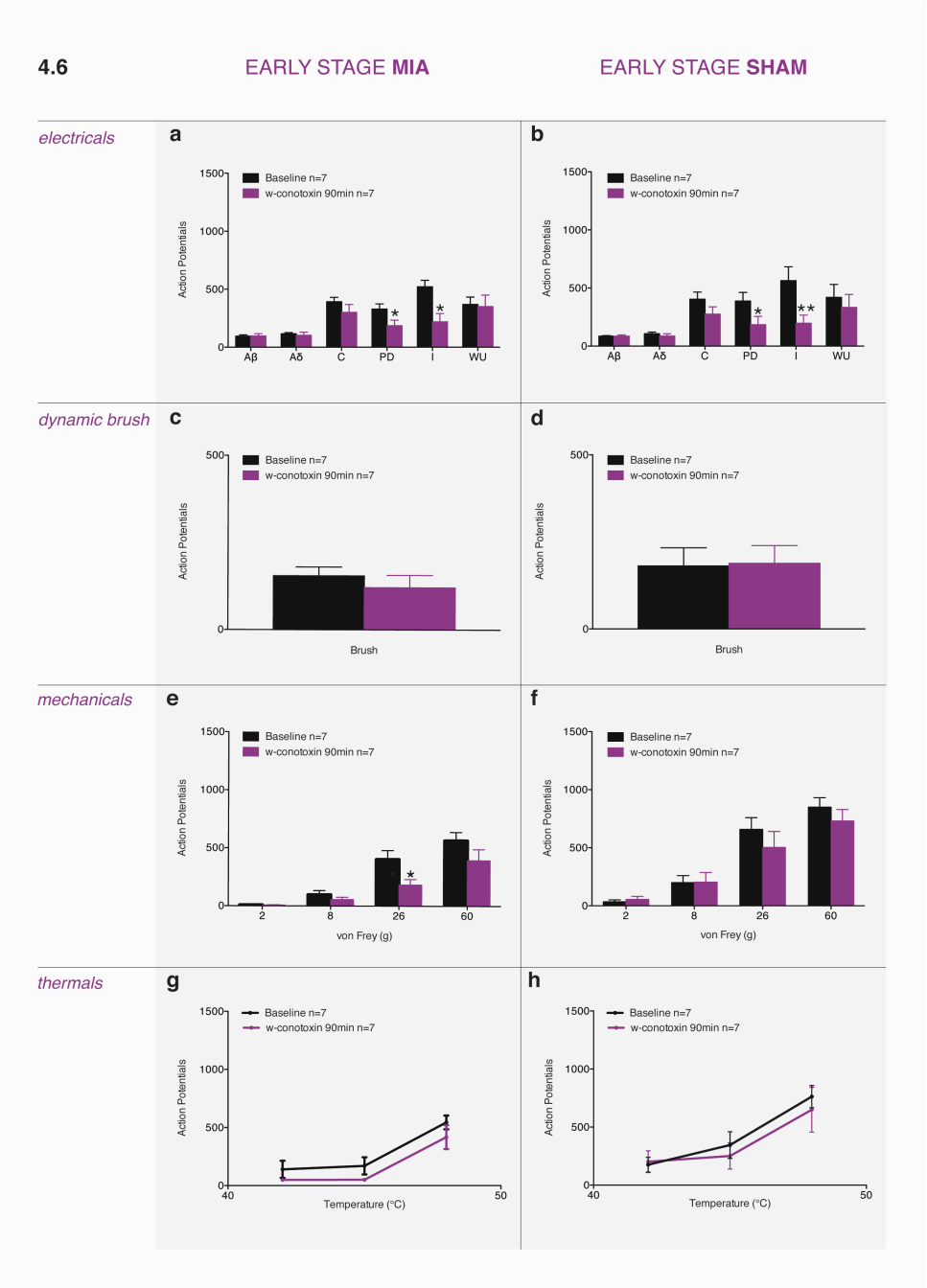

Figure 4.6. Effects of spinally applied ω-conotoxin GVIA on spinal neuronal evoked responses in both early stage MIA and sham-operated animals. **a)** WDR neuronal evoked responses to electrical stimulation in the early stage MIA group showed that ω-conotoxin significantly inhibited electrical responses attributed to post-discharge (PD) and input (I), (PD: $t_{(6)}=2.478$, $p=0.047$(*); I: $t_{(6)}=3.345$, $p=0.015$(**), while others remained unchanged. **b)** WDR neuronal evoked responses to electrical stimulation in the early stage sham-operated control group. ω-conotoxin significantly inhibited indicators of neuronal excitability post-discharge (PD) and input (I) PD: $t_{(6)}=2.596$, $p=0.041$(*); I: $t_{(6)}=3.974$, $p=0.007$(**), while others remained unchanged. **c,d)** WDR neuronal evoked responses to dynamic brush stimulation in early stage MIA and sham-operated groups showed that ω-conotoxin failed to inhibit evoked responses in both groups. **e)** WDR neuronal evoked responses to mechanical punctuated stimulation in the early stage MIA group were significantly inhibited after ω-conotoxin ($F_{(3,6)}=8.220$, $p=0.035$(**)).Pairwise comparisons with Bonferroni correction, shows a significant inhibition of 26g vF compared to baseline (26g vF, $p=0.022$(*)) **f)** WDR neuronal evoked responses to mechanical punctuated stimulation in early stage sham-operated animals showed that spinally applied ω-conotoxin had no significant effects in this group. **g,h)** WDR neuronal evoked responses to thermal simulation in early stage MIA and sham-operated groups remained unaffected after spinally applied ω-conotoxin.

4.4.5. Spinally applied ω-conotoxin inhibits all modality neuronal evoked responses in the late stage MIA rat model of OA

In the late stage of the MIA, spinal administration of ω-conotoxin caused a significant inhibition of C-fiber evoked responses after 90 minutes ($t_{(5)}$=4.750, p=0.005(**)) while Aβ and Aδ-fiber activity were unaffected. No changes were observed in the sham-operated control group. Indicators of neuronal excitability, post-discharge and input were significantly inhibited (PD: $t_{(5)}$=3.521, p=0.017(*); I: $t_{(5)}$=3.338, p=0.021(*), **Figure 4.7a**) but wind-up remained unaffected in the late stage MIA. Late sham-operated control animals however, showed an inhibitory on wind-up (WU) ($t_{(3)}$=*3.935 p=0.029(*)*) (**Figure 4.7b**).

Dynamic Brush was also significantly inhibited in the late stage MIA group ($t_{(5)}$=2.678, p=0.044(*)) (**Figure 4.7c and d**). WDR neuronal evoked responses to mechanical punctate stimuli showed an overall significant inhibition ($F_{(2,5)}$=*27.125 p=0.003(**)*), and post-hoc test revealed a change when 8g (p=0.024(*)), 26g (p=0.015(*)) and 60g (p=0.001(***)) vF were applied to the receptive field, while 2g vF did not change (**Figure 4.7.e**). Thermal heat responses were all inhibited 90min post-drug in the MIA group ($F_{(2,5)}$=*14.570, p=0.012(*)*) and post-hoc test were all significant (42°C: *p=0.022(*), 45°C; p=0.023(*), 48°C; p=0.018(*)*, **Figure 4.6g**).

After spinally applied ω-conotoxin, late sham-operated control animals showed an inhibitory effect to wind-up (WU) ($t_{(3)}$=*3.935 p=0.029(*)*) while other electrical measurements, dynamic brush and mechanical stimulation were unaffected (**Figure 4.7b,d and f**). Thermal responses in late stage sham-operated animals were significantly inhibited following spinal application of ω-conotoxin ($F_{(2,4)}$=11.711, p=0.027(*)); only responses to with 48°C heat were significantly inhibited after post-hoc test (*p=0.043(*)*) (**Figure 4.7h**).

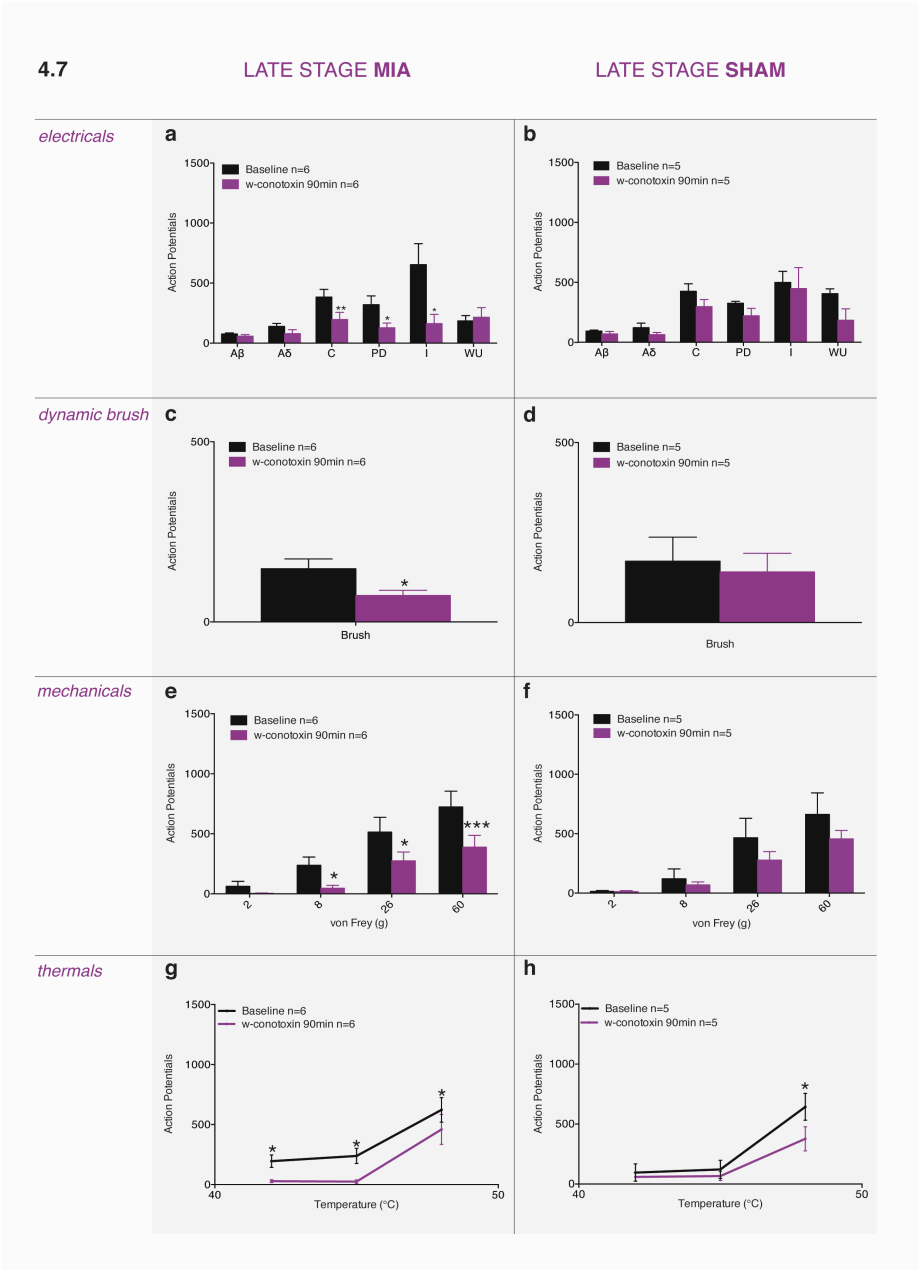

Figure 4.7. Effects of spinally applied ω-conotoxin GVIA on spinal neuronal evoked responses in both late stage MIA and sham-operated animals. **a)** Spinal administration of ω-conotoxin caused a significant inhibition WDR neuronal responses attributed to C-fibers attributed action potentials ($t_{(5)}$=4.750, p=0.005(**)), post-discharge and input (PD: $t_{(5)}$=3.521, p=0.017(*); I: $t_{(5)}$=3.338, p=0.021(*) after electrical stimulation. Aβ, Aδ-fibers activity remained unaffected. **b)** Spinal administration of ω-conotoxin had no effects on WDR neuronal evoked responses to electrical stimulation in late stage sham-operated rats.. **c)** WDR neuronal evoked responses to dynamic brush stimulation in late stage MIA were significantly inhibited after ω-conotoxin spinal application ($t_{(5)}$=2.678, p=0.044(*)) **d)** WDR neuronal evoked responses to dynamic brush in the late stage sham-operated group were unaffected after ω-conotoxin spinal application. **e)** WDR neuronal evoked responses to mechanical punctuated stimulation in the late stage MIA animals were significantly inhibited after ω-conotoxin spinal application ($F_{(2,5)}$=27.125, p=0.003(**)). Pairwise comparison with Bonferroni correction showed a significant inhibition to 8g (p=0.024(*)), 26g (p=0.015(*)) and 60g (p=0.001(***)) vF filaments. **f)** Spinal administration of ω-conotoxin had no effects on WDR neuronal evoked responses to mechanical punctuated stimulation in late stage sham-operated rats. **g)** WDR neuronal evoked responses to thermal simulation in late stage MIA group were all significantly inhibited after ω-conotoxin spinal application (($F_{(2,5)}$=14.570, p=0.012(*)), pairwise comparisons with Bonferroni correction show, 42°C: p=0.022(*), 45°C; p=0.023(*), 48°C; p=0.018(*)). **h)** WDR neuronal evoked responses to thermal simulation in late stage sham-operated group were significantly inhibited after application of ω-conotoxin (($F_{(2,4)}$=11.711, p=0.027(*), pairwise comparison with Bonferroni correction (48°C, (p=0.043(*))).

4.5 Discussion

4.5.1. State dependent vs. state independent inhibitors of Ca_V2 channels

State independent blockers such as ω-conotoxin, exert their function under most conditions of electrical excitability regardless of the channels state in contrast to state dependent inhibitors such as TROX-1, which blocks the channel under depolarized conditions when the channel is in an open or inactivated state (Abbadie et al., 2010). This differential role in antagonism action between the different types of state inhibitors suggests that while state dependent blockers would be able to inhibit nociceptive signalling while preserving other neurological functions, state independent blockers would not, as they would act on channels that are not contributing to the pathology. In fact, locally delivered treatment with state-independent blocker ziconotide through the use of an intrathecal pump still causes side effects.

Previous studies in our laboratory have reported the inhibitory effects of high doses of spinally applied ω-conotoxin GVIA on WDR neuronal evoked effects of WDR to peripherally applied stimuli in both SNL and sham-operated rats (Matthews and Dickenson, 2001). This demonstrates an ability of the toxin to inhibit responses regardless of physiological condition when applied at high concentrations. This proves to be a disadvantaged when using state independent blockers because the effects of the drug are no longer specific to the pathology itself and not only that, but can interfere with normal physiological function. In contrast, Matthews and Dickenson, observed that ω-conotoxin GVIA had a lower inhibitory effect in Sham animals compared to SNL animals but still produced significant inhibitory effects to electrical, innocuous and noxious mechanical punctuated stimuli as well as thermal noxious stimulation in SNL animals (Matthews and Dickenson, 2001). Therefore, using lower concentrations of the toxins is recommended as it still inhibits channel activity without having such a big effect to normal physiological functions.

In the present study, a low dose of 0.5μg of ω-conotoxin GVIA were spinally applied into the spinal cord in both early and late of MIA-induced OA rats. Results show that ω-conotoxin GVIA had no effects on late sham animals in terms of spinal neuronal responses to all modalities tested while early sham animals showed a statistically significant inhibitory effect in response to input and post-discharge. This differential effect in response to the toxin observed between early and late sham animals can be due to slight inflammation that occurs post injection even in early sham animals that is not due to the MIA itself.

Additionally, a differential effect on ω-conotoxin GVIA was observed between the early and late stage MIA group proving that ω-conotoxin GVIA is more potent in the late stage. Both early and late stage MIA animals exhibit inhibition of neuronal indicators of excitability input and post-discharge. Prolonged afferent fiber activation occurs both during the early MIA acute inflammatory stage and the late stage MIA group with neuropathic pain-like features. Non-potentiated input is inhibited in both stages suggesting that there is a decrease in synaptic transmission between primary afferent fibers and second order neurones, while post-discharge is a measurement of neuronal hyperexcitability mediated by post-synaptic events. Therefore it is not a surprise that these are inhibited in both early and late stages. However, C-fiber activity is inhibited in the late stage MIA group but does not appear so in the early stage MIA animals. C-fibers become active in response to noxious heat and mechanical stimulation thus it makes sense that an inhibition of C-fiber activity would harmonise with a decrease in neuronal responses to thermal heat and mechanical punctuated stimuli in the late stage MIA group (Figure 4.6). Interestingly, in the early stage MIA group, where C-fiber activity remained unchanged a significant inhibition was observed in mechanical evoked responses while thermal responses remained unchanged compared to baseline.

From changes in the peripheral drive, to changes in descending controls modulating spinal activity, to the changes in VGCC expression and function, such events could contribute to an increased inhibitory potency of ω-conotoxin in the late stage MIA rat model of OA, and this will be further discussed in the next section.

The role of state dependent blocker TROX-1 has been previously studied in the late stages of the MIA model. In contrary to previous results, the present study found, it is shown that TROX-1 failed to inhibit evoked neuronal responses to electrical, dynamic brush, mechanical and thermal stumuli both in early stage and late stage MIA groups. TROX-1 also failed to increase paw withdrawal thresholds both in early and late stages of MIA. In the SNL model of neuropathic pain, TROX-1 was shown to increase paw withdraw thresholds as well as inhibiting neuronal evoked responses to electrical, dynamic brush, mechanical and thermal stimulation (Patel et al., 2015). Prolonged peripheral stimulation causes the activation of NMDA receptors, which leads to wind-up as well as contributing to cell depolarization, which leads to VGCC open state. It is possible that during the early stages of MIA development the acute inflammation is not enough to promote an open state for the channel.

4.5.2. Maladaptive changes in voltage-gated calcium channels expression and action under pathological conditions

During pathological conditions voltage-gated calcium channel activity and function might differ from its action under normal conditions. There are different factors that might contribute to this change of function of the channel and will influence analgesic action obtain by targeting these channels.

Alternative splicing is necessary in order to assure that specific proteins are functional in specific cell types (Jiang et al., 2013). In nociceptors, $Ca_V2.2$ mRNA exhibits two mutually exclusive exons, e37a and e37b. Interestingly, e37a is less abundant elsewhere in the nervous system and plays a crucial role in thermal nociception; it is expressed almost exclusively in capsaicin-sensitive nociceptive DRG neurones (Park and Luo, 2010) (Jiang et al., 2013). Additionally, both splice isoforms exhibit different properties. Exon 37a exhibits larger currents than e37b, remains open longer upon activation and when silenced with siRNA a reduction in basal thermal nociception as well as a decrease in the development of mechanical and thermal hyperalgesia in both neuropathy and inflammatory pain is observed (Park and Luo, 2010, Altier et al., 2007). Additionally, expression of both exons contributes to tactile and mechanical allodynia (Altier et al., 2007). Cumulatively this data suggests a differential contribution of each isoform on modality specific stimuli.

The differential biophysical properties of these two splice isoforms is important when considering the inhibition of $Ca_V2.2$ by state dependent or independent blockers. Because e37a-$Ca_V2.2$ channels remain open for longer periods, state dependent antagonist such as TROX-1 could act on these channels with a higher efficiency. Interestingly in a neuropathic pain model, Altier and colleagues observed a ~50% reduction on $Ca_V2.2$ mRNA levels but no changes in e37b mRNA were observed (Altier et al., 2007), suggesting that perhaps this exon was in charge of producing large currents and contributing to thermal and mechanical hyperalgesia.

In the present study TROX-1 failed to inhibit neuronal evoked responses in both early and late stage MIA and Sham animals while ω-conotoxin inhibited mechanical responses in early stage MIA animals. Evoked neuronal responses to all modality stimuli were inhibited after ω-conotoxin spinal application in the late stage MIA group. Perhaps in this model of OA changes in splice variant isoforms of $Ca_V2.2$ could contribute to the changes in the state dependency of the channel interfering with the action of TROX-1. It would be interesting to look at what splice variants are present or upregulated in this model of OA to get a better understanding of the mechanisms that are driving nociceptive signalling in this model. Previous studies using Ziconotide showed that this toxin inhibited $Ca_V2.2$ channel currents equally well in e37a-$Ca_V2.2$ e37b-$Ca_V2.2$ channel

isoforms (Jiang et al., 2013). Additionally, intrathecal injection of Ziconotide in nerve injury mice exerted analgesic actions in response to mechanical and thermal hypersensitivity in both wild-type and e37b-only mice (Jiang et al., 2013). This suggests that conotoxin inhibitory action is effective regardless of splice variant expression. Thus, these results could explain the inhibition of neuronal evoked responses observed in this thesis study in both early and late stage MIA animals after w-conotoxin GVIA topical application.

In the SNL model, immunohistochemical studies have revealed an upregulation of $\alpha_2\delta$-1 in the ipsilateral injured side, thus suggestive of increased $Ca_V2.2$ trafficking into the plasma membrane (Bauer et al., 2009). However it is as yet unclear whether it is the upregulation of the channel into the plasma membrane, the continuous activation of 5-HT3 receptors due to enhanced serotonergic drive, or a combination of both that is required for the inhibitory actions of the gabapentinoids in neuropathic conditions. *In-vivo* electrophysiological studies from our laboratory have shown that pharmacological blockade of 5-HT3 receptors in spinal cord blocks gabapentin (GBP) inhibitory action, suggesting that it is the increased facilitatory drive, rather than the increased trafficking of the channel, that promotes GBP efficacy (Suzuki et al., 2005). In inflammatory conditions, descending serotonergic drive is unaltered in carrageenan model and GBP does not have inhibitory effect (Rahman et al., 2004).

Previous studies have shown that, in the late stage of the MIA model, pregabalin (PGB) inhibits WDR neuronal evoked responses to dynamic brush, mechanical and thermal stimuli, and reduces Ad, C and PD activity (Rahman et al., 2009). In addition, high doses of ondansetron, a 5-HT3 receptor agonist, inhibit neuronal evoked responses in late stage MIA animals in response to dynamic brush, mechanical and thermal stimulation when compared to the sham group. Spinal application of ondansetron reduced PGB efficacy (Rahman et al., 2009). This suggests that, in the late stages of the MIA mode, an increased descending serotonergic drive might also be present. In the early stages of MIA, PGB fails to inhibit neuronal evoked responses to mechanical stimuli (Lockwood, 2018).Thus, suggesting that an increased descending serotonergic drive might not be present in the early acute inflammatory stage of the MIA model.

Altogether, these results could explain the potentiated action of ω-conotoxin GVIA in the late stage MIA group as presented in this study. During the acute inflammatory early stage of the model, descending controls might not be enhanced but as the disease progresses an increased descending facilitation could appear in the late stages, which promotes channel activity through the constant activation of 5-HT3 receptors and potentiates the inhibitory action of the toxin. Increased $\alpha_2\delta$-1 mRNA levels are present in lumbar region 3 and 4 on the ipsilateral side of late stage MIA animals (Rahman et al.,

2009). However more recent studies have shown there is no increased expression of mRNA levels in either lumbar DRGs or dorsal horn of both early and late stage MIA animals (Lockwood, 2018). The MIA model provides a lot of variability, with some animals developing neuropathic pain like features, which could explain for the difference in results. Most likely, based on most data, the inhibitory action of pregabalin in the late stage MIA model is due to the continuous activation of 5-HT3 receptors rather than an upregulation of VGCC in plasma membrane.

A recent study has shown that NMDA receptors form a complex with $\alpha_2\delta$-1 subunits and that this interaction promotes the increased trafficking of NMDA receptors to the plasma membrane under neuropathic conditions (Chen et al., 2018). The authors suggest that GBP acts by blocking this interaction and reducing NMDA receptors trafficking and conclude that inhibition of the $\alpha_2\delta$-1-NMDA receptor complex by GBP could explain the exclusive inhibitory action of the drug under persistent pain conditions (Chen et al., 2018). However, the inhibition of ω-conotoxin GVIA presented in this work suggests that VGCC are still a crucial target for the treatment of chronic pain in the late stages of the MIA model of OA, independent of GBP's mechanism of action. In addition this study also suggests that targeting the channel itself, rather than channel trafficking, might prove to me a more efficient as seen by reduction of neuronal evoked responses in MIA animals by the occlusion of the α1 main pore exerted by spinal administration of ω-conotoxin. Additionally, targeting channel trafficking would not have any effects on already up-regulated channels in the plasma membrane.

4.5.3. The role of N-type channels in the RVM and amygdala

N-type channels may contribute to nociception via actions outside of the spinal cord. In the rostral ventromedial medulla (RVM) blockade of N-type channels with ω-conotoxin MVIIA (local injection), produced an inhibition of SNL-induced allodynia that was not observed in sham animals (Urban et al., 2005). Because the RVM is involved in sending descending projections into the spinal cord and modulating spinal activity, inhibition of N-type channels might reduce descending serotonergic drive and ensuring receptor mediated facilitations, therefore alleviating SNL-induced allodynia.

The amygdala plays a crucial role in processing the emotional component of pain. The central amygdala (CeA) has been shown to be involved in the expression of behavioural responses to aversive stimuli such as fear and anxiety (Finn et al., 2003). N-type channels are also present in the CeA, and intra-CeA administration of ω-conotoxin GVIA produced a reduction in condition aversive behaviour (Finn et al., 2003). In the same study, the authors found that in the formalin-induced nociceptive model, ω-

conotoxin GVIA treated rats had an earlier onset of nociceptive responses as well as increased formalin-evoked nociceptive behaviours (Finn et al., 2003). This data suggests that N-type channels are crucial for amygdala processing of aversive behaviour, but at the same time a decrease of CeA activity leads to pro-nociceptive behavioural effects. The latter might be attributed to the fact that the CeA sends projections to the midbrain periaqueductal grey (PAG), which is a major relay site for descending inhibitory pathways (Todd, 2010) and decreased CeA activity may impact descending modulation from the PAG (da Costa Gomez and Behbehani, 1995).

4.5. Summary

Spinal administration of TROX-1 did not modulate spinal neuronal activity in response to evoked stimuli in the early or late stages of the MIA rat model of OA. Additionally intra-peritoneal injection of TROX-1 had no effects on paw withdraw thresholds in MIA and Sham induced animals. On the other hand, targeting Cav2.2 with state independent blocker ω-conotoxin GVIA causes an inhibition of WDR neuronal responses in both early and late MIA stage animals, and a more potent action was observed in the late stages of the MIA model. This data suggests that N-type channels may play a differential role in nociceptive signalling during the acute inflammatory early stage of the MIA model and in the late stage of the MIA model of OA where neuropathic pain-like features are observed.

Chapter 5. Targeting the USP5/$Ca_V3.2$ interaction withTAT-cUBPI-USP5 peptide in the late stages of the MIA rat model of OA

5.1. Introduction

5.1.1. Properties of T-type voltage gated calcium channels

T-type (Ca_V3) voltage gated calcium channels are key players in regulating neuronal excitability both in the central and peripheral nervous system. These channels are extremely sensitive to voltage changes and are able to open upon small membrane depolarization (Gray and Macdonald, 2006). Calcium entry through these channels allows for further membrane depolarization and action potential bursts. Interestingly, these channels are capable of recovering a small portion of current when hyperpolarization is followed by depolarization (Iftinca and Zamponi, 2009). This recovery enables them to become activated at resting membrane potentials and leading to the generation of low-threshold calcium spikes known as “rebound bursting” (Iftinca and Zamponi, 2009) (Rajakulendran and Hanna, 2016). Once the membrane is sufficiently depolarized, activation of sodium channels can initiate high frequency firing called “burst firing” (Steinmeyer et al., 2018). The vast majority of T-type channels remain inactivate at normal neuronal resting membrane potentials, becoming activated during hyperpolarization. When eventually the membrane depolarizes these channels can immediately open in order to trigger the bursts (Weiss and Zamponi, 2019). However, a small percentage of T-type channels are able to remain open and tonically active at resting state creating a “window” for calcium influx into the cell at rest (Crunelli et al., 2005). This “window” is important to generate neuronal firing patterns during sleep, in cardiac automaticity and to mediate hormone release. Additionally, T-type channels located in pre-synaptic neve terminals can mediate neurotransmitter release near the resting potential state (Waxman and Zamponi, 2014).

5.1.2. Role of $Ca_V3.2$ in nociceptive processing

Voltage gated calcium channel $Ca_V3.2$ is present at various locations along sensory dorsal root ganglion (DRG) neurones and is essential for pain transmission (Zamponi et al., 2009). From the periphery, where it plays a role in mechanotransduction, to the axons, where it plays a role in initiating and maintaining neuronal excitability, and up to the pre-synaptic terminals in the spinal dorsal horn where it mediates neurotransmitter release (Zamponi et al., 2009). $Ca_V3.2$ can be found in small diameter unmyelinated fibers (C-fibers) as well as in medium diameter thinly myelinated (Aδ-fibers) fibers (Jagodic et al., 2008). Additionally, $Ca_V3.2$ channels have also been identified in a subgroup of small diameter subtype of DRG neurones classed as T-rich cells (Rose et

al., 2013). These T-cells express high density T-currents, have a robust response to capsaicin and respond to high-threshold mechanical stimuli (Nelson et al., 2007). Small and medium diameter sensory fibers exhibit TTX-resistant sodium (Na^+) currents supported by $Na_V1.8$ and $Na_V1.9$ channels (Coste et al., 2007). Electrophysiological studies have showed that T-rich cells co-express with these TTX-resistant currents (Coste et al., 2007), suggesting that these may play a part in nociceptive transmission. Other studies using $Ca_V3.2$ knockdown mice revealed the pronociceptive role of this channel in acute pain. $Ca_V3.2$ knockdown mice display increased latency of tail licking/biting in response to tail clip test (Choi et al., 2007). The authors also observed an increased latency to heat-induced behaviour in hot plate test and reduced licking behaviour upon capsaicin administration (Choi et al., 2007). Interestingly, after spinal nerve ligation $Ca_V3.2$ (-/-) mice still developed neuropathic behaviours (Choi et al., 2007). Contrary to these results, intrathecal administration of an antisense oligonucleotide targeting $Ca_V3.2$ caused a reduction in T-type large currents in dissociated DRG neurones, as well as a decrease in mechanical and thermal nociception and tactile allodynia in both in healthy and neuropathic rats (Bourinet et al., 2005).

Although these studies studies have shed some light on the role of $Ca_V3.2$ in nociception, the cellular mechanisms by which these T-type channels regulate pain signalling in afferent fibers are still unclear. Their presence at different locations in primary afferent fibers hints that they might regulate afferent fiber activity through different mechanisms (Waxman and Zamponi, 2014). In the periphery, $Ca_V3.2$ channels are expressed in nerve endings in the skin. D-hair mechanoreceptors are involved in cutaneous mechanosensation, they have low mechanical threshold, a large receptive field and they can become activated by forces 10 times lower than other fibers (Heppenstall and Lewin, 2006). It is thought that D-hair mechanoreceptors require $Ca_V3.2$ to modulate their function and suggest a role for $Ca_V3.2$ in tactile sensation (Heppenstall and Lewin, 2006). As discussed in the previous section (5.1.1), $Ca_V3.2$ exhibit rebound bursting activity and this activity which is thought to regulate excitability of primary afferents by facilitating the opening of co-localized Na_V channels (Hildebrand et al., 2011). In dorsal horn $Ca_V3.2$ is present in pre-synaptic terminals, where they have been associated with synaptic release machinery suggesting a role in low-threshold exocytosis (Waxman and Zamponi, 2014). The literature has provided extensive research showing how these channels contribute to nociception at different levels and suggesting that $Ca_V3.2$ is an important target for the therapeutic treatment of pain.

5.1.3. Targeting USP5 and $Ca_V3.2$ interaction for analgesia

$Ca_V3.2$ calcium currents are upregulated in various painful pathological disorders (Weiss and Zamponi, 2019). However the mechanisms behind this upregulation remain unclear. Ion channel protein levels can by regulated by ubiquitination, a process, mediated by E3 ubiquitin ligase (Garcia-Caballero et al., 2014). Ubiquitin-specific proteases (USP) remove ubiquitin groups from ubiquitin-conjugated proteins that are a target for degradation (Gadotti and Zamponi, 2018). By removing ubiquitin groups, proteases restore the protein stability and decrease their chances of undergoing degradation (Gadotti and Zamponi, 2018).

Ubiquitin specific protease USP5, is an 835 residue multidomain enzyme that has been shown to bind to the intracellular domain III-IV of $Ca_V3.2$ through a specific region called cUBPI (Garcia-Caballero et al., 2016). USP5-$Ca_V3.2$ interaction reduces $Ca_V3.2$ ubiquitination and enhances the stability of this channel at the cell surface, allowing for its accumulation. This increase of the channel in the plasma membrane, results in an increase in whole cell current. Since an increased activity of $Ca_V3.2$ is observed in models of chronic pain, it is inevitable to ask the question of whether USP5 is involved in the stability of the channel during this pathology. Previous research, demonstrated that USP5 is upregulated in various pain models; after intraplatar injection of CFA, in the nerve injury model, inflammatory pain models and in a post-surgical pain model (Garcia-Caballero et al., 2014) (Gadotti and Zamponi, 2018) (Joksimovic et al., 2018). Additionally Garcia-Caballero and colleagues observed that, silencing UPS5 by delivery of shRNA results in decreased USP5 protein levels in DRG neurones and dorsal horn tissue and prevented $Ca_V3.2$ upregulation after chronic constriction injury (CCI). In the same study, injection of USP5 (short hairpin RNA) shRNA reversed mechanical hyperalgesia in CFA treated mice (Garcia-Caballero et al., 2014), suggesting a role of this enzyme in $Ca_V3.2$ stability during chronic pain states.

Disruption of the interaction between these two proteins has been shown to produce analgesic effects in animal models. This has been achieved by generating a trans-activating transcriptional activator (TAT) conjugated peptide that disrupts the binding of USP5 to $Ca_V3.2$ (Garcia-Caballero et al., 2014). *In-vitro*, Tat-$Ca_V3.2$-III-IV linker peptide, which interacts with USP5, has been shown to attenuate calcium entry in dissociated DRG neurones and to reduce spontaneous neurotransmitter release in spinal cord slices (Garcia-Caballero et al., 2014). This suggests a role for the channel in both cell bodies and pre-synaptic terminals. Additionally, intrathecal injection of this peptide in the CFA model in mice has shown to attenuate mechanical hypersensitivity 30min post-injection and lasting up to 6h (Garcia-Caballero et al., 2014). In CFA-treated

animals, a reduction of $Ca_V3.2$ was observed in dissected DRG neurones 90min post-TAT-$Ca_V3.2$-III-IV linker peptide administration. Garcia-Caballero and collegues, showed that, in the CCI mice model of neuropathic pain, this peptide also reversed mechanical hyperalgesia.

cUBPI was identified as the region of USP5 that interacts with the intracellular domain III-IV of $Ca_V3.2$. Additionally, a TAT-cUBPI-USP5 peptide has also has been shown to reduce mechanical allodynia both in CFA-treated animals and in male mice subject to sciatic nerve injury (PSI) (Garcia-Caballero et al., 2016). In a diabetic neuropathy model, TAT-cUBPI-USP5 peptide reduces thermal hyperalgesia (Garcia-Caballero et al., 2016), and in CFA-treated female mice, these peptide increased paw withdraw thresholds (Gadotti and Zamponi, 2018).

Altogether these studies demonstrate not only that $Ca_V3.2$ is a crucial player in developing pain hypersensitivity followed both inflammation and neuropathy, but also that targeting the interaction of the channel with USP5 through small peptides provides analgesic effects in various animal models of chronic pain. Hence, analgesics that targeting the molecular processes, such as channel trafficking, that occur after pathology and lead to $Ca_V3.2$ malfunction, might prove more beneficial than focusing on blocking channel activity (Garcia-Caballero et al., 2016). This is because, normal channel function won't be altered. However, there are different isoforms of T-type channels and producing blockers that distinguish between these is challenging.

5.1.4. Ca_V3 blockers for the treatment of chronic pain

There are currently two types of calcium channel blockers being tested in humans for safety and efficacy for the treatment of chronic pain. These are Z944 and ABT-639 (LeBlanc et al., 2016, Jarvis et al., 2014, Lee, 2014).

Z944 is first-in-class T-type calcium channel blocker with enhanced affinity for the channels inactivated state of the channel (Zamponi et al., 2015). Z944 inhibits calcium currents from all types of T-type channels isoforms with a 200 fold higher selectivity for T-type over N-type channels (Lee, 2014). In preclinical models, oral administration of Z944 has shown to reverse mechanical hypersensitivity in animals subject to the Complete Freud's Adjuvant (CFA) model of inflammatory pain (Lee, 2014). Z944 reduce flinch responses during the inflammatory pain phase in CFA-treated rats and in both acute and inflammatory phases in mice (Lee, 2014). Additionally, Z944 is thought to inhibit burst firing of T-type channels in thalamic neurones (LeBlanc et al., 2016). Administration of this compound in rats with CCI showed a normalization of thalamic activity as well reversing thermal hyperalgesia and producing an increase in conditioned

place preference (CCP) (LeBlanc et al., 2016). Z944 has demonstrated to have clinical efficacy in phase 1 clinical trial in patients suffering from post-operative pain, fibromyalgia and inflammatory bowel syndrome (Lee, 2014). This drug is currently in second phase clinical trials.

ABT-639 is a peripherally acting T-type calcium channel blocker that shows less affinity to $Ca_V2.2$ channels and weak or no activity on other calcium channels including L-type and P/Q-type channels (Jarvis et al., 2014). In animal models, ABT-639 decreases nociception in different neuropathic pain and inflammatory models (Ziegler et al., 2015). In the spinal nerve ligation (SNL) model, ABT-639 has been shown to decrease mechanical hypersensitivity by increasing paw withdrawal thresholds in rats (Jarvis et al., 2014). In the same study the author found a decrease in neuronal evoked responses to mechanical stimuli (10gvF) after ABT-639 administration through *in-vivo* electrophysiological recordings of WDR neurones.

In the late stage of the MIA model, orally administrated ABT-639 caused a reversal of pain measured by hind limb grip force deficit (Jarvis et al., 2014). Lastly, in the chronic constriction injury (CCI) model of neuropathic pain ABT-639 also increased paw withdrawal thresholds as well as attenuated cold allodynia (Jarvis et al., 2014). In contrast, the authors found that systemic administration of ABT-639 produced weak antinociceptive effects in the CFA and carrageenan-induced models of inflammatory pain, suggesting that ABT-639 might not be as efficient at treating this type of pain. In phase 1 clinical trials ABT-639 demonstrated an acceptable safety profile at all doses and is currently in phase 2 trials (Ziegler et al., 2015).

5.2. Chapter Aims

The aim of this chapter was to address, through *in-vivo* electrophysiological recordings, the effects of spinally delivered TAT-cUBPI-USP5 peptide on WDR neuronal responses to evoked stimuli. The results presented in this chapter are preliminary data.

5.3. Methods

5.3.1. Animals

In this study, a total of 9 Male Sprague-Dawley rats (230g-300g), bred by the Biological Service Unit (UCL, London, UK), were used for electrophysiological experiments. Weights of all animals can be found in Appendix III: Chapter 5.

5.3.2. *In-vivo* electrophysiology

Refer to Chapter 2: Methods and Materials, section 2.4, in order to obtain more information on in-vivo electrophysiological recordings. In-vivo electrophysiology was performed between day 14 and day 21 post-injection in late stage MIA and sham groups. Single WDR neurones were characterized for responses to dynamic brush, mechanical and thermal stimulation.

Three baseline responses to all modality stimuli were recorded in both late stage MIA and sham animals before spinal administration of 10µg TAT-peptide-USP5-cUBT was spinally applied in a volume of 50µL and neuronal events were recorded in response to all modality stimuli 15, 45, 90 and 130min post-dosing. Maximal neuronal changes following administration of TAT-peptide-USP5-cUBT compared to baseline were plotted for each neuron.

5.3.3. Statistics

All statistical tests were performed on raw data using SPSS, version 25 (IBM, Armonk, NY). Mechanical and Heat coding of neurones were compared using a two-way repeated-measures (RM) ANOVA, followed by a Bonferroni post-hoc test for pair comparisons as well as DNIC. Brush neuronal responses were compared using a paired sample Student's *t*-test. $^{*}p < 0.05$, $^{**}p < 0.01$, $^{***}p < 0$ .001. All data is expressed as mean ± SEM. Additionally all statistical values for both studies can be found in Appendix III: Chapter 5.

5.4. Results

5.4.1. TAT-cUBPI-USP5 peptide increase neuronal evoked responses to dynamic brush of WDR in the late stage MIA rat model of OA but does not affect mechanical and thermal evoked activity

Intrathecal administration of TAT-peptide-UPS5-cUBT caused a significant increase ($t_{(5)}$=*3.041*; *p=0.011(*))* of neuronal activity of deep dorsal horn WDR neurones in response to dynamic brush stimulation of the receptive field (**Figure 5.1a**). However, neuronal evoked responses of WDR neuron to mechanical punctuate stimulation and heat remained unchanged after intrathecal administration of the peptide (**Figure 5.1c,e**). Additionally, TAT-peptide-UPS5-cUBT had no significant effect in neuronal evoked responses to dynamic brush and mechanical stimulation (**Figure 5.1b,d**). However, thermal evoked neuronal responses were significantly inhibited ($F_{(2,3)}$=*3.888*; *p=0.033(*))* and pairwise comparisons with Bonferroni correction showed a significant inhibition to thermal stimulation to 42°C (*p=0.023(*))* and 48°C (*p=0.041(*)*) compared to baseline responses (**Figure 5.1f**).

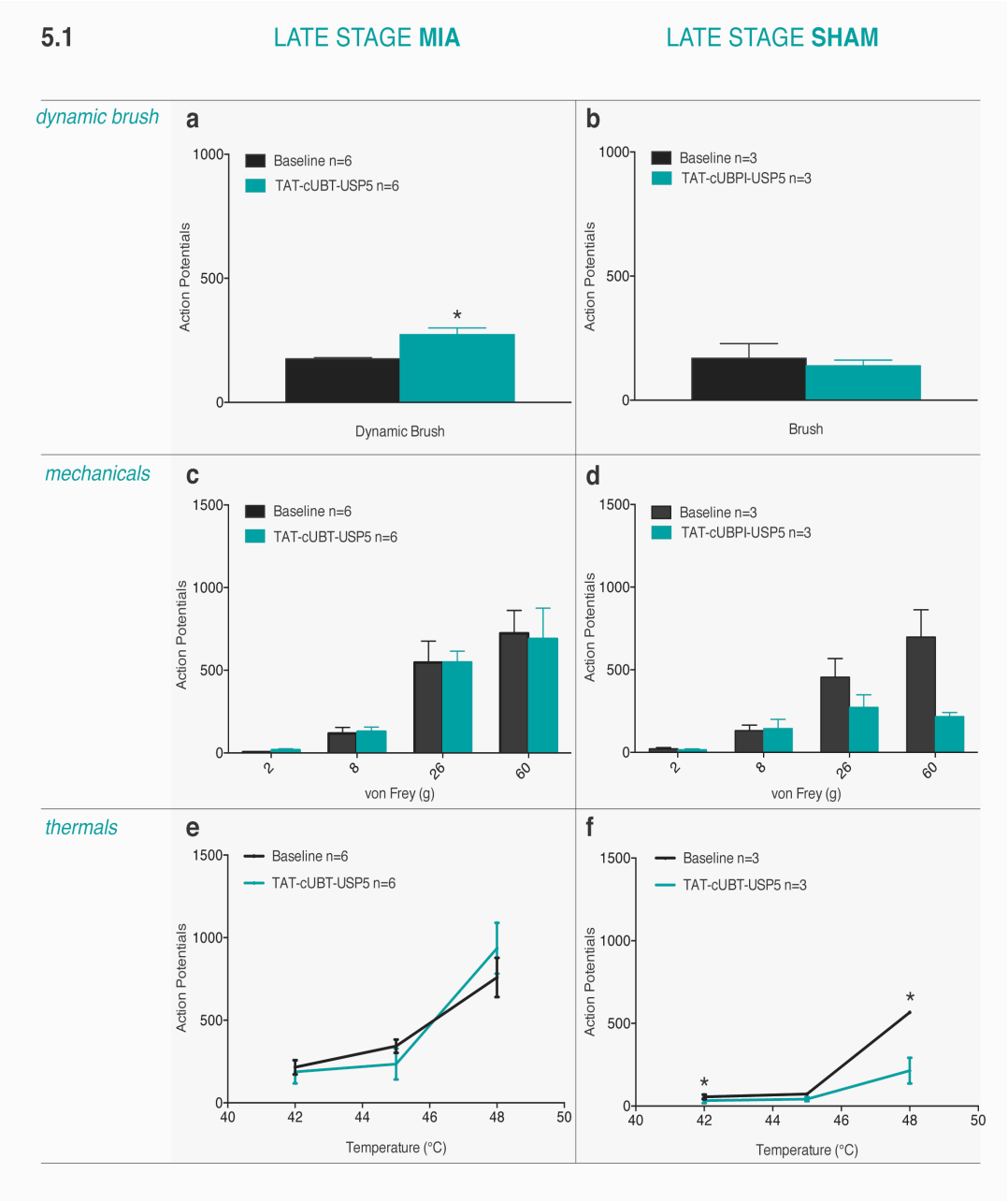

Figure 5.1. Effect of spinally applied TAT-cUBT-USP5 peptide on spinal neuronal evoked responses in both late stage MIA and late stage sham-operated rats in response to different modality stimulus. **a) WDR** neuronal evoked responses to dynamic brush were significantly increased after TAT-cUBT-USP5 administration (t_{as}=3.041; p=0.011(*)). b) WDR neuronal evoked responses to dynamic bru **c)** WDR neuronal evoked responses to mechanical punctuated stimuli remained unaffected after spinal administration TAT-cUBT-USP5 peptide. **e)** WDR neuronal evoked responses to thermal stimulation remained unaffected post spinal administration of TAT-cUBT-USP5 peptide **b,d)** WDR neuronal evoked responses to dynamic brush and mechanical stimulation were unaffected after TAT-cUBT-USP5 administration in the late stage sham group. **f)** WDR neuronal evoked responses to thermal stimulation were significantly inhibited in the late stage sham group after spinally administrated TAT-cUBT-USP5 peptide (*F_{as}=3.888; p=0.033(*)*) and pairwise comparisons with Bonferroni correction showed a significant inhibition to thermal stimulation to 42°C *(p=0.023(*))* and 48°C (*p=0.041(*))* compared to baseline responses.

5.5. Discussion

The T-type voltage gated calcium channel $Ca_V3.2$ plays a crucial role in mediating pain sensation at various locations along the small primary afferent fibers (Zamponi et al., 2015). Their fast rate of activation, strong-voltage dependency and slow deactivation rate allow them to modulate transmembrane calcium influx (Jarvis et al., 2014).

In the periphery, $Ca_V3.2$ channels are expressed in low-threshold mechanoreceptors, more specifically in D-hairs (Wang and Lewin, 2011, Bernal Sierra et al., 2017). These are Aδ-fibers, with low mechanical thresholds and are sensitive to slow moving stimuli. The role of Cav3.2 expressed in these mechanoreceptors is to amplify the mechanosensory signals (Wang and Lewin, 2011). Bernal Sierra and colleagues also identified a second population of $Ca_V3.2$ positive neurones within the DRG that are CGRP+, innervate muscles and project to the superficial laminas of spinal dorsal horn (Bernal Sierra et al., 2017). Additionally, another study also proposed that C-low threshold mechano receptors (LTMR), a subgroup of C-fibers, also express $Ca_V3.2$ along its axons. Thus, $Ca_V3.2$ is not only present in nerve endings, but also, along the axons of peripheral nociceptors and in spinal dorsal horn. Recent immunofluorescence studies have identified the presence of this channel in laminas I, II and II of the dorsal horn (Candelas et al., 2019). More specifically, the authors found that ~60% of lamina II neurones express $Ca_V3.2$ (Candelas et al., 2019). $Ca_V3.2$ has been identified pre-synaptically in the terminals of primary afferent fibers, where it contributes to spontaneous neurotransmitter release (Jacus et al., 2012) as well as post-synaptically in lamina I in NK1+ projection neurones (Ikeda et al., 2003). The role of the channel post-synaptically is to contribute, together with NMDA receptors, to the intracellular rise of calcium in order to generate long term potentiation (LTP) (Ikeda et al., 2003). Thus, $Ca_V3.2$ is a key mediator of the pain signal both in the periphery and central nervous system making it a great target for the treatment of pain. Targeting both peripheral and central $Ca_V3.2$ channels pharmacologically has been proven to reduce nociceptive behaviour in rats in different chronic pain states (Ziegler et al., 2015, Zamponi et al., 2015, M'Dahoma et al., 2016, Lee, 2014, LeBlanc et al., 2016). Because most drugs target the main a1 pore of the channel, and although they have proven to be effective, targeting channel dysregulations might be a good approach to be able to reduce the influx of calcium through the channel, while maintaining their normal activity (Gadotti and Zamponi, 2018). Additionally, the use of small organic molecules is also crucial as it provides an easier delivery.

In this study, TAT-cUBPI-USP5 peptide was intrathecally delivered onto the spinal cord of late stage MIA and sham animals and neuronal evoked responses of WDR to dynamic brush, mechanical and thermal were measure at 15, 45, 90 and 140min post-dosing. The peptide, acts by interrupting the interaction of ubiquitin USP5 to the $Ca_V3.2$

cUBPI region. This interruption disputes the stability of the channel at the plasma membrane that is normally acquired by the interaction with USP5 prompting degradation of the channel by ubiquitination. Although the peptide has never been tested in an animal model of OA before, it has been shown to attenuate mechanical withdrawal thresholds at 45, 90 and 180 min post-dosing in the CFA model of inflammatory pain as well as in the PSI model of neuropathy (Garcia-Caballero et al., 2014, Garcia-Caballero et al., 2016, Gadotti and Zamponi, 2018) Similarly, in a mouse model of diabetic neuropathy, intrathecal administration of TAT-cUBPI-USP5 peptide appeared to have a mild but significant increase in thermal withdrawal thresholds in these animals 90min post-dosing (Garcia-Caballero et al., 2016). Thus, it is surprising that in this chapter's study, TAT-cUBPI-USP5 peptide failed to inhibit neuronal responses of WDR neurones evoked by mechanical punctuated stimuli as in the late stages (14-21 days post injection), since this is when the animals start exhibiting neuropathic pain-like features (**Figure 5.1a,c and e**). It is possible that delivering the peptide at even later stages (28 days) would produce an inhibitory effect, as the neuropathic pain-like component would be further developed as previously observed in other studies (Ivanavicius et al., 2007, Liu et al., 2011, Havelin et al., 2016, Ferreira-Gomes et al., 2012). In addition, delivering the peptide in the early acute inflammatory stage of the MIA model, which may replicate the acute CFA model, might provide a better insight on the ability of the peptide to inhibit WDR evoked responses. Although, in late sham group TAT-cUBPI-USP5 peptide inhibited neuronal evoked responses to thermal heat, the number of sham animals was quite low and more experiments need to be done in order to properly address if this inhibitory effect is significant in a bigger sized sample number.

Deep dorsal horn WDR neurones receive input from nociceptive and non-nociceptive neurones, conveying information from multiple sources. Since $Ca_V3.2$ channels in spinal cord are mainly present in the superficial laminae (Candelas et al., 2019) effects of the TAT-cUBPI-USP5 might be restricted to superficial laminae and might not translate to effects on the deeper laminae. In addition, $Ca_V3.2$ are also present in post-synaptic terminals of lamina I projection neurones. Therefore, extracellular in-vivo electrophysiological recordings of lamina I-II neurones would provide more information on the effects of this peptide on neuronal evoked responses than the lamina V recordings presented here . Although $Ca_V3.2$ contributes to spontaneous neurotransmitter release from primary afferent fibers, it is $Ca_V2.2$ that plays the main role in the release of neurotransmitters. Thus, targeting $Ca_V3.2$ activity might not be enough to produce a decrease in neurotransmitter release leading to an inhibitory effect on WDR neuronal evoked responses. In addition, as shown through this thesis, suprathreshold stimuli can be gauged with extracellular *in-vivo* neuronal recordings in anaesthetised animals. These suprathreshold stimuli are greater than the threshold stimuli that are applied in behavioural assays and perhaps that may explain the differences between the electrophysiological and behavioural studies and indicates that $Ca_V3.2$ plays a

small roll in sensory transmission. Combination treatment of state dependent blockers that target both $Ca_V3.2$ and $Ca_V2.2$ may lead to a more efficient inhibitory approach.

T-type channels control subthreshold excitability of DRG neurones by lowering the threshold of action potential initiation in a subpopulation of medium size DRG neurones that are IB_4 positive as well as in D-hair mechanoreceptors (Jarvis et al., 2014).. Furthermore, small DRG cells exhibit T-type currents that are sensitive to capsaicin (Jarvis et al., 2014). Therefore, T-type channels are present in cell bodies of DRG neurones of both Aδ and C-fibers and perhaps targeting $Ca_V3.2$ channels in the periphery might prove a better and more efficient strategy. As previously mentioned the peripherally acting T-type channel blocker ABT-639 is in phase II clinical trials and acts by selectively blocking $Ca_V3.2$ in the inactivated and resting state in rat DRG neurones as well as producing a less than 10% block at resting state in human DRG neurones (Ziegler et al., 2015)

In the MIA rat model of OA, peripherally acting T-type channel blocker ABT-639 delivered orally produced a significant increase in grip force strength 21 days post-MIA injection (Jarvis et al., 2014). Moreover, it increased paw withdraw thresholds in spinal nerve ligated rats as well as in a chronic constriction injury model. *In-vivo* electrophysiological recordings of WDR neurones showed a decrease in neuronal evoked responses to 10g vF stimulation after ABT-639 was delivered in SNL animals while in the CFA-model, ABT-639 did not alter neuronal evoked responses to mechanical stimulation. Although authors did not address if ABT-639 could inhibit responses evoked by more noxious stimuli, these results suggest that peripheral blockers may alter WDR neuronal excitability during neuropathic pain conditions but less so during inflammatory pain.

While T-type blocker might prove to be effective in certain animal models, most of the research has been aimed at looking into animal pain behaviours. Electrophysiological studies might also give us a better insight on the action of these drugs or molecules as seen in this study. Furthermore, it will be important to address electrophysiological changes not only at the level of spinal cord but also in the brain, since T-type channels are abundant in the thalamus and it is a crucial relay station for nociceptive inputs from projection neurones could be helpful (Timic Stamenic et al., 2019).

5.6. Summary

This study shows that TAT-cUBT-USP5 peptide fails to inhibit neuronal responses of WDR neurons to evoked thermal and mechanical stimulation, while increasing evoked responses to dynamic brush.

Chapter 6. Descending modulation functionality in the early and late stage of the MIA rat model of OA

6.1. Introduction

6.1.1. The role of descending serotonergic and noradrenergic controls

Superficial and deep dorsal spinal nociceptive neurones send ascending projections into multiple brain areas from which descending modulatory controls originate. The periaqueductal grey (PAG) located in the midbrain is a crucial relay site that coordinates nociceptive inputs by sending descending projections to other brainstem regions such as the rostral ventromedial medulla (RVM) and locus coeruleus (LC) (Ossipov et al., 2010). From here direct projections to the spinal cord modulate spinal dorsal horn activity.

The RVM has a biphasic function in terms of pain modulation. On one hand, it has been shown that microinjection of lidocaine into the RVM abolishes anti-nociception arising from electrical stimulation of PAG (Sandkuhler and Gebhart, 1984). On the other hand, lesion of the dorsolateral funiculus (DLF), a tract where descending pathways from the RVM arrive into the spinal dorsal horn, reverses tactile allodynia in spinal nerve ligated (SNL) animals (Ossipov et al., 2000). This suggesting that RVM descending facilitatory projections contribute to the development of allodynia in this model. Thus the RVM can either facilitate or inhibit spinal activity. Within the RVM the nucleus raphe magnus is the main site from where descending serotonergic projections to the spinal cord originate. These projections can have inhibitory or facilitator effects depending on the 5-HT receptor subtype that they activate in the spinal dorsal horn (Ossipov et al., 2010). For instance, 5-HT can exert powerful excitatory effects through activation of pronociceptive 5-HT3 receptors (Bannister and Dickenson, 2016). In contrast, activation of 5-HT7 or 5-HT2A receptors is proposed to be antinociceptive (Bannister and Dickenson, 2016) (Bannister et al., 2015).

In-vivo electrophysiological studies in the SNL model have so far revealed that antagonizing 5-HT3 receptors through intrathecal injection of ondansetron causes an inhibition in WDR neuron evoked activity (Bannister et al., 2015). In the monosodium iodoacetate (MIA) rat model of osteoarthritis, in the late stages of the model ondansetron inhibited neuronal evoked response of WDR neurones to mechanical, thermal and dynamic brush stimulation (Rahman et al., 2009). In many chronic conditions the proposed increased excitatory serotonergic drive as observed here may drive the transition from acute to chronic state, as the descending inhibitory drive is ‘masked’.

The PAG and RVM do not contain noradrenergic neurones, rather the locous coruleus (LC) is one of the brainstem site where these neurones are contained. Descending noradrenergic projections from the LC are proposed to be inhibitory in terms of modulation of spinal activity because of actions at α_2-adrenoreceptors. In the MIA model neuronal evoked responses to mechanical stimulation of WDR neurones are enhanced after spinal administration of α_2-adrenoreceptors antagonist atipamezole (Lockwood et al., 2019a). However, noradrenaline can also act on facilitatory α_1-adrenoreceptors causing the depolarization of GABA interneurones and enhancing inhibition (Gassner et al., 2009)

Descending control functionality from midbrain and brainstem regions is altered in patients with chronic pain as detected using functional magnetic resonance imaging. In a subgroup of human OA patients that score high in the PainDETECT, increased PAG activity following the application of mechanical punctuated stimuli is observed (Soni et al., 2018). In contrast increased PAG activity is not observed in OA patients who scored low on the PainDETECT test and who exhibit pain perception with nociceptive features comparably to control patients (Soni et al., 2018). This study suggests that the differential engagement of PAG in the two OA groups might contribute to an altered descending modulation in the subgroup of patients that leads them to score high on the PainDETECT test (Soni et al., 2018). Other studies have also suggested that this subgroup of patients exhibits neuropathic pain-like features driven by altered descending serotonergic controls. These studies demonstrated that this subgroup exhibits temporal summation (Clauw and Hassett, 2017), referred pain with mechanical and thermal hyperalgesia (Gwilym et al., 2009), ongoing pain even when at rest, and a reduced response to NSAIDs treatment (Thakur et al., 2014).

Additionally after knee replacement surgery a subgroup of OA patients with neuropathic pain like features still suffered from chronic pain with increased RVM activity (Soni et al., 2018). Therefore, pharmacological agents that centrally target descending modulation to counteract the increased PAG and RVM activity might prove to be an efficient way to provide pain relief for OA patients with neuropathic pain-like features (Chappell et al., 2009).

6.1.2. Diffuse Noxious Inhibitory Controls (DNIC)

Diffuse noxious inhibitory controls (DNIC) are a form of endogenous inhibitory controls whereby the evoked activity of wide dynamic range neurones becomes inhibited upon simultaneous application of a noxious stimulus applied away from the receptive field of the original pain complaint (Bannister et al., 2015). The efficiency of

DNIC allows for the prediction of pain chronification as well as treatment responses (Phelps et al., 2019).

Previously it was shown that, in the MIA model, DNIC is present in the early stage of OA disease progression and in early and late sham-operated animals, but is dysfunctional by the late stage. Blocking α_2-adrenoreceptors with atipamezole abolishes the DNIC response in early stage MIA animals (Lockwood et al., 2019a). This data is keeping with earlier studies in neuropathic animals that hypothesized that in fact DNIC requires a tonic activation of these receptors for its inhibitory action (Bannister et al., 2015). Treating late stage MIA animals with tapentadol, which acts both as an agonist for μ-opioid receptor (MOR) and as an agonist for norepinephrine reuptake inhibitor (NRI), restores DNIC (Lockwood et al., 2019a).

The role that descending serotonergic modulation plays on DNIC still remains unclear. It has been shown that in the SNL model antagonizing 5-HT3 receptors with ondansetron restores DNIC (Bannister et al., 2015). Surprisingly, in the same model of neuropathy, increasing synaptic content of serotonin by using selective serotonin reuptake inhibitors (SSRIs), such as fluoxetine, restores DNIC (Bannister et al., 2017). In contrast, dual spinal administration of fluroxetine and 5-HT7 receptor antagonists SB26997, led to abolish DNIC. The authors concluded that the increased synaptic content of serotonin activates proposed-upregulated 5-HT7 receptors, which themselves exert an anti-nociceptive role (Bannister et al., 2017). These results are supported from a previous study showing that, antagonism of 5-HT7 receptors blocks the inhibitory effects of milnacipran a serotonin, norepinephrine reuptake inhibitor (SNRIs), in the late stages of the MIA model (Burnham and Dickenson, 2013). In the late stages of this model, where there is evidence for altered descending drives, the inhibitory action of milnacipran requires 5-HT7 receptor activation. However, the role of serotonin in pain modulation is extremely complex due to the aformementioned myriad of dorsal horn spinally expressed different types 5-HT receptors and their different functions.

In conclusion, the studies outlined indicate that it is both a decrease in serotonergic signalling and/or function, and an increase in inhibitory tone, (by way of α_2-adrenoreceptors activation) alone or in concert with activation of 5-HT7 receptors that contribute to restoring DNIC in neuropathic pain models. Perhaps the increased descending facilitation observed in neuropathic pain models masks DNIC inhibitory responses by lowering levels of noradrenaline in the spinal cord as it has been previously suggested (Phelps et al., 2019).

6.1.3 Serotonin, norepinephrine reuptake inhibitors for the treatment of chronic pain

Serotonin, norepinephrine reuptake inhibitors (SNRIs) are commonly used anti depressant drugs that, unlike SSRIs, are effective for the treatment of chronic pain (Kremer et al., 2018). Duloxetine is a commonly used SNRI that has demonstrated clinical efficacy in chronic pain conditions such as diabetic peripheral neuropathy and fibromyalgia, and it has recently been approved for the treatment of OA pain (Chappell et al., 2009). Duloxetine acts by blocking the pre-synaptical terminal reuptake site, thus increasing synaptic levels of noradrenaline and promoting inhibition through the activation of post-synaptic α_2-adrenoreceptors (Havelin et al., 2016). In a study using high (4.8mg/60μL) versus low (3.0mg/60μL) doses of MIA, authors found a reversal of weight bearing asymmetry when using duloxetine, 30min after drug delivery in the high dose group (Havelin et al., 2016). In the same study lidocaine injection into the RVM induced CPP in the high dose MIA animals but not in the lower dose animal group. The data suggests that high dose late stage MIA animals exhibit spontaneous pain driven by increased descending facilitatory controls and central sensitization (Havelin et al., 2016). Additionally, duloxetine delivery in the high dose late stage group 30min before localized lidocaine injection in the RVM blocked CPP (Havelin et al., 2016). In conclusion, the authors stated that perhaps duloxetine may be effective for the relief spontaneous ongoing pain in osteoarthritis patients that exhibit neuropathic pain-like features and are insensitive to pain relieving effects of the NSAIDs.

A recent study has uncovered the mechanism of action of duloxetine in an animal model of neuropathy. The authors suggest that duloxetine acts through two mechanisms in order to produce pain relief (Kremer et al., 2018). The first mechanisms, acts centrally through descending inhibitory controls and α_2-adrenoreceptors in the spinal dorsal horn. It exerts a rapid and transitory action to relieve mechanical allodynia. This action also requires the activation of μ-opioid receptors (MOR) and d-opioid receptors DOR (Kremer et al., 2018). The second mechanism is a long lasting antiallodynic effect that requires the activation of β_2-adrenoreceptors in the periphery as well as the activation of centrally expressing DORs (Kremer et al., 2018).

The action of other SNRI's, such as milnacipran, has also been studied in both early and late stages of the MIA model. Subcutaneous administration of milnacipran inhibited neuronal evoked responses of WDR neurones to electrical, mechanical and thermal stimulation in both MIA groups as well as in naïve animals (Burnham and Dickenson, 2013). Interestingly, spinal administration of atipamezole after administration of milnacipran blocked the SNRI inhibitory action in both early MIA and naïve animals but not in late stage MIA animals (Burnham and Dickenson, 2013). This data suggests that in

the early acute inflammatory stage descending inhibition is engaged but is aberrant in the late stages. Additionally this acute effect of milnacipran was partly blocked by spinal administration naloxone in all groups (Burnham and Dickenson, 2013). This work by our laboratory is in accordance with the work of Kremer et al., as milnacipran not only acts by engaging descending facilitation and α_2-adrenoreceptors but also requires opioid activity (Burnham and Dickenson, 2013) (Kremer et al., 2018). Perhaps the mechanism described by Kremer et al., could be common amongst all SNRIs.

6.2. Chapter Aims

The aims of this chapter are to address if descending controls are altered in during the early acute inflammatory stage and late stage of the MIA rat model of OA by addressing changes in descending serotonergic drive as well as changes in diffuse noxious inhibitory controls. Lastly, to address weather SNRIs modulate changes in neuronal evoked responses of WDR neurones in the late stages of the MIA model and are a good target for the treatment of OA pain.

6.3. Methods

6.3.1. Animals

In this study, a total of 42 Male Sprague-Dawley rats (230g-300g), bred by the Biological Service Unit (UCL, London, UK), were used for electrophysiological experiments. Weights of all animals can be found on Appendix III: Chapter 6. 29 rats were used for the ondansetron studies (n=29 cells, one cell per animal) and 13 rats for the duloxetine study (n=13 cells, one cell per animal)

6.3.2. *In-vivo* electrophysiology

Refer to Chapter 2: Methods and Materials, section 2.4, in order to obtain more information on in-vivo electrophysiological recordings. In-vivo electrophysiology was performed between day 2 and day 4 post-injection in early stage MIA and sham groups and day 14 and day 21 post-injection in late stage MIA and sham groups. Single WDR neurones were characterized for responses to electrical stimulation, followed by dynamic brush, mechanical and thermal stimulation for the ondansetron study. For duloxetine study electrical stimulation was not performed.

For the ondansetron study, three baseline responses to all modality stimuli were recorded in both early and late stage MIA and sham animals before spinal administration of ondansetron. 100μg (taken from a 2mg/mL vial) of ondansetron was spinally applied in a volume of 50uL and neuronal events were recorded in response to all modality

stimuli 10, 30 and 50min post-dosing. Maximal change following administration of ondansetron compared to baseline was plotted for each neuron.

For the duloxetine study, three consecutive baselines where recorded for dynamic brush, mechanical, mechanical + condition noxious pinch stimuli applied in the ear ipsilateral for the neuron being recorded to test DNIC and lastly thermal stimulation. Duloxetine was dissolved in ddH_20 saline and 30mg/kg of duloxetine were subcutaneously injected using a syringe. Responses to duloxetine to all modality stimuli were recorded in late stage MIA and sham animals, 10, 30, 50, 70 and 90min post dosing.

6.3.3. Statistics

All statistical tests were performed on raw data using SPSS, version 25 (IBM, Armonk, NY). Mechanical and Heat coding of neurones were compared using a two-way repeated-measures (RM) ANOVA, followed by a Bonferroni post-hoc test for pair comparisons as well as DNIC. Brush neuronal responses were compared using a paired sample Student's *t*-test. $^{*}p < 0.05$, $^{**}p < 0.01$, $^{***}p < 0$ .001. Additionally all statistical values for both studies can be found in Appendix III: Chapter 6.

6.4. Results

6.4.1. Ondansetron fails to inhibit neuronal evoked responses in the early stages of the MIA rat model of OA

In the early stage MIA and early sham-operated control animals, spinally applied ondansetron failed to inhibit neuronal evoked responses to dynamic brush, mechanical and thermal stimulation applied into the receptive field (**Figure 6.1c-h**). Regarding electrical stimulation parameters, ondansetron failed to inhibit action potentials attributed to Ab, Ad and C-fibers in both MIA and control group. However, the indicator of neuronal excitability input (I) was significantly inhibited in both early MIA ($t_{(6)}=3.371$; $p=0.020(*)$) and early sham control group ($t_{(5)}=3.847$; $p=0.012(*)$), while post-discharge (PD) and wind-up remained unaffected in both groups (**Figure 6.1a-b**).

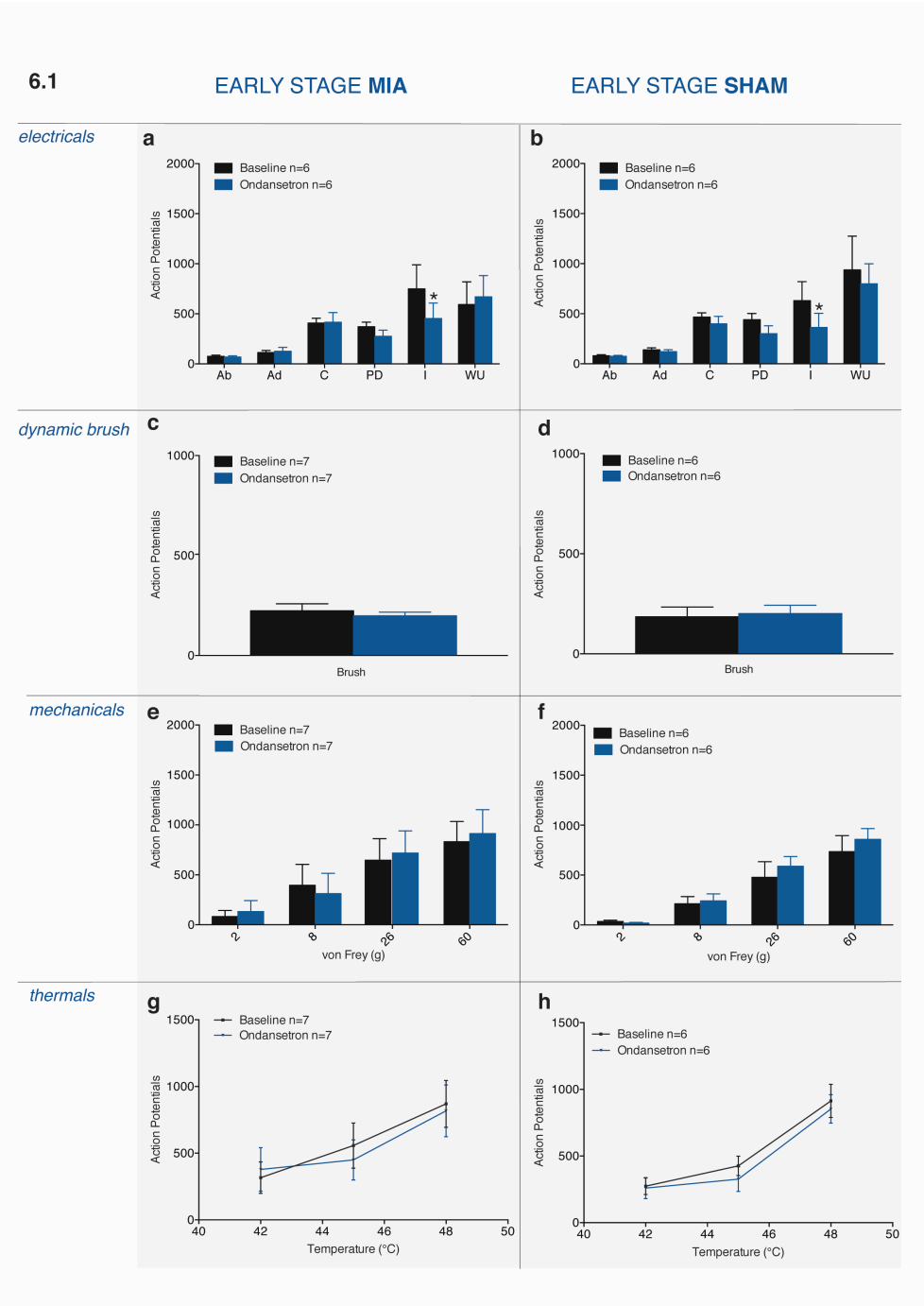

Figure 6.1. Effects of spinally applied ondansetron on neuronal evoked responses to early stage MIA and sham rats. **a,b)** WDR neuronal evoked responses of WDR neurones to electrical stimulation shows an inhibition of input in early MIA ($t_{(6)}=3.371$; $p=0.020(*)$) and early sham control group ($t_{(5)}=3.847$; $p=0.012(*)$). While action potentials attributed to Aβ, Aδ and C-fibers remain unaffected as well as post-discharge (PD) and wind-up (WU). **c,d)** WDR neuronal evoked responses to dynamic brush in both early MIA and sham control group remained unaffected after ondansetron spinal administration. **e,f)** WDR neuronal evoked responses to mechanical stimulation remained unchanged after spinal administration of ondansetron in both early MIA and Sham groups. **g.h)** WDR neuronal evoked responses to thermal stimulation were unchanged after spinally applied ondansetron in the early stage MIA and sham control group.

6.4.2. Ondansetron on neuronal evoked response of WDR neuron in the late stage of MIA rat model of OA

In both late stage MIA and sham-operated control groups spinally applied ondansetron inhibited input (I ($t_{(6)}$=*3.041*; *p=0.023(*)*) ($t_{(5)}$=*3.754*; *p=0.013(*)*) while other electrically-stimulated recorded parameters remained unchanged (Ab, Ad and C-fibers, PD, WU) (**Figure 6.2a-b**). Ondansetron did not inhibit neuronal evoked responses of WDR neurones to stimulation of the receptive field with dynamic brush, mechanical and thermal stimulation in the late stage MIA group (**Figure 6.2c,e and g**).

In the late stage sham-operated control group, in response to mechanical stimulation, evoked response of deep dorsal horn neurones was statistically significantly inhibited ($F_{(5,6)}$=*12.206*; *p=0.0017(**)*) with significant differences in response to 8g (p=0.026(*)) and 60g (*p=0.008(**)*) vF compared to baseline (**Figure 6.2f**). Ondansetron also significantly inhibited thermal responses in this group ($F_{(5,6)}$=*24.55*; *p=0.0017(**)*) with post hoc test showing a significant reduction to 45°C (*p=0.043(*)*) and 48°C (p=0.041(*)) (**Figure 6.2h**). Dynamic brush remained unchanged after drug application (**Figure 6.2d**).

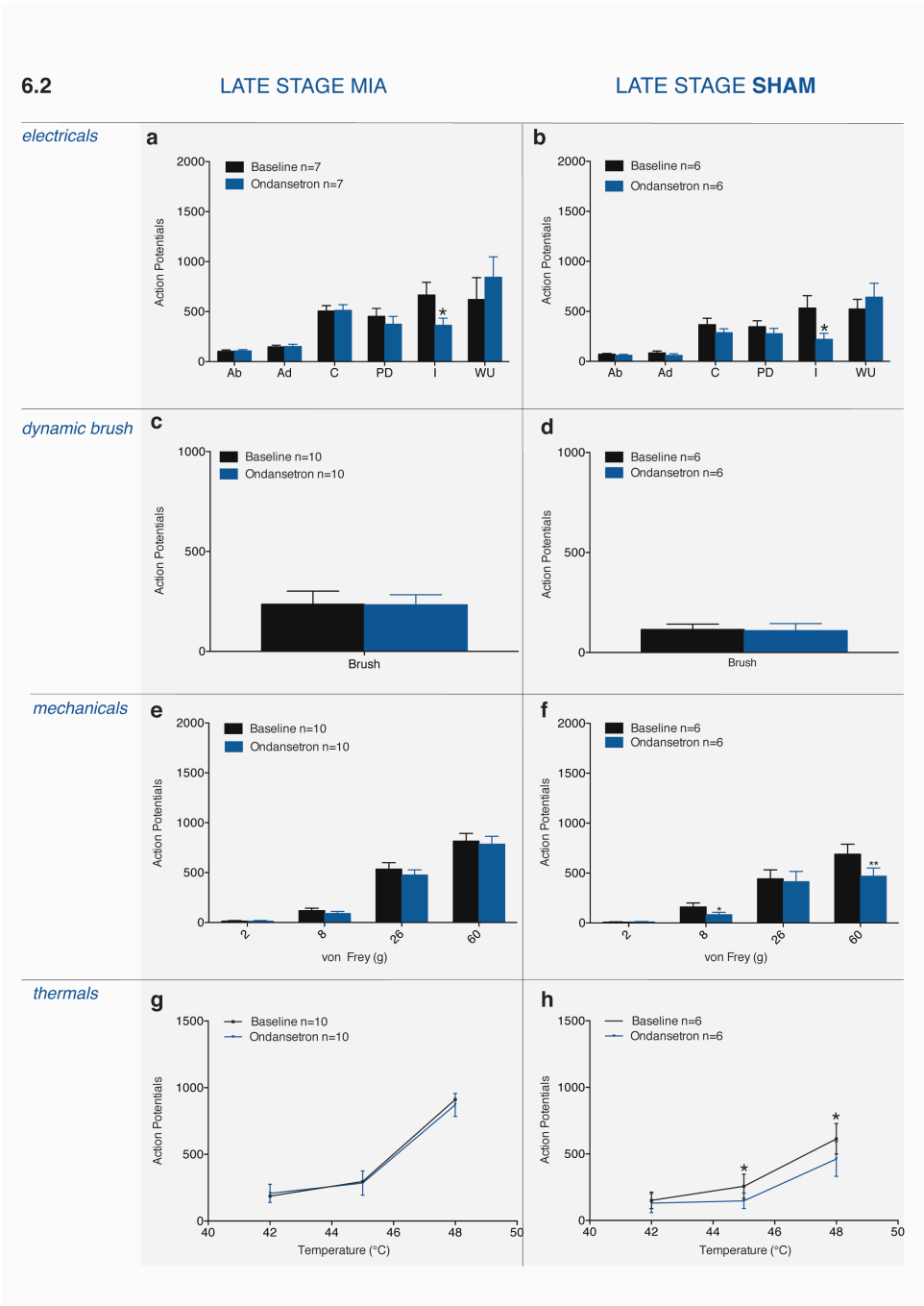

Figure 6.2. Effects of spinally applied ondansetron on neuronal evoked responses to late stage MIA and sham rats. **a,b)** WDR neuronal evoked responses to electrical stimulation in MIA and sham-operated groups showed a significant inhibition of input (I) in both groups after spinal application of ondansetron ($t_{(6)}$=3.041; p=0.023(*)) ($t_{(5)}$=3.754; p=0.013(*)). While action potentials attributed to Aβ, Aδ and C-fibers remain unaffected as well as post-discharge (PD) and wind-up (WU). **c,d)** WDR neuronal evoked responses to dynamic brush in both late MIA and sham control group remained unchanged after spinal administration of ondansetron. **e)** WDR neuronal evoked responses to mechanical stimulation in the MIA group remained unchanged after spinal administration of ondansetron. **f)** In the sham control group, WDR neuronal evoked responses to mechanical stimulation were significantly inhibited after spinal administration of ondansetron ($F_{(5,6)}$=12.206; p=0.0017(**)). Pairwise comparison with Bonferroni correction showed a significant difference to 8g (p=0.026(*)) and 60g (p=0.008(**)) vF compared to baseline. **g)** WDR neuronal evoked responses to thermal stimulation were unchanged after spinally applied ondansetron in the late stage MIA group. **h)** Ondansetron significantly inhibited neuronal responses to thermal heat in the sham control group ($F_{(5,6)}$=24.55; p=0.0017(**)). Pairwise comparison with Bonferroni correction showed a significant reduction to 45°C (p=0.043(*)) and 48°C (p=0.041(*)).

6.4.2.1 Individual variability: Identification of subgroups in late stage MIA rat model of OA in terms of response to ondansetron

In the late stage MIA group, spinally applied ondansetron did not statistically significantly inhibit WDR neuronal evoked responses to any natural or electrical stimuli (**Figure 6.3**). However, a subgroup of 4 neurones (n5, n7, n9 and n10 shown in **Figure 6.3a**) show an overall significant inhibition of WDR neuron evoked action potentials post-ondansetron after mechanical stimulation *($F_{(3,4)}$=95.547, p=0.002(**)).* (**Figure 6.3b**).

6.3 *Individual neuronal responses to mechanical stimulation before and after ondansetron*

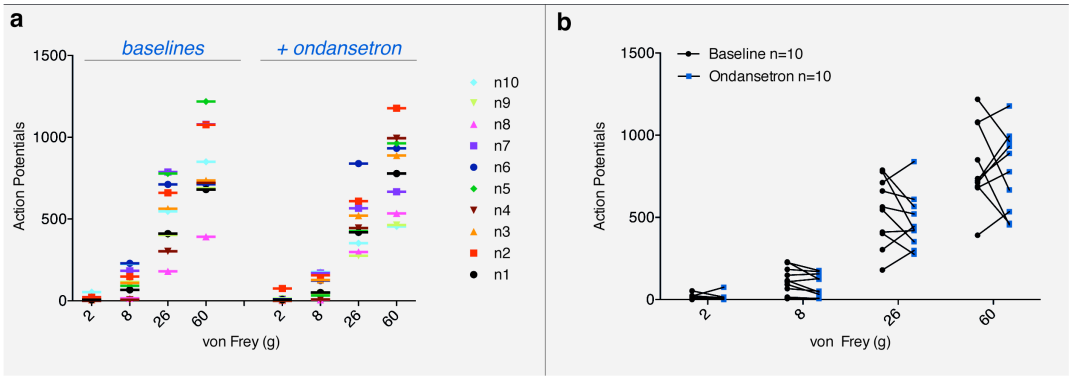

Figure 6.3. Individual neuronal evoked responses to mechanical stimulation before and after ondansetron in late stage MIA animals. **a)** Individual neuronal evoked responses of 10 WDR neurons to 2g, 8g, 26g and 60g vF. Each neuron is color-coded before and after ondansetron spinal administration. Notice neurons number 5, 7, 9 and 10 show decreased neuronal responses to ondansetron. **b)** Before-after plots showing different neuronal evoked responses of the 10 WDR neurons from baseline to post ondansetron after 2g, 8g, 26g and 60g vF stimulation.

Specifically, a significant reduction of evoked responses to 8g (*p=0.03(*)*), 26g (*p=0.018(*)*) and to 60g (*p=0.007(**)*) vF (**Figure 6.4**) is observed. Thermal and dynamic brush responses were unaffected. My data indicates the possibility of a subgroup of neurones that are sensitive to ondansetron and this impact is masked by the overall group.

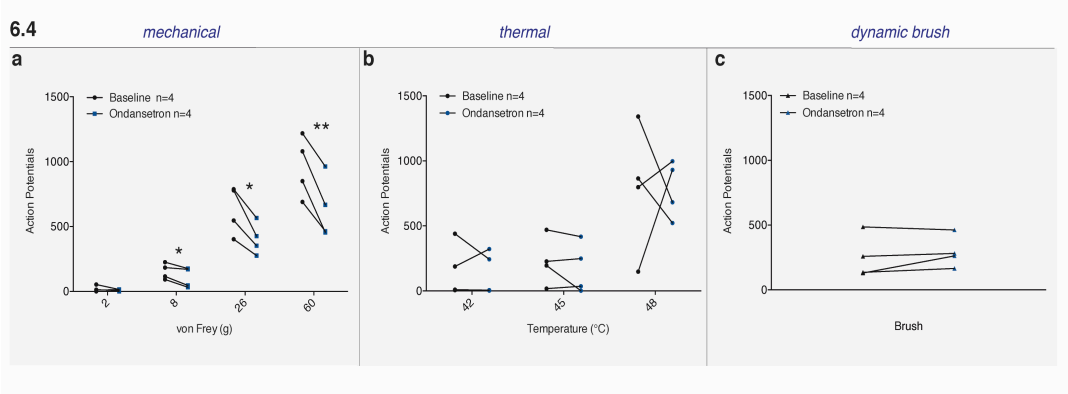

Figure 6.4. Before-after plots of neuronal evoked responses of WDR to mechanical, thermal and dynamic brush, in late stage MIA neuronal subgroup sensitive to ondansetron. **a)** In this subgroup, neuronal evoked responses to mechanical stimulation of the receptive field, are significantly inhibited by ondansetron *($F_{(3,4)}$=95.547, p=0.002(**)).* Pairwise comparison with Bonferroni correction showed a significant inhibition to 8g (*p=0.03(*)*), 26g (*p=0.018(*)*) and to 60g (*p=0.007(**)*) vF, after ondansetron spinal administration compared to baseline responses. **b,c)** Thermal and dynamic brush evoked responses remained unchanged before and after ondansetron spinal administration in this subgroup of neurones of the late stage MIA animals.

6.4.3. Duloxetine fails to inhibit neuronal evoked responses in the late stage MIA rat model of OA

In the late stage MIA group subcutaneous administration of duloxetine failed to inhibit neuronal evoked responses to dynamic brush, mechanical and thermal stimulation (**Figure 6.5a, c and e**). In the late stage sham-operated control group duloxetine did not inhibit neuronal evoked responses to any modality stimuli compared to baseline (**Figure 6.5b,d and f**).

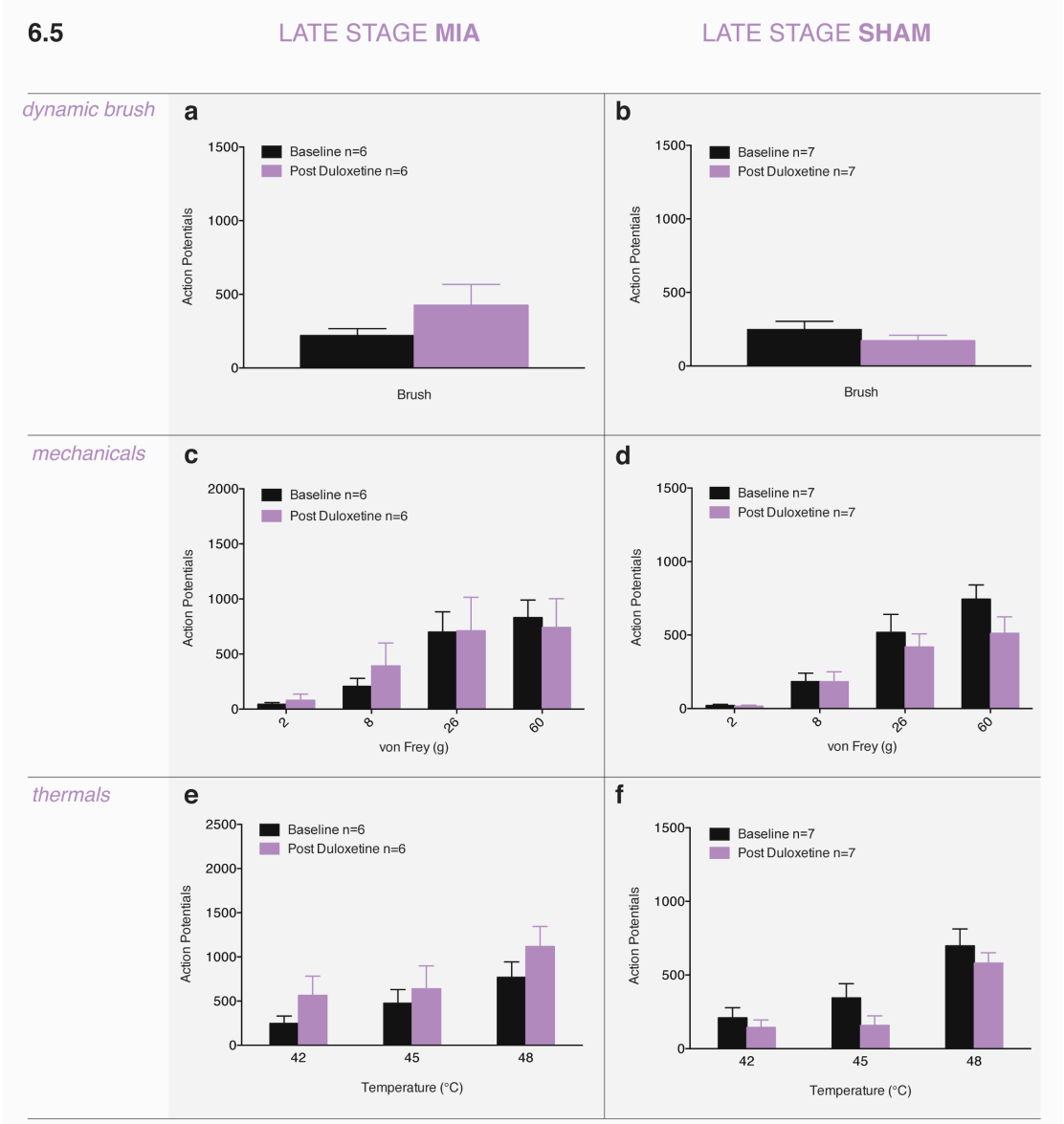

Figure 6.5 Effects of systemic administration of Duloxetine on neuronal evoked responses of wide dynamic range neurones in late stage MIA and sham animals. a,b) In both late stage MIA and sham control group, duloxetine failed to significantly inhibit WDR neuronal responses to dynamic brush. **c,d)** WDR neuronal evoked responses to mechanical stimulation were unaffected by duloxetine in both MIA and sham control groups. **e)** WDR neuronal evoked responses to thermal stimulation were unaffected in the MIA group after systemic administration of duloxetine. **f)** In the sham control group, WDR neuronal evoked responses to thermal stimulation also remained unchanged after systemic administration of ondansetron.

6.4.4. DNIC is abolished in the late stage MIA rat model of OA

Through this study DNIC was induced by applying a noxious ear pinch ipsilateral to the neuron being recorded concurrently to stimulation of the ipsilateral injured hind paw using 8g, 26g and 60g vF filaments.

In the late stage sham-operated control group the presence of DNIC was quantified a significant reduction in WDR neuronal firing in response to non-noxious and noxious mechanical punctuated stimulus application (8g, 26g and 60g vF) as compared to baseline responses ($F_{(6,7)}=7.687;\ p=0.032(*)$). Specifically, post-hoc test indicate significance when 60g vF to baseline ($p=0.008(**)$) while 8g and 26g vF remained unchanged.

In contrast, DNIC responses were abolished in the late stage MIA group; application of the conditioning stimulus (noxious ear pinch) failed to inhibit neuronal evoked responses to mechanical stimuli of WDR neurones **(Figure 6.6)**.

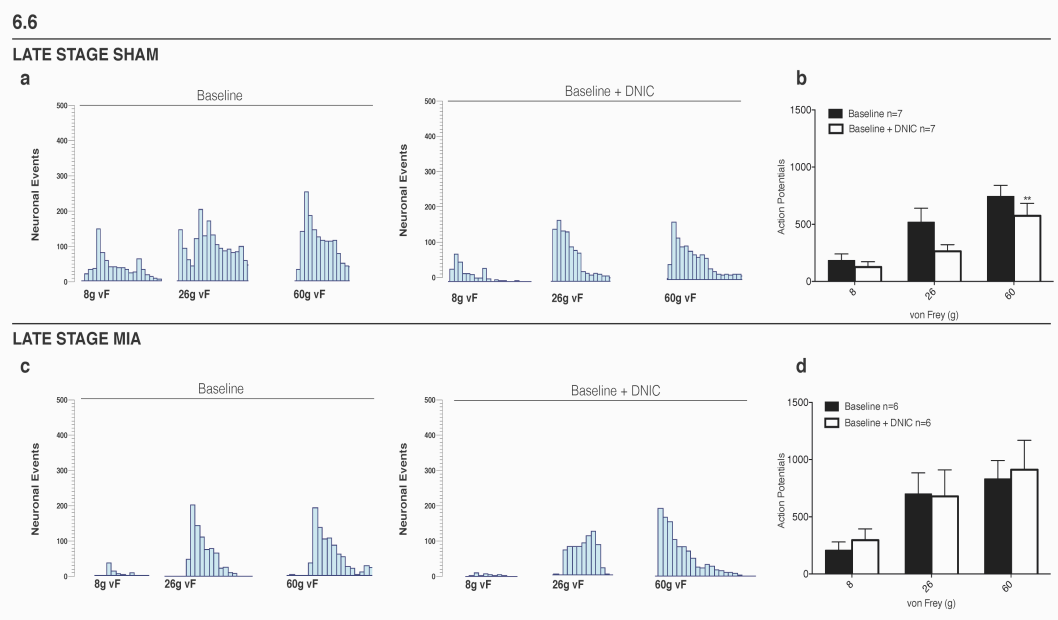

Figure 6.6 Effects of DNIC in neuronal evoked responses of wide dynamic range neurones in late stage MIA and sham animals. a) Example of neuronal traces of late stage baseline sham animals alone or with DNIC (conditioned stimuli elicited with an ear pinch), in response to mechanical punctuated stimuli (8g, 26g and 60g vF). **b)** A noxious ear pinch applied ipsilateral to neuronal receptive field significantly reduced neuronal evoked responses to mechanical stimuli in late stage sham animals (n=7) ($F_{6,7}=7.687;\ p=0.032(*)$), thus producing DNIC. Post-hoc Pairiwise comparison test with Bonferroni correction showing decreased mechanical evoked responses to noxious mechanical 60g vF stimulation ($p=0.008(**)$). **c)** Example of neuronal traces of late stage baseline MIA animals alone or with DNIC, in response to mechanical punctuated stimuli (8g, 26g and 60g vF). **d)** Noxious ear pinch did not induce DNIC in the late stage MIA group as it failed to inhibit neuronal evoked responses of WDR neurones to mechanical noxious and innocuous stimuli.

6.4.5. Duloxetine fails to restore DNIC in the late stage MIA rat model of OA

In the late stage MIA animals, systemic administration of Duloxetine failed to restore functional DNIC. Additionally, in the late stage sham group, DNIC was lost after duloxetine systemic administration **(Figure 6.7).**

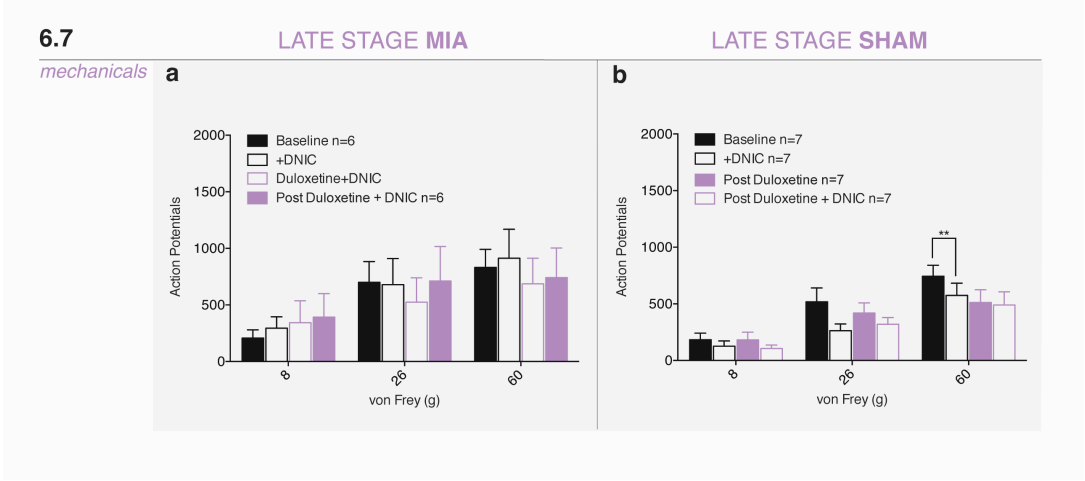

Figure 6.7. Duloxetine fails to restore DNIC. a) Late stage MIA neuronal evoked responses of WDR neurones to mechanical punctuated stimulation. No significant differences are observed between groups. **b)** In the late stage sham group the conditioning stimulus produces DNIC (n=7) ($F_{6,7}$*=7.687; p=0.032(*)*) with post-hoc, pairwise comparison with Bonferroni correction showing decreased mechanical evoked responses to noxious mechanical 60g vF stimulation (*p=0.008(**)*). However DNIC is lost after duloxetine administration.

6.5. Discussion

6.5.1 Descending control functionality is altered in the late stages of the MIA rat model of OA

Descending serotonergic controls originate in the RVM and project to the spinal cord dorsal horn where they may activate activation of 5-HT3 receptors; this contributes to the maintenance of persistent pain states (Cortes-Altamirano et al., 2018). 5-HT3 receptors are ligand gated ion channels that produce fast depolarization of cells. In the spinal cord, immunoreactivity studies have shown that these receptors are localized between laminas I-III. 5-HT3 receptors can be present in pre-synaptic terminals of unmylinated primary afferent fibers or post-synaptically.

The proposed role of this channel in pre-synaptic terminals is to produce a local depolarization of the terminal, inducing the increase of calcium influx through VGGC, contributing to spontaneous neurotransmitter release (Maricq et al., 1991). Post-synaptic

5-HT3 receptors are present in spinal cord GABAergic interneurones where they can either increase or inhibit the activity of projection neurones, 40% of 5-HT3 binding sites are associated with their pre-synaptic role (Cortes-Altamirano et al., 2018). Thus, suggesting that 5-HT3 receptors mainly play a pronociceptive role in pain transmission.

In the study presented in this chapter, spinally applied ondansetron, a 5-HT3 antagonist, inhibited the input (I), a theoretical non-potentiated response, in all animal groups (Early MIA/Sham and Late MIA/Sham) (**Figure 6.1a,b and 6.2a,b**). This suggests that indeed 5-HT3 receptors, via their pre-synaptic role reduce inputs send from primary afferent fibers to spinal neurones, in this case wide-dynamic range (WDR) neurones. Compared to baseline, ondansetron failed to inhibit electrical evoked responses to Ab, Ad and C-fibers as well as post-discharge (PD) and wind-up (WU) in all groups (Early MIA/Sham and Late MIA/Sham) (**Figure 6.1a,b and 6.2a,b**). This was observed in previous studies in sham-operated and neuropathic animals (Suzuki et al., 2004).

Targeting 5-HT3 receptors can lead to an anti-nociceptive effect in a number of pain states. Previous work has shown that descending serotonergic drive is not enhanced in inflammatory disorders, such as the carrageenan model of inflammation, unlike the situation in neuropathic pain models (Rahman et al., 2004, Suzuki et al., 2005). The early stages of the MIA rat model of OA are characterized by an acute inflammatory state. In this current study ondansetron failed to inhibit neuronal evoked responses to dynamic brush, mechanical and thermal stimulation in early stages as well as in early-stage sham-operated animals (**Figure 6.1**). This suggests that, in the acute inflammatory phase, the descending serotonergic drive is not enhanced as has been shown in other inflammatory disorders or that an enhanced drive is masked by a compensatory inhibition. Additionally, in nociceptive OA patients there is no increased PAG activity, suggesting that descending control modulation from this brain region is not altered in these patients (Soni et al., 2018).

Previous work proposed that an increased descending serotonergic drive is present in the late stages of the MIA model (Rahman et al., 2009). However in the presented study spinally applied ondansetron failed to inhibit neuronal evoked responses to electrical, dynamic bush, mechanical and thermal stimulation in the late stage MIA group (**Figure 6.2**). In contrast, in the late stage sham-operated control group, there was a significant decrease in neuronal responses to mechanically applied stimulation, notably at the most noxious intensity (60g vF). A significant decrease in neuronal response to thermal stimulation was also observed following ondansetron administration (**Figure 6.2 f and h**). Recent studies have shown that spinally applied ondansetron reduces thalamic neuronal responses to mechanical stimulation in sham-operated animals (Patel and

Dickenson, 2018). This data suggests that these receptors play a role in facilitating evoked spinal neuronal responses to mechanical punctuated stimuli. Therefore it is not a surprise that in the control group ondansetron inhibited neuronal evoked responses to high intensity mechanical stimuli (**Figure 6.2f**). The thermal inhibition observed in the late sham-operated control group following ondansetron administration is in line with other studies that also report decreased neuronal responses to thermal stimulation in sham animals (Suzuki et al., 2004).

In the late stage MIA animals a subgroup of 4 neurones showed reduced responses exclusively to mechanical stimulation following application of spinal ondansetron. Because 5-HT3 receptors are present in unmylinated fibers and are mainly involved in transmission mechanical stimulation, it could explain why this subgroup shows reduced responses to mechanical stimulation inhibition only (**Figure 6.4a**). These results raise the possibility that a subgroup of MIA OA rats develop the neuropathic pain-like features whereas others do not; this variability could depend on the functionality of the descending controls. MIA model variability exists and may be due to a variety of reasons including, animal susceptibility, the amount of MIA injected, the experimenter's way of injecting the MIA (example, the angle of injection, location) and the development or not of nerve damage. In the late stages of the MIA model some studies report increased ATF-3 expression in the DRG, an indicator of neuronal damage, (Thakur et al., 2012) whereas others do not report an increase in ATF-3 expression in the late stages of the model (Lockwood et al., 2019b). Additionally, we need to bear in mind that only around 14% of OA patients develop neuropathic pain-like features (Hochman et al., 2010). Thus perhaps only a small percentage of MIA animals might be developing the neuropathic pain like component.

Diffused noxious inhibitory controls (DNIC) expression is altered following neuropathic pain injury in a rat model; it is proposed that an increased facilitatory serotonergic drive in spinal nerve ligated animals may mask the tonic inhibitory noradrenergic drive that ordinarily is vital or the functional expression of DNIC (Bannister et al., 2015). In this present study, I have demonstrated that in the late stage MIA animals DNIC is abolished but its expression is present in late stage sham-operated control animals (**Figure 6.7**). These results are in line with other work presented by our laboratory using the same model (Lockwood et al., 2019a).

In conclusion, in the late stages of MIA model, descending controls are altered as indicated by abolished DNIC in this group. There is also a possibility of an increased descending serotonergic drive in a subgroup of neurones that exhibit decreased activity to mechanical stimulation following spinal application of ondansetron.

6.5.2 Duloxetine as a modulator of pain in the MIA model

Duloxetine has been recently approved for the treatment of OA pain. Duloxetine's main action is to increase serotonin (5-HT) and norepinephrine (NE) levels both centrally and in the periphery by inhibiting the reuptake of these two neurotransmitters (Karpa et al., 2002). Clinical trials show mixed results in the improvement of pain scores in pain patients (Chappell et al., 2009), and many open-label studies do not take into consideration the possible effect of placebo.

Two different studies have looked at the effects of systemic administration of duloxetine on spontaneous pain in the late stages of the MIA model (2mg of MIA per animal in both studies). Both studies report that, following duloxetine administration weight bearing asymmetry was decreased in the MIA animals (Havelin et al., 2016), (Ishikawa et al., 2014). In contrast, Ishikawa et al., showed that duloxetine did not have any effects on the maximal contact area or swing speed of the MIA animals measured with Catwalk Gateway system. The authors concluded that duloxetine inhibited spontaneous pain but did not have any effects in reliving pain upon movement (Ishikawa et al., 2014).

In the present study, systemic administration of duloxetine failed to inhibit neuronal evoked responses to dynamic brush, mechanical and thermal stimulation in the late stage MIA group (**Figure 6.5a, c and e**). I demonstrated abolished DNIC in the late stage MIA model and speculated the possibility of an increased descending serotonergic drive in the late stages of the disease. The possible increase in descending serotonergic drive might mask descending inhibitory pathways leading to the disappearance of DNIC as observed in neuropathic pain models (Bannister et al., 2015). Additionally, this increased descending facilitatory drive could alter 5-HT receptor expression, as this receptor could be upregulated after injury, as well as increase 5-HT spinal levels. Such effects could account for the ineffective action of duloxetine as an anti-nociceptive drug in the late stage MIA gorup. In the late stage sham-operated control animals, duloxetine had no effects in neuronal evoked responses to all modality stimuli (**Figure 6.5b, d and f**), thus perhaps drug action might vary depending on the levels of 5-HT/NE present.

In vitro studies in rat hippocampal slices show that duloxetine is twice as potent at inhibiting 5-HT than NE (Mantovani et al., 2009). Contrasting *ex vivo* experiments using hippocampal slices of rats that had been treated over a two-day period with duloxetine show that duloxetine inhibits the reuptake of both neurotransmitters equally (Mantovani et al., 2009). The action of duloxetine may vary when duloxetine is administrated acutely or when it is chronically administrated, in line with Kremer et al., studies (see section 6.1.3) (Kremer et al., 2018). In this study, duloxetine was administrated acutely, which might be a possible reason why duloxetine failed to inhibit neuronal evoked responses

and rather had a trend to increase them as well as failed to bring back DNIC in the late stage MIA group (**Figure 6.7**).

Another possible reason why duloxetine may not have had an inhibitory action on WDR neuron responses is the delivery route chosen. In animal models of neuropathy, systemic administration of fluoxetine a SSRI, did not bring back DNIC where as spinal administration of the drug did (Bannister et al., 2017). This may be due to a localized high dose action of the drug and also due to the proposed activation of 5-HT7 receptors in spinal cord, which are known to play an anti-nociceptive role (Bannister et al., 2017). Increased serotonergic levels in the spinal cord allow for 5-HT7 inhibitory actions, whereas systemic administration is not enough to raise spinal serotonin levels in synaptic on the deeper laminas of spinal cord.

The same mechanism might be happening with systemic administration of duloxetine. Thus, the inhibitory effects on spontaneous pain observed by Havelin et al., and Ishikawa et al., after systemic administration of duloxetine might not be affecting neuronal evoked responses of WDR neurones, but rather could affecting supraspinal interaction between the monamines, contributing to changes in the final output of descending pathway modulation.

6.6 Summary

In this study ondansetron fails to inhibit neuronal evoked responses to all modality stimuli in both early stage MIA and sham control animals, suggesting that in the acute inflammatory state, either a) descending serotonergic projections are not enhanced and/or b) that receptor drive actions that predominate are altered. However in a subgroup of late stage MIA animals ondansetron inhibited neuronal evoked responses to mechanical stimulation. It is proposed that this subgroup of animals had developed a neuropathic-pain like features, making them susceptible to ondansetron. Additionally, in the late stage MIA group DNIC is lost but is present in late stage sham control group. Duloxetine failed to inhibit neuronal evoked responses of WDR neurones to dynamic brush, mechanical and thermal stimulation in both sham and MIA. In the late stage MIA group, there was a trend for neuronal responses to be increased. These could be due to increased 5-HT levels compared to NA levels in the synaptic cleft may be due to the altered descending controls. Lastly, duloxetine failed to bring back DNIC in the late stage MIA group.

Chapter 7. General Discussion

7.1. What the MIA model of Osteoarthritis has taught us, and its translational relevance

The MIA rat model of OA has been used in the present study in order to study behavioural and neuronal changes in pain processing that occur during OA progression. Intra-articular injection 2mg of MIA diluted in 25μL of 0.9% sterile saline into the knee joint space, has been shown to provide two distinct stages; an early acute inflammatory stage (2-4 days post-MIA injection) and a later stage that exhibits neuropathic pain-like features (Udo et al., 2016, Thakur et al., 2012, Orita et al., 2011, Havelin et al., 2016, Ferreira-Gomes et al., 2012, Combe et al., 2004). These stages differ regarding changes in knee joint structures, to changes in behaviour and lastly, to changes in neuronal pain processing.

7.1.1. The role of inflammation driving pain processing in the MIA rat model of OA

Osteoarthritis pain has often been classed as nociceptive because of the inflammatory response that appears due to damage of the articular cartilage (Thakur et al., 2014). Clinical changes in the early stages of OA include, joint pain, minor radiographic changes as well as articular cartilage and/or subchondral bone lesions (Cucchiarini et al., 2016). Early damage to the articular cartilage leads to altered chondrocyte activity, which in turn causes the induction of inflammatory mediators such as cytokines and chemokines amongst others (Goldring and Otero, 2011). These inflammatory factors infiltrate the synovial fluid leading to inflammation of the synovial membrane and contribute to further cartilage damage and OA progression (Mathiessen and Conaghan, 2017).

In OA patients, levels of pro-inflammatory cytokines IL-1β and IL-6 are increased in both serum and synovial fluid (Sohn et al., 2012, Finn et al., 2014). On the other hand TNF-α has only been shown to increase in synovial fluid but not serum (Sohn et al., 2012, Finn et al., 2014), suggesting that the role of TNF-α is mainly local.

In the present study increased levels of pro-inflammatory chemokine KC/GRO were present at day 4 post-MIA injection while others remained unchanged. IL-6 has been reported to be increased in serum of MIA animals (Finn et al., 2014), it is possible that increased levels of cytokines in this model are increased locally rather than globally. Therefore, measuring levels of cytokines in synovial fluid might be a

better approach. Additionally, other techniques could be used to measure cytokines levels in serum such as the enzyme-linked immunosorbant assay (ELISA).

Although, in the early stages of the disease changes in cytokine profile in serum were not detected, MIA animals exhibited behavioural hypersensitivity. Paw withdrawal thresholds (g) were decreased at days 2 and 4 post MIA injection and a weight bearing deficit of the ipsilateral injured hind-paw was observed at the same time points. In the late stages of the MIA model, there was an increase in the anti-inflammatory cytokine IL-10 (day 14 post-MIA injection) that coincided with an increase in withdrawal thresholds at this time point. Additionally, the catwalk gateway system revealed changes in gait parameters in the early acute inflammatory stages of the MIA model but not in the later stages. In contrast, LABORAS data did not provide much information on differences in naturalistic behaviours of MIA animals.

While *in-vivo* electrophysiological neuronal recordings of lamina V WDR neurones did not show any changes in action potential firing, between early and late stage MIA animals, it is clear that behavioural hypersensitivity is enhanced in the early acute inflammatory stage. It may be possible that a transitional stage is present between days 7-14 post injection as seen behaviourally, with increased withdrawal thresholds, increased weight bearing (%) of ipsilateral hind-paws and increased levels of anti-inflammatory cytokines. Thus, contributing to the decrease in inflammation, while more severe neuropathic pain-like features in the MIA model do not develop until later time points (21-28 days post-MIA injection). This is supported by previous studies that have shown the increase of pro-inflammatory cytokines, decreased paw withdrawal thresholds, weight bearing deficits, increased ATF-3 expression and increased neuronal evoked responses of WDR neurones at days 21 and 28 post-MIA injection (Finn et al., 2014, Ferreira-Gomes et al., 2012, Thakur, 2012, Sagar et al., 2010).

7.1.2. Central sensitization and changes in descending modulation in the MIA rat model of OA

Human studies with OA patients have revealed the presence of central sensitization in OA. It is important to identify the presence of central sensitization because it will have implications for the treatment of OA pain as peripheral acting agents might not proved to be efficient in patients with central sensitization. Knee OA patients report wide spread allodynia and hyperalgesia and referred pain in areas around the joint and tibia (Lesher et al., 2008). Referred pain in these patients has been shown to be accompanied by cutaneous mechanical hyperalgesia and

pressure-induced pain (Gwilym et al., 2009). In line with human studies, in the present study, behavioural analysis of the responses different intensity mechanical stimuli applied into the ipsilateral (injured) hind-paw show the presence of referred hypersensitivity in both the early and late stages of the MIA model. Ongoing pain while at rest is another feature of central sensitization that OA patients suffer from. While peripheral drive can contribute to central sensitization, ongoing pain can also be driven by central mechanisms. In the late stages of the MIA model (14 days post injection), local injection of lidocaine into the intra-articular space of the knee joint reversed MIA induced weight bearing deficiency at 1mg, 3mg and 4.8mg MIA doses. However, local lidocaine injection only induced CPP in the high doses of MIA (4.8mg**)**. This suggests that while peripheral drive can contribute to pain processing, on going pain is present in the high dose of MIA animals in the late stages of the model. Thus, central sensitization can drive on going pain independently of peripheral inputs.

OA patients exhibit temporal summation (Thakur et al., 2014) and *in-vivo* electrophysiological neuronal recordings of WDR neurones in early and late stages of the MIA model show the presence of wind-up after electrical stimulation of the electric field.

Descending inhibitory or excitatory controls may contribute to the maintenance of central sensitization in OA. While most of OA patients describe their pain as nociceptive and do not present altered midbrain and brainstem functionality, a subgroup of OA patients has been shown to describe their pain with neuropathic pain-like indicators as shown by their high scores on the PainDETECT test (Gwilym et al., 2009). Additionally, the subgroup of patients exhibit increased PAG activity following stimulation of their injured side with mechanical punctuated stimuli compared to controls and to nociceptive OA patients (Gwilym et al., 2009). Most of this subgroup of OA patients also do not respond to NSAIDs treatment and after knee replacement surgery they still suffer from chronic pain with increased RVM activity. Thus, they exhibit neuropathic pain-like features and have enhanced descending facilitation (Soni et al., 2018).

In neuropathic pain models an altered descending serotonergic drive facilitates neuronal evoked responses of WDR neurones by acting on 5-HT3 R (Rahman et al., 2009). Thus, spinal application of 5-HT3 receptor antagonist, ondansetron, inhibits neuronal evoked responses of WDR neurones in these neuropathic animals (Rahman et al., 2009).

In the present study, altered descending controls are not present in the early acute inflammatory stage of the MIA model, as has been shown by the inability of ondansetron, to inhibit neuronal evoked responses of WDR neurones. This is in line with previous studies that show that in the carrageenan model of inflammation increased descending facilitation is not enhanced (Rahman et al., 2004). On the other hand, in the present study, in the late stages of the MIA model only a subgroup of animals exhibited decreased neuronal activity of WDR neurones to mechanical stimulation raising the possibility that, like in human studies, only a subgroup develop the neuropathic pain-like component. Several studies report the presence of neuropathic markers, which could contribute to the altered descending modulation (Thakur et al., 2012, Ferreira-Gomes et al., 2012, Orita et al., 2011, Harvey and Dickenson, 2009, Ivanavicius et al., 2007). However, some of these studies show the presence of neuropathic pain-like features at later time points of the late stage MIA group (21-28 days post injection).

Another way to address altered descending modulation is by recording the presence of diffuse noxious inhibitory controls (DNIC). In the present study, DNIC was abolished in the late stage MIA animals while it as present in the late stage sham group. This result is in line with previous work from our laboratory that showed that DNIC was present in the early acute inflammatory stage but abolished in the late stages in MIA animals (Lockwood et al., 2019a). In addition, in neuropathic pain models DNIC is not present (Bannister et al., 2017). Therefore, measuring conditioned pain modulation (CPM), the human counterpart of DNIC, could be a good approach to diagnose the presence of altered descending controls in OA patients. The subgroup of patients with altered descending controls will have to be treated with alternative treatment to NSAID and may not be eligible for knee replacement surgery. Altogether these data suggest that descending controls might become altered in a subgroup of animals during the late stages of the MIA model.

7.2. Lamina V spinal neuronal recordings and their relation to pain processing

A series of behavioural assays have been developed in order to assess pain hypersensitivity in animal models of chronic pain before and after injury as well as to address the efficacy of analgesic agents. However, behavioural tests do not provide information that relates to suprathreshold stimuli, as high noxious stimuli cannot be delivered to awake animals without anaesthesia. *In-vivo* electrophysiological extracellular single cell neuronal recordings in anaesthetised animals provide information regarding pain processing of suprathreshold stimuli.

Primary afferent fibers transmit sensory signals to both the superficial and deep layers of the dorsal horn sending mono and polysynaptic input to interneurones and projection neurones (Woolf and Fitzgerald, 1986). WDR neurones receive direct or indirect inputs from all types of primary afferent fibers, thus becoming active upon both innocuous and noxious stimulation. While WDR neurones can be found in the superficial lamina I, the vast majority of WDR neurones are present in the deep laminas (V-VI) (McGaraughty et al., 2018). WDR neurones respond to stimuli in a coded manner, thus their response frequency increases as the stimulus intensity increases likely because of the number of neurones activated and firing frequency (Quevedo and Coghill, 2009). Nociceptive specific (NS) neurones in the superficial lamina I, also respond to stimuli in a coded manner. However, studies have shown that they have lower discharge frequencies to thermal and mechanical stimulation compared to WDR neurones (Sikandar et al., 2013). This is because WDR neurones exhibit wind-up; an NMDA receptor driven event similar to LTP whereabouts repetitive stimulation of these neurones causes an increased firing of action potentials as well as post-discharge (Dickenson and Sullivan, 1987). In chronic pain conditions constant primary afferent drive leads to the activation of WDR neurones leading to the production of wind-up. In chronic pain models increase WDR neuron activity and sensitivity causes hyperalgesia and/or allodynia. In OA, patients that exhibit central sensitization features also exhibit temporal summation, the human counterpart of wind-up (Thakur et al., 2014). Thus, measuring wind-up provides a read out of sensitization and inhibiting wind-up could reverse central sensitization (Herrero et al., 2000). Importantly, these WDR neurones code for a controlled thermal stimuli in a manner that exactly reflects human pain ratings to the same stimulus (Sikandar et al., 2013). Furthermore, these neurones show altered responses that mirror changes in human sensory testing in a model of UVA radiation with heat rekindling that can be attributed to both peripheral and central sensitization (Bishop et al., 2009). A final point of the translational aspects of recording these neurones comes from their modulation by DNIC, a descending system that does not act on NS neurones and again has a human counterpart, CPM (Le Bars et al., 1979) .

Lastly, because most of projections from lamina V are direct spinothalamic projections transmitting information to insular and somatosensory cortices, WDR neurones are able to transmit information regarding stimuli intensity (Todd, 2002, Sikandar et al., 2013). Whereas, lamina I projection neurones in the rat target medullary and parabrachial areas, thus sending information regarding autonomic and emotional responses (Todd, 2002, Sikandar et al., 2013).

7.3. Limitations

7.3.1. Measuring paw withdrawal responses in the MIA rat model of OA

One of the limitations found in the present study was measuring paw withdrawal threshold and paw withdrawal frequencies in late stage MIA animals. These were measured by applying von Frey filaments (vF) of different weights onto the plantar surface of the both ipsilateral (injured) and contralateral hind-paw and recording the withdraw reflexes. This provides a measurement of hypersensitivity and allows us to test whether the MIA injection produced referred pain. While in the early acute inflammatory stage MIA animals exhibited decreased ipsilateral paw withdrawal thresholds (PWT) and increase paw withdraw frequency (PWF) (%) to both innocuous and noxious vF, in the later stages of the MIA model, PWT appeared unaltered when comparing them to baseline. Although the increase in anti-inflammatory cytokines observed at days 7 and 14 post-MIA injection might be contributing to this increase in PWT observed in the late stage, some animals appeared to be in pain yet failed to withdraw suggestive of guarding behaviour that would confound the evoked measures.

7.3.2. The effects of anaesthetics on neuronal evoked responses in spinal cord

Anaesthetics depress reflex activity (nocifensive movements) by supressing spinal motor neurones in a dose dependent manner as well as suppressing responses of spinal nociceptive neurones. However, in order to perform *in-vivo* electrophysiological recordings of WDR neurones animals need to be anaesthetised.

In the present study *in-vivo* evoked neuronal responses of deep dorsal horn WDR neurones were recorded in isoflurane anaesthetised rats. A constant delivery of isoflurane was delivered through a cannula inserted and secured into the exposed trachea of the animal and connected to the isoflurane tank. Animals were maintained at 1.5% isoflurane for the duration of the experiment.

Several studies have looked at the effects of various anaesthetic agents on WDR neuronal responses. In most animal studies, the use of anaesthetics has been shown to reduce receptive field size as well as reducing nociceptive and non-nociceptive neuronal activity (Vahle-Hinz and Detsch, 2002). A study showed that reducing concentrations of isoflurane from a high (2%) to low (1%) dose of isoflurane in mice increased the number of neurones that exhibited wind-up from 16.7% to 43.4% after electrical stimulation of the receptive field (Guan and Raja, 2010). In contrary, another study showed that increasing the dose of isoflurane in rats had no effects on WDR neuronal evoked responses to thermal stimulation, while NS neuronal responses appeared reduced after increased isoflurane levels (Barter et al., 2009).

It is clear that the use of anaesthetic could somehow affect neuronal evoked responses of spinal neurones and interfere with pain modulation. However, for the present study, the level of anaesthesia was maintained at a minimally sufficient dose to induce areflexia and levels of anaesthesia were constant and always the same for all experiments, allowing for a controlled use of the anaesthetic. As discussed in section 7.2, the responses of these neurones equate with human measures even under anaesthesia suggestive that this is not a major confound.

7.3.3. Limitations of single cell *in-vivo* extracellular neuronal recordings of spinal dorsal horn neurones

There are several limitations in the use of in-vivo electrophysiological recordings presented in this thesis. For instance in the present study the only neurones recorded from were WDR neurones in lamina V. Thus, the search criteria were limited to finding neurones in the deep dorsal horn that responded to threshold innocuous (dynamic brush) and high and low noxious stimuli (mechanical, thermal and electrical) and exhibited wind-up. Additionally, the neurones chosen did not exhibit high spontaneous activity, as neurones with high spontaneous activity tend to be very unstable across baselines and on many occasions end up bursting after repetitive noxious stimulation. Therefore, comparisons across studies of diverse neuronal populations were not made as WDR neurones in lamina I-II and NS neurones in superficial and deep laminas were not studied. Another important factor to take into consideration is that we are unable to know if the WDR neurones we are recording from are interneurones or projection neurones.

7.4. Future studies

A number of future studies could be carried out in order to continue the work presented in this thesis. The first important aspect that needs addressing is the possibility of studying behavioural responses of late stage MIA animals at time points later than 14-21 days post MIA injection. In the present work, behavioural studies showed that MIA animals exhibit mechanical hypersensitivity to vF stimulation during the early acute inflammatory stage, while increased paw withdraw thresholds were present in the late stage at day 14 post MIA injection. Several studies have demonstrated that paw withdraw threshold decrease again in the later stage at 21-28 days post-MIA injection. Behavioural data was consistent with other studies that showed the presence of pro-inflammatory cytokines in the early acute stage and in the later stages of the MIA model also at days 21-28 post-MIA injection (Finn et al., 2014, Sohn et al., 2012, Orita et al., 2011). Thus, it would be very

interesting to be able to address behavioural withdrawal thresholds and frequencies at later time points in the late stage, which in this present study were not addressed due to Home Office animal licence regulations.

One of the most discussed topics in this thesis was the presence of a subgroup of animals that exhibited neuropathic pain-like features in the late stages of the MIA model. Late stage MIA animals did not exhibit DNIC suggestive of changes in descending modulation. However, only a subgroup of late stage MIA animals (40% of animals) showed reduced neuronal evoked responses to mechanical evoked stimulation after the 5-HT3 receptor antagonist ondansetron was spinally delivered. Thus, raising the possibility that perhaps only a subgroup of animals develops the neuropathic pain-like component of altered descending facilitation. These may reflect the subgroups of patients with OA recently described by Soni et al., with neuropathic pain-like features and enhanced descending facilitation. Because *in-vivo* electrophysiological recordings in the late stage MIA group were carried out 14-21 days post injection, it would be interesting to repeat this experiment at a later time point (28 days post-injection). This would give us further information in regards of whether only a subgroup of animals develops the neuropathic pain-like component, as observed in human OA patients (Gwilym et al., 2009), or if neuropathic pain-like component develops at later time points as observed in several studies described in this thesis (Havelin et al., 2016, Abaei et al., 2016, Thakur et al., 2012, Orita et al., 2011, Liu et al., 2011, Combe et al., 2004).

The role of VGCC state dependent vs. state independent blockers has also been addressed in the present study. While state dependent blocker TROX-1 failed to inhibit neuronal evoked responses in both early and late stage MIA animals, state independent blocker w-conotoxin inhibited neuronal evoked responses in both early and late stage MIA animals, but not in shams, with a higher potency in animals in the late stage. It would be interesting to address if the role of an enhanced descending modulation is contributing to this increase in potency in the late stage MIA group. This could be done by blocking 5-HT3 receptor activity after ω-conotoxin spinal administration and recording neuronal evoked responses of WDR neurones.

Lastly, the role of T-type VGCC in pain transmission has been investigated in this study targeting the USP5/$Ca_V3.2$ interaction through TAT-cUBPI-USP5 peptide in the late stages of MIA. However, the data presented in this thesis chapter is preliminary and additional experiments need to be done in order to address the effects of the TAT-cUBPI-USP5 peptide. Additionally, it would be important to address if USP5 is upregulated in both early and late stage MIA animals as that would give more information on whether targeting this interaction in the MIA model would be efficient as well as looking at the effects of the peptide in the early acute inflammatory stage of the MIA model.

7.5. Main findings and closing remarks

The work presented in this thesis aimed to provide further insight into mechanisms driving OA associated pain in the MIA rat model of OA. This model provides two distinct stages of OA-associated pain. In the early stage acute inflammation drives nociceptive pain while in the later stages of the disease the pain is thought to acquire neuropathic-pain like features (Thakur et al., 2012). Because recent human studies have shown that a subgroup of OA patients exhibits pain with neuropathic pain-like features as well as enhanced PAG and RVM activity, it is important to get a better understanding of the mechanisms driving pain in this subgroup of patients to provide a better treatment (Gwilym et al., 2009, Soni et al., 2018).

Using the MIA model, I have demonstrated that rats at both stages present different behavioural phenotypes. In the early acute inflammatory stage, paw withdrawal thresholds are decreased, gait abnormalities are present, while histological data of the knee joint shows that damage to the articular cartilage is little to none. In the later stages of the MIA model, rats show increased paw withdraw thresholds as inflammation is thought to resolve and while animals exhibit weight bearing asymmetry, gait abnormalities measured with Catwalk Gateway system were not present. Additionally, cartilage damage is present but remains moderate and a significant increase of anti-inflammatory cytokine IL-10 is present at day 14 post MIA-injection.

The presence of neuropathic-pain like features, that is thought to appear on the late stage of the MIA model, remains a controversial topic. With some studies reporting nerve damage and altered descending modulation while other studies do not report the presence of a later stage with neuropathic-pain like features. In the present study, I have demonstrated that in the early stages of the MIA-induced arthritis in rats, descending serotonergic drive does not appear altered. Although I have demonstrated that diffused noxious inhibitory controls (DNIC) disappear in the late stages of the MIA model, suggestive of changes in descending modulation, only a subgroup of animals exhibit increased descending serotonergic modulation. This increase of descending serotonergic modulation has been previously reported in both the MIA model as well as in the SNL model of neuropathic pain. These results raise the possibility that either neuropathic-pain like features only develop in a subgroup of rats, as observed in humans and in previous animal? studies, or that the neuropathic-pain like features in this model develop at later stages of the disease as observed in other studies (around day 24-28).

Another aim of the thesis was to investigate the role of voltage gated calcium channels (VGCCs) blockers in modulating OA associated pain. While VGCCs blockers have not been

used for the treatment of pain, drugs such as pregabalin and gabapentin that modulate this channel's activity are commonly prescribed for the treatment of neuropathic pain.

T-type channel blockers have been used to relief pain related behaviours in both neuropathic and inflammatory rodent models. In the work presented in this thesis, a TAT-cUBPI-USP5 peptide that interrupts the interaction between VGCC $Ca_V3.2$ and USP5, promoting channel ubiquitination and degradation. Thus, reducing channels stability in the plasma membrane. TAT-cUBPI-USP5 failed to inhibit neuronal evoked responses of WDR neurons. Additionally, another aim was to address if state-dependent blockers of VGCC $Ca_V2.2$, that act by blocking the channel when it is in an open state, are better modulators than state-independent blockers. In this work, I have demonstrated that the state-independent blocker TROX-1, which targets $Ca_V2.2$, failed to inhibit neuronal evoked responses of WDR neurons in both early and late stages of the MIA model in rats. On the other hand targeting $Ca_V2.2$ using state-independent blocker ω-conotoxin significantly inhibited neuronal evoked responses of deep dorsal horn WDR neurons in both early and late stages of the MIA model. However, ω-conotoxin proved to be more potent in the later stages of the model. These finding raise the question whether descending controls are influencing channel activity and drug potency. Previous work has demonstrated that gabapentin action is dependent on the activation of 5HT-3 receptors in the spinal cord driven by an increased descending serotonergic drive (Rahman et al., 2009, Rahman et al., 2004). Further studies should aim to investigate the relationship between this increased descending serotonergic drive and $Ca_V2.2$ activity, as the increased potency of ω-conotoxin could be modulated by altered descending controls. Altogether, the work presented in this PhD thesis provides further insight on pain mechanisms in both the early and late stages of the rat MIA model of OA.

APPENDIX I: CHAPTER 3

1. Cytokine profile in serum in the MIA rat model of OA

Statistical Analysis

IL-4

One Way ANOVA, $F_{(8,24)}$=2.569, p=0.1031 ns

Multiple comparisons Bonferroni correction ns

Baseline – Day 4	*p=0.939*	$t_{(8)}$= 0.079
Baseline – Day 7	*p=0.630*	$t_{(8)}$= *0.500*
Baseline – Day 14	*p=0.05(*)*	$t_{(8)}$= *3.531*

IL-10

One Way ANOVA, $F_{(8,24)}$=6.116, p=0.0093(**)

Multiple comparisons Bonferroni correction

Baseline – Day 4	*p=0.55*	$t_{(8)}$= 0.622
Baseline – Day 7	*p=0.087*	$t_{(8)}$= *1.950*
Baseline – Day 14	*p=0.0003(***)*	$t_{(8)}$= *5980*

IL-13

One Way ANOVA, $F_{(8,24)}$=2.843, p=0.0.07 ns

Multiple comparisons Bonferroni correction ns

Baseline – Day 4	*p=0.504*	$t_{(8)}$= 0.700
Baseline – Day 7	*p=0.022*	$t_{(8)}$= *2.823*
Baseline – Day 14	*p=0.096*	$t_{(8)}$= *1.884*

IFNγ

One Way ANOVA, $F_{(8,24)}$=1.813, p=0.1921 ns

Multiple comparisons Bonferroni correction ns

Baseline – Day 4	*p=0.537*	$t_{(8)}$= 0.646
Baseline – Day 7	*p=0.052*	$t_{(8)}$= *2.288*
Baseline – Day 14	*p=0.950*	$t_{(8)}$= *0.0646*

TNFα

One Way ANOVA, $F_{(8,24)}$=4.494, p=0.0431 (*)

Multiple comparisons Bonferroni correction ns

Baseline – Day 4	*p=0.084*	$t_{(8)}$= 1.976
Baseline – Day 7	*p=0.732*	$t_{(8)}$= *0.355*
Baseline – Day 14	*p=0.143*	$t_{(8)}$= *1.623*

KC/GRO

One Way ANOVA, $F_{(8,24)}$=4.184, p=0.0356 (*)

Multiple comparisons Bonferroni correction ns

Baseline – Day 4	*p=0.016(*)*	$t_{(8)}$= 3.036
Baseline – Day 7	*p=0.148*	$t_{(8)}$= *1.603*
Baseline – Day 14	*p=ns*	$t_{(8)}$= 3.015

2. Knee Histology

Statistical Analysis

- Condyle Average

Early MIA vs. Early Sham
Non-parametric test 2-Independent samples
Mann Whitney – U test

Medial Tibia	*p=0.517*
Medial Femur	*p=0.135*
Lateral Tibia	*p=0.744*
Lateral Femur	*p=0.744*

Late MIA vs. Late Sham
Non-parametric test 2-Independent samples
Mann Whitney – U test

Medial Tibia	*p=0.218*
Medial Femur	*p=0.017(*)*
Lateral Tibia	*p=0.155*
Lateral Femur	*p=0.008(**)*

- Average Maximum Knee Score

Non-parametric test 2-Independent samples
Kruskal-Wallis to compare all groups, showed p=0.05(*)
Pair-wise comparisons

Early MIA – Early Sham	*p=1.00*
Late MIA – Late Sham	*p=1.00*
Early Sham – Late Sham	*p=1.00*
Late MIA – Early MIA	*p=0.040(*)*

3. Paw withdraw thresholds (g)

Statistical Analysis

MIA ANIMALS

Non-parametric Related Samples Friedman test

Baseline IPSILATERAL – Day 2 IPSILATERAL	*p=0.046(*)*

Friedman test showed p=0.026, Paired Comparisons with Bonferroni Correction

Baseline IPSILATERAL – Day 4 IPSILATERAL	*p=0.049(*)*
Baseline IPSILATERAL – Day 7 IPSILATERAL	*p=0.310*
Baseline IPSILATERAL – Day 14 IPSILATERAL	*p=0.765*
Baseline CONTRALATERAL – Day 2 CONTRALATERAL	*p=0.317*

Friedman test showed ns. p=0.873

Baseline CONTRALATERAL – Day 4 CONTRALATERAL	*ns*

Baseline CONTRALATERAL – Day 7 CONTRALATERAL	*ns*
Baseline CONTRALATERAL – Day 14 CONTRALATERAL	*ns*

Non-parametric 2-Related Samples Wilcoxon test

Baseline IPSILATERAL – Baseline CONTRALATERAL	*p=0.317(*)*
Day 2 IPSILATERAL – Day 2 CONTRALATERAL	*p=0.0446(*)*
Day 4 ISPILATERAL – Day 4 CONTRALATERAL	*p=0.012(*)*
Day 7 ISPILATERAL – Day 7 CONTRALTERAL	*p=0.040(*)*
Day 14 IPSILATERAL – Day 14 CONTRALERAL	*p=0.102*

SHAM ANIMALS

Non-parametric Related Samples Friedman test

Baseline IPSILATERAL – Day 2 IPSILATERAL	*p=1.000*
Friedman test showed ns. p=0.714	
Baseline IPSILATERAL – Day 4 IPSILATERAL	*ns*
Baseline IPSILATERAL – Day 7 IPSILATERAL	*ns*
Baseline IPSILATERAL – Day 14 IPSILATERAL	*ns*
Baseline CONTRALATERAL – Day 2 CONTRALATERAL	*p=1.00*
Friedman test showed ns. p=0.318	
Baseline CONTRALATERAL – Day 4 CONTRALATERAL	*ns*
Baseline CONTRALATERAL – Day 7 CONTRALATERAL	*ns*
Baseline CONTRALATERAL – Day 14 CONTRALATERAL	*ns*

Non-parametric 2-Related Samples Wilcoxon test

Baseline IPSILATERAL – Baseline CONTRALATERAL	*p=1.00*
Day 2 IPSILATERAL – Day 2 CONTRALATERAL	*p=1.00*
Day 4 ISPILATERAL – Day 4 CONTRALATERAL	*p=0.109*
Day 7 ISPILATERAL – Day 7 CONTRALTERAL	*p=0.317*
Day 14 IPSILATERAL – Day 14 CONTRALERAL	*p=0.317*

MIA ANIMALS vs. SHAM ANIMALS

Non-parametric 2-Related Samples Wilcoxon test

Baseline IPSILATERAL – Baseline IPSILATERAL	*p=0.0317*
Day 2 IPSILATERAL – Day 2 IPSILATERAL	*p=0.083*
Baseline IPSILATERAL – Baseline IPSILATERAL	*p=0.655*
Day 4 ISPILATERAL – Day 4 IPSILATERAL	*p=0.235*
Day 7 ISPILATERAL – Day 7 IPSILATERAL	*p=0.073*
Day 14 IPSILATERAL – Day 14 IPSILATERAL	*p=0.713*

Non-parametric 2-Related Samples Wilcoxon test

Baseline CONTRALATERAL – Baseline CONTRALATERAL	*p=1.00*
Day 2 CONTRALATERAL – Day 2 CONTRALATERAL	*p=0.317*
Baseline CONTRALATERAL – Baseline CONTRALATERAL	*p=1.00*
Day 4 CONTRALATERAL – Day 4 CONTRALATERAL	*p=0.414*
Day 7 CONTRALATERAL – Day 7 CONTRALATERAL	*p=0.655*
Day 14 CONTRALATERAL – Day 14 I CONTRALATERAL	*p=1.000*

3. Paw withdraw frequency (%)

Statistical Analysis

MIA ANIMALS: 1g vF

Non-parametric Related Samples Friedman test

Baseline IPSILATERAL – Day 2 IPSILATERAL	*p=0.527*
Friedman test showed p=0.936 ns	
Baseline IPSILATERAL – Day 4 IPSILATERAL	*ns*
Baseline IPSILATERAL – Day 7 IPSILATERAL L	*ns*
Baseline IPSILATERAL L – Day 14 IPSILATERAL	*ns*

Baseline CONTRALATERAL – Day 2 CONTRALATERAL	*p=0.205*
Friedman test showed ns. p=0.873	
Baseline CONTRALATERAL – Day 4 CONTRALATERAL	*ns*
Baseline CONTRALATERAL – Day 7 CONTRALATERAL	*ns*
Baseline CONTRALATERAL – Day 14 CONTRALATERAL	*ns*

Non-parametric 2-Related Samples Wilcoxon test

Baseline IPSILATERAL – Baseline CONTRALATERAL	*p=0.887*
Day 2 IPSILATERAL – Day 2 CONTRALATERAL	*p=0.157*
Baseline IPSILATERAL – Baseline CONTRALATERAL	*p=0.268*
Day 4 ISPILATERAL – Day 4 CONTRALATERAL	*p=1.000*
Day 7 ISPILATERAL – Day 7 CONTRALTERAL	*p=0.107*
Day 14 IPSILATERAL – Day 14 CONTRALERAL	*p=0.496*

MIA ANIMALS: 4g vF

Non-parametric Related Samples Friedman test

Baseline IPSILATERAL – Day 2 IPSILATERAL	*p=0.366*
Friedman test showed p=0.936 ns	
Baseline IPSILATERAL – Day 4 IPSILATERAL	*ns*
Baseline IPSILATERAL – Day 7 IPSILATERAL L	*ns*
Baseline IPSILATERAL L – Day 14 IPSILATERAL	*ns*

Baseline CONTRALATERAL – Day 2 CONTRALATERAL	*p=0.205*
Friedman test showed p=0.022,	
Paired Comparisons with Bonferroni Correction	
Baseline CONTRALATERAL – Day 4 CONTRALATERAL	*p=0.162*
Baseline CONTRALATERAL – Day 7 CONTRALATERAL	*p=0.292*
Baseline CONTRALATERAL – Day 14 CONTRALATERAL	*p=0.139*

Non-parametric 2-Related Samples Wilcoxon test

Baseline IPSILATERAL – Baseline CONTRALATERAL	*p=0.541*
Day 2 IPSILATERAL – Day 2 CONTRALATERAL	*p=0.644*
Baseline IPSILATERAL – Baseline CONTRALATERAL	*p=0.943*
Day 4 ISPILATERAL – Day 4 CONTRALATERAL	*p=0.010(**)*
Day 7 ISPILATERAL – Day 7 CONTRALTERAL	*p=0.571*
Day 14 IPSILATERAL – Day 14 CONTRALERAL	*p=0.045(*)*

MIA ANIMALS: 10g vF

Non-parametric Related Samples Friedman test

Baseline IPSILATERAL – Day 2 IPSILATERAL	*p=0.205*
Friedman test showed p=0.190 ns	
Baseline IPSILATERAL – Day 4 IPSILATERAL	*ns*
Baseline IPSILATERAL – Day 7 IPSILATERAL L	*ns*
Baseline IPSILATERAL L – Day 14 IPSILATERAL	*ns*
Baseline CONTRALATERAL – Day 2 CONTRALATERAL	*p=0.109*
Friedman test showed ns. p=0.000	
Baseline CONTRALATERAL – Day 4 CONTRALATERAL	*p=0.030(**)*
Baseline CONTRALATERAL – Day 7 CONTRALATERAL	*p=0.000(***)*
Baseline CONTRALATERAL – Day 14 CONTRALATERAL	*p=0.006(**)*

Non-parametric 2-Related Samples Wilcoxon test

Baseline IPSILATERAL – Baseline CONTRALATERAL	*p=0.437*
Day 2 IPSILATERAL – Day 2 CONTRALATERAL	*p=0.107*
Baseline IPSILATERAL – Baseline CONTRALATERAL	*p=0.095*
Day 4 ISPILATERAL – Day 4 CONTRALATERAL	*p=0.0009(**)*
Day 7 ISPILATERAL – Day 7 CONTRALTERAL	*p=0.03(*)*
Day 14 IPSILATERAL – Day 14 CONTRALERAL	*p=0.004(**)*

MIA ANIMALS: 15g vF

Non-parametric Related Samples Friedman test

Baseline IPSILATERAL – Day 2 IPSILATERAL	*p=0.248*
Friedman test showed p=0.788 ns	
Baseline IPSILATERAL – Day 4 IPSILATERAL	*ns*
Baseline IPSILATERAL – Day 7 IPSILATERAL L	*ns*
Baseline IPSILATERAL L – Day 14 IPSILATERAL	*ns*
Baseline CONTRALATERAL – Day 2 CONTRALATERAL	*p=0.782*
Friedman test showed ns. p=0.000	
Baseline CONTRALATERAL – Day 4 CONTRALATERAL	*p=0.566*
Baseline CONTRALATERAL – Day 7 CONTRALATERAL	*p=0.025(*)*
Baseline CONTRALATERAL – Day 14 CONTRALATERAL	*p=0.002(**)*

Non-parametric 2-Related Samples Wilcoxon test

Baseline IPSILATERAL – Baseline CONTRALATERAL	*p=0.928*
Day 2 IPSILATERAL – Day 2 CONTRALATERAL	*p=0.632*
Baseline IPSILATERAL – Baseline CONTRALATERAL	*p=0.354*
Day 4 ISPILATERAL – Day 4 CONTRALATERAL	*p=0.024(**)*
Day 7 ISPILATERAL – Day 7 CONTRALTERAL	*p=0.001(***)*
Day 14 IPSILATERAL – Day 14 CONTRALERAL	*p=0.001(***)*

MIA ANIMALS vs. SHAM ANIMALS: 1g vF

Non-parametric 2-Related Samples Wilcoxon test

Baseline IPSILATERAL – Baseline IPSILATERAL	*p=0.351*
Day 2 IPSILATERAL – Day 2 IPSILATERAL	*p=0.655*
Baseline IPSILATERAL – Baseline IPSILATERAL	*p=0.026*
Day 4 ISPILATERAL – Day 4 IPSILATERAL	*p=0.760*
Day 7 ISPILATERAL – Day 7 IPSILATERAL	*p=0.764*
Day 14 IPSILATERAL – Day 14 IPSILATERAL	*p=0.723*

MIA ANIMALS vs. SHAM ANIMALS: 5g vF

Non-parametric 2-Related Samples Wilcoxon test

Baseline IPSILATERAL – Baseline IPSILATERAL	*p=0.238*
Day 2 IPSILATERAL – Day 2 IPSILATERAL	*p=0.803*
Baseline IPSILATERAL – Baseline IPSILATERAL	*p=0.531*
Day 4 ISPILATERAL – Day 4 IPSILATERAL	*p=0.692*
Day 7 ISPILATERAL – Day 7 IPSILATERAL	*p=0.685*
Day 14 IPSILATERAL – Day 14 IPSILATERAL	*p=0.542*

MIA ANIMALS vs. SHAM ANIMALS: 10g vF

Non-parametric 2-Related Samples Wilcoxon test

Baseline IPSILATERAL – Baseline IPSILATERAL	*p=0.094*
Day 2 IPSILATERAL – Day 2 IPSILATERAL	*p=0.359*
Baseline IPSILATERAL – Baseline IPSILATERAL	*p=0.878*
Day 4 ISPILATERAL – Day 4 IPSILATERAL	*p=0.113*
Day 7 ISPILATERAL – Day 7 IPSILATERAL	*p=0.255*
Day 14 IPSILATERAL – Day 14 IPSILATERAL	*p=0.464*

MIA ANIMALS vs. SHAM ANIMALS: 15g vF

Non-parametric 2-Related Samples Wilcoxon test

Baseline IPSILATERAL – Baseline IPSILATERAL	*p=0.317*
Day 2 IPSILATERAL – Day 2 IPSILATERAL	*p=0.083*
Baseline IPSILATERAL – Baseline IPSILATERAL	*p=0.655*
Day 4 ISPILATERAL – Day 4 IPSILATERAL	*p=0.235*
Day 7 ISPILATERAL – Day 7 IPSILATERAL	*p=0.073*
Day 14 IPSILATERAL – Day 14 IPSILATERAL	*p=0.713*

S.1 PAW WITHDRAW FREQUENCY: MIA vs. SHAM IPSILATERAL

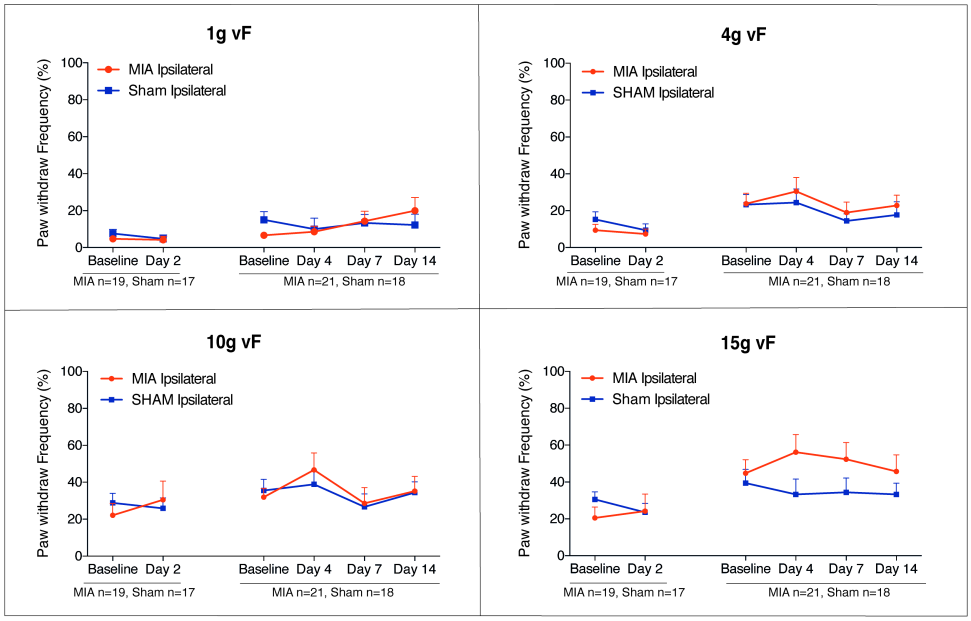

Supplementary figure 1. Paw withdrawal frequency (%): MIA vs. Sham Ipsilateral hind-paw. This figure shows the paw withdraw frequency of 1g, 4g, 10g and 15g vF filaments applied to the ipsilateral hind-paw of MIA and sham animals at baseline and at different post injection time points. No significant changes in paw withdraw frequency (%) are present upon stimulation with any of the presented vF filaments when comparing MIA ipsilateral to sham ipsilateral responses.

4. Weight Bearing (%)

Statistical Analysis

MIA ANIMALS

Non-parametric Related Samples Friedman test

Baseline IPSILATERAL – Day 2 IPSILATERAL	*p=0.002(*)*

Friedman test showed p=0.026,
Paired Comparisons with Bonferroni Correction

Baseline IPSILATERAL – Day 4 IPSILATERAL	*p=0.000(***)*
Baseline IPSILATERAL – Day 7 IPSILATERAL	*p=0.139*
Baseline IPSILATERAL – Day 14 IPSILATERAL	*p=0.721*

Non-parametric Related Samples Friedman test

Baseline CONTRALATERAL – Day 2 CONTRALATERAL	*p=0.033(*)*

Friedman test showed p=0.003,
Paired Comparisons with Bonferroni Correction

Baseline CONTRALATERAL – Day 2 CONTRALATERAL	*p=0.033(*)*
Baseline CONTRALATERAL – Day 4 CONTRALATERAL	*p=0.001(**)*
Baseline CONTRALATERAL – Day 7 CONTRALATERAL	*p=0.023(*)*
Baseline CONTRALATERAL – Day 14 CONTRALATERAL	*p=0.056*

Non-parametric 2-Related Samples Wilcoxon test

Baseline IPSILATERAL – Baseline CONTRALATERAL	*p=0.73*
Day 2 IPSILATERAL – Day 2 CONTRALATERAL	*p=0.005*
Day 4 ISPILATERAL – Day 4 CONTRALATERAL	*p=0.000281(###)*
Day 7 ISPILATERAL – Day 7 CONTRALTERAL	*p=0.001(###)*
Day 14 IPSILATERAL – Day 14 CONTRALERAL	*p=0.102(###)*

SHAM ANIMALS

Non-parametric Related Samples Friedman test

Baseline IPSILATERAL – Day 2 IPSILATERAL	*p=0.285*

Friedman test showed ns. p=0.163

Baseline IPSILATERAL – Day 4 IPSILATERAL	*ns*
Baseline IPSILATERAL – Day 7 IPSILATERAL	*ns*
Baseline IPSILATERAL – Day 14 IPSILATERAL	*ns*

Baseline CONTRALATERAL – Day 2 CONTRALATERAL	*p=0.55*

Friedman test showed ns. p=0.189

Baseline CONTRALATERAL – Day 4 CONTRALATERAL	*ns*
Baseline CONTRALATERAL – Day 7 CONTRALATERAL	*ns*
Baseline CONTRALATERAL – Day 14 CONTRALATERAL	*ns*

Non-parametric 2-Related Samples Wilcoxon test

Baseline IPSILATERAL – Baseline CONTRALATERAL	*p=0.826*
Day 2 IPSILATERAL – Day 2 CONTRALATERAL	*p=0.686*
Day 4 ISPILATERAL – Day 4 CONTRALATERAL	*p=0.407*
Day 7 ISPILATERAL – Day 7 CONTRALTERAL	*p=0.653*
Day 14 IPSILATERAL – Day 14 CONTRALERAL	*p=0.227*

MIA ANIMALS vs. SHAM ANIMALS

Non-parametric 2-Related Samples Wilcoxon test

Baseline IPSILATERAL – Baseline IPSILATERAL	*p=0.975*
Day 2 IPSILATERAL – Day 2 IPSILATERAL	*p=0.003(**)*
Baseline IPSILATERAL – Baseline IPSILATERAL	*p=0.435*
Day 4 ISPILATERAL – Day 4 IPSILATERAL	*p=0.006(**)*
Day 7 ISPILATERAL – Day 7 IPSILATERAL	*p=0.001(***)*
Day 14 IPSILATERAL – Day 14 IPSILATERAL	*p=0.007(**)*

Non-parametric 2-Related Samples Wilcoxon test

Baseline IPSILATERAL – Baseline IPSILATERAL	*p=0.594*
Day 2 IPSILATERAL – Day 2 IPSILATERAL	*p=0.003(**)*
Baseline IPSILATERAL – Baseline IPSILATERAL	*p=0.381*
Day 4 ISPILATERAL – Day 4 IPSILATERAL	*p=0.001(***)*
Day 7 ISPILATERAL – Day 7 IPSILATERAL	*p=0.000(****)*
Day 14 IPSILATERAL – Day 14 IPSILATERAL	*p=0.002(**)*

5. Catwalk Gateway System

Statistical Analysis

- PRINT AREA (cm^2)

MIA ANIMALS

Non-parametric Related Samples Friedman test p=0.004(**)
Paired Comparisons with Bonferroni Correction

Baseline LH/RH ratio – Day 2 LH/RH ratio	*p=0.003(**)*
Baseline LH/RH ratio – Day 4 LH/RH ratio	*p=0.067*
Baseline LH/RH ratio – Day 7 LH/RH ratio	*p=1.00*
Baseline LH/RH ratio – Day 14 LH/RH ratio	*p=1.00*

Non-parametric Related Samples Friedman test p=0.025
Paired Comparisons with Bonferroni Correction

Baseline LF/RF ratio – Day 2 LF/RF ratio	*p=0.019*
Baseline LF/RF ratio – Day 4 LF/RF ratio	*p=0.933*
Baseline LF/RF ratio – Day 7 LF/RF ratio	*p=1.00*
Baseline LF/RF ratio – Day 14 LF/RF ratio	*p=1.00*

SHAM ANIMALS

Non-parametric Related Samples Friedman test p=0.569
Baseline LH/RH ratio – post Sham-injection LH/RH ns

Non-parametric Related Samples Friedman test p=0.504
Baseline LF/RF ratio – post Sham-injection LF/RF ns

MIA vs. SHAM ANIMALS

Non-parametric 2-Related Samples Wilcoxon test

Baseline LH/RH ratio – Baseline LH/RH ratio	*p=0.463*
Day 2 LH/RH ratio – Day 2 LH/RH ratio	*p=0.028(#)*

Day 4 LH/RH ratio – Day 4 LH/RH ratio	*p=0.028(##)*
Day 7 LH/RH ratio – Day 7 LH/RH ratio	*p=0.345*
Day 14 LH/RH ratio – Day 14 LH/RH ratio	*p=0.046(#)*

Non-parametric 2-Related Samples Wilcoxon test

Baseline LF/RF ratio – Baseline LF/RF ratio	*p=0.249*
Day 2 LF/RF ratio – Day 2 LF/RF ratio	*p=0.173*
Day 4 LF/RF ratio – Day 4 LF/RF ratio	*p=0.075*
Day 7 LF/RF ratio – Day 7 LF/RF ratio	*p=0.917*
Day 14 LF/RF ratio – Day 14 LF/RF ratio	*p=6.00*

- SWING (s)

MIA ANIMALS

Non-parametric Related Samples Friedman test p=0.002(**)
Paired Comparisons with Bonferroni Correction

Baseline LH/RH ratio – Day 2 LH/RH ratio	*p=0.001(**)*
Baseline LH/RH ratio – Day 4 LH/RH ratio	*p=0.389*
Baseline LH/RH ratio – Day 7 LH/RH ratio	*p=1.00*
Baseline LH/RH ratio – Day 14 LH/RH ratio	*p=0.282*

Non-parametric Related Samples Friedman test p=0.048

Baseline LF/RF ratio – post-MIA injection LH/RH	*ns*

SHAM ANIMALS

Non-parametric Related Samples Friedman test p=0.371

Baseline LH/RH ratio – post Sham-injection LH/RH	*ns*

Non-parametric Related Samples Friedman test p=0.547

Baseline LF/RF ratio – post Sham-injection LF/RF	*ns*

MIA vs. SHAM ANIMALS

Non-parametric 2-Related Samples Wilcoxon test

Baseline LH/RH ratio – Baseline LH/RH ratio	*p=0.075*
Day 2 LH/RH ratio – Day 2 LH/RH ratio	*p=0.028(#)*
Day 4 LH/RH ratio – Day 4 LH/RH ratio	*p=0.345*
Day 7 LH/RH ratio – Day 7 LH/RH ratio	*p=0.463*
Day 14 LH/RH ratio – Day 14 LH/RH ratio	*p=0.116*

Non-parametric 2-Related Samples Wilcoxon test

Baseline LF/RF ratio – Baseline LF/RF ratio	*p=0.753*
Day 2 LF/RF ratio – Day 2 LF/RF ratio	*p=0.917*
Day 4 LF/RF ratio – Day 4 LF/RF ratio	*p=0.917*
Day 7 LF/RF ratio – Day 7 LF/RF ratio	*p=0.600*
Day 14 LF/RF ratio – Day 14 LF/RF ratio	*p=0.173*

- SWING SPEED (cm/s)

MIA ANIMALS

Non-parametric Related Samples Friedman test p=0.007(**)
Paired Comparisons with Bonferroni Correction

Baseline LH/RH ratio – Day 2 LH/RH ratio	*p=0.003(**)*
Baseline LH/RH ratio – Day 4 LH/RH ratio	*p=1.00*
Baseline LH/RH ratio – Day 7 LH/RH ratio	*p=1.00*
Baseline LH/RH ratio – Day 14 LH/RH ratio	*p=1.00*

Non-parametric Related Samples Friedman test p=0.255
Baseline LF/RF ratio – post-MIA injection LH/RH ns

SHAM ANIMALS

Non-parametric Related Samples Friedman test p=0.139

Baseline LH/RH ratio – post Sham-injection LH/RH	*ns*

Non-parametric Related Samples Friedman test p=0.525

Baseline LF/RF ratio – post Sham-injection LF/RF	*ns*

MIA vs. SHAM ANIMALS

Non-parametric 2-Related Samples Wilcoxon test

Baseline LH/RH ratio – Baseline LH/RH ratio	*p=0.753*
Day 2 LH/RH ratio – Day 2 LH/RH ratio	*p=0.028(#)*
Day 4 LH/RH ratio – Day 4 LH/RH ratio	*p=0.345*
Day 7 LH/RH ratio – Day 7 LH/RH ratio	*p=0.173*
Day 14 LH/RH ratio – Day 14 LH/RH ratio	*p=0.347*

Non-parametric 2-Related Samples Wilcoxon test

Baseline LF/RF ratio – Baseline LF/RF ratio	*p=0.028(#)*
Day 2 LF/RF ratio – Day 2 LF/RF ratio	*p=0.248*
Day 4 LF/RF ratio – Day 4 LF/RF ratio	*p=0.345*
Day 7 LF/RF ratio – Day 7 LF/RF ratio	*p=0.463*
Day 14 LF/RF ratio – Day 14 LF/RF ratio	*p=0.116*

- SWING SPEED (cm/s)

MIA ANIMALS

Non-parametric Related Samples Friedman test p=0.000(***)
Paired Comparisons with Bonferroni Correction

Baseline LH/RH ratio – Day 2 LH/RH ratio	*p=0.000(***)*
Baseline LH/RH ratio – Day 4 LH/RH ratio	*p=0.933*
Baseline LH/RH ratio – Day 7 LH/RH ratio	*p=0.282*
Baseline LH/RH ratio – Day 14 LH/RH ratio	*p=1.00*

Non-parametric Related Samples Friedman test p=0.001
Paired Comparisons with Bonferroni Correction

Baseline LF/RF ratio – Day 2 LF/RF ratio	*p=0.012(**)*
Baseline LF/RF ratio – Day 4 LF/RF ratio	*p=0.001(***)*
Baseline LF/RF ratio – Day 7 LF/RF ratio	*p=0.005(**)*
Baseline LF/RF ratio – Day 14 LF/RF ratio	*p=0.03(*)*

SHAM ANIMALS

Non-parametric Related Samples Friedman test p=0.424

Baseline LH/RH ratio – post Sham-injection LH/RH	*ns*

Non-parametric Related Samples Friedman test p=0.004
Paired Comparisons with Bonferroni Correction

Baseline LF/RF ratio – Day 2 LF/RF ratio	*p=0.176*
Baseline LF/RF ratio – Day 4 LF/RF ratio	*p=0.106*
Baseline LF/RF ratio – Day 7 LF/RF ratio	*p=0.285*
Baseline LF/RF ratio – Day 14 LF/RF ratio	*p=0.0001(***)*

MIA vs. SHAM ANIMALS

Non-parametric 2-Related Samples Wilcoxon test

Baseline LH/RH ratio – Baseline LH/RH ratio	*p=0.024*
Day 2 LH/RH ratio – Day 2 LH/RH ratio	*p=0.028(#)*
Day 4 LH/RH ratio – Day 4 LH/RH ratio	*p=0.345*
Day 7 LH/RH ratio – Day 7 LH/RH ratio	*p=0.046(##)*
Day 14 LH/RH ratio – Day 14 LH/RH ratio	*p=0.116*

Non-parametric 2-Related Samples Wilcoxon test

Baseline LF/RF ratio – Baseline LF/RF ratio	*p=0.917*
Day 2 LF/RF ratio – Day 2 LF/RF ratio	*p=0.249*
Day 4 LF/RF ratio – Day 4 LF/RF ratio	*p=0.753*
Day 7 LF/RF ratio – Day 7 LF/RF ratio	*p=0.249*
Day 14 LF/RF ratio – Day 14 LF/RF ratio	*p=0.116*

6. LABORAS

Statistical Analysis

- LOCOMOTOR DURATION

MIA DARK CYCLE
Non-parametric Related Samples Friedman test
p=0.592 ns

MIA LIGHT CYCLE
Non-parametric Related Samples Friedman test
p=0.002(**)
Paired Comparisons with Bonferroni Correction

Baseline – Day 2	*p=0.098*
Baseline – Day 4	*p=0.019(*)*
Baseline – Day 7	*p=0.001(**)*
Baseline – Day 14	*p=0.389*

SHAM DARK CYCLE
Non-parametric Related Samples Friedman test
p=0.294

SHAM LIGHT CYCLE
Non-parametric Related Samples Friedman test
p=0.015(**)
Paired Comparisons with Bonferroni Correction

Baseline – Day 2	*p=0.176*
Baseline – Day 4	*p=0.062*
Baseline – Day 7	*p=0.035(*)*
Baseline – Day 14	*p=0.035(*)*

MIA DARK CYCLE vs. SHAM DARK CYCLE
Non-parametric 2-Related Samples Wilcoxon test

Baseline MIA – Baseline Sham	*p=0.600*
Day 2 MIA – Day 2 Sham	*p=0.753*
Day 4 MIA – Day 4 Sham	*p=0.753*
Day 7 MIA – Day 7 Sham	*p=0.345*
Day 14 MIA – Day 14 Sham	*p=0.753*

MIA LIGHT CYCLE vs. SHAM LIGHT CYCLE
Non-parametric 2-Related Samples Wilcoxon test

Baseline MIA – Baseline Sham	*p=0.116*
Day 2 MIA – Day 2 Sham	*p=0.463*
Day 4 MIA – Day 4 Sham	*p=0.463*
Day 7 MIA – Day 7 Sham	*p=0.917*
Day 14 MIA – Day 14 Sham	*p=0.463*

- MAXIMUM SPEED (mm/s)

MIA DARK CYCLE
Non-parametric Related Samples Friedman test
p=0.616 ns

MIA LIGHT CYCLE
Non-parametric Related Samples Friedman test
p=0.001(**)
Paired Comparisons with Bonferroni Correction

Baseline – Day 2	*p=0.933*
Baseline – Day 4	*p=0.528*
Baseline – Day 7	*p=0.707*
Baseline – Day 14	*p=1.00*

SHAM DARK CYCLE
Non-parametric Related Samples Friedman test
p=0.107 ns

SHAM LIGHT CYCLE
Non-parametric Related Samples Friedman test
p=0.063 ns

MIA DARK CYCLE vs. SHAM DARK CYCLE
Non-parametric 2-Related Samples Wilcoxon test

Baseline MIA – Baseline Sham	*p=0.917*
Day 2 MIA – Day 2 Sham	*p=0.173*
Day 4 MIA – Day 4 Sham	*p=0.173*
Day 7 MIA – Day 7 Sham	*p=0.173*
Day 14 MIA – Day 14 Sham	*p=0.046(#)*

MIA LIGHT CYCLE vs. SHAM LIGHT CYCLE
Non-parametric 2-Related Samples Wilcoxon test

Baseline MIA – Baseline Sham	*p=0.249*
Day 2 MIA – Day 2 Sham	*p=0.028(#)*
Day 4 MIA – Day 4 Sham	*p=0.753*
Day 7 MIA – Day 7 Sham	*p=0.116*
Day 14 MIA – Day 14 Sham	*p=0.028(#)*

- DISTANCE (m)

MIA DARK CYCLE
Non-parametric Related Samples Friedman test
p=0.075 ns

MIA LIGHT CYCLE
Non-parametric Related Samples Friedman test
p=0.167 ns

SHAM DARK CYCLE
Non-parametric Related Samples Friedman test
p=0.547 ns

SHAM LIGHT CYCLE
Non-parametric Related Samples Friedman test
p=0.006(**)
Paired Comparisons with Bonferroni Correction

Baseline – Day 2	*p=0.106*
Baseline – Day 4	*p=0.003(**)*
Baseline – Day 7	*p=0.285*
Baseline – Day 14	*p=0.106*

MIA DARK CYCLE vs. SHAM DARK CYCLE
Non-parametric 2-Related Samples Wilcoxon test

Baseline MIA – Baseline Sham	*p=0.173*
Day 2 MIA – Day 2 Sham	*p=0.600*
Day 4 MIA – Day 4 Sham	*p=0.075*
Day 7 MIA – Day 7 Sham	*p=0.753*
Day 14 MIA – Day 14 Sham	*p=0.600*

MIA LIGHT CYCLE vs. SHAM LIGHT CYCLE
Non-parametric 2-Related Samples Wilcoxon test

Baseline MIA – Baseline Sham	*p=0.173*
Day 2 MIA – Day 2 Sham	*p=0.249*
Day 4 MIA – Day 4 Sham	*p=0.173*
Day 7 MIA – Day 7 Sham	*p=0.345*
Day 14 MIA – Day 14 Sham	*p=0.917*

- DRINKING FREQUENCY (counts)

MIA DARK CYCLE
Non-parametric Related Samples Friedman test
p=0.001(**)

Baseline – Day 2	*p=0.814*
Baseline – Day 4	*p=1.00*
Baseline – Day 7	*p=1.00*
Baseline – Day 14	*p=0.239*

MIA LIGHT CYCLE
Non-parametric Related Samples Friedman test
p=0.167

Baseline – Day 2	*p=0.389*
Baseline – Day 4	*p=0.169*
Baseline – Day 7	*p=0.118*
Baseline – Day 14	*p=0.008(**)*

SHAM DARK CYCLE
Non-parametric Related Samples Friedman test
p=0.026(**)

Baseline – Day 2	*p=1.000*
Baseline – Day 4	*p=1.000*
Baseline – Day 7	*p=1.00*
Baseline – Day 14	*p=0.176*

SHAM LIGHT CYCLE
Non-parametric Related Samples Friedman test
p=0.006(**)
Paired Comparisons with Bonferroni Correction

Baseline – Day 2	*p=0.106*
Baseline – Day 4	*p=1.000*
Baseline – Day 7	*p=0.285*
Baseline – Day 14	*p=0.003(**)*

MIA DARK CYCLE vs. SHAM DARK CYCLE
Non-parametric 2-Related Samples Wilcoxon test

Baseline MIA – Baseline Sham	*p=0.249*
Day 2 MIA – Day 2 Sham	*p=0.753*
Day 4 MIA – Day 4 Sham	*p=0.463*
Day 7 MIA – Day 7 Sham	*p=0.600*
Day 14 MIA – Day 14 Sham	*p=0.917*

MIA LIGHT CYCLE vs. SHAM LIGHT CYCLE
Non-parametric 2-Related Samples Wilcoxon test

Baseline MIA – Baseline Sham	*p=0.752*
Day 2 MIA – Day 2 Sham	*p=0.600*
Day 4 MIA – Day 4 Sham	*p=0.173*
Day 7 MIA – Day 7 Sham	*p=0.141*
Day 14 MIA – Day 14 Sham	*p=0.686*

- FEEDING FREQUENCY (counts)

MIA DARK CYCLE
Non-parametric Related Samples Friedman test
p=0.051 ns

MIA LIGHT CYCLE
Non-parametric Related Samples Friedman test
p=0.003(**)

Baseline – Day 2	*p=0.142*
Baseline – Day 4	*p=1.00*
Baseline – Day 7	*p=0.01(**)*
Baseline – Day 14	*p=0.01(**)*

SHAM DARK CYCLE
Non-parametric Related Samples Friedman test
p=0.338

SHAM LIGHT CYCLE
Non-parametric Related Samples Friedman test
p=0.012(*)
Paired Comparisons with Bonferroni Correction

Baseline – Day 2	*p=0.106*
Baseline – Day 4	*p=0.446*
Baseline – Day 7	*p=0.446*
Baseline – Day 14	*p=0.005(**)*

MIA DARK CYCLE vs. SHAM DARK CYCLE
Non-parametric 2-Related Samples Wilcoxon test

Baseline MIA – Baseline Sham	*p=0.345*
Day 2 MIA – Day 2 Sham	*p=0.600*
Day 4 MIA – Day 4 Sham	*p=0.463*
Day 7 MIA – Day 7 Sham	*p=0.916*
Day 14 MIA – Day 14 Sham	*p=0.116*

MIA LIGHT CYCLE vs. SHAM LIGHT CYCLE
Non-parametric 2-Related Samples Wilcoxon test

Baseline MIA – Baseline Sham	*p=0.917*
Day 2 MIA – Day 2 Sham	*p=0.463*
Day 4 MIA – Day 4 Sham	*p=0.833*
Day 7 MIA – Day 7 Sham	*p=0.0028(*)*
Day 14 MIA – Day 14 Sham	*p=0.753*

- GROOMING FREQUENCY (counts)

MIA DARK CYCLE
Non-parametric Related Samples Friedman test
p=0.000(****)

Baseline – Day 2	*p=0.000(****)*
Baseline – Day 4	*p=0.005(**)*
Baseline – Day 7	*p=0.0067*
Baseline – Day 14	*p=1.000*

MIA LIGHT CYCLE

Non-parametric Related Samples Friedman test

p=0.002(**)

Baseline – Day 2	*p=0.707*
Baseline – Day 4	*p=0.282*
Baseline – Day 7	*p=0.001(***)*
Baseline – Day 14	*p=0.019(*)*

SHAM DARK CYCLE

Non-parametric Related Samples Friedman test

p=0.043(*)

Baseline – Day 2	*p=0.062*
Baseline – Day 4	*p=1.000*
Baseline – Day 7	*p=0.679*
Baseline – Day 14	*p=1.000*

SHAM LIGHT CYCLE

Non-parametric Related Samples Friedman test

p=0.013(*)

Paired Comparisons with Bonferroni Correction

Baseline – Day 2	*p=1.000*
Baseline – Day 4	*p=0.035(*)*
Baseline – Day 7	*p=0.176*
Baseline – Day 14	*p=0.019(*)*

MIA DARK CYCLE vs. SHAM DARK CYCLE

Non-parametric 2-Related Samples Wilcoxon test

Baseline MIA – Baseline Sham	*p=0.345*
Day 2 MIA – Day 2 Sham	*p=0.600*
Day 4 MIA – Day 4 Sham	*p=0.463*
Day 7 MIA – Day 7 Sham	*p=0.916*
Day 14 MIA – Day 14 Sham	*p=0.116*

MIA LIGHT CYCLE vs. SHAM LIGHT CYCLE

Non-parametric 2-Related Samples Wilcoxon test

Baseline MIA – Baseline Sham	*p=0.917*
Day 2 MIA – Day 2 Sham	*p=0.753*
Day 4 MIA – Day 4 Sham	*p=0.600*
Day 7 MIA – Day 7 Sham	*p=0.345*
Day 14 MIA – Day 14 Sham	*p=0.345*

- REARING FREQUENCY (counts)

MIA DARK CYCLE

Non-parametric Related Samples Friedman test

p=0.004(**)

Baseline – Day 2	*p=0.024(*)*
Baseline – Day 4	*p=1.000*
Baseline – Day 7	*p=1.000*
Baseline – Day 14	*p=1.000*

MIA LIGHT CYCLE

Non-parametric Related Samples Friedman test

p=0.006(**)

Baseline – Day 2	*p=0.142*
Baseline – Day 4	*p=0.087*
Baseline – Day 7	*p=0.008(**)*
Baseline – Day 14	*p=0.019(*)*

SHAM DARK CYCLE

Non-parametric Related Samples Friedman test

p=0.180

SHAM LIGHT CYCLE

Non-parametric Related Samples Friedman test

p=0.012(*)

Paired Comparisons with Bonferroni Correction

Baseline – Day 2	*p=0.176*
Baseline – Day 4	*p=0.010(**)*
Baseline – Day 7	*p=0.062*
Baseline – Day 14	*p=0.106*

MIA DARK CYCLE vs. SHAM DARK CYCLE

Non-parametric 2-Related Samples Wilcoxon test

Baseline MIA – Baseline Sham	*p=0.075*
Day 2 MIA – Day 2 Sham	*p=0.917*
Day 4 MIA – Day 4 Sham	*p=0.173*
Day 7 MIA – Day 7 Sham	*p=0.917*
Day 14 MIA – Day 14 Sham	*p=0.600*

MIA LIGHT CYCLE vs. SHAM LIGHT CYCLE

Non-parametric 2-Related Samples Wilcoxon test

Baseline MIA – Baseline Sham	*p=0.463*
Day 2 MIA – Day 2 Sham	*p=0.249*
Day 4 MIA – Day 4 Sham	*p=0.600*
Day 7 MIA – Day 7 Sham	*p=0.345*
Day 14 MIA – Day 14 Sham	*p=0.753*

7. Electrophysiology statistics

EARLY MIA vs. EARLY SHAM

ELECTRICALS

Paired Sample t-test

Aβ	*p=0.324*	$t_{(27)}$*=1.003*
Aδ	*p=0.502*	$t_{(27)}$*=0.679*
C	*p=0.432*	$t_{(27)}$*=0.795*
PD	*p=0.449*	$t_{(27)}$*=0.765*
I	*p=0.576*	$t_{(27)}$*=0.564*
WU	*p=0.061*	$t_{(27)}$*=1.933*

DYNAMIC BRUSH
Paired Sample t-test

p=0.337	$t_{(27)}=1.025$

MECHANICALS
Repeated measures 2-way ANOVA

p=0.337	$F_{(34,35)}=1.181$

THERMALS
Repeated measures 2-way ANOVA

p=0.495	$F_{(34,35)}=0.815$

LATE MIA vs. LATE SHAM

ELECTRICALS
Paired Sample t-test

Aβ	*p=0.512*	$t_{(45)}=0.835$
Aδ	*p=0.935*	$t_{(45)}=0.935$
C	*p=0.815*	$t_{(45)}=0.815$
PD	*p=0.635*	$t_{(45)}=0.635$
I	*p=0.555*	$t_{(45)}=0.555$
WU	*p=0.184*	$t_{(45)}=0.18$

DYNAMIC BRUSH
Paired Sample t-test

p=0.523	$t_{(56)}=1.210$

MECHANICALS
Repeated measures 2-way ANOVA

p=0.381	$F_{(50,51)}=1.071$

THERMALS
Repeated measures 2-way ANOVA

p=0.492	$F_{(52,53)}=0.813$

EARLY MIA vs. LATE MIA

ELECTRICALS
Paired Sample t-test

Aβ	*p=0.369*	$t_{(47)}=0.714$
Aδ	*p=0.760*	$t_{(47)}=0.451$
C	*p=0.401*	$t_{(47)}=0.690$
PD	*p=0.208*	$t_{(47)}=0.836$
I	*p=0.141*	$t_{(47)}=0.888$
WU	*p=0.024(*)*	$t_{(47)}=0.981$

DYNAMIC BRUSH
Paired Sample t-test

p=0.077	$t_{(53)}=1.806$

MECHANICALS

Repeated measures 2-way ANOVA

p=0.366	$F_{(47,48)}$*=1.104*

THERMALS

Repeated measures 2-way ANOVA

p=0.687	$F_{(49,50)}$*=0.037*

EARLY SHAM vs. LATE SHAM

ELECTRICALS

Paired Sample t-test

Aβ	*p=0.091*	$t_{(35)}$*=1.771*
Aδ	*p=0.869*	$t_{(35)}$*=0.167*
C	*p=0.532*	$t_{(35)}$*=0.631*
PD	*p=0.310*	$t_{(35)}$*=1.029*
I	*p=0.819*	$t_{(35)}$*=0.231*
WU	*p=0.416*	$t_{(35)}$*=0.822*

DYNAMIC BRUSH

Paired Sample t-test

p=0.977	$t_{(40)}$*=0.977*

MECHANICALS

Repeated measures 2-way ANOVA

p=0.185	$F_{(37,38)}$*=1.640*

THERMALS

Repeated measures 2-way ANOVA

p=0.343	$F_{(37,38)}$*=1.146*

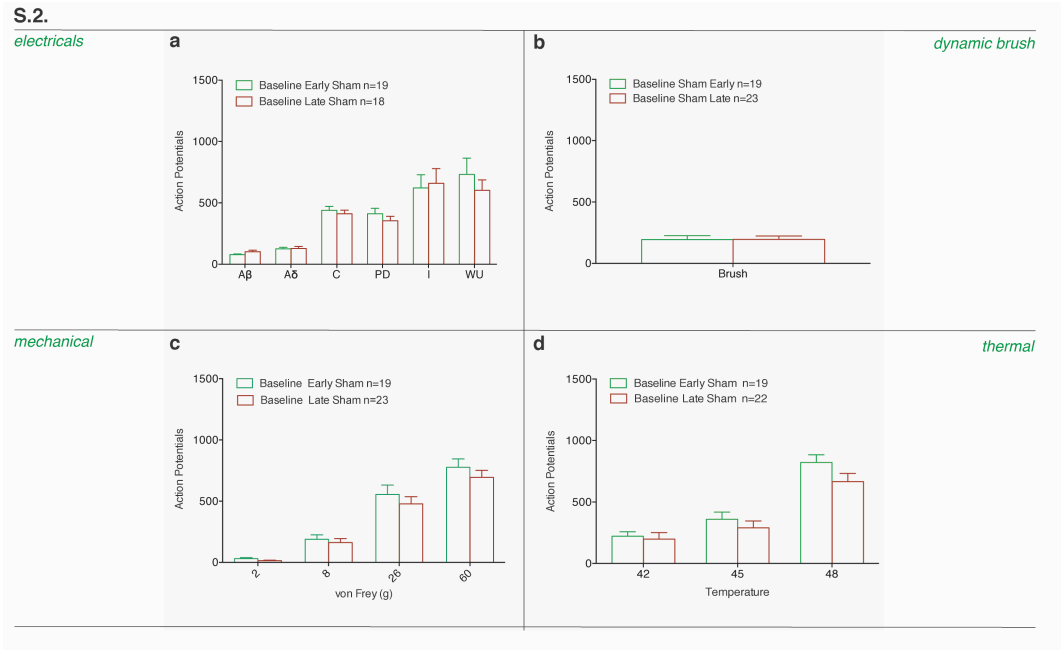

Supplementary Figure 2. Baseline neuronal evoked responses of deep dorsal horn WDR neurones in early sham and late shams animals. **a)** Electrical evoked responses of WDR neurones. **b)** Dynamic Brush of neuronal evoked response. **c)** Mechanical evoked responses of WDR neurones to 2g, 8g, 26g and 60g vF. **d)** Thermal evoked neuronal responses of WDR neurones t0 45, 42 and 48°C.

8. Electrophysiology statistics comparing MIA and sham baseline responses to 10 and 30min post-spinally applied 0.9% saline

MIA ANIMALS

ELECTRICALS

One Way ANOVA

Aβ	*p=0.474*	$F_{(2,6)}$*=1.003*
Aδ	*p=0.630*	$F_{(2,6)}$*=0.500*
C	*p=0.512*	$F_{(2,6)}$*=0.623*
PD	*p=0.443*	$F_{(2,6)}$*=0.930*
I	*p=0.759*	$F_{(2,6)}$*=0.289*
WU	*p=0.515*	$F_{(2,6)}$*=0.742*

DYNAMIC BRUSH

One Way ANOVA

	p=0.958	$F_{(2,6)}$*=0.044*

MECHANICALS

Repeated measures 2-way ANOVA

	p=0.520	*$F_{(2,6)}$=0.730*

THERMALS

Repeated measures 2-way ANOVA

	p=0.841	*$F_{(2,6)}$=0.178*

SHAM ANIMALS

ELECTRICALS

One Way ANOVA

Aβ	*p=0.811*	*$F_{(2,9)}$=1.003*
Aδ	*p=0.863*	*$F_{(2,9)}$=0.150*
C	*p=0.419*	*$F_{(2,9)}$=0.960*
PD	*p=0.524*	*$F_{(2,9)}$=0.694*
I	*p=0.824*	*$F_{(2,9)}$=0.198*
WU	*p=0.287*	*$F_{(2,9)}$=1.439*

DYNAMIC BRUSH

One Way ANOVA

	p=0.824	*$F_{(2,12)}$=1.97*

MECHANICALS

Repeated measures 2-way ANOVA

	p=0.915	*$F_{(2,8)}$=0.090*

THERMALS

Repeated measures 2-way ANOVA

	p=0.132	*$F_{(2,8)}$=2.637*

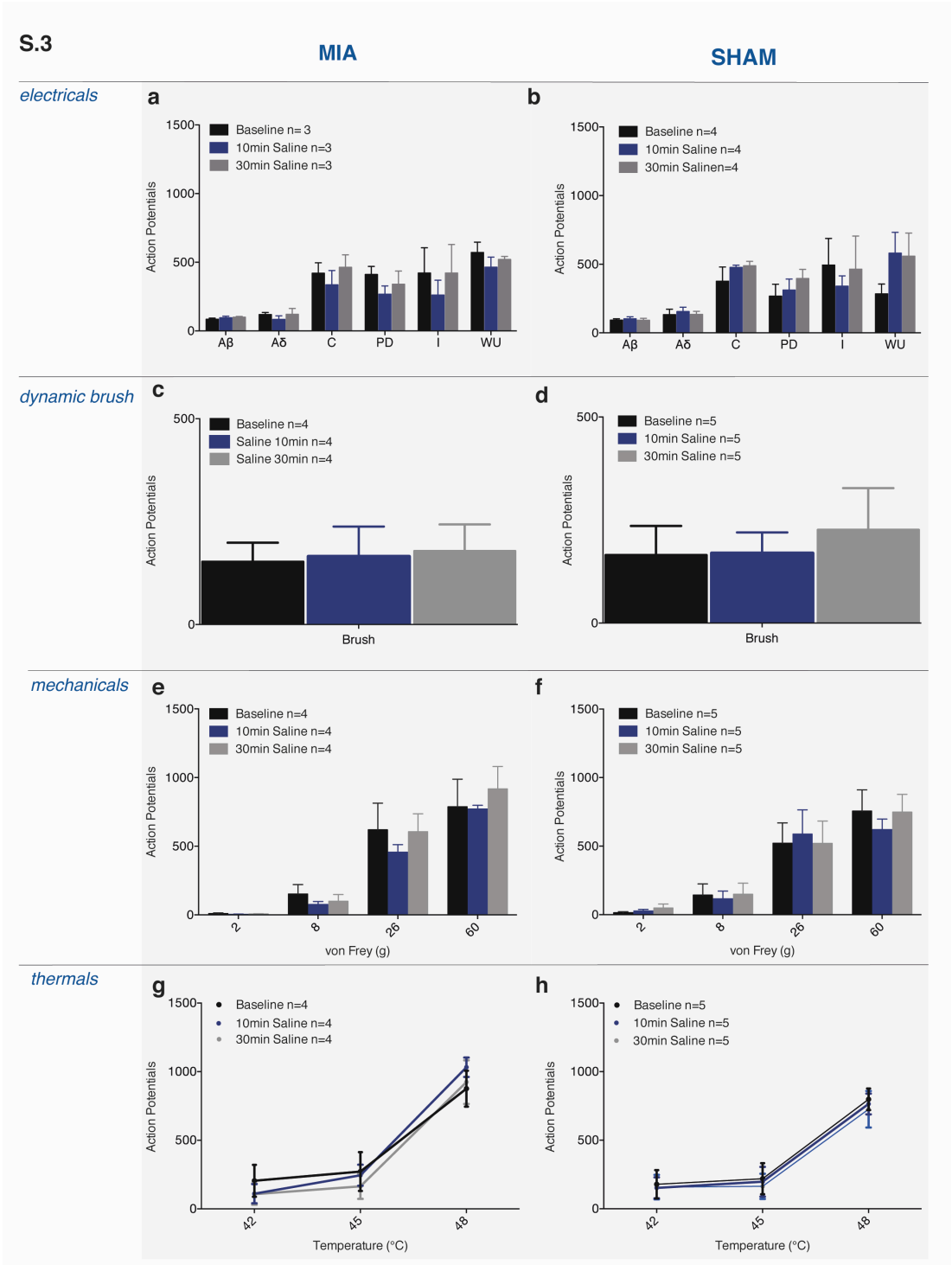

Supplementary figure 3. Effects of spinally applied 0.9% saline on neuronal evoked responses in MIA and Sham animals. Data from early and late stage MIA pulled together for MIA group. Data from early and late stage sham pulled together for Sham group. 0.9% saline was spinally applied and WDR neuronal responses were recorded 10 and 30min post dosing. Saline had no effects in electrical (**a,b**), dynamic brush (**c,d**), mechanical (**e,f**) and thermal (**g,h**) evoked responses of WDR neurones 10 and 30min post-dosing compared to baseline.

APPENDIX II: CHAPTER 4

1.TROX-1 STUDY

Weight of animals on electrophysiology day

TROX-1			
Weight (g)			
Early Sham	Early MIA	Late Sham	Late MIA
235	230	252	236
242	276	282	219
243	249	236	235
248	238	235	290
263	250	237	233
246	244	-	268
235	230	252	236
242	276	282	219

Electrophysiology statistics

EARLY SHAM

ELECTRICALS

Paired Sample t-test

Baseline vs. TROX-1

Aβ	*p=0.973*	$t_{(5)}$*=0.035*
Aδ	*p=0.355*	$t_{(5)}$*=1.019*
C	*p=0.183*	$t_{(5)}$*=1.545*
PD	*p=0.263*	$t_{(5)}$*=1.267*
I	*p=0.385*	$t_{(5)}$*=0.953*
WU	*p=0.220*	$t_{(5)}$*=1.402*

DYNAMIC BRUSH

Paired Sample t-test

Baseline vs. TROX-1 *p=0.684* $t_{(5)}$*=0.431*

MECHANICALS

Repeated measures 2-way ANOVA

Baseline vs. TROX-1 *p=0.946* $F_{(5,6)}$*=0.005*

THERMALS

Repeated measures 2-way ANOVA

Baseline vs. TROX-1 *p=0.593* $F_{(5,6)}$*=0.325*

EARLY MIA

ELECTRICALS

Paired Sample t-test

Baseline vs. TROX-1

Aβ	*p=0.442*	$t_{(5)}$*=0.835*
Aδ	*p=0.215*	$t_{(5)}$*=1.420*
C	*p=0.716*	$t_{(5)}$*=0.385*
PD	*p=0.833*	$t_{(5)}$*=0.223*
I	*p=0.421*	$t_{(5)}$*=0.876*
WU	*p=0.202*	$t_{(5)}$*=1.469*

DYNAMIC BRUSH

Paired Sample t-test

Baseline vs. TROX-1	*p=0.280*	$t_{(5)}$*=1.210*

MECHANICALS

Repeated measures 2-way ANOVA

Baseline vs. TROX-1n	*p=0.0419(*)*	$F_{(5,6)}$*=7.478*

Pairwise comparisons with Bonferroni Correction

Baseline 02g vs. 02g + TROX-1	*p=0.136*
Baseline 08g vs. 08g + TROX-1	*p=0.696*
Baseline 26g vs. 26g + TROX-1	*p=0.088*
Baseline 60g vs. 60g + TROX-1	*p=0.110*

THERMALS

Repeated measures 2-way ANOVA

Baseline vs. TROX-1	*p=0.981*	$F_{(4,5)}$*=0.001*

LATE SHAM

ELECTRICALS

Paired Sample t-test

Baseline vs. TROX-1

Aβ	*p=0.031(*)*	$t_{(4)}$*=3.259*
Aδ	*p=0.181*	$t_{(4)}$*=1.620*
C	*p=0.756*	$t_{(4)}$*=0.332*
PD	*p=0.704*	$t_{(4)}$*=0.408*
I	*p=0.641*	$t_{(4)}$*=0.504*
WU	*p=0.184*	$t_{(4)}$*=1.604*

DYNAMIC BRUSH

Paired Sample t-test

Baseline vs. TROX-1	*p=0.718*	$t_{(4)}$*=0.388*

MECHANICALS

Repeated measures 2-way ANOVA

Baseline vs. TROX-1	*p=0.919*	$F_{(4,5)}$*=0.12*

THERMALS

Repeated measures 2-way ANOVA

Baseline vs. TROX-1	*p=0.856*	$F_{(4,5)}$*=0.037*

LATE MIA

ELECTRICALS

Paired Sample t-test

Baseline vs. TROX-1

Aβ	*p=0.839*	$t_{(5)}$*=0.214*
Aδ	*p=2.046*	$t_{(5)}$*=2.046*
C	*p=1.463*	$t_{(5)}$*=1.463*
PD	*p=1.954*	$t_{(5)}$*=1.954*
I	*p=3.425*	$t_{(5)}$*=3.425*
WU	*p=0.180*	$t_{(5)}$*=0.180*

DYNAMIC BRUSH

Paired Sample t-test

Baseline vs. TROX-1 *p=0.422* $t_{(5)}$*=0.875*

MECHANICALS

Repeated measures 2-way ANOVA

Baseline vs. TROX-1 *p=0.546* $F_{(5,6)}$*=0.419*

THERMALS

Repeated measures 2-way ANOVA

Baseline vs. TROX-1 *p=0.284* $F_{(5,6)}$*=1.439*

2. ω-CONTOXIN STUDY

Weight of animals on electrophysiology day

ω-CONTOXIN			
Weight (g)			
Early Sham	Early MIA	Late Sham	Late MIA
228	244	279	255
230	244	240	220
228	250	232	244
-	232	268	232
270	279	240	225
230	225	227	260
222	240		260

Electrophysiology statistics

EARLY SHAM

ELECTRICALS

Paired Sample t-test

Baseline vs. ω-contoxin

Aβ	*p=0.995*	$t_{(6)}$*=0.007*
Aδ	*p=0.198*	$t_{(6)}$*=1.446*
C	*p=0.170*	$t_{(6)}$*=1.558*
PD	*p=0.041(*)*	$t_{(6)}$*=2.596*
I	*p=0.007(**)*	$t_{(6)}$*=3.974*
WU	*p=0.489*	$t_{(6)}$*=0.721*

DYNAMIC BRUSH

Paired Sample t-test

Baseline vs. ω-contoxin	*p=0.826*	$t_{(6)}$*=0.230*

MECHANICALS

Repeated measures 2-way ANOVA

Baseline vs. ω-contoxin	*p=0.395*	$F_{(6,7)}$*=0.840*

THERMALS

Repeated measures 2-way ANOVA

Baseline vs. ω-contoxin	*p=0.526*	$F_{(6,7)}$*=0.463*

EARLY MIA

ELECTRICALS

Paired Sample t-test

Baseline vs. ω-contoxin

Aβ	*p=0.813*	$t_{(6)}$*=0.242*
Aδ	*p=0.593*	$t_{(6)}$*=0.562*
C	*p=0.176*	$t_{(6)}$*=1.533*
PD	*p=0.047(*)*	$t_{(6)}$*=2.478*
I	*p=0.015(*)*	$t_{(6)}$*=3.345*
WU	*p=0.866*	$t_{(6)}$*=0.176*

DYNAMIC BRUSH

Paired Sample t-test

Baseline vs. ω-contoxin	*p=0.092*	$t_{(5)}$*=3.084*

MECHANICALS

Repeated measures 2-way ANOVA

Baseline vs. ω-contoxin	*p=0.035(*)*	$F_{(5,6)}$*=8.220*

Pairwise comparisons with Bonferroni Correction

Baseline 02g vs. 02g + TROX-1	*p=0.851*
Baseline 08g vs. 08g + TROX-1	*p=0.379*
Baseline 26g vs. 26g + TROX-1	*p=0.022(*)*
Baseline 60g vs. 60g + TROX-1	*p=0.089*

THERMALS

Repeated measures 2-way ANOVA

Baseline vs. ω-contoxin	*p=0.140*	$F_{(5,6)}$=*3.076*

LATE SHAM

ELECTRICALS

Paired Sample t-test

Baseline vs. ω-contoxin

Aβ	*p=0.227*	$t_{(3)}$=*1.513*
Aδ	*p=0.344*	$t_{(3)}$=*1.122*
C	*p=0.367*	$t_{(3)}$=*1.061*
PD	*p=0.225*	$t_{(3)}$=*1.522*
I	*p=0.834*	$t_{(3)}$=*0.228*
WU	*p=0.029(*)*	$t_{(3)}$=*3.935*

DYNAMIC BRUSH

Paired Sample t-test

Baseline vs. ω-contoxin	*p=0.166*	$t_{(4)}$=*0.1.690*

MECHANICALS

Repeated measures 2-way ANOVA

Baseline vs. ω-contoxin	*p=0.208*	$F_{(4,5)}$=*2.225*

THERMALS

Repeated measures 2-way ANOVA

Baseline vs. ω-contoxin	*p=0.027(*)*	$F_{(4,5)}$=*11.711*

Pairwise comparisons with Bonferroni Correction

Baseline 42°C vs. 42°C + ω-contoxin	*p=0.397*
Baseline 45°C vs. 45°C + ω-contoxin	*p=0.250*
Baseline 48°C vs. 48°C + ω-contoxin	*p=0.043(*)*

LATE MIA

ELECTRICALS

Paired Sample t-test

Baseline vs. ω-contoxin

Aβ	*p=0.073*	$t_{(5)}$=*2.286*
Aδ	*p=0.072*	$t_{(5)}$=*2.278*
C	*p=0.005(**)*	$t_{(5)}$=*4.750*
PD	*p=0.017(*)*	$t_{(5)}$=*3.521*
I	*p=0.021(*)*	$t_{(5)}$=*3.338*
WU	*p=0.656*	$t_{(5)}$=*0.473*

DYNAMIC BRUSH

Paired Sample t-test

Baseline vs. ω-contoxin	*p=0.044(*)*	$t_{(5)}$=*2.678*

MECHANICALS

Repeated measures 2-way ANOVA

Baseline vs. ω-contoxin *p=0.003(**)* $F_{(5,6)}$*=27.125*

Pairwise comparisons with Bonferroni Correction

Baseline 02g vs. 02g + TROX-1	*p=0.235*
Baseline 08g vs. 08g + TROX-1	*p=0.024(*)*
Baseline 26g vs. 26g + TROX-1	*p=0.015(*)*
Baseline 60g vs. 60g + TROX-1	*p=0.001(***)*

THERMALS

Repeated measures 2-way ANOVA

Baseline vs. ω-contoxin *p=0.0012(**)* $F_{(5,6)}$*=14.570*

Pairwise comparisons with Bonferroni Correction

Baseline 42°C vs. 42°C + ω-contoxin	*p=0.022(*)*
Baseline 45°C vs. 45°C + ω-contoxin	*p=0.023(*)*
Baseline 48°C vs. 48°C + ω-contoxin	*p=0.018(*)*

APENDIX III: CHAPTER 5

1. TAT-cUBT-USP5 peptide STUDY

Weights of animals on electrophysiology day

DULOXETINE	
Weight (g)	
Late Sham	Late MIA
230	248
282	268
265	-
	285
	300
	320

Electrophysiology statistics

LATE MIA

DYNAMIC BRUSH

Paired Sample t-test

Baseline vs. TAT-cUBT-USP5 peptide *p=0.011(*)* $t_{(5)}=3.904$

MECHANICALS

Repeated measures 2-way ANOVA

Baseline vs. TAT-cUBT-USP5 peptide *p=0.987* $F_{(5,6)}=0.001$

THERMALS

Repeated measures 2-way ANOVA

Baseline vs. TAT-cUBT-USP5 peptide *p=0.880* $F_{(5,6)}=0.0025$

LATE SHAM

DYNAMIC BRUSH

Paired Sample t-test

Baseline vs. TAT-cUBT-USP5 peptide *p=0.644* $t_{(2)}=0.539$

MECHANICALS

Repeated measures 2-way ANOVA

Baseline vs. TAT-cUBT-USP5 peptide *p=0.187* $F_{(2,3)}=3.88$

THERMALS

Repeated measures 2-way ANOVA

Baseline vs. TAT-cUBT-USP5 peptide *p=0.033(*)* $F_{(2,3)}=28.478$

Pairwise comparisons with Bonferroni Correction

Baseline 42°C vs. 42°C + TAT-cUBT-USP5 peptide *p=0.023(*)*

Baseline 45°C vs. 45°C + TAT-cUBT-USP5 peptide *p=0.180*

Baseline 48°C vs. 48°C + TAT-cUBT-USP5 peptide *p=0.041(*)*

APENDIX IV: CHAPTER 6

1. ONDANSETRON STUDY

Weight of animals on electrophysiology day

ONDANSETRON			
Weight (g)			
Early Sham	Early MIA	Late Sham	Late MIA
300	230	223	221
280	233	245	223
245	280	238	238
252	258	287	224
249	256	277	330
247	220	270	315
-	-	-	270
-	-	-	240

Electrophysiology statistics

EARLY MIA

ELECTRICALS

Paired Sample t-test

Baseline vs. Ondansetron

Ab	*p=0.229*	$t_{(5)}$*=1.370*
Ad	*p=0.592*	$t_{(5)}$*=0.571*
C	*p=0.917*	$t_{(5)}$*=0.110*
I	*p=0.020(*)*	$t_{(5)}$*=3.371*
WU	*p=0.0751*	$t_{(5)}$=0.335

DYNAMIC BRUSH

Paired Sample t-test

Baseline vs. Ondansetron *p=0.449* $t_{(5)}$*=0.809*

MECHANICALS

Repeated measures 2-way ANOVA

Baseline vs. Ondansetron *p=0.410* $F_{(6,7)}$*=0.784*

THERMALS

Repeated measures 2-way ANOVA

Baseline vs. Ondansetron *p=0.508* $F_{(6,7)}$*=0.496*

2. DULOXETINE STUDY

Weights of animals on electrophysiology day

DULOXETINE	
Weight (g)	
Late Sham	Late MIA
218	248
240	255
262	245
248	225
282	299
272	263
252	-

Electrophysiology statistics

LATE SHAM

DYNAMIC BRUSH
Paired Sample t test
Baseline vs. Duloxetine — *p=0.157* — $t_{(6)=}1.617$

MECHANICALS
Repeated Measures 2-way ANOVA
Baseline vs. Duloxetine — *p=0.076* — $F_{(6,7)}=4.578$

THERMALS
Repeated Measures 2-way ANOVA
Baseline vs. Duloxetine — *p=0.103* — $F_{(5,6)}=3.965$

DNIC
Repeated Measures 2-way ANOVA
Baseline vs. +DNIC — *p=0.032(*)* — $F_{(6,7)}=7.687$
Pairwise comparisons with Bonferroni Correction
Baseline 08g vs. 08g + DNIC — *p=0.118*
Baseline 26g vs. 26g + DNIC — *p=0.117*
Baseline 60g vs. 60g + DNIC — *p=0.008(**)*
Baseline vs. Duloxetine + DNIC — *p=0.061* — $F_{(6,7)}=5.276$
Duloxetine vs. Duloxetine + DNIC — *p=0.126* — $F_{(6,7)}=3.156$

LATE MIA

DYNAMIC BRUSH
Paired Sample t test
Baseline vs. Duloxetine — *p=0.155* — $t_{(5)}=1.674$

MECHANICALS
Repeated Measures 2-way ANOVA
Baseline vs. Duloxetine — *p=0.858* — $F_{(5,6)}=0.035$

THERMALS

Repeated Measures 2-way ANOVA

Baseline vs. Duloxetine	*p=0.162*	$F_{(4,5)}$=*0.035*

DNIC

Repeated Measures 2-way ANOVA

Baseline vs. +DNIC	*p=0.641*	$F_{(5,6)}$=*0.246*
Baseline vs. Duloxetine + DNIC	*p=0.780*	$F_{(5,6)}$=*0.087*
Duloxetine vs. Duloxetine + DNIC	*p=0.183*	$F_{(5,6)}$=*2.393*

REFERENCES

ABAEI, M., SAGAR, D. R., STOCKLEY, E. G., SPICER, C. H., PRIOR, M., CHAPMAN, V. & AUER, D. P. 2016. Neural correlates of hyperalgesia in the monosodium iodoacetate model of osteoarthritis pain. *Mol Pain,* 12.

ABBADIE, C., MCMANUS, O. B., SUN, S. Y., BUGIANESI, R. M., DAI, G., HAEDO, R. J., HERRINGTON, J. B., KACZOROWSKI, G. J., SMITH, M. M., SWENSEN, A. M., WARREN, V. A., WILLIAMS, B., ARNERIC, S. P., EDULJEE, C., SNUTCH, T. P., TRINGHAM, E. W., JOCHNOWITZ, N., LIANG, A., EUAN MACINTYRE, D., MCGOWAN, E., MISTRY, S., WHITE, V. V., HOYT, S. B., LONDON, C., LYONS, K. A., BUNTING, P. B., VOLKSDORF, S. & DUFFY, J. L. 2010. Analgesic effects of a substituted N-triazole oxindole (TROX-1), a state-dependent, voltage-gated calcium channel 2 blocker. *J Pharmacol Exp Ther,* 334**,** 545-55.

ABOU-RAYA, S., ABOU-RAYA, A. & HELMII, M. 2012. Duloxetine for the management of pain in older adults with knee osteoarthritis: randomised placebo-controlled trial. *Age Ageing,* 41**,** 646-52.

ABRAHAMSEN, B., ZHAO, J., ASANTE, C. O., CENDAN, C. M., MARSH, S., MARTINEZ-BARBERA, J. P., NASSAR, M. A., DICKENSON, A. H. & WOOD, J. N. 2008. The cell and molecular basis of mechanical, cold, and inflammatory pain. *Science,* 321**,** 702-5.

AKKIRAJU, H. & NOHE, A. 2015. Role of Chondrocytes in Cartilage Formation, Progression of Osteoarthritis and Cartilage Regeneration. *J Dev Biol,* 3**,** 177-192.

AKOPIAN, A. N., SIVILOTTI, L. & WOOD, J. N. 1996. A tetrodotoxin-resistant voltage-gated sodium channel expressed by sensory neurons. *Nature,* 379**,** 257-62.

ALLISTON, T., HERNANDEZ, C. J., FINDLAY, D. M., FELSON, D. T. & KENNEDY, O. D. 2018. Bone marrow lesions in osteoarthritis: What lies beneath. *J Orthop Res,* 36**,** 1818-1825.

ALTIER, C., DALE, C. S., KISILEVSKY, A. E., CHAPMAN, K., CASTIGLIONI, A. J., MATTHEWS, E. A., EVANS, R. M., DICKENSON, A. H., LIPSCOMBE, D., VERGNOLLE, N. & ZAMPONI, G. W. 2007. Differential role of N-type calcium channel splice isoforms in pain. *J Neurosci,* 27**,** 6363-73.

ALTMAN, R., ASCH, E., BLOCH, D., BOLE, G., BORENSTEIN, D., BRANDT, K., CHRISTY, W., COOKE, T. D., GREENWALD, R., HOCHBERG, M. & ET AL. 1986. Development of criteria for the classification and reporting of osteoarthritis. Classification of osteoarthritis of the knee. Diagnostic and Therapeutic Criteria Committee of the American Rheumatism Association. *Arthritis Rheum,* 29**,** 1039-49.

AMIN, S., GUERMAZI, A., LAVALLEY, M. P., NIU, J., CLANCY, M., HUNTER, D. J., GRIGORYAN, M. & FELSON, D. T. 2008. Complete anterior cruciate ligament tear and the risk for cartilage loss and progression of symptoms in men and women with knee osteoarthritis. *Osteoarthritis Cartilage,* 16**,** 897-902.

ANDREW, D., KROUT, K. E. & CRAIG, A. D. 2003. Differentiation of lamina I spinomedullary and spinothalamic neurons in the cat. *J Comp Neurol,* 458**,** 257-71.

ARENDT-NIELSEN, L. 2017. Pain sensitisation in osteoarthritis. *Clin Exp Rheumatol,* 35 Suppl 107**,** 68-74.

ARENDT-NIELSEN, L., SKOU, S. T., NIELSEN, T. A. & PETERSEN, K. K. 2015. Altered Central Sensitization and Pain Modulation in the CNS in Chronic Joint Pain. *Curr Osteoporos Rep,* 13**,** 225-34.

ASHRAF, S., WIBBERLEY, H., MAPP, P. I., HILL, R., WILSON, D. & WALSH, D. A. 2011. Increased vascular penetration and nerve growth in the meniscus: a potential source of pain in osteoarthritis. *Ann Rheum Dis,* 70**,** 523-9.

BANNISTER, K. & DICKENSON, A. H. 2010. Opioid hyperalgesia. *Curr Opin Support Palliat Care,* 4**,** 1-5.

BANNISTER, K. & DICKENSON, A. H. 2016. What the brain tells the spinal cord. *Pain,* 157**,** 2148-51.

BANNISTER, K., LOCKWOOD, S., GONCALVES, L., PATEL, R. & DICKENSON, A. H. 2017. An investigation into the inhibitory function of serotonin in diffuse noxious inhibitory controls in the neuropathic rat. *Eur J Pain,* 21**,** 750-760.

BANNISTER, K., PATEL, R., GONCALVES, L., TOWNSON, L. & DICKENSON, A. H. 2015. Diffuse noxious inhibitory controls and nerve injury: restoring an imbalance between descending monoamine inhibitions and facilitations. *Pain,* 156**,** 1803-11.

BAPAT, S., HUBBARD, D., MUNJAL, A., HUNTER, M. & FULZELE, S. 2018. Pros and cons of mouse models for studying osteoarthritis. *Clin Transl Med,* 7**,** 36.

BARTER, L. S., CARSTENS, E. E., JINKS, S. L. & ANTOGNINI, J. F. 2009. Rat dorsal horn nociceptive-specific neurons are more sensitive than wide dynamic range neurons to depression by immobilizing doses of volatile anesthetics: an effect partially reversed by the opioid receptor antagonist naloxone. *Anesth Analg,* 109**,** 641-7.

BASBAUM, A. I., BAUTISTA, D. M., SCHERRER, G. & JULIUS, D. 2009. Cellular and molecular mechanisms of pain. *Cell,* 139**,** 267-84.

BAUER, C. S., NIETO-ROSTRO, M., RAHMAN, W., TRAN-VAN-MINH, A., FERRON, L., DOUGLAS, L., KADURIN, I., SRI RANJAN, Y., FERNANDEZ-ALACID, L., MILLAR, N. S., DICKENSON, A. H., LUJAN, R. & DOLPHIN, A. C. 2009. The increased trafficking of the calcium channel subunit alpha2delta-1 to presynaptic terminals in neuropathic pain is inhibited by the alpha2delta ligand pregabalin. *J Neurosci,* 29**,** 4076-88.

BEE, L. A. & DICKENSON, A. H. 2007. Rostral ventromedial medulla control of spinal sensory processing in normal and pathophysiological states. *Neuroscience,* 147**,** 786-93.

BENARROCH, E. E. 2016. Dorsal horn circuitry: Complexity and implications for mechanisms of neuropathic pain. *Neurology,* 86**,** 1060-9.

BERNAL SIERRA, Y. A., HASELEU, J., KOZLENKOV, A., BEGAY, V. & LEWIN, G. R. 2017. Genetic Tracing of Cav3.2 T-Type Calcium Channel Expression in the Peripheral Nervous System. *Front Mol Neurosci,* 10**,** 70.

BERNSTEIN, G. M. & JONES, O. T. 2007. Kinetics of internalization and degradation of N-type voltage-gated calcium channels: role of the alpha2/delta subunit. *Cell Calcium,* 41**,** 27-40.

BEVILAQUA-GROSSI, D., ZANIN, M., BENEDETTI, C., FLORENCIO, L. & OLIVEIRA, A. 2019. Thermal and mechanical pain sensitization in patients with osteoarthritis of the knee. *Physiother Theory Pract,* 35**,** 139-147.

BHARATE, S. S. & BHARATE, S. B. 2012. Modulation of thermoreceptor TRPM8 by cooling compounds. *ACS Chem Neurosci,* 3**,** 248-67.

BISHOP, T., BALLARD, A., HOLMES, H., YOUNG, A. R. & MCMAHON, S. B. 2009. Ultraviolet-B induced inflammation of human skin: characterisation and comparison with traditional models of hyperalgesia. *Eur J Pain,* 13**,** 524-32.

BONADIO, M. B., FILHO, A. G. O., HELITO, C. P., STUMP, X. M. & DEMANGE, M. K. 2017. Bone Marrow Lesion: Image, Clinical Presentation, and Treatment. *Magn Reson Insights,* 10**,** 1178623x17703382.

BOURINET, E., ALLOUI, A., MONTEIL, A., BARRERE, C., COUETTE, B., POIROT, O., PAGES, A., MCRORY, J., SNUTCH, T. P., ESCHALIER, A. & NARGEOT, J. 2005. Silencing of the Cav3.2 T-type calcium channel gene in sensory neurons demonstrates its major role in nociception. *Embo j,* 24**,** 315-24.

BOURINET, E. & ZAMPONI, G. W. 2017. Block of voltage-gated calcium channels by peptide toxins. *Neuropharmacology,* 127**,** 109-115.

BOVE, S. E., CALCATERRA, S. L., BROOKER, R. M., HUBER, C. M., GUZMAN, R. E., JUNEAU, P. L., SCHRIER, D. J. & KILGORE, K. S. 2003. Weight bearing as a measure of disease progression and efficacy of anti-inflammatory compounds in a model of monosodium iodoacetate-induced osteoarthritis. *Osteoarthritis Cartilage,* 11**,** 821-30.

BRANDT, K. D., RADIN, E. L., DIEPPE, P. A. & VAN DE PUTTE, L. 2006. Yet more evidence that osteoarthritis is not a cartilage disease. *Ann Rheum Dis,* 65**,** 1261-4.

BRAZ, J., SOLORZANO, C., WANG, X. & BASBAUM, A. I. 2014. Transmitting pain and itch messages: a contemporary view of the spinal cord circuits that generate gate control. *Neuron,* 82**,** 522-36.

BURNHAM, L. J. 2012. Monoaminergic Control of the Central Processing of Sensory Stimuli in a Rat Model of Osteoarthritis *UCL Library,* Thesis.

BURNHAM, L. J. & DICKENSON, A. H. 2013. The antinociceptive effect of milnacipran in the monosodium iodoacetate model of osteoarthritis pain and its relation to changes in descending inhibition. *J Pharmacol Exp Ther,* 344**,** 696-707.

CANDELAS, M., REYNDERS, A., ARANGO-LIEVANO, M., NEUMAYER, C., FRUQUIERE, A., DEMES, E., HAMID, J., LEMMERS, C., BERNAT, C., MONTEIL, A., COMPAN, V., LAFFRAY, S., INQUIMBERT, P., LE FEUVRE, Y., ZAMPONI, G. W., MOQRICH, A., BOURINET, E. & MERY, P. F. 2019. Cav3.2 T-type calcium channels shape electrical firing in mouse Lamina II neurons. *Sci Rep,* 9**,** 3112.

CASSIDY, J. S., FERRON, L., KADURIN, I., PRATT, W. S. & DOLPHIN, A. C. 2014. Functional exofacially tagged N-type calcium channels elucidate the interaction with auxiliary alpha2delta-1 subunits. *Proc Natl Acad Sci U S A,* 111**,** 8979-84.

CATERINA, M. J., SCHUMACHER, M. A., TOMINAGA, M., ROSEN, T. A., LEVINE, J. D. & JULIUS, D. 1997. The capsaicin receptor: a heat-activated ion channel in the pain pathway. *Nature,* 389**,** 816-24.

CATTERALL, W. A. 2000. Structure and regulation of voltage-gated Ca2+ channels. *Annu Rev Cell Dev Biol,* 16**,** 521-55.

CATTERALL, W. A. 2011. Voltage-gated calcium channels. *Cold Spring Harb Perspect Biol,* 3**,** a003947.

CATTERALL, W. A., CESTELE, S., YAROV-YAROVOY, V., YU, F. H., KONOKI, K. & SCHEUER, T. 2007. Voltage-gated ion channels and gating modifier toxins. *Toxicon,* 49**,** 124-41.

CHAO, M. V. 2003. Neurotrophins and their receptors: a convergence point for many signalling pathways. *Nat Rev Neurosci,* 4**,** 299-309.

CHAPLAN, S. R., BACH, F. W., POGREL, J. W., CHUNG, J. M. & YAKSH, T. L. 1994a. Quantitative assessment of tactile allodynia in the rat paw. *J Neurosci Methods,* 53**,** 55-63.
CHAPLAN, S. R., POGREL, J. W. & YAKSH, T. L. 1994b. Role of voltage-dependent calcium channel subtypes in experimental tactile allodynia. *J Pharmacol Exp Ther,* 269**,** 1117-23.
CHAPMAN, V., SUZUKI, R., CHAMARETTE, H. L., RYGH, L. J. & DICKENSON, A. H. 1998. Effects of systemic carbamazepine and gabapentin on spinal neuronal responses in spinal nerve ligated rats. *Pain,* 75**,** 261-72.
CHAPPELL, A. S., OSSANNA, M. J., LIU-SEIFERT, H., IYENGAR, S., SKLJAREVSKI, V., LI, L. C., BENNETT, R. M. & COLLINS, H. 2009. Duloxetine, a centrally acting analgesic, in the treatment of patients with osteoarthritis knee pain: a 13-week, randomized, placebo-controlled trial. *Pain,* 146**,** 253-60.
CHEN, A., GUPTE, C., AKHTAR, K., SMITH, P. & COBB, J. 2012. The Global Economic Cost of Osteoarthritis: How the UK Compares. *Arthritis,* 2012**,** 698709.
CHEN, J., LI, L., CHEN, S. R., CHEN, H., XIE, J. D., SIRRIEH, R. E., MACLEAN, D. M., ZHANG, Y., ZHOU, M. H., JAYARAMAN, V. & PAN, H. L. 2018. The alpha2delta-1-NMDA Receptor Complex Is Critically Involved in Neuropathic Pain Development and Gabapentin Therapeutic Actions. *Cell Rep,* 22**,** 2307-2321.
CHOI, S., NA, H. S., KIM, J., LEE, J., LEE, S., KIM, D., PARK, J., CHEN, C. C., CAMPBELL, K. P. & SHIN, H. S. 2007. Attenuated pain responses in mice lacking Ca(V)3.2 T-type channels. *Genes Brain Behav,* 6**,** 425-31.
CHUANG, H. H., PRESCOTT, E. D., KONG, H., SHIELDS, S., JORDT, S. E., BASBAUM, A. I., CHAO, M. V. & JULIUS, D. 2001. Bradykinin and nerve growth factor release the capsaicin receptor from PtdIns(4,5)P2-mediated inhibition. *Nature,* 411**,** 957-62.
CLARK, A. K., GENTRY, C., BRADBURY, E. J., MCMAHON, S. B. & MALCANGIO, M. 2007. Role of spinal microglia in rat models of peripheral nerve injury and inflammation. *Eur J Pain,* 11**,** 223-30.
CLAUW, D. J. & HASSETT, A. L. 2017. The role of centralised pain in osteoarthritis. *Clin Exp Rheumatol,* 35 Suppl 107**,** 79-84.
COMBE, R., BRAMWELL, S. & FIELD, M. J. 2004. The monosodium iodoacetate model of osteoarthritis: a model of chronic nociceptive pain in rats? *Neurosci Lett,* 370**,** 236-40.
COOKE, M. E., LAWLESS, B. M., JONES, S. W. & GROVER, L. M. 2018. Matrix degradation in osteoarthritis primes the superficial region of cartilage for mechanical damage. *Acta Biomater,* 78**,** 320-328.
CORTES-ALTAMIRANO, J. L., OLMOS-HERNANDEZ, A., JAIME, H. B., CARRILLO-MORA, P., BANDALA, C., REYES-LONG, S. & ALFARO-RODRIGUEZ, A. 2018. Review: 5-HT1, 5-HT2, 5-HT3 and 5-HT7 Receptors and their Role in the Modulation of Pain Response in the Central Nervous System. *Curr Neuropharmacol,* 16**,** 210-221.
COSTE, B., CREST, M. & DELMAS, P. 2007. Pharmacological dissection and distribution of NaN/Nav1.9, T-type Ca2+ currents, and mechanically activated cation currents in different populations of DRG neurons. *J Gen Physiol,* 129**,** 57-77.
COSTE, B., MATHUR, J., SCHMIDT, M., EARLEY, T. J., RANADE, S., PETRUS, M. J., DUBIN, A. E. & PATAPOUTIAN, A. 2010. Piezo1 and Piezo2 are essential components of distinct mechanically activated cation channels. *Science,* 330**,** 55-60.
CRAIG, A. D. 2003. Pain mechanisms: labeled lines versus convergence in central processing. *Annu Rev Neurosci,* 26**,** 1-30.
CRUNELLI, V., TOTH, T. I., COPE, D. W., BLETHYN, K. & HUGHES, S. W. 2005. The 'window' T-type calcium current in brain dynamics of different behavioural states. *J Physiol,* 562**,** 121-9.
CUCCHIARINI, M., DE GIROLAMO, L., FILARDO, G., OLIVEIRA, J. M., ORTH, P., PAPE, D. & REBOUL, P. 2016. Basic science of osteoarthritis. *J Exp Orthop,* 3**,** 22.
D'MELLO, R. & DICKENSON, A. H. 2008. Spinal cord mechanisms of pain. *Br J Anaesth,* 101**,** 8-16.
DA COSTA GOMEZ, T. M. & BEHBEHANI, M. M. 1995. An electrophysiological characterization of the projection from the central nucleus of the amygdala to the periaqueductal gray of the rat: the role of opioid receptors. *Brain Res,* 689**,** 21-31.
DAVIES, A., KADURIN, I., ALVAREZ-LAVIADA, A., DOUGLAS, L., NIETO-ROSTRO, M., BAUER, C. S., PRATT, W. S. & DOLPHIN, A. C. 2010. The alpha2delta subunits of voltage-gated calcium channels form GPI-anchored proteins, a posttranslational modification essential for function. *Proc Natl Acad Sci U S A,* 107**,** 1654-9.
DENK, F., MCMAHON, S. B. & TRACEY, I. 2014. Pain vulnerability: a neurobiological perspective. *Nat Neurosci,* 17**,** 192-200.
DERRY, S., CONAGHAN, P., DA SILVA, J. A., WIFFEN, P. J. & MOORE, R. A. 2016. Topical NSAIDs for chronic musculoskeletal pain in adults. *Cochrane Database Syst Rev,* 4**,** Cd007400.
DERRY, S., RICE, A. S., COLE, P., TAN, T. & MOORE, R. A. 2017. Topical capsaicin (high concentration) for chronic neuropathic pain in adults. *Cochrane Database Syst Rev,* 1**,** Cd007393.

DEVONSHIRE, I. M., BURSTON, J. J., XU, L., LILLYWHITE, A., PRIOR, M. J., WATSON, D. J. G., GREENSPON, C. M., IWABUCHI, S. J., AUER, D. P. & CHAPMAN, V. 2017. Manganese-enhanced magnetic resonance imaging depicts brain activity in models of acute and chronic pain: A new window to study experimental spontaneous pain? *Neuroimage,* 157**,** 500-510.

DICKENSON, A. H. 1995. Spinal cord pharmacology of pain. *Br J Anaesth,* 75**,** 193-200.

DICKENSON, A. H. & SULLIVAN, A. F. 1987. Evidence for a role of the NMDA receptor in the frequency dependent potentiation of deep rat dorsal horn nociceptive neurones following C fibre stimulation. *Neuropharmacology,* 2**6,** 1235-8.

DOLPHIN, A. C. 2012. Calcium channel auxiliary alpha2delta and beta subunits: trafficking and one step beyond. *Nat Rev Neurosci,* 13**,** 542-55.

DOLPHIN, A. C. 2013. The alpha2delta subunits of voltage-gated calcium channels. *Biochim Biophys Acta,* 1828**,** 1541-9.

DOLPHIN, A. C. 2016. Voltage-gated calcium channels and their auxiliary subunits: physiology and pathophysiology and pharmacology. *J Physiol,* 594**,** 5369-90.

DOLPHIN, A. C. 2018. Voltage-gated calcium channel alpha 2delta subunits: an assessment of proposed novel roles. *F1000Res,* 7.

DRAKE, R. W. V., A. MITCHELL, A. 2009. Gray's Anatomy for Students. *Philadelphia: Elsevier/Churchill Livingstone.*

DREIER, R. 2010. Hypertrophic differentiation of chondrocytes in osteoarthritis: the developmental aspect of degenerative joint disorders. *Arthritis Res Ther,* 12**,** 216.

DRIBAN, J. B., PRICE, L., LO, G. H., PANG, J., HUNTER, D. J., MILLER, E., WARD, R. J., EATON, C. B., LYNCH, J. A. & MCALINDON, T. E. 2013. Evaluation of bone marrow lesion volume as a knee osteoarthritis biomarker--longitudinal relationships with pain and structural changes: data from the Osteoarthritis Initiative. *Arthritis Res Ther,* 15**,** R112.

DUA, A. B., NEOGI, T., MIKOLAITIS, R. A., BLOCK, J. A. & SHAKOOR, N. 2018. Somatosensation in OA: exploring the relationships of pain sensitization, vibratory perception and spontaneous pain. *BMC Musculoskelet Disord,* 19**,** 307.

DUAN, B., CHENG, L. & MA, Q. 2018. Spinal Circuits Transmitting Mechanical Pain and Itch. *Neurosci Bull,* 34**,** 186-193.

EDD, S. N., GIORI, N. J. & ANDRIACCHI, T. P. 2015. The role of inflammation in the initiation of osteoarthritis after meniscal damage. *J Biomech,* 48**,** 1420-6.

EITNER, A., HOFMANN, G. O. & SCHAIBLE, H. G. 2017. Mechanisms of Osteoarthritic Pain. Studies in Humans and Experimental Models. *Front Mol Neurosci,* 10**,** 349.

ENE, R., SINESCU, R. D., ENE, P., CIRSTOIU, M. M. & CIRSTOIU, F. C. 2015. Synovial inflammation in patients with different stages of knee osteoarthritis. *Rom J Morphol Embryol,* 56**,** 169-73.

ETHGEN, O., BRUYERE, O., RICHY, F., DARDENNES, C. & REGINSTER, J. Y. 2004. Health-related quality of life in total hip and total knee arthroplasty. A qualitative and systematic review of the literature. *J Bone Joint Surg Am,* 86-a**,** 963-74.

FANG, H., HUANG, L., WELCH, I., NORLEY, C., HOLDSWORTH, D. W., BEIER, F. & CAI, D. 2018. Early Changes of Articular Cartilage and Subchondral Bone in The DMM Mouse Model of Osteoarthritis. *Sci Rep,* 8**,** 2855.

FELSON, D. T., CHAISSON, C. E., HILL, C. L., TOTTERMAN, S. M., GALE, M. E., SKINNER, K. M., KAZIS, L. & GALE, D. R. 2001. The association of bone marrow lesions with pain in knee osteoarthritis. *Ann Intern Med,* 134**,** 541-9.

FELSON, D. T. & NEVITT, M. C. 2004. Epidemiologic studies for osteoarthritis: new versus conventional study design approaches. *Rheum Dis Clin North Am,* 30**,** 783-97, vii.

FERLAND, C. E., LAVERTY, S., BEAUDRY, F. & VACHON, P. 2011. Gait analysis and pain response of two rodent models of osteoarthritis. *Pharmacol Biochem Behav,* 97**,** 603-10.

FERREIRA-GOMES, J., ADAES, S., SOUSA, R. M., MENDONCA, M. & CASTRO-LOPES, J. M. 2012. Dose-dependent expression of neuronal injury markers during experimental osteoarthritis induced by monoiodoacetate in the rat. *Mol Pain,* 8**,** 50.

FIELD, M. J., COX, P. J., STOTT, E., MELROSE, H., OFFORD, J., SU, T. Z., BRAMWELL, S., CORRADINI, L., ENGLAND, S., WINKS, J., KINLOCH, R. A., HENDRICH, J., DOLPHIN, A. C., WEBB, T. & WILLIAMS, D. 2006. Identification of the alpha2-delta-1 subunit of voltage-dependent calcium channels as a molecular target for pain mediating the analgesic actions of pregabalin. *Proc Natl Acad Sci U S A,* 103**,** 17537-42.

FINAN, P. H., BUENAVER, L. F., BOUNDS, S. C., HUSSAIN, S., PARK, R. J., HAQUE, U. J., CAMPBELL, C. M., HAYTHORNTHWAITE, J. A., EDWARDS, R. R. & SMITH, M. T. 2013. Discordance between pain and radiographic severity in knee osteoarthritis: findings from quantitative sensory testing of central sensitization. *Arthritis Rheum,* 65**,** 363-72.

FINN, A., ANGEBY MOLLER, K., GUSTAFSSON, C., ABDELMOATY, S., NORDAHL, G., FERM, M. & SVENSSON, C. 2014. Influence of model and matrix on cytokine profile in rat and human. *Rheumatology (Oxford),* 53**,** 2297-305.

FINN, D. P., CHAPMAN, V., JHAVERI, M. D., SAMANTA, S., MANDERS, T., BOWDEN, J., MATTHEWS, L., MARSDEN, C. A. & BECKETT, S. R. 2003. The role of the central nucleus of the amygdala in nociception and aversion. *Neuroreport,* 14**,** 981-4.

GADOTTI, V. M. & ZAMPONI, G. W. 2018. Disrupting USP5/Cav3.2 interactions protects female mice from mechanical hypersensitivity during peripheral inflammation. *Mol Brain,* 11**,** 60.

GARCIA-CABALLERO, A., GADOTTI, V. M., CHEN, L. & ZAMPONI, G. W. 2016. A cell-permeant peptide corresponding to the cUBP domain of USP5 reverses inflammatory and neuropathic pain. *Mol Pain,* 12.

GARCIA-CABALLERO, A., GADOTTI, V. M., STEMKOWSKI, P., WEISS, N., SOUZA, I. A., HODGKINSON, V., BLADEN, C., CHEN, L., HAMID, J., PIZZOCCARO, A., DEAGE, M., FRANCOIS, A., BOURINET, E. & ZAMPONI, G. W. 2014. The deubiquitinating enzyme USP5 modulates neuropathic and inflammatory pain by enhancing Cav3.2 channel activity. *Neuron,* 83**,** 1144-58.

GASSNER, M., RUSCHEWEYH, R. & SANDKUHLER, J. 2009. Direct excitation of spinal GABAergic interneurons by noradrenaline. *Pain,* 145**,** 204-10.

GERWIN, N., BENDELE, A. M., GLASSON, S. & CARLSON, C. S. 2010. The OARSI histopathology initiative - recommendations for histological assessments of osteoarthritis in the rat. *Osteoarthritis Cartilage,* 18 Suppl 3**,** S24-34.

GOLDRING, M. B. 2012. Chondrogenesis, chondrocyte differentiation, and articular cartilage metabolism in health and osteoarthritis. *Ther Adv Musculoskelet Dis,* 4**,** 269-85.

GOLDRING, M. B. & OTERO, M. 2011. Inflammation in osteoarthritis. *Curr Opin Rheumatol,* 23**,** 471-8.

GOLDRING, S. R. & GOLDRING, M. B. 2016. Changes in the osteochondral unit during osteoarthritis: structure, function and cartilage-bone crosstalk. *Nat Rev Rheumatol,* 12**,** 632-644.

GRÄSSEL, S. & MUSCHTER, D. 2017. Peripheral Nerve Fibers and Their Neurotransmitters in Osteoarthritis Pathology. *Int J Mol Sci,* 18.

GRAY, L. S. & MACDONALD, T. L. 2006. The pharmacology and regulation of T type calcium channels: new opportunities for unique therapeutics for cancer. *Cell Calcium,* 40**,** 115-20.

GREENSPON, C. M., BATTELL, E. E., DEVONSHIRE, I. M., DONALDSON, L. F., CHAPMAN, V. & HATHWAY, G. J. 2019. Lamina-specific population encoding of cutaneous signals in the spinal dorsal horn using multi-electrode arrays. *J Physiol,* 597**,** 377-397.

GUAN, Y. & RAJA, S. N. 2010. Wide-dynamic-range neurons are heterogeneous in windup responsiveness to changes in stimulus intensity and isoflurane anesthesia level in mice. *J Neurosci Res,* 88**,** 2272-83.

GUINGAMP, C., GEGOUT-POTTIE, P., PHILIPPE, L., TERLAIN, B., NETTER, P. & GILLET, P. 1997. Mono-iodoacetate-induced experimental osteoarthritis: a dose-response study of loss of mobility, morphology, and biochemistry. *Arthritis Rheum,* 40**,** 1670-9.

GUZMAN, R. E., EVANS, M. G., BOVE, S., MORENKO, B. & KILGORE, K. 2003. Mono-iodoacetate-induced histologic changes in subchondral bone and articular cartilage of rat femorotibial joints: an animal model of osteoarthritis. *Toxicol Pathol,* 31**,** 619-24.

GWILYM, S. E., KELTNER, J. R., WARNABY, C. E., CARR, A. J., CHIZH, B., CHESSELL, I. & TRACEY, I. 2009. Psychophysical and functional imaging evidence supporting the presence of central sensitization in a cohort of osteoarthritis patients. *Arthritis Rheum,* 61**,** 1226-34.

HARVEY, V. L. & DICKENSON, A. H. 2009. Behavioural and electrophysiological characterisation of experimentally induced osteoarthritis and neuropathy in C57Bl/6 mice. *Mol Pain,* 5**,** 18.

HATAKEYAMA, S., WAKAMORI, M., INO, M., MIYAMOTO, N., TAKAHASHI, E., YOSHINAGA, T., SAWADA, K., IMOTO, K., TANAKA, I., YOSHIZAWA, T., NISHIZAWA, Y., MORI, Y., NIIDOME, T. & SHOJI, S. 2001. Differential nociceptive responses in mice lacking the alpha(1B) subunit of N-type Ca(2+) channels. *Neuroreport,* 12**,** 2423-7.

HAVELIN, J., IMBERT, I., CORMIER, J., ALLEN, J., PORRECA, F. & KING, T. 2016. Central Sensitization and Neuropathic Features of Ongoing Pain in a Rat Model of Advanced Osteoarthritis. *J Pain,* 17**,** 374-82.

HEIDARI, B. 2011. Knee osteoarthritis diagnosis, treatment and associated factors of progression: part II. *Caspian J Intern Med,* 2**,** 249-55.

HEPPENSTALL, P. A. & LEWIN, G. R. 2006. A role for T-type Ca2+ channels in mechanosensation. *Cell Calcium,* 40**,** 165-74.

HERRERO, J. F., LAIRD, J. M. & LOPEZ-GARCIA, J. A. 2000. Wind-up of spinal cord neurones and pain sensation: much ado about something? *Prog Neurobiol,* 61**,** 169-203.

HILDEBRAND, M. E., SMITH, P. L., BLADEN, C., EDULJEE, C., XIE, J. Y., CHEN, L., FEE-MAKI, M., DOERING, C. J., MEZEYOVA, J., ZHU, Y., BELARDETTI, F., PAJOUHESH, H., PARKER, D., ARNERIC, S. P., PARMAR, M., PORRECA, F., TRINGHAM, E., ZAMPONI, G. W. & SNUTCH, T. P. 2011. A novel slow-inactivation-specific ion channel modulator attenuates neuropathic pain. *Pain,* 152**,** 833-43.

HILL, R. Z. & BAUTISTA, D. M. 2018. A trio of ion channels takes the heat. *Nature,* 555**,** 591-592.

HILL, R. Z., HOFFMAN, B. U., MORITA, T., CAMPOS, S. M., LUMPKIN, E. A., BREM, R. B. & BAUTISTA, D. M. 2018. The signaling lipid sphingosine 1-phosphate regulates mechanical pain. *Elife,* 7.

HOCHMAN, J. R., FRENCH, M. R., BERMINGHAM, S. L. & HAWKER, G. A. 2010. The nerve of osteoarthritis pain. *Arthritis Care Res (Hoboken),* 62**,** 1019-23.

IFTINCA, M. C. & ZAMPONI, G. W. 2009. Regulation of neuronal T-type calcium channels. *Trends Pharmacol Sci,* 30**,** 32-40.

IKEDA, H., HEINKE, B., RUSCHEWEYH, R. & SANDKUHLER, J. 2003. Synaptic plasticity in spinal lamina I projection neurons that mediate hyperalgesia. *Science,* 299**,** 1237-40.

ISHIKAWA, G., NAGAKURA, Y., TAKESHITA, N. & SHIMIZU, Y. 2014. Efficacy of drugs with different mechanisms of action in relieving spontaneous pain at rest and during movement in a rat model of osteoarthritis. *Eur J Pharmacol,* 738**,** 111-7.

IVANAVICIUS, S. P., BALL, A. D., HEAPY, C. G., WESTWOOD, F. R., MURRAY, F. & READ, S. J. 2007. Structural pathology in a rodent model of osteoarthritis is associated with neuropathic pain: increased expression of ATF-3 and pharmacological characterisation. *Pain,* 128**,** 272-82.

JACUS, M. O., UEBELE, V. N., RENGER, J. J. & TODOROVIC, S. M. 2012. Presynaptic Cav3.2 channels regulate excitatory neurotransmission in nociceptive dorsal horn neurons. *J Neurosci,* 32**,** 9374-82.

JAGODIC, M. M., PATHIRATHNA, S., JOKSOVIC, P. M., LEE, W., NELSON, M. T., NAIK, A. K., SU, P., JEVTOVIC-TODOROVIC, V. & TODOROVIC, S. M. 2008. Upregulation of the T-type calcium current in small rat sensory neurons after chronic constrictive injury of the sciatic nerve. *J Neurophysiol,* 99**,** 3151-6.

JARVIS, M. F., SCOTT, V. E., MCGARAUGHTY, S., CHU, K. L., XU, J., NIFORATOS, W., MILICIC, I., JOSHI, S., ZHANG, Q. & XIA, Z. 2014. A peripherally acting, selective T-type calcium channel blocker, ABT-639, effectively reduces nociceptive and neuropathic pain in rats. *Biochem Pharmacol,* 89**,** 536-44.

JIANG, Y. Q., ANDRADE, A. & LIPSCOMBE, D. 2013. Spinal morphine but not ziconotide or gabapentin analgesia is affected by alternative splicing of voltage-gated calcium channel CaV2.2 pre-mRNA. *Mol Pain,* 9**,** 67.

JOHN, T., MULLER, R. D., OBERHOLZER, A., ZREIQAT, H., KOHL, B., ERTEL, W., HOSTMANN, A., TSCHOEKE, S. K. & SCHULZE-TANZIL, G. 2007. Interleukin-10 modulates pro-apoptotic effects of TNF-alpha in human articular chondrocytes in vitro. *Cytokine,* 40**,** 226-34.

JOKSIMOVIC, S. L., JOKSIMOVIC, S. M., TESIC, V., GARCIA-CABALLERO, A., FESEHA, S., ZAMPONI, G. W., JEVTOVIC-TODOROVIC, V. & TODOROVIC, S. M. 2018. Selective inhibition of CaV3.2 channels reverses hyperexcitability of peripheral nociceptors and alleviates postsurgical pain. *Sci Signal,* 11.

JULIUS, D. & BASBAUM, A. I. 2001. Molecular mechanisms of nociception. *Nature,* 413**,** 203-10.

KANG, S. J., LIU, M. G., SHI, T. Y., ZHAO, M. G., KAANG, B. K. & ZHUO, M. 2013. N-type voltage gated calcium channels mediate excitatory synaptic transmission in the anterior cingulate cortex of adult mice. *Mol Pain,* 9**,** 58.

KARPA, K. D., CAVANAUGH, J. E. & LAKOSKI, J. M. 2002. Duloxetine pharmacology: profile of a dual monoamine modulator. *CNS Drug Rev,* 8**,** 361-76.

KATSURAGAWA, Y., SAITOH, K., TANAKA, N., WAKE, M., IKEDA, Y., FURUKAWA, H., TOHMA, S., SAWABE, M., ISHIYAMA, M., YAGISHITA, S., SUZUKI, R., MITOMI, H. & FUKUI, N. 2010. Changes of human menisci in osteoarthritic knee joints. *Osteoarthritis Cartilage,* 18**,** 1133-43.

KIDD, B. 2012. Mechanisms of pain in osteoarthritis. *Hss j,* 8**,** 26-8.

KINGSBURY, S. R., GROSS, H. J., ISHERWOOD, G. & CONAGHAN, P. G. 2014. Osteoarthritis in Europe: impact on health status, work productivity and use of pharmacotherapies in five European countries. *Rheumatology (Oxford),* 53**,** 937-47.

KIRKLEY, A., BIRMINGHAM, T. B., LITCHFIELD, R. B., GIFFIN, J. R., WILLITS, K. R., WONG, C. J., FEAGAN, B. G., DONNER, A., GRIFFIN, S. H., D'ASCANIO, L. M., POPE, J. E. & FOWLER, P. J. 2008. A randomized trial of arthroscopic surgery for osteoarthritis of the knee. *N Engl J Med,* 359**,** 1097-107.

KLEMENT, M. R. & SHARKEY, P. F. 2019. The Significance of Osteoarthritis-associated Bone Marrow Lesions in the Knee. *J Am Acad Orthop Surg*.

KOBAYASHI, Y., KIGUCHI, N., FUKAZAWA, Y., SAIKA, F., MAEDA, T. & KISHIOKA, S. 2015. Macrophage-T cell interactions mediate neuropathic pain through the glucocorticoid-induced tumor necrosis factor ligand system. *J Biol Chem,* 290**,** 12603-13.

KOSEK, E., FINN, A., ULTENIUS, C., HUGO, A., SVENSSON, C. & AHMED, A. S. 2018. Differences in neuroimmune signalling between male and female patients suffering from knee osteoarthritis. *J Neuroimmunol,* 321**,** 49-60.

KOTLARZ, H., GUNNARSSON, C. L., FANG, H. & RIZZO, J. A. 2010. Osteoarthritis and absenteeism costs: evidence from US National Survey Data. *J Occup Environ Med,* 52**,** 263-8.

KREMER, M., YALCIN, I., GOUMON, Y., WURTZ, X., NEXON, L., DANIEL, D., MEGAT, S., CEREDIG, R. A., ERNST, C., TURECKI, G., CHAVANT, V., THEROUX, J. F., LACAUD, A., JOGANAH, L. E., LELIEVRE, V., MASSOTTE, D., LUTZ, P. E., GILSBACH, R., SALVAT, E. & BARROT, M. 2018. A Dual Noradrenergic Mechanism for the Relief of Neuropathic Allodynia by the Antidepressant Drugs Duloxetine and Amitriptyline. *J Neurosci,* 38**,** 9934-9954.

KUYINU, E. L., NARAYANAN, G., NAIR, L. S. & LAURENCIN, C. T. 2016. Animal models of osteoarthritis: classification, update, and measurement of outcomes. *J Orthop Surg Res,* 11**,** 19.

LAMPROPOULOU-ADAMIDOU, K., LELOVAS, P., KARADIMAS, E. V., LIAKOU, C., TRIANTAFILLOPOULOS, I. K., DONTAS, I. & PAPAIOANNOU, N. A. 2014. Useful animal models for the research of osteoarthritis. *Eur J Orthop Surg Traumatol,* 24**,** 263-71.

LANE, N. E., SCHNITZER, T. J., BIRBARA, C. A., MOKHTARANI, M., SHELTON, D. L., SMITH, M. D. & BROWN, M. T. 2010. Tanezumab for the treatment of pain from osteoarthritis of the knee. *N Engl J Med,* 363**,** 1521-31.

LE BARS, D., DICKENSON, A. H. & BESSON, J. M. 1979. Diffuse noxious inhibitory controls (DNIC). I. Effects on dorsal horn convergent neurones in the rat. *Pain,* 6**,** 283-304.

LEBLANC, B. W., LII, T. R., HUANG, J. J., CHAO, Y. C., BOWARY, P. M., CROSS, B. S., LEE, M. S., VERA-PORTOCARRERO, L. P. & SAAB, C. Y. 2016. T-type calcium channel blocker Z944 restores cortical synchrony and thalamocortical connectivity in a rat model of neuropathic pain. *Pain,* 157**,** 255-63.

LEE, M. 2014. Z944: a first in class T-type calcium channel modulator for the treatment of pain. *J Peripher Nerv Syst,* 19 Suppl 2**,** S11-2.

LESHER, J. M., DREYFUSS, P., HAGER, N., KAPLAN, M. & FURMAN, M. 2008. Hip joint pain referral patterns: a descriptive study. *Pain Med,* 9**,** 22-5.

LIU, P., OKUN, A., REN, J., GUO, R. C., OSSIPOV, M. H., XIE, J., KING, T. & PORRECA, F. 2011. Ongoing pain in the MIA model of osteoarthritis. *Neurosci Lett,* 493**,** 72-5.

LOCKWOOD, S. 2018. An Investigation of the Pharmacological Modulation of Diffuse Noxious Inhibitory Controls in a Monoiodoacetate Model of Osteoarthritis *UCL Library,* Thesis.

LOCKWOOD, S. M., BANNISTER, K. & DICKENSON, A. H. 2019a. An investigation into the noradrenergic and serotonergic contributions of diffuse noxious inhibitory controls in a monoiodoacetate model of osteoarthritis. *J Neurophysiol,* 121**,** 96-104.

LOCKWOOD, S. M., LOPES, D. M., MCMAHON, S. B. & DICKENSON, A. H. 2019b. Characterisation of peripheral and central components of the rat monoiodoacetate model of Osteoarthritis. *Osteoarthritis Cartilage,* 27**,** 712-722.

LOESER, R. F., GOLDRING, S. R., SCANZELLO, C. R. & GOLDRING, M. B. 2012. Osteoarthritis: a disease of the joint as an organ. *Arthritis Rheum,* 64**,** 1697-707.

LUMPKIN, E. A. & CATERINA, M. J. 2007. Mechanisms of sensory transduction in the skin. *Nature,* 445**,** 858-65.

M'DAHOMA, S., GADOTTI, V. M., ZHANG, F. X., PARK, B., NAM, J. H., ONNIS, V., BALBONI, G., LEE, J. Y. & ZAMPONI, G. W. 2016. Effect of the T-type channel blocker KYS-05090S in mouse models of acute and neuropathic pain. *Pflugers Arch,* 468**,** 193-9.

MAJEED, M. H., SHERAZI, S. A. A., BACON, D. & BAJWA, Z. H. 2018. Pharmacological Treatment of Pain in Osteoarthritis: A Descriptive Review. *Curr Rheumatol Rep,* 20**,** 88.

MAKRIS, E. A., HADIDI, P. & ATHANASIOU, K. A. 2011. The knee meniscus: structure-function, pathophysiology, current repair techniques, and prospects for regeneration. *Biomaterials,* 32**,** 7411-31.

MALFAIT, A. M., LITTLE, C. B. & MCDOUGALL, J. J. 2013. A commentary on modelling osteoarthritis pain in small animals. *Osteoarthritis Cartilage,* 21**,** 1316-26.

MANTOVANI, M., DOOLEY, D. J., WEYERBROCK, A., JACKISCH, R. & FEUERSTEIN, T. J. 2009. Differential inhibitory effects of drugs acting at the noradrenaline and 5-hydroxytryptamine transporters in rat and human neocortical synaptosomes. *Br J Pharmacol,* 158**,** 1848-56.

MANTYH, P. W., ROGERS, S. D., HONORE, P., ALLEN, B. J., GHILARDI, J. R., LI, J., DAUGHTERS, R. S., LAPPI, D. A., WILEY, R. G. & SIMONE, D. A. 1997. Inhibition of hyperalgesia by ablation of lamina I spinal neurons expressing the substance P receptor. *Science,* 278**,** 275-9.

MAPP, P. I., SAGAR, D. R., ASHRAF, S., BURSTON, J. J., SURI, S., CHAPMAN, V. & WALSH, D. A. 2013. Differences in structural and pain phenotypes in the sodium monoiodoacetate and meniscal transection models of osteoarthritis. *Osteoarthritis Cartilage,* 21**,** 1336-45.

MARICQ, A. V., PETERSON, A. S., BRAKE, A. J., MYERS, R. M. & JULIUS, D. 1991. Primary structure and functional expression of the 5HT3 receptor, a serotonin-gated ion channel. *Science,* 254**,** 432-7.

MARX, R. G. 2008. Arthroscopic surgery for osteoarthritis of the knee? *N Engl J Med,* 359**,** 1169-70.

MATHIESSEN, A. & CONAGHAN, P. G. 2017. Synovitis in osteoarthritis: current understanding with therapeutic implications. *Arthritis Res Ther,* 19**,** 18.

MATTHEWS, E. A. & DICKENSON, A. H. 2001. Effects of spinally delivered N- and P-type voltage-dependent calcium channel antagonists on dorsal horn neuronal responses in a rat model of neuropathy. *Pain,* 92**,** 235-46.
MCALINDON, T. & DIEPPE, P. 1989. Osteoarthritis: definitions and criteria. *Ann Rheum Dis,* 48**,** 531-2.
MCGARAUGHTY, S., CHU, K. L. & XU, J. 2018. Characterization and pharmacological modulation of noci-responsive deep dorsal horn neurons across diverse rat models of pathological pain. *J Neurophysiol,* 120**,** 1893-1905.
MELCHIORRI, C., MELICONI, R., FRIZZIERO, L., SILVESTRI, T., PULSATELLI, L., MAZZETTI, I., BORZI, R. M., UGUCCIONI, M. & FACCHINI, A. 1998. Enhanced and coordinated in vivo expression of inflammatory cytokines and nitric oxide synthase by chondrocytes from patients with osteoarthritis. *Arthritis Rheum,* 41**,** 2165-74.
MELZACK, R. & WALL, P. D. 1965. Pain mechanisms: a new theory. *Science,* 150**,** 971-9.
MENDELL, L. M. 1966. Physiological properties of unmyelinated fiber projection to the spinal cord. *Exp Neurol,* 16**,** 316-32.
MICHAELIS, M., HABLER, H. J. & JAENIG, W. 1996. Silent afferents: a separate class of primary afferents? *Clin Exp Pharmacol Physiol,* 23**,** 99-105.
MILLER, R. E., MALFAIT, A. M. & BLOCK, J. A. 2017. Current status of nerve growth factor antibodies for the treatment of osteoarthritis pain. *Clin Exp Rheumatol,* 35 Suppl 107**,** 85-87.
MILLER, R. E., MILLER, R. J. & MALFAIT, A. M. 2014. Osteoarthritis joint pain: the cytokine connection. *Cytokine,* 70**,** 185-93.
MILLER, R. E., TRAN, P. B., DAS, R., GHOREISHI-HAACK, N., REN, D., MILLER, R. J. & MALFAIT, A. M. 2012. CCR2 chemokine receptor signaling mediates pain in experimental osteoarthritis. *Proc Natl Acad Sci U S A,* 109**,** 20602-7.
MIYAGI, M., ISHIKAWA, T., KAMODA, H., SUZUKI, M., INOUE, G., SAKUMA, Y., OIKAWA, Y., ORITA, S., UCHIDA, K., TAKAHASHI, K., TAKASO, M. & OHTORI, S. 2017. Efficacy of nerve growth factor antibody in a knee osteoarthritis pain model in mice. *BMC Musculoskelet Disord,* 18**,** 428.
MOAYEDI, M. & DAVIS, K. D. 2013. Theories of pain: from specificity to gate control. *J Neurophysiol,* 109**,** 5-12.
MOEHRING, F., HALDER, P., SEAL, R. P. & STUCKY, C. L. 2018. Uncovering the Cells and Circuits of Touch in Normal and Pathological Settings. *Neuron,* 100**,** 349-360.
MOORE, R. A., WIFFEN, P. J., DERRY, S., TOELLE, T. & RICE, A. S. 2014. Gabapentin for chronic neuropathic pain and fibromyalgia in adults. *Cochrane Database Syst Rev***,** Cd007938.
MOSS, P., KNIGHT, E. & WRIGHT, A. 2016. Subjects with Knee Osteoarthritis Exhibit Widespread Hyperalgesia to Pressure and Cold. *PLoS One,* 11**,** e0147526.
NAIR, A. S., POORNACHAND, A. & KODISHARAPU, P. K. 2018. Ziconotide: Indications, Adverse Effects, and Limitations in Managing Refractory Chronic Pain. *Indian J Palliat Care,* 24**,** 118-119.
NELSON, M. T., WOO, J., KANG, H. W., VITKO, I., BARRETT, P. Q., PEREZ-REYES, E., LEE, J. H., SHIN, H. S. & TODOROVIC, S. M. 2007. Reducing agents sensitize C-type nociceptors by relieving high-affinity zinc inhibition of T-type calcium channels. *J Neurosci,* 27**,** 8250-60.
NEOGI, T. 2017. Structural correlates of pain in osteoarthritis. *Clin Exp Rheumatol,* 35 Suppl 107**,** 75-78.
OGBONNA, A. C., CLARK, A. K., GENTRY, C., HOBBS, C. & MALCANGIO, M. 2013. Pain-like behaviour and spinal changes in the monosodium iodoacetate model of osteoarthritis in C57Bl/6 mice. *Eur J Pain,* 17**,** 514-26.
ORGANIZATION, G. W. H. 2003. The burden of musculoskeletal conditions at the start of the new millenium: report of a WHO scientific group. *WHO technical report series ; 919*.
ORITA, S., ISHIKAWA, T., MIYAGI, M., OCHIAI, N., INOUE, G., EGUCHI, Y., KAMODA, H., ARAI, G., TOYONE, T., AOKI, Y., KUBO, T., TAKAHASHI, K. & OHTORI, S. 2011. Pain-related sensory innervation in monoiodoacetate-induced osteoarthritis in rat knees that gradually develops neuronal injury in addition to inflammatory pain. *BMC Musculoskelet Disord,* 12**,** 134.
OSSIPOV, M. H., DUSSOR, G. O. & PORRECA, F. 2010. Central modulation of pain. *J Clin Invest,* 120**,** 3779-87.
OSSIPOV, M. H., HONG SUN, T., MALAN, P., JR., LAI, J. & PORRECA, F. 2000. Mediation of spinal nerve injury induced tactile allodynia by descending facilitatory pathways in the dorsolateral funiculus in rats. *Neurosci Lett,* 290**,** 129-32.
OSSIPOV, M. H., MORIMURA, K. & PORRECA, F. 2014. Descending pain modulation and chronification of pain. *Curr Opin Support Palliat Care,* 8**,** 143-51.
PARK, J. & LUO, Z. D. 2010. Calcium channel functions in pain processing. *Channels (Austin),* 4**,** 510-7.
PATEL, R., BAUER, C. S., NIETO-ROSTRO, M., MARGAS, W., FERRON, L., CHAGGAR, K., CREWS, K., RAMIREZ, J. D., BENNETT, D. L., SCHWARTZ, A., DICKENSON, A. H. & DOLPHIN, A. C. 2013. alpha2delta-1 gene deletion affects somatosensory neuron function and delays

mechanical hypersensitivity in response to peripheral nerve damage. *J Neurosci,* 33**,** 16412-26.
PATEL, R. & DICKENSON, A. H. 2016. Neuronal hyperexcitability in the ventral posterior thalamus of neuropathic rats: modality selective effects of pregabalin. *J Neurophysiol,* 116**,** 159-70.
PATEL, R. & DICKENSON, A. H. 2018. Modality selective roles of pro-nociceptive spinal 5-HT2A and 5-HT3 receptors in normal and neuropathic states. *Neuropharmacology,* 143**,** 29-37.
PATEL, R., GONCALVES, L., NEWMAN, R., JIANG, F. L., GOLDBY, A., REEVE, J., HENDRICK, A., TEALL, M., HANNAH, D., ALMOND, S., BRICE, N. & DICKENSON, A. H. 2014. Novel TRPM8 antagonist attenuates cold hypersensitivity after peripheral nerve injury in rats. *J Pharmacol Exp Ther,* 349**,** 47-55.
PATEL, R., MONTAGUT-BORDAS, C. & DICKENSON, A. H. 2018. Calcium channel modulation as a target in chronic pain control. *Br J Pharmacol,* 175**,** 2173-2184.
PATEL, R., RUTTEN, K., VALDOR, M., SCHIENE, K., WIGGE, S., SCHUNK, S., DAMANN, N., CHRISTOPH, T. & DICKENSON, A. H. 2015. Electrophysiological characterization of activation state-dependent Ca(v)2 channel antagonist TROX-1 in spinal nerve injured rats. *Neuroscience,* 297**,** 47-57.
PETERSEN, K. K., SIMONSEN, O., LAURSEN, M. B., NIELSEN, T. A., RASMUSSEN, S. & ARENDT-NIELSEN, L. 2015. Chronic postoperative pain after primary and revision total knee arthroplasty. *Clin J Pain,* 31**,** 1-6.
PHELPS, C. E., NAVRATILOVA, E., DICKENSON, A. H., PORRECA, F. & BANNISTER, K. 2019. Kappa Opioid Signaling in the Right Central Amygdala Causes Hindpaw Specific Loss of Diffuse Noxious Inhibitory Controls (DNIC) in Experimental Neuropathic Pain. *Pain*.
POMONIS, J. D., BOULET, J. M., GOTTSHALL, S. L., PHILLIPS, S., SELLERS, R., BUNTON, T. & WALKER, K. 2005. Development and pharmacological characterization of a rat model of osteoarthritis pain. *Pain,* 114**,** 339-46.
PRATO, V., TABERNER, F. J., HOCKLEY, J. R. F., CALLEJO, G., ARCOURT, A., TAZIR, B., HAMMER, L., SCHAD, P., HEPPENSTALL, P. A., SMITH, E. S. & LECHNER, S. G. 2017. Functional and Molecular Characterization of Mechanoinsensitive "Silent" Nociceptors. *Cell Rep,* 21**,** 3102-3115.
QUEVEDO, A. S. & COGHILL, R. C. 2009. Filling-in, spatial summation, and radiation of pain: evidence for a neural population code in the nociceptive system. *J Neurophysiol,* 102**,** 3544-53.
RAHMAN, W., BANNISTER, K., BEE, L. A. & DICKENSON, A. H. 2011. A pronociceptive role for the 5-HT2 receptor on spinal nociceptive transmission: an in vivo electrophysiological study in the rat. *Brain Res,* 1382**,** 29-36.
RAHMAN, W., BAUER, C. S., BANNISTER, K., VONSY, J. L., DOLPHIN, A. C. & DICKENSON, A. H. 2009. Descending serotonergic facilitation and the antinociceptive effects of pregabalin in a rat model of osteoarthritic pain. *Mol Pain,* 5**,** 45.
RAHMAN, W., PATEL, R. & DICKENSON, A. H. 2015. Electrophysiological evidence for voltage-gated calcium channel 2 (Cav2) modulation of mechano- and thermosensitive spinal neuronal responses in a rat model of osteoarthritis. *Neuroscience,* 305**,** 76-85.
RAHMAN, W., SUZUKI, R., RYGH, L. J. & DICKENSON, A. H. 2004. Descending serotonergic facilitation mediated through rat spinal 5HT3 receptors is unaltered following carrageenan inflammation. *Neurosci Lett,* 361**,** 229-31.
RAHMAN, W., SUZUKI, R., WEBBER, M., HUNT, S. P. & DICKENSON, A. H. 2006. Depletion of endogenous spinal 5-HT attenuates the behavioural hypersensitivity to mechanical and cooling stimuli induced by spinal nerve ligation. *Pain,* 123**,** 264-74.
RAJAKULENDRAN, S. & HANNA, M. G. 2016. The Role of Calcium Channels in Epilepsy. *Cold Spring Harb Perspect Med,* 6**,** a022723.
RAOOF, R., WILLEMEN, H. & EIJKELKAMP, N. 2018. Divergent roles of immune cells and their mediators in pain. *Rheumatology (Oxford),* 57**,** 429-440.
RENGANATHAN, M., CUMMINS, T. R. & WAXMAN, S. G. 2001. Contribution of Na(v)1.8 sodium channels to action potential electrogenesis in DRG neurons. *J Neurophysiol,* 86**,** 629-40.
ROSE, K. E., LUNARDI, N., BOSCOLO, A., DONG, X., ERISIR, A., JEVTOVIC-TODOROVIC, V. & TODOROVIC, S. M. 2013. Immunohistological demonstration of CaV3.2 T-type voltage-gated calcium channel expression in soma of dorsal root ganglion neurons and peripheral axons of rat and mouse. *Neuroscience,* 250**,** 263-74.
SAEED, A. W. & RIBEIRO-DA-SILVA, A. 2013. De novo expression of neurokinin-1 receptors by spinoparabrachial lamina I pyramidal neurons following a peripheral nerve lesion. *J Comp Neurol,* 521**,** 1915-28.
SAEGUSA, H., KURIHARA, T., ZONG, S., KAZUNO, A., MATSUDA, Y., NONAKA, T., HAN, W., TORIYAMA, H. & TANABE, T. 2001. Suppression of inflammatory and neuropathic pain symptoms in mice lacking the N-type Ca2+ channel. *Embo j,* 20**,** 2349-56.

SAGAR, D. R., NWOSU, L., WALSH, D. A. & CHAPMAN, V. 2015. Dissecting the contribution of knee joint NGF to spinal nociceptive sensitization in a model of OA pain in the rat. *Osteoarthritis Cartilage,* 23**,** 906-13.

SAGAR, D. R., STANIASZEK, L. E., OKINE, B. N., WOODHAMS, S., NORRIS, L. M., PEARSON, R. G., GARLE, M. J., ALEXANDER, S. P., BENNETT, A. J., BARRETT, D. A., KENDALL, D. A., SCAMMELL, B. E. & CHAPMAN, V. 2010. Tonic modulation of spinal hyperexcitability by the endocannabinoid receptor system in a rat model of osteoarthritis pain. *Arthritis Rheum,* 62**,** 3666-76.

SANDELL, L. J. 2012. Etiology of osteoarthritis: genetics and synovial joint development. *Nat Rev Rheumatol,* 8**,** 77-89.

SANDKUHLER, J. & GEBHART, G. F. 1984. Relative contributions of the nucleus raphe magnus and adjacent medullary reticular formation to the inhibition by stimulation in the periaqueductal gray of a spinal nociceptive reflex in the pentobarbital-anesthetized rat. *Brain Res,* 305**,** 77-87.

SANTOS, S. F., LUZ, L. L., SZUCS, P., LIMA, D., DERKACH, V. A. & SAFRONOV, B. V. 2009. Transmission efficacy and plasticity in glutamatergic synapses formed by excitatory interneurons of the substantia gelatinosa in the rat spinal cord. *PLoS One,* 4**,** e8047.

SCHAIBLE, H. G., VON BANCHET, G. S., BOETTGER, M. K., BRAUER, R., GAJDA, M., RICHTER, F., HENSELLEK, S., BRENN, D. & NATURA, G. 2010. The role of proinflammatory cytokines in the generation and maintenance of joint pain. *Ann N Y Acad Sci,* 1193**,** 60-9.

SCHLAAK, J. F., PFERS, I., MEYER ZUM BUSCHENFELDE, K. H. & MARKER-HERMANN, E. 1996. Different cytokine profiles in the synovial fluid of patients with osteoarthritis, rheumatoid arthritis and seronegative spondylarthropathies. *Clin Exp Rheumatol,* 14**,** 155-62.

SCHMIDT, R., SCHMELZ, M., FORSTER, C., RINGKAMP, M., TOREBJORK, E. & HANDWERKER, H. 1995. Novel classes of responsive and unresponsive C nociceptors in human skin. *J Neurosci,* 15**,** 333-41.

SCHROEDER, C. I. & LEWIS, R. J. 2006. ω-Conotoxins GVIA, MVIIA and CVID: SAR and Clinical Potential. *Mar Drugs,* 4**,** 193-214.

SEGOND VON BANCHET, G., BOETTGER, M. K., FISCHER, N., GAJDA, M., BRAUER, R. & SCHAIBLE, H. G. 2009. Experimental arthritis causes tumor necrosis factor-alpha-dependent infiltration of macrophages into rat dorsal root ganglia which correlates with pain-related behavior. *Pain,* 145**,** 151-9.

SIKANDAR, S., RONGA, I., IANNETTI, G. D. & DICKENSON, A. H. 2013. Neural coding of nociceptive stimuli-from rat spinal neurones to human perception. *Pain,* 154**,** 1263-73.

SIMMS, B. A. & ZAMPONI, G. W. 2014. Neuronal voltage-gated calcium channels: structure, function, and dysfunction. *Neuron,* 82**,** 24-45.

SIMON, D., MASCARENHAS, R., SALTZMAN, B. M., ROLLINS, M., BACH, B. R., JR. & MACDONALD, P. 2015. The Relationship between Anterior Cruciate Ligament Injury and Osteoarthritis of the Knee. *Adv Orthop,* 2015**,** 928301.

SIQUEIRA, M. B., FRANGIAMORE, S., KLIKA, A. K., GAJEWSKI, N., BARSOUM, W. K. & HIGUERA, C. A. 2017. Comparison of Synovial Fluid Cytokine Levels between Traumatic Knee Injury and End-Stage Osteoarthritis. *J Knee Surg,* 30**,** 128-133.

SNIDER, W. D. & MCMAHON, S. B. 1998. Tackling pain at the source: new ideas about nociceptors. *Neuron,* 20**,** 629-32.

SOHN, D. H., SOKOLOVE, J., SHARPE, O., ERHART, J. C., CHANDRA, P. E., LAHEY, L. J., LINDSTROM, T. M., HWANG, I., BOYER, K. A., ANDRIACCHI, T. P. & ROBINSON, W. H. 2012. Plasma proteins present in osteoarthritic synovial fluid can stimulate cytokine production via Toll-like receptor 4. *Arthritis Res Ther,* 14**,** R7.

SONI, A., WANIGASEKERA, V., MEZUE, M., COOPER, C., JAVAID, M. K., PRICE, A. J. & TRACEY, I. 2018. Central sensitisation in knee osteoarthritis: Relating pre-surgical brainstem neuroimaging and PainDETECT based patient stratification to arthroplasty outcome. *Arthritis Rheumatol*.

SPIKE, R. C., PUSKAR, Z., ANDREW, D. & TODD, A. J. 2003. A quantitative and morphological study of projection neurons in lamina I of the rat lumbar spinal cord. *Eur J Neurosci,* 18**,** 2433-48.

STEINMEYER, J., BOCK, F., STOVE, J., JEROSCH, J. & FLECHTENMACHER, J. 2018. Pharmacological treatment of knee osteoarthritis: Special considerations of the new German guideline. *Orthop Rev (Pavia),* 10**,** 7782.

SURI, S., GILL, S. E., MASSENA DE CAMIN, S., WILSON, D., MCWILLIAMS, D. F. & WALSH, D. A. 2007. Neurovascular invasion at the osteochondral junction and in osteophytes in osteoarthritis. *Ann Rheum Dis,* 66**,** 1423-8.

SURI, S. & WALSH, D. A. 2012. Osteochondral alterations in osteoarthritis. *Bone,* 51**,** 204-11.

SUZUKI, R., MORCUENDE, S., WEBBER, M., HUNT, S. P. & DICKENSON, A. H. 2002. Superficial NK1-expressing neurons control spinal excitability through activation of descending pathways. *Nat Neurosci,* 5**,** 1319-26.

SUZUKI, R., RAHMAN, W., HUNT, S. P. & DICKENSON, A. H. 2004. Descending facilitatory control of mechanically evoked responses is enhanced in deep dorsal horn neurones following peripheral nerve injury. *Brain Res,* 1019**,** 68-76.

SUZUKI, R., RAHMAN, W., RYGH, L. J., WEBBER, M., HUNT, S. P. & DICKENSON, A. H. 2005. Spinal-supraspinal serotonergic circuits regulating neuropathic pain and its treatment with gabapentin. *Pain,* 117**,** 292-303.

SWENSEN, A. M., HERRINGTON, J., BUGIANESI, R. M., DAI, G., HAEDO, R. J., RATLIFF, K. S., SMITH, M. M., WARREN, V. A., ARNERIC, S. P., EDULJEE, C., PARKER, D., SNUTCH, T. P., HOYT, S. B., LONDON, C., DUFFY, J. L., KACZOROWSKI, G. J. & MCMANUS, O. B. 2012. Characterization of the substituted N-triazole oxindole TROX-1, a small-molecule, state-dependent inhibitor of Ca(V)2 calcium channels. *Mol Pharmacol,* 81**,** 488-97.

SZCZOT, M., LILJENCRANTZ, J., GHITANI, N., BARIK, A., LAM, R., THOMPSON, J. H., BHARUCHA-GOEBEL, D., SAADE, D., NECAISE, A., DONKERVOORT, S., FOLEY, A. R., GORDON, T., CASE, L., BUSHNELL, M. C., BONNEMANN, C. G. & CHESLER, A. T. 2018. PIEZO2 mediates injury-induced tactile pain in mice and humans. *Sci Transl Med,* 10.

TEEPLE, E., JAY, G. D., ELSAID, K. A. & FLEMING, B. C. 2013. Animal models of osteoarthritis: challenges of model selection and analysis. *Aaps j,* 15**,** 438-46.

TER HEEGDE, F., LUIZ, A. P., SANTANA-VARELA, S., CHESSELL, I. P., WELSH, F., WOOD, J. N. & CHENU, C. 2019. Noninvasive Mechanical Joint Loading as an Alternative Model for Osteoarthritic Pain. *Arthritis Rheumatol,* 71**,** 1078-1088.

THAKUR, M. 2012. Pharmocological, Neurochemical and Functional Characterisation of the MIA Model of Experimental Osteoarthritis. *UCL Library,* Thesis.

THAKUR, M., DICKENSON, A. H. & BARON, R. 2014. Osteoarthritis pain: nociceptive or neuropathic? *Nat Rev Rheumatol,* 10**,** 374-80.

THAKUR, M., RAHMAN, W., HOBBS, C., DICKENSON, A. H. & BENNETT, D. L. 2012. Characterisation of a peripheral neuropathic component of the rat monoiodoacetate model of osteoarthritis. *PLoS One,* 7**,** e33730.

TIMIC STAMENIC, T., FESEHA, S., VALDEZ, R., ZHAO, W., KLAWITTER, J. & TODOROVIC, S. M. 2019. Alterations in Oscillatory Behavior of Central Medial Thalamic Neurons Demonstrate a Key Role of CaV3.1 Isoform of T-Channels During Isoflurane-Induced Anesthesia. *Cereb Cortex*.

TODD, A. J. 2002. Anatomy of primary afferents and projection neurones in the rat spinal dorsal horn with particular emphasis on substance P and the neurokinin 1 receptor. *Exp Physiol,* 87**,** 245-9.

TODD, A. J. 2010. Neuronal circuitry for pain processing in the dorsal horn. *Nat Rev Neurosci,* 11**,** 823-36.

TODD, A. J., MCGILL, M. M. & SHEHAB, S. A. 2000. Neurokinin 1 receptor expression by neurons in laminae I, III and IV of the rat spinal dorsal horn that project to the brainstem. *Eur J Neurosci,* 12**,** 689-700.

TRACEY, I. & MANTYH, P. W. 2007. The cerebral signature for pain perception and its modulation. *Neuron,* 55**,** 377-91.

TRAN, P. B., MILLER, R. E., ISHIHARA, S., MILLER, R. J. & MALFAIT, A. M. 2017. Spinal microglial activation in a murine surgical model of knee osteoarthritis. *Osteoarthritis Cartilage,* 25**,** 718-726.

TRAN-VAN-MINH, A. & DOLPHIN, A. C. 2010. The alpha2delta ligand gabapentin inhibits the Rab11-dependent recycling of the calcium channel subunit alpha2delta-2. *J Neurosci,* 30**,** 12856-67.

UDO, M., MUNETA, T., TSUJI, K., OZEKI, N., NAKAGAWA, Y., OHARA, T., SAITO, R., YANAGISAWA, K., KOGA, H. & SEKIYA, I. 2016. Monoiodoacetic acid induces arthritis and synovitis in rats in a dose- and time-dependent manner: proposed model-specific scoring systems. *Osteoarthritis Cartilage,* 24**,** 1284-91.

URBAN, M. O., REN, K., SABLAD, M. & PARK, K. T. 2005. Medullary N-type and P/Q-type calcium channels contribute to neuropathy-induced allodynia. *Neuroreport,* 16**,** 563-6.

URCH, C. E. & DICKENSON, A. H. 2003. In vivo single unit extracellular recordings from spinal cord neurones of rats. *Brain Res Brain Res Protoc,* 12**,** 26-34.

URCH, C. E., DONOVAN-RODRIGUEZ, T. & DICKENSON, A. H. 2003. Alterations in dorsal horn neurones in a rat model of cancer-induced bone pain. *Pain,* 106**,** 347-56.

VAHLE-HINZ, C. & DETSCH, O. 2002. What can in vivo electrophysiology in animal models tell us about mechanisms of anaesthesia? *Br J Anaesth,* 89**,** 123-42.

VANDEWAUW, I., DE CLERCQ, K., MULIER, M., HELD, K., PINTO, S., VAN RANST, N., SEGAL, A., VOET, T., VENNEKENS, R., ZIMMERMANN, K., VRIENS, J. & VOETS, T. 2018. A TRP channel trio mediates acute noxious heat sensing. *Nature,* 555**,** 662-666.

WALSH, D. A., BONNET, C. S., TURNER, E. L., WILSON, D., SITU, M. & MCWILLIAMS, D. F. 2007. Angiogenesis in the synovium and at the osteochondral junction in osteoarthritis. *Osteoarthritis Cartilage,* 15**,** 743-51.

WALSH, D. A., MCWILLIAMS, D. F., TURLEY, M. J., DIXON, M. R., FRANSES, R. E., MAPP, P. I. & WILSON, D. 2010. Angiogenesis and nerve growth factor at the osteochondral junction in rheumatoid arthritis and osteoarthritis. *Rheumatology (Oxford),* 49**,** 1852-61.
WANG, R. & LEWIN, G. R. 2011. The Cav3.2 T-type calcium channel regulates temporal coding in mouse mechanoreceptors. *J Physiol,* 589**,** 2229-43.
WAXMAN, S. G. & ZAMPONI, G. W. 2014. Regulating excitability of peripheral afferents: emerging ion channel targets. *Nat Neurosci,* 17**,** 153-63.
WEISS, N. & ZAMPONI, G. W. 2019. T-type calcium channels: From molecule to therapeutic opportunities. *Int J Biochem Cell Biol,* 108**,** 34-39.
WIELAND, H. A., MICHAELIS, M., KIRSCHBAUM, B. J. & RUDOLPHI, K. A. 2005. Osteoarthritis - an untreatable disease? *Nat Rev Drug Discov,* 4**,** 331-44.
WIFFEN, P. J., MCQUAY, H. J., EDWARDS, J. E. & MOORE, R. A. 2005. Gabapentin for acute and chronic pain. *Cochrane Database Syst Rev***,** Cd005452.
WINQUIST, R. J., PAN, J. Q. & GRIBKOFF, V. K. 2005. Use-dependent blockade of Cav2.2 voltage-gated calcium channels for neuropathic pain. *Biochem Pharmacol,* 70**,** 489-99.
WOJDASIEWICZ, P., PONIATOWSKI, L. A. & SZUKIEWICZ, D. 2014. The role of inflammatory and anti-inflammatory cytokines in the pathogenesis of osteoarthritis. *Mediators Inflamm,* 2014**,** 561459.
WOOLF, C. J. & FITZGERALD, M. 1986. Somatotopic organization of cutaneous afferent terminals and dorsal horn neuronal receptive fields in the superficial and deep laminae of the rat lumbar spinal cord. *J Comp Neurol,* 251**,** 517-31.
WYLDE, V., PALMER, S., LEARMONTH, I. D. & DIEPPE, P. 2012. Somatosensory abnormalities in knee OA. *Rheumatology (Oxford),* 51**,** 535-43.
XIAOMING ZHANG, D. B. A. J. W. 2015. Classifications and Definitions of Normal Joints. *IntechOpen*.
YU, D., LIU, F., LIU, M., ZHAO, X., WANG, X., LI, Y., MAO, Y. & ZHU, Z. 2013. The inhibition of subchondral bone lesions significantly reversed the weight-bearing deficit and the overexpression of CGRP in DRG neurons, GFAP and Iba-1 in the spinal dorsal horn in the monosodium iodoacetate induced model of osteoarthritis pain. *PLoS One,* 8**,** e77824.
YUSUF, E., KORTEKAAS, M. C., WATT, I., HUIZINGA, T. W. & KLOPPENBURG, M. 2011. Do knee abnormalities visualised on MRI explain knee pain in knee osteoarthritis? A systematic review. *Ann Rheum Dis,* 70**,** 60-7.
ZAMPONI, G. W., LEWIS, R. J., TODOROVIC, S. M., ARNERIC, S. P. & SNUTCH, T. P. 2009. Role of voltage-gated calcium channels in ascending pain pathways. *Brain Res Rev,* 60**,** 84-9.
ZAMPONI, G. W., STRIESSNIG, J., KOSCHAK, A. & DOLPHIN, A. C. 2015. The Physiology, Pathology, and Pharmacology of Voltage-Gated Calcium Channels and Their Future Therapeutic Potential. *Pharmacol Rev,* 67**,** 821-70.
ZHANG, J., CAVANAUGH, D. J., NEMENOV, M. I. & BASBAUM, A. I. 2013. The modality-specific contribution of peptidergic and non-peptidergic nociceptors is manifest at the level of dorsal horn nociresponsive neurons. *J Physiol,* 591**,** 1097-110.
ZHUO, M. & GEBHART, G. F. 1992. Characterization of descending facilitation and inhibition of spinal nociceptive transmission from the nuclei reticularis gigantocellularis and gigantocellularis pars alpha in the rat. *J Neurophysiol,* 67**,** 1599-614.
ZIEGLER, D., DUAN, W. R., AN, G., THOMAS, J. W. & NOTHAFT, W. 2015. A randomized double-blind, placebo-, and active-controlled study of T-type calcium channel blocker ABT-639 in patients with diabetic peripheral neuropathic pain. *Pain,* 156**,** 2013-20.
ZYLKA, M. J., RICE, F. L. & ANDERSON, D. J. 2005. Topographically distinct epidermal nociceptive circuits revealed by axonal tracers targeted to Mrgprd. *Neuron,* 45**,** 17-25.